



Synthesis and applications of new *hydrophilic*
aldehyde-functional methacrylic polymers

Emma Elizabeth Brotherton

A thesis submitted in partial fulfilment for the degree of
Doctor of Philosophy

The University of Sheffield
Department of Chemistry

October 2022

Declaration

The work described in this thesis was undertaken at the University of Sheffield under the supervision of Professor Steven P. Armes between October 2018 and October 2022 and has not been submitted, either wholly or in part, for this or any other degree. All the work is the original work of the author, except where acknowledged.

Signature: _____

Emma Elizabeth Brotherton

October 2022

Declarations for published Chapters

Chapter III

The synthesis of GEO5MA was conducted by Dr C. P. Jesson at GEO Specialty Chemicals. Its characterisation and all other work in that Chapter was done by E. E. Brotherton.

Chapter IV

All of the work in this Chapter was conducted by E. E. Brotherton.

Chapter V

The rheology and SAXS were conducted by Dr T. J. Neal (in Figure 5.6, 5.9 and 5.11 and Appendix). The mucoadhesion studies (Figure 5.12 and 5.13) were performed at University of Reading. All other work was conducted by E. E. Brotherton.

Acknowledgements

Firstly, thanks to Steve for your supervision and constant ideas throughout this project. Thanks, Denise, for helping me out when I inevitably tried to book things without all of the correct forms. Thank you to Debbie Hammond for your XPS expertise. Cheers to Andy Parnell for teaching me the basics of ellipsometry and to Gary Dunderdale for your early help with ARGET ATRP. A big thanks to Vitaliy Khutoryanskiy and Daulet Kaldybekov at the University of Reading for your work on the mucoadhesion studies. Thanks also to Tom Neal for all of your work on this project, especially all of the rheology experiments you conducted.

Thanks to GEO Specialty Chemicals for partly sponsoring my PhD and cheers to everyone at GEO who whole-heartedly welcomed me during my brief stint down south. Thanks to the whole of the R&D team: Mel, George, Tash, Léon, Becky, Jade and Tom. Especially thanks to George for your supervision throughout my placement and for all the F1 chat.

Thanks to every member of the CDT's Cohort 5, you all made this experience a lot more fun. Thank you to the Armes group past and present; cheers to the oldies who really helped me and welcomed me at the start and the newbies who continued to make Fridays pub day. Thanks to both of my Masters' students for all of your hard work and giving me the opportunity to supervise.

A massive thanks to Ed Johnson for all of your help with the brush work and for the moral support with that project. Without you, I'd still be banging my head against the proverbial brick wall. T. J. Neal, thanks for being the best friend throughout this: thank you for always taking me for a coffee when times got tough, for proof reading everything, always offering advice and for being an all-round good guy.

A big thanks to the O. G. lunch crew for making these past four years so good; from waterpark trips to lockdown quizzes, it's been a laugh. Courtney Thompson, you legend, thank you for being the best friend I could ask for. I don't know how I would have got through these past four years without the weekly lockdown chats/walks, all the coffee breaks, writing days and all the rubbish we've chatted. To some my undergrad friends: Jen, Beth, Charlotte; thank you for always being there for me through everything and always listening to me moaning about PhD life.

A massive thank you to my wonderful boyfriend; thank you for always being there for me, we got through these past few months together (even if we were 3000+ miles apart for a lot of it). I'm so excited to see the world with you. Dad, thanks for helping me move house 1,000,000 times over the past eight years and always being on the other end of the phone when I've needed you. Cheers to my little bro for always keeping me grounded and reminding me how uncool I am. Finally, thank you to my brilliant mother who has always championed me and taught me "girls can do anything". Without your hard work, I wouldn't have got this far.

Publications

Primary publications resulting from this work:

E. E. Brotherton, C. P. Jesson, N. J. Warren, M. J. Smallridge and S. P. Armes, 'New Aldehyde-Functional Methacrylic Water-Soluble Polymers', *Angew. Chemie Int. Ed.*, 2021, **60**, 12032–12037.

E. E. Brotherton, M. J. Smallridge and S. P. Armes, 'Aldehyde-Functional Diblock Copolymer Nano-Objects *via* RAFT Aqueous Dispersion Polymerization', *Biomacromolecules*, 2021, **22**, 5382–5389.

E. E. Brotherton, T. J. Neal, D. B. Kaldybekov, M. J. Smallridge, V. V. Khutoryanskiy and S. P. Armes, 'Aldehyde-Functional Thermoresponsive Diblock Copolymer Worm Gels Exhibit Strong Mucoadhesion', *Chem. Sci.*, 2022, **13**, 6888–6898.

E. E. Brotherton, E. C. Johnson, M. J. Smallridge, G. J. Leggett and S. P. Armes, 'New Hydrophilic Aldehyde-Functional Polymer Brushes: Synthesis, Characterization and Potential Bioapplications', *manuscript submitted*.

Other publications:

E. E. Brotherton, F. L. Hatton, A. A. Cockram, M. J. Derry, A. Czajka, E. J. Cornel, P. D. Topham, O. O. Mykhaylyk and S. P. Armes, '*In Situ* SAXS Studies During the RAFT Aqueous Emulsion Polymerization of 2-Methoxyethyl Methacrylate', *J. Am. Chem. Soc.*, 2019, **141**, 13664–13675.

J. Engström, M. S. Reid, E. E. Brotherton, E. Malmström, S. P. Armes and F. L. Hatton, 'Investigating the Adsorption of Anisotropic Diblock Copolymer Worms onto Planar Silica and Nanocellulose Surfaces Using a Quartz Crystal Microbalance', *Polym. Chem.*, 2021, **12**, 6088–6100.

E. E. Brotherton, D. Josland, C. György, E. C. Johnson, D. H. H. Chan, M. J. Smallridge and S. P. Armes, 'Histidine-Functionalized Diblock Copolymer Nanoparticles Exhibit Enhanced Adsorption onto Planar Stainless Steel', *accepted Macromol. Rapid Commun.*, 2022.

Conferences

Oral presentations

- July 2019 Polymer, Soft Matter and Colloids CDT Annual Summer School,
Sheffield, UK
- August 2019 258th ACS National Meeting, San Diego, USA
- July 2021 Polymer, Soft Matter and Colloids CDT Annual Summer School,
Sheffield, UK
- March 2022 263rd ACS National Meeting, San Diego, USA
- August 2022 264th ACS National Meeting, Chicago, USA

Poster presentations

- June 2022 Bordeaux Polymer Conference, Bordeaux, France

Abstract

This Thesis explores the synthesis of a new hydrophilic aldehyde-functional vinyl monomer, AGE05MA, and its corresponding (co)polymers. AGE05MA can be synthesised from a precursor *cis*-diol based monomer (GEO5MA) by oxidation under relatively mild conditions using an aqueous solution of sodium periodate (NaIO₄). This chemistry can also be employed for the derivatisation of PGEO5MA homopolymer, whereby the extent of oxidation can be tuned by using sub-stoichiometric amounts of NaIO₄. Moreover, the same approach can be employed to introduce aldehyde groups into both water-soluble PGEO5MA-based diblock copolymers and PGEO5MA-based diblock copolymer nanoparticles. PAGE05MA homopolymer was derivatised using various amino acids *via* reductive amination. High extents of functionalisation (>99% as judged by ¹H NMR spectroscopy) were achieved in all cases. This chemistry was then extended to include PAGE05MA₂₆-PHPMA_y diblock copolymer spheres, worms or vesicles, with similarly high extents of functionalisation being obtained. Aqueous electrophoresis studies were conducted to determine zeta potential vs. pH curves for the derivatised nanoparticles. As expected, the precursor PGEO5MA₂₆-PHPMA_y and PAGE05MA₂₆-PHPMA_y nanoparticles exhibited zeta potentials close to zero across the whole pH range. In contrast, zeta potentials for the amino acid-functionalised nanoparticles proved to be strongly pH-dependent. Oxidation of PGEO5MA₂₆-PHPMA₃₅₀ vesicles led to partial loss of the original copolymer morphology (TEM studies indicated a worm population). In view of this unexpected problem, membrane-crosslinked PAGE05MA₂₆-PHPMA₃₅₀-PEGDMA₂₀ vesicles were prepared prior to functionalisation with a model globular protein, bovine serum albumin (BSA). The electrophoretic behaviour of the BSA-functionalised vesicles closely resembled that of the BSA protein alone. In contrast, no change in zeta potential was observed after attempted BSA functionalisation of the analogous PGEO5MA₂₆-PHPMA₃₅₀-PEGDMA₂₀ vesicles. This suggests that the surface aldehyde groups introduced *via* NaIO₄ oxidation are essential for successful BSA conjugation. PGEO5MA brushes were grown from planar silicon wafers and then oxidised using a 3.0 mg mL⁻¹ aqueous NaIO₄ solution. The extent of oxidation was determined to be more than 99% by X-ray photoelectron spectroscopy (XPS). The resulting PAGE05MA brushes were reacted in turn with 2,2,2-trifluoroethylamine, (2-aminoethyl)trimethylammonium chloride hydrochloride (AETMA) or histidine at 35 °C *via* reductive amination; XPS studies indicated extents of functionalisation of 29, 20 or 13%, respectively. Notably, the surface zeta potential vs. pH curves for the AETMA- and histidine-functionalised brushes were dramatically altered after such derivatisation. Interestingly, increasing the temperature from 35 °C to 50 °C led to higher extents of functionalisation (up to 82% for histidine). Selective oxidation of thermoresponsive PGEO5MA₁₃-PHPMA₁₅₅ worm gels targeting extents of oxidation of 10, 20, 30 or 50% was conducted. The mucoadhesive properties of these worm gels on porcine bladder tissue was assessed in collaboration with a team at the University of Reading. The 30% aldehyde-functional worm gel exhibited the highest mucoadhesion (comparable to that of chitosan) while retaining the thermoresponsive behaviour exhibited by the precursor PGEO5MA₁₃-PHPMA₁₅₅ worm gel.

Abbreviations

ACVA	4,4'-azobis-4-cyanopentanoic acid
AETMA	(2-aminoethyl)trimethylammonium chloride hydrochloride
AGEO5MA	aldehyde-functional GEO5MA
APTES	(3-aminopropyl)triethoxysilane
ARGET ATRP	activator regenerated by electron transfer atom transfer radical polymerisation
ATRP	atom transfer radical polymerisation
AU	artificial urine
BiBB	α -bromoisobutyryl bromide
BSA	bovine serum albumin
CECPA	4-(((2-carboxyethyl)thio)carbonothioyl)thio)-4-cyanopentanoic acid
CPDB	2-cyano-2-propyl benzodithioate
CTA(s)	chain transfer agent(s)
CuCl ₂	copper (II) chloride
\mathcal{D}	dispersity
DAAM	diacetone acrylamide
D_h	hydrodynamic diameter
DLS	dynamic light scattering
DMF	dimethylformamide
DMSO	dimethyl sulfoxide
D_n	number-average diameter
DP(s)	degree(s) of polymerisation
D_v	hydrodynamic volume-average diameter
D ₂ O	deuterium oxide
EGDMA	ethylene glycol dimethacrylate
FHMA	3-formyl-4-hydroxybenzyl methacrylate
FITC	fluorescein isothiocyanate
FMA	fluorescein methacrylate
FRP	free radical polymerisation
FT-IR	fourier transform infrared spectroscopy
G'	storage modulus
G''	loss modulus

GMA	glycerol monomethacrylate
GPC	gel permeation chromatography
HCl	hydrochloric acid
HEMA	2-hydroxyethyl methacrylate
HPMA	2-hydroxypropyl methacrylate
IEP	isoelectric point
Macro-CTA	macromolecular chain transfer agent
MEHQ	4-methoxyphenol
METAC	[2-(methacryloyloxy)ethyl] trimethylammonium chloride
MMA	methyl methacrylate
M_n	number-average molecular weight
MPC	(methacryloyloxy)ethyl phosphorylcholine
M_w	weight-average molecular weight
NaCNBH ₃	sodium cyanoborohydride
NaIO ₄	sodium periodate
NaOH	sodium hydroxide
NMP	nitroxide-mediated polymerisation
NMR	nuclear magnetic resonance
OEGMA	oligo(ethylene glycol) methacrylate
P or <i>p</i>	packing parameter
PAGEO5MA	poly(aldehyde-functional GEO5MA)
PAGMA	poly(aldehyde-functional glycerol monomethacrylate)
PDI	polydispersity index
PEG	poly(ethylene glycol)
PEGDMA	poly(ethylene glycol dimethacrylate)
PEO	poly(ethylene oxide)
PGlyGEO5MA	poly(glycine-functionalised GEO5MA)
PGMA	poly(glycerol monomethacrylate)
PHEMA	poly(2-hydroxyethyl methacrylate)
PHisGEO5MA	poly(histidine-functionalised GEO5MA)
PHPMA	poly(2-hydroxypropyl methacrylate)
PISA	polymerisation-induced self-assembly
PMDETA	<i>N,N,N',N'',N'''</i> -pentamethyldiethylenetriamine
PMETAC	poly([2-(methacryloyloxy)ethyl] trimethylammonium chloride)

PMMA	poly(methyl methacrylate)
PMPC	poly[(methacryloyloxy)ethyl phosphorylcholine]
PNAM	poly(<i>N</i> -acryloylmorpholine)
PSEM	poly(ammonium 2-sulfatoethyl methacrylate)
PVBA	poly(4-vinylbenzaldehyde)
RAFT	reversible addition-fragmentation chain transfer
RDRP(s)	reversible-deactivation radical polymerisation(s)
SAXS	small-angle X-ray scattering
SEM	ammonium 2-sulfatoethyl methacrylate
SI-ARGET ATRP	surface-initiated activators regenerated by electron transfer atom-transfer radical polymerisation
SI-ATRP	surface-initiated atom-transfer radical polymerisation
SI-CRP	surface-initiated controlled radical polymerisation
TEM	transmission electron microscopy
TFEA	2,2,2-trifluoroethylamine
THF	tetrahydrofuran
VBA	4-vinylbenzaldehyde

Contents

Chapter I: Introduction	1
1.1. What is a polymer?	2
1.2. Polymer architectures	2
1.3. Polymerisation techniques	3
1.3.1. Free radical polymerisation (FRP)	3
1.3.2. Ionic polymerisation	4
1.3.3. Reversible-deactivation radical polymerisations (RDRPs).....	5
1.3.3.1. Nitroxide-mediated polymerisation (NMP)	6
1.3.3.2. Atom transfer radical polymerisation (ATRP).....	7
1.3.3.3. Reversible addition-fragmentation chain transfer (RAFT) polymerisation.....	8
1.4. Polymerisation methods	11
1.4.1. Bulk polymerisation	11
1.4.2. Solution polymerisation	11
1.4.3. Aqueous emulsion polymerisation.....	11
1.4.4. Aqueous dispersion polymerisation	13
1.4.5. Surface-initiated (SI) polymerisation.....	15
1.4.5.1. Polymer brushes.....	15
1.4.5.2. Surface-initiated controlled radical polymerisation (SI-CRP)	16
1.4.5.3. Surface-initiated atom transfer radical polymerisation (SI-ATRP).....	17
1.5. Diblock copolymer nanoparticles	20
1.5.1. Block copolymer self-assembly	20
1.5.2. Post-polymerisation modification.....	21
1.5.3. Polymerisation-induced self-assembly (PISA)	22
1.5.3.1. Pseudo-phase diagrams	23
1.5.3.2. Thermoresponsive nanoparticles.....	24
1.5.3.3. Diblock copolymer worm gels for biological applications.....	25

1.6. Aldehyde-functional polymers.....	27
1.6.1. Chemistry of the aldehyde functional group	27
1.6.2. Synthesis of linear aldehyde-functional polymers.....	28
1.6.2.1. <i>Synthesis using aldehyde-functional initiators</i>	28
1.6.2.2. <i>Incorporation of aldehyde functionality after polymerisation</i>	29
1.6.2.3. <i>Synthesis using aldehyde-functional monomers</i>	30
1.6.3. Synthesis of aldehyde-functional nanoparticles	32
1.6.3.1. <i>Synthesis by post-polymerisation modification</i>	32
1.6.3.2. <i>Synthesis via PISA</i>	34
1.6.4. Applications of aldehyde-functional polymers.....	36
1.6.4.1. <i>Aldehyde-functional polymers as drug conjugates</i>	36
1.6.4.2. <i>Aldehyde-functional polymers as biosensors</i>	39
1.6.4.3. <i>Aldehyde-functional polymers for protein binding</i>	41
1.7. Thesis outline.....	42
1.8. References.....	43
Chapter II: Materials and methods.....	53
2.1. Materials.....	54
2.2. Methods.....	55
2.3. References	60
Chapter III: New aldehyde-functional methacrylic water-soluble polymers.....	61
3.1. Introduction.....	62
3.2. Experimental.....	64
3.2.1. Synthesis.....	64
3.3. Results and Discussion.....	69
3.3.1. Synthesis of GEO5MA monomer	69
3.3.2. Synthesis of AGE05MA monomer <i>via</i> NaIO ₄ oxidation	70
3.3.3. Homopolymerisation of GEO5MA and AGE05MA.....	71
3.3.4. Functionalisation of PAGE05MA ₃₇ homopolymer <i>via</i> reductive amination.....	75

3.3.5. Synthesis of PAGEO5MA _x -PX _y diblock copolymers	76
3.4. Conclusion	77
3.5. References	78
Chapter IV: Aldehyde-functional diblock copolymer nano-objects <i>via</i> RAFT aqueous dispersion polymerisation	81
4.1. Introduction.....	82
4.2. Experimental.....	84
4.2.1. Synthesis.....	84
4.3. Results and Discussion.....	86
4.3.1. Synthesis of PGEO5MA ₂₆ -HPMA _y diblock copolymer nanoparticles <i>via</i> RAFT aqueous dispersion polymerisation.....	86
4.3.2. Oxidation of PGEO5MA ₂₆ -PHPMA _y diblock copolymer nanoparticles using NaIO ₄	88
4.3.3. Functionalisation of PAGEO5MA ₂₆ -PHPMA _y (-PEGDMA ₂₀) block copolymer nanoparticles <i>via</i> reductive amination.....	91
4.4. Conclusion	97
4.5. References	98
Chapter V: Aldehyde-functional thermoresponsive diblock copolymer worm gels exhibit strong mucoadhesion	102
5.1. Introduction.....	103
5.2. Experimental.....	105
5.2.1. Synthesis.....	105
5.3. Results and Discussion.....	107
5.3.1. Synthesis of PGEO5MA _x -PHPMA _y diblock copolymer worms.....	107
5.3.2. Investigating the thermoresponsive nature of PGEO5MA _x -PHPMA _y worms.....	110
5.3.3. Synthesis and oxidation of PGEO5MA ₁₃ -P(HPMA ₁₅₅ - <i>stat</i> -FMA _{0.15}) copolymer worms	112
5.3.4. Investigating the mucoadhesive properties of PGEO5MA ₁₃ -P(HPMA ₁₅₅ - <i>stat</i> -FMA _{0.15}) based worms	118
5.4. Conclusion	119
5.5. References	120

Chapter VI: New hydrophilic aldehyde-functional polymer brushes: synthesis, characterisation and potential bioapplications	125
6.1. Introduction.....	126
6.2. Experimental.....	127
6.2.1. Synthesis.....	127
6.3. Results and Discussion.....	129
6.3.1. Kinetics of PGEO5MA brush synthesis.....	129
6.3.2. X-ray photoelectron spectroscopy (XPS) studies of PGEO5MA brush oxidation	132
6.3.3. Functionalisation of PAGEO5MA brushes <i>via</i> reductive amination.....	136
6.3.4. Characterisation of PGEO5MA, PAmGEO5MA and PHisGEO5MA polymer brushes using surface zeta potential measurements	138
6.3.5. The effect of temperature on extent of functionalisation for the reductive amination of NaIO ₄ -oxidised PGEO5MA polymer brushes	141
6.4. Conclusion	142
6.5. References	143
Chapter VII: Conclusions and outlook	146
7.1. References.....	152
Chapter VIII: Appendix.....	154

Chapter I: Introduction

Chapter I: Introduction

Polymers can exhibit a wide range of chemical and physical properties, which makes them extremely useful. Naturally derived polymers such as proteins, deoxyribonucleic acid and cellulose are the basic building blocks of life. Synthetic polymers like polyamides (e.g., Nylon), poly(vinyl chloride) (PVC), or polytetrafluoroethylene (Teflon) offer highly desirable properties for specific applications. For example, PVC has excellent weatherability and hence is used for double glazing, while Teflon is an inert polymer with a very low coefficient of friction so it is a very useful non-stick coating for kitchenware.¹

1.1. What is a polymer?

A polymer is a long-chain molecule composed of identical repeat units (or monomers) covalently linked together. The mean number of monomer units per chain is known as the degree of polymerisation (DP). Unlike small molecules, polymer chains do not possess a unique molecular weight. Instead, polymer chains vary in length and hence exhibit a molecular weight distribution (MWD), whose width can be crudely described by the dispersity (\mathcal{D}). This parameter is defined as follows:

$$\mathcal{D} = M_w / M_n$$

where M_w and M_n are the weight-average and number-average molecular weight, respectively. M_n is defined as

$$M_n = \sum X_i M_i$$

where M_i is the molar mass and X_i is the mole fraction. Similarly, M_w is defined as

$$M_w = \sum w_i M_i$$

where w_i is the weight fraction. If $\mathcal{D} = 1$, then the polymer is perfectly monodisperse and all chains have the same length. This can be achieved for certain biopolymers, e.g., proteins. However, \mathcal{D} is always greater than unity for all synthetic polymers.

1.2. Polymer architectures

Polymers can exhibit a wide range of architectures (Figure 1.1). The simplest is a linear homopolymer. Other polymer architectures include block, statistical or alternating copolymers, as well as combs, brushes and stars.

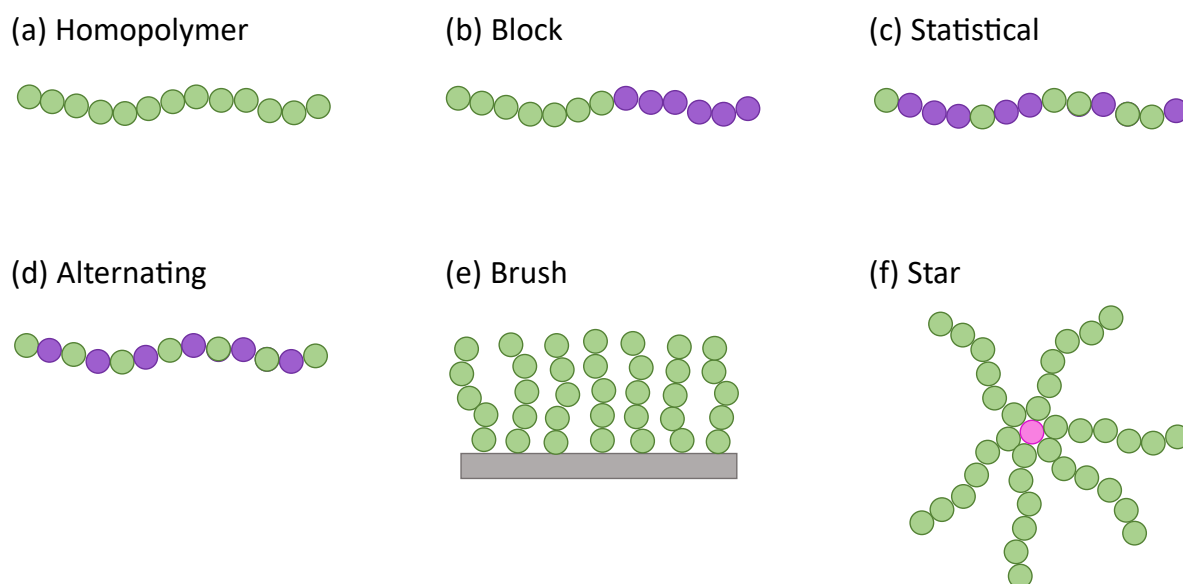


Figure 1.1. Schematic cartoon showing six examples of copolymer architectures: (a) homopolymer, (b) block, (c) statistical, (d) alternating, (e) brush and (f) star. The green and purple circles represent different monomer units, and the pink circles are the branching points on the polymer chain.

1.3. Polymerisation techniques

1.3.1. Free radical polymerisation (FRP)

FRP is a highly versatile, well-established technique that is tolerant to both protic and aprotic solvents. It has been widely used on an industrial scale for the polymerisation of a broad range of functional vinyl monomers.² If chain transfer side-reactions are ignored, the FRP mechanism consists of four main steps: thermal decomposition, initiation, propagation and termination (Scheme 1.1).³ Thermal decomposition involves homolytic cleavage of an initiator to produce two $R\bullet$ radicals. Because this is a relatively slow process, it is usually the rate-determining step. Moreover, some fraction of the initiator radicals can undergo recombination, which reduces the initiator efficiency (the so-called ‘cage effect’).⁴ Initiation involves the reaction of an initiator-derived radical with a single monomer unit.

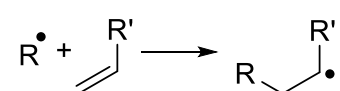
Propagation involves the resulting monomer-initiator adduct radical reacting with many further monomer units to produce relatively long chains. The final step in the FRP mechanism is termination, which can occur *via* either combination or disproportionation. Combination is where two radicals react together to form one longer polymer chain. Conversely, disproportionation involves hydrogen abstraction from one of the polymer radicals by another and results in one saturated and one unsaturated polymer chain-end. The dominant termination mechanism depends on the type of monomer that is being polymerised. For example, styrenes and acrylates generally favour termination *via*

combination. On the other hand, methacrylate termination mainly occurs *via* disproportionation.³ This affects the characteristic dispersity of the resulting polymer chains: a typical \mathcal{D} value for combination is around 1.5, whereas $\mathcal{D} \sim 2.0$ for disproportionation. Unfortunately, both dispersities indicate a relatively broad MWD, which is one disadvantage of FRP. This is due to several factors including the slow rate of initiation resulting in some polymer chains becoming very high molecular weight, quickly. Moreover, FRP offers rather limited control over the copolymer architecture (for example, well-defined diblock copolymers cannot be prepared) and the target DP cannot be calculated without extensive knowledge of various kinetic parameters.

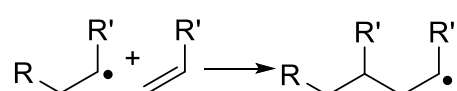
Initiator decomposition



Initiation



Propagation



Termination

i) Combination



ii) Disproportionation



Scheme 1.1. Mechanism of free radical polymerisation, including initiator decomposition, initiation, propagation and termination steps.

The rate of polymerisation is proportional to the monomer concentration and the square root of the initiator concentration. To produce higher molecular weight polymers, the monomer concentration needs to be increased whilst the initiator concentration needs to be reduced. Thus, it can be difficult to produce higher molecular weight polymers efficiently *via* conventional FRP.

1.3.2. Ionic polymerisation

There are two different types of ionic polymerisation: cationic and anionic polymerisation. Cationic polymerisation is where an initiator reacts with a monomer to produce a carbocation. However, termination can readily occur *via* nucleophilic addition of an anion to the growing polymer chain or by β -eliminations on the cationic chain-ends e.g., from

water impurities.⁵ Moreover, chain transfer with solvent, monomer and *via* β -hydride elimination can occur, which leads to relatively broad MWDs ($D > 2.0$). However, the use of Lewis acids as catalysts can increase the rate of the initiation steps, which results in a controlled polymerisation. This can increase the molecular weight of the polymers and reduce the MWDs.⁶ Vinyl monomers with electron-donating groups (e.g., styrene, isobutylene or vinyl ethers) can be polymerised *via* cationic polymerisation.⁷⁻¹⁰

In contrast, anionic polymerisation of vinyl monomers involves carbanions. Thus, an essential prerequisite for successful anionic polymerisation is that the monomer must be able to stabilise anionic charge. Examples include styrene,^{11,12} butadiene,^{13,14} isoprene,¹⁵ 2-vinylpyridine¹⁶ or 4-vinylpyridine.¹⁶ One of the main advantages of anionic polymerisation is that there is no intrinsic termination mechanism: the anionic chain-ends are highly reactive towards protic impurities but they cannot react with each other. Thus, if anionic polymerisation is conducted under rigorously anhydrous conditions, this results in a so-called living polymerisation, which exhibits no irreversible chain transfer or chain termination reactions.^{3,17} Polymerisations continue until all of the monomer is consumed and such homopolymer precursors can be chain-extended by adding a second monomer to produce well-defined diblock copolymers.¹⁸ This is known as sequential monomer addition.

Unlike FRP or cationic polymerisations, anionic polymerisations typically lead to very narrow MWDs ($D < 1.10$).¹⁹ Moreover, the target DP is simply given by the number of moles of monomer divided by the number of moles of initiator. Anionic polymerisations are very intolerant to water. Therefore, the monomer, solvent and initiator have to be dried prior to anionic polymerisation and surface moisture must be removed from the inner walls of the reaction vessel.²⁰ Nevertheless, this technique has been used to prepare various styrene-based block copolymers on an industrial scale for more than four decades by companies such as Kraton. For example, hydrogenated polystyrene-polybutadiene-polystyrene triblock copolymers are widely used as thermoplastic elastomers (synthetic rubber).²¹

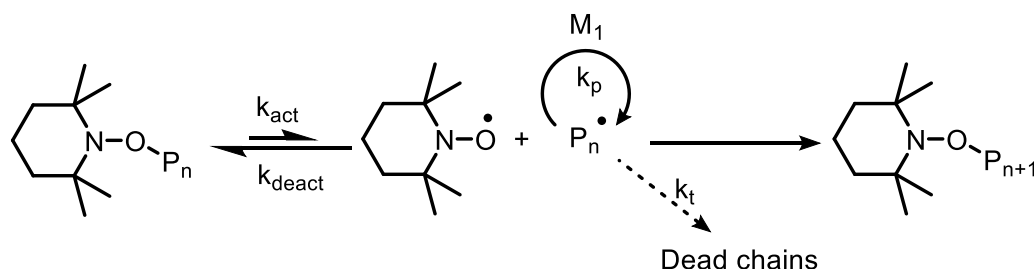
1.3.3. Reversible-deactivation radical polymerisations (RDRPs)

RDRPs are examples of pseudo-living polymerisations, which means that they exhibit many of the same properties as classical living polymerisation techniques such as anionic polymerisation.¹⁷ However, they are not truly living as they suffer from low levels of radical-radical termination. Nevertheless, the rate of termination is suppressed relative to

the rate of propagation,³ which allows the synthesis of well-defined polymers with narrow MWDs ($\mathcal{D} < 1.20$) and complex architectures (e.g., block or star polymers). The target molecular weight of such polymers can be readily controlled with minimal prior knowledge of kinetic parameters. Another benefit of RDRP compared with living polymerisations is that they can be conducted under various physical conditions e.g., *via* bulk, solution, dispersion or emulsion polymerisation and in the presence of protic sources (including water). Importantly, RDRP techniques are also tolerant of a wide range of monomer functionality. Thus, in contrast to anionic polymerisation, RDRP enables the convenient synthesis of functional polymers without recourse to protecting group chemistry. The RDRP mechanism is based on the fast, reversible activation/deactivation of propagating polymer radicals, which minimises the probability of their premature termination. The three main types of RDRP are nitroxide-mediated polymerisation (NMP), atom transfer radical polymerisation (ATRP) and reversible addition-fragmentation chain transfer (RAFT) polymerisation. Two types of dynamic equilibria can be employed in RDRP, either reversible transfer (e.g., RAFT) or reversible deactivation/activation (e.g., ATRP or NMP).

1.3.3.1. Nitroxide-mediated polymerisation (NMP)

NMP involves a rapid equilibrium between a persistent stable radical (e.g., a nitroxide such as TEMPO) and a reactive carbon-centred radical (Scheme 1.2).²² Polymers with relatively narrow dispersities can be produced ($\mathcal{D} \sim 1.10$ for acrylates and $\mathcal{D} \sim 1.20$ – 1.30 for styrene).^{23,24} However, high temperatures are usually required to overcome the slow polymerisation kinetics, methacrylates cannot be homopolymerised by NMP, and the preparation of nitroxides/alkoxyamines is rather difficult (and few are commercially available).^{25,26} Further drawbacks include side reactions such as chain transfer to solvent, nitroxide decomposition, oxidation of alkyne-bearing monomers and the unwanted cleavage of the N-O bond, rather than the N-C bond.²⁷



Scheme 1.2. Reversible reaction between a stable nitroxide (TEMPO) and a growing polymer radical.

1.3.3.2. Atom transfer radical polymerisation (ATRP)

ATRP is another example of a reversible-deactivation polymerisation. It was discovered simultaneously by Kato et al.²⁸ and Wang and Matyjaszewski²⁹ in 1994 and has provided a powerful and versatile method for the preparation of many well-defined functional polymers with good control. ATRP uses a transition metal catalyst and an alkyl halide initiator. The initiator structure (Figure 1.2) varies but should normally resemble the chemical structure of the monomer to be polymerised. This ensures that the initiator radical is at least as stable as the growing polymer radical with regard to further propagation.

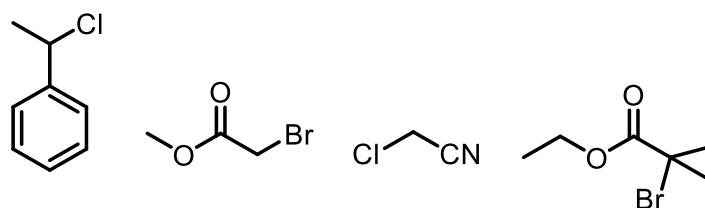
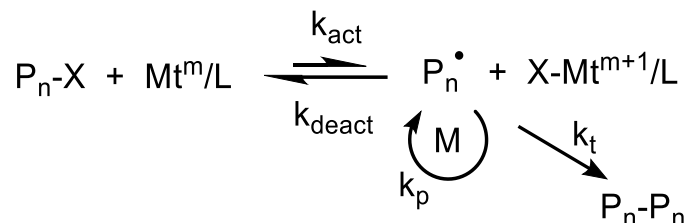


Figure 1.2. Chemical structures of several ATRP initiators; (a) (1-chloroethyl)benzene, (b) methyl bromoacetate, (c) chloroacetonitrile and (d) ethyl α -bromoisobutyrate.

Various transition metal complexes can be used to mediate ATRP but the Cu^I/Cu^{II} redox couple is most commonly used.³⁰ Copper is the preferred transition metal owing to its relatively low cost and high catalytic activity. Either Br and/or Cl atoms have suitable C-X bond dissociation energies for use as the halogen end-group (X) in ATRP, whereas the C-I and C-F bonds are too weak and too strong, respectively. The choice of ligand for the transition metal complex is very important; the catalyst is more active if the ligand can stabilise the Cu^{II} complex relative to the Cu^I species. The most common ligands are multidentate amines or bipyridine derivatives owing to their low cost and wide availability. If initiation is sufficiently fast, concurrent growth of all chains occurs to produce polymers with low dispersities ($\mathcal{D} \sim 1.10$).³¹ Initiation is the rate-determining step in ATRP. An equilibrium between propagating polymer radicals and dormant species is set up with the transition metal complex acting as the catalyst (Scheme 1.3).



Scheme 1.3. Reaction equilibrium set up in conventional ATRP.

The dormant species (typically a halide-capped polymer chain) reacts reversibly with the transition metal complex in its lower oxidation state (e.g., a Cu^I species) to produce a

polymer radical, which undergoes a short burst of chain growth before becoming reversibly deactivated by the catalyst in its higher oxidation state (e.g., a Cu^{II} species). The rate of polymerisation depends on the temperature, the monomer concentration and the catalyst concentration. The ATRP equilibrium is set up to ensure that the dormant species is the predominant one. Thus, the mean lifetime of the radical species is reduced, which lowers the rate of termination relative to that of propagation.²⁹ Halide exchange is an effective method to increase the control of the polymerisation. This is where the initiating species and the catalytic species contain different halogen atoms (usually Br and Cl). This is especially useful for the synthesis of block copolymers, whereby the second monomer produces a less stable polymer radical than that of the first monomer.

ATRP can be conducted in either polar or non-polar media.³² However, particular attention has been paid to ATRP syntheses conducted in water.^{32–36} This is because water is an inexpensive and environmentally-friendly solvent with a high heat capacity, making it ideal for exothermic vinyl polymerisations. The catalyst structure and the reaction conditions have to be adjusted to account for the lower complex stability and the very high equilibrium constants for aqueous ATRP formulations.³⁷ Various aqueous reaction conditions have been investigated, including emulsion, suspension, dispersion and precipitation.³⁸ One of the main drawbacks of conventional ATRP is the relatively large amount of the toxic copper catalyst that is required. Although attempts have been made to minimise and/or recycle this catalyst, this usually results in reduced polymerisation control in biphasic systems or more expensive catalysts.³⁹ It is usually necessary to remove the toxic catalyst residues from ATRP-synthesised polymers, which precludes many potential applications.

1.3.3.3. Reversible addition-fragmentation chain transfer (RAFT) polymerisation

RAFT polymerisation is based on the principle of rapid reversible transfer. It was first reported by Rizzardo et al.⁴⁰ in 1998 and has since proven to be an extremely versatile technique for the synthesis of many complex copolymer architectures. An organosulfur-based RAFT chain transfer agent (CTA) reacts rapidly and reversibly with the growing polymer radicals, thus reducing their effective concentration in the reaction mixture. This equilibrium suppresses the probability of termination relative to that of propagation. Several classes of CTAs are known, including trithiocarbonates, dithiobenzoates and xanthates. In each case, the general chemical structure (Figure 1.3) comprises a C=S double bond, an R group and a Z group.

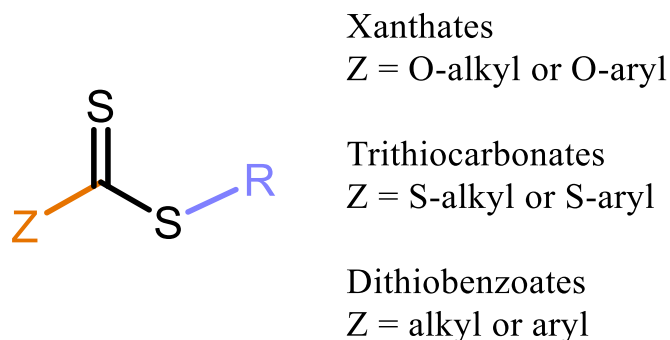


Figure 1.3. Generic chemical structure of a RAFT CTA, where R is a good radical leaving group and Z is the stabilising group.

There are several important features regarding the RAFT CTA structure. The R group is a good radical leaving group and influences the rate of radical addition/fragmentation.^{40,41} It is essential that the R group is able to reinitiate the polymerisation. The Z group stabilises the polymer radicals in both the chain equilibria and the reversible chain transfer steps.⁴² The most reactive RAFT CTAs are dithiobenzoates, which are suitable for the polymerisation of styrene and methacrylic monomers. However, they are highly susceptible to retardation, hydrolysis and decomposition by Lewis acids.⁴¹ They are also unsuitable for the polymerisation of acrylic monomers at high concentrations as this can lead to retardation. On the other hand, trithiocarbonates are less prone to hydrolysis due to their less reactive nature.⁴² They are suitable for acrylates and can also be used for methacrylates if they contain a cyano substituent on the R group.^{43,44} Several examples of RAFT CTAs are shown below in Figure 1.4.

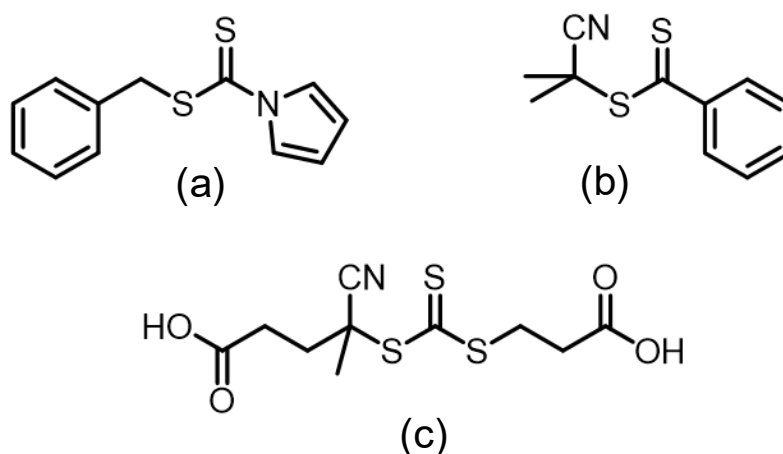
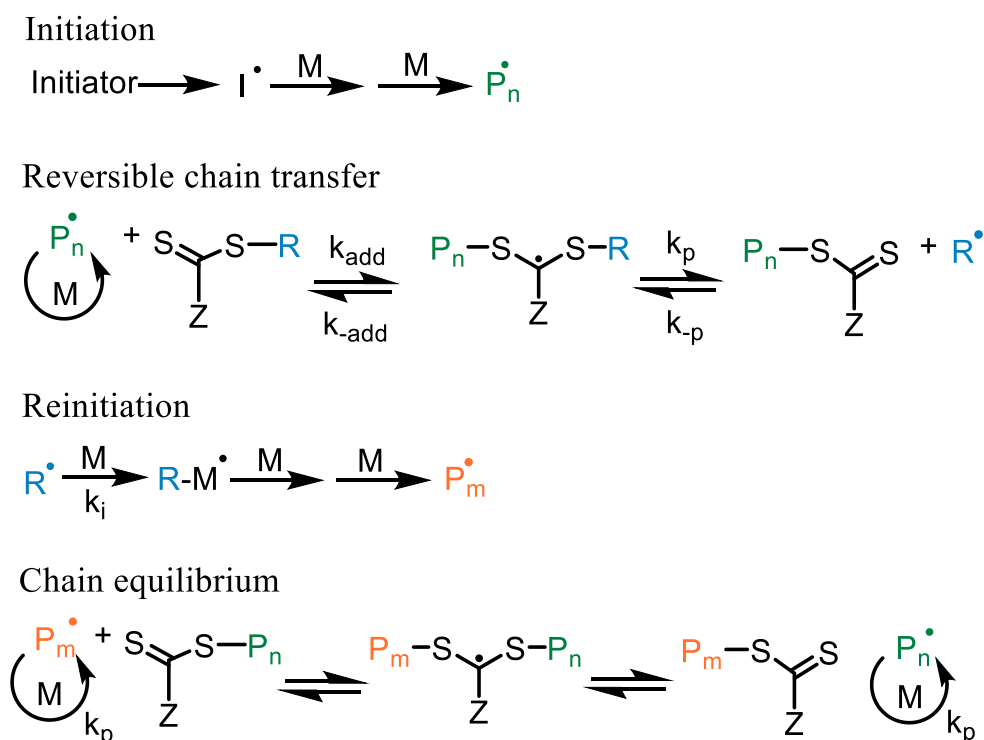


Figure 1.4. Chemical structures of three common RAFT CTAs. (a) benzyl 1*H*-pyrrole-1-carbodithioate, (b) 2-cyano-2-propyl dithiobenzoate and (c) 4-(((2-(carboxyethyl)thio)carbonothioyl)thio)-4-cyanopentanoic acid.

The first step in a RAFT polymerisation involves the relatively slow thermal decomposition of the initiator to generate radical species (Scheme 1.4). This is the rate-determining step for all RAFT polymerisations. These radicals then react rapidly with

monomer to produce polymer radicals. The CTA/initiator molar ratio used for a RAFT polymerisation determines the number of dead polymer chains at the end of the polymerisation. ⁴⁵ Therefore, a relatively high CTA/initiator molar ratio of 5–10 is usually required to produce polymers with narrow molecular weight distributions. However, lower ratios speed up the rate of polymerisation, so a compromise in the CTA/initiator molar ratio is sometimes necessary to produce well-defined polymers within reasonable time scales. ⁴⁴ Owing to the pseudo-living character of the polymerisation, all chains begin to grow at the start of the polymerisation and continue to do so until all monomer has been consumed. This leads to a linear evolution of molecular weight with monomer conversion. ⁴⁰ If a RAFT polymerisation proceeds to full conversion, the target DP is simply determined by the number of moles of monomer divided by the number of moles of RAFT agent.



Scheme 1.4. The RAFT polymerisation mechanism according to Rizzardo and co-workers.

The next step in a RAFT polymerisation is chain transfer. This is where the polymer radical reversibly reacts with the C=S bond of the CTA. The C=S bond can then reform with either the polymer radical or R• acting as the leaving group. Although this is reversible, the equilibrium favours fragmentation such that the polymer chain remains attached to the CTA. Such CTA-capped polymer chains cannot propagate and are said to be in their dormant form. To ensure this scenario, the R group must be at least as good a leaving group as the polymer radical. The C=S bond of the CTA also needs to be sufficiently reactive to prevent side-reactions. ³¹

The $R\bullet$ radical can then react with further monomer and create new polymer radicals. This step is called reinitiation and imposes another important constraint on the RAFT CTA; the $R\bullet$ radical must be able to reinitiate the monomer. This requires the rate of initiation to be greater than the rate of propagation. The next step is the chain equilibrium, where the polymer radicals react with the CTA-capped chains. This rapid equilibrium minimises the amount of radical-radical termination and consequently gives all chains an equal probability to grow. This leads to a linear increase in polymer molecular weight with conversion and the resulting polymers have relatively low dispersities ($\mathcal{D} < 1.20$).^{40,46} One of the few examples of the successful commercialisation of RAFT polymerisation was reported by Lubrizol, who used this chemistry to prepare multiple-arm star polymers as viscosity modifiers for automotive engine oils.⁴⁷

1.4. Polymerisation methods

1.4.1. Bulk polymerisation

Bulk polymerisation is the simplest polymerisation method and involves only monomer and an initiator (or catalyst). Bulk polymerisation produces polymers with little contamination. However, one of its main drawbacks is that the reaction mixtures are very viscous, resulting in poor heat dissipation and inefficient stirring.

1.4.2. Solution polymerisation

Solution polymerisation involves a solvent-soluble monomer, a suitable solvent and a soluble initiator to produce a soluble polymer. This method overcomes some of the disadvantages of bulk polymerisation: the lower solution viscosity means that there is better heat dissipation and more efficient stirring.

1.4.3. Aqueous emulsion polymerisation

Conventional aqueous emulsion polymerisation involves a water-immiscible monomer, a water-soluble initiator and water. A suitable surfactant (or water-soluble polymer) is also usually required to act as a stabiliser in order to prevent macroscopic precipitation. Aqueous emulsion polymerisation typically produces low-viscosity, colloiddally stable latex particles comprising high molecular weight polymer chains at high solids, which makes it very attractive for various industrial applications, e.g., paints, coatings and varnishes.⁴⁸⁻⁵² Moreover, most vinyl monomers are water-immiscible and hence well-suited for aqueous emulsion polymerisation.³¹

The mechanism for emulsion polymerisation is split into three main intervals (Figure 1.5).⁵³ Interval I is where the water-immiscible monomer and the surfactant are emulsified. Surfactant micelles are formed spontaneously *via* self-assembly and mechanical stirring produces surfactant-stabilised monomer droplets of $\sim 1\text{--}10\ \mu\text{m}$ diameter.⁵⁴ Some of the monomer is located within monomer-swollen micelles of $\sim 5\text{--}10\ \text{nm}$ diameter and a relatively small amount of the monomer will be molecularly dissolved within the aqueous phase. Propagation begins with the dissolved monomer reacting with the water-soluble initiator radicals. As propagation proceeds, the oligomers that are created quickly become hydrophobic. At some critical chain length, these oligomers diffuse into the surfactant-stabilised micelles and propagation continues within these micelles. As the polymerisation proceeds and monomer is consumed, further monomer diffuses from the large monomer droplets to replenish the reacted monomer within the micelles. During Interval II, the surfactant-stabilised monomer-swollen micelles gradually grow in size to become latex particles (particle growth stage). Within this period, the number of latex particles remains constant, and monomer is continuously replenished from the monomer droplet reservoirs. This means that the rate of polymerisation is relatively fast and roughly constant. Once all of the μm -sized monomer droplets have been consumed, this marks the beginning of Interval III. The remaining monomer inside the latex particles is gradually consumed to produce colloiddally stable latex particles. The rate of polymerisation is lower during Interval III owing to the progressive reduction in the monomer concentration.

One of the main advantages of aqueous emulsion polymerisation is that reactions are typically much faster than the equivalent solution polymerisation. This is because most of the polymerisation occurs within micelles and, on average, there is only one propagating polymer radical per particle, which means that termination is suppressed relative to propagation.⁵⁴ This is beneficial for paints and coatings applications because high molecular weight polymer chains lead to stronger, more durable films. Further important advantages of aqueous emulsion polymerisation are that the rapid rate of polymerisation usually enables very high monomer conversions to be achieved and water is an environmentally friendly and cost-effective solvent. In practice, this means that many millions of tonnes of vinyl polymers are produced by aqueous emulsion polymerisation each year.⁵³

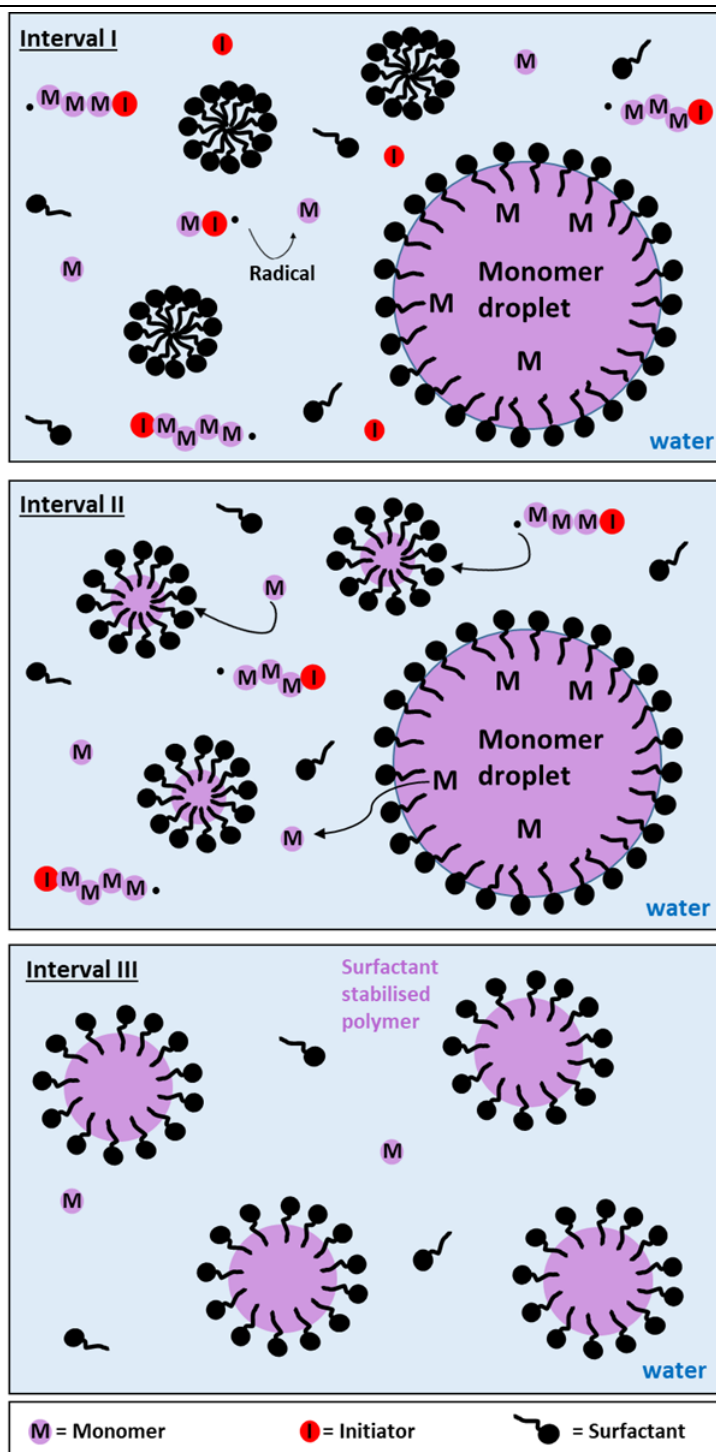


Figure 1.5. Scheme representing the three intervals that occur during conventional emulsion polymerisation as described by C. S. Chern and R. G. Gilbert.

1.4.4. Aqueous dispersion polymerisation

Conventional aqueous dispersion polymerisation involves a water-miscible monomer and a water-soluble initiator to produce a water-insoluble polymer in aqueous solution. A suitable water-soluble polymer is employed to confer steric stabilisation and hence prevent macroscopic precipitation.

The mechanism is split into six distinct stages (Figure 1.6). In Stage 1, all components are water-soluble, which results in a homogeneous solution. Radicals are produced during Stage 2 by decomposition of the initiator. These free radicals react with the monomer to produce water-soluble oligomers. As propagation continues (Stage 3), the growing polymer chains become water-insoluble at some critical DP, which induces their aggregation to form nascent particles (or nuclei). In the absence of a polymeric stabiliser, these nascent particles would eventually form a macroscopic precipitate. Immediately after their formation, the particles become monomer-swollen, and polymerisation occurs within them until all of the monomer is consumed. Step 4 involves further aggregation of the growing particles with concomitant adsorption of a polymeric stabiliser. By Step 5, these particles are fully coated with the steric stabiliser chains, which confer colloidal stability (Step 6).⁵⁵

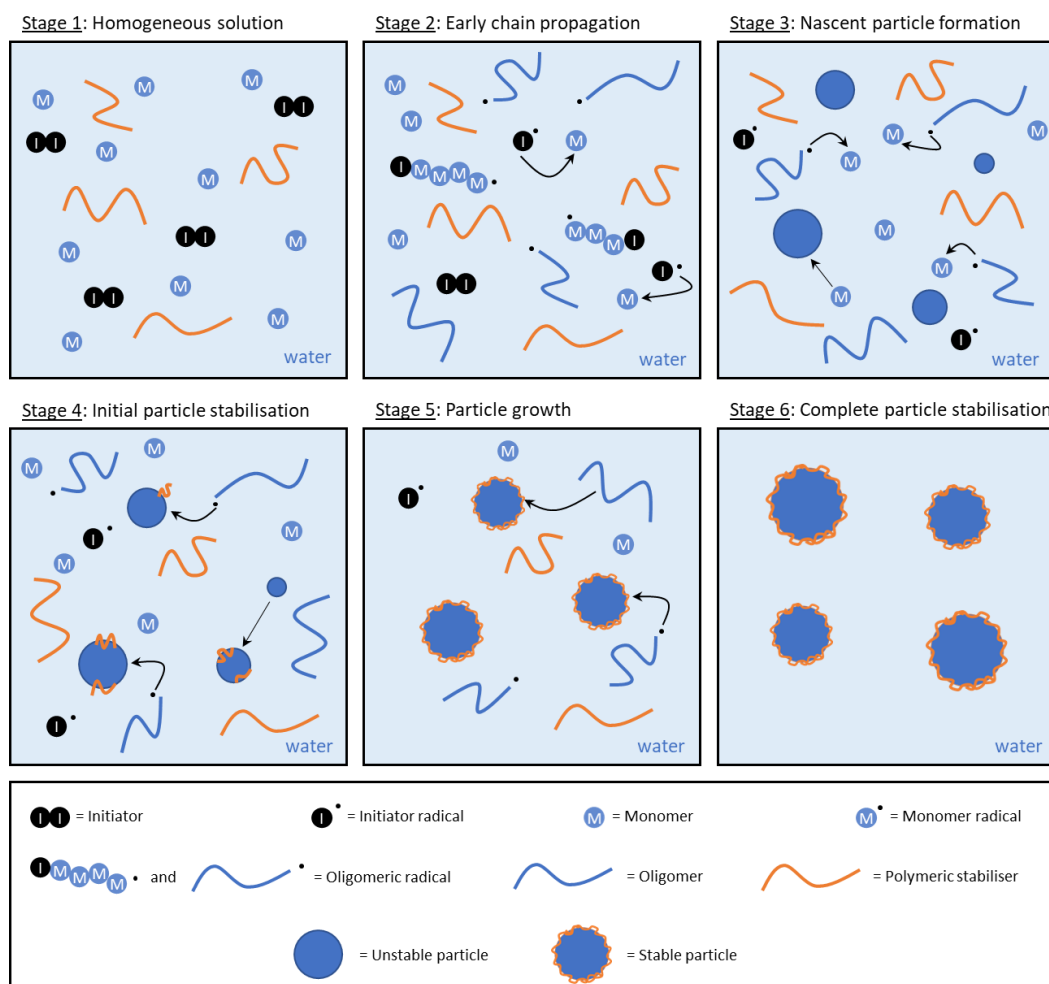


Figure 1.6. Schematic representation of the mechanism for an aqueous dispersion polymerisation.

Like aqueous emulsion polymerisation, aqueous dispersion polymerisation produces low-viscosity, colloidally stable latexes. However, the latter technique is not as widely used

as the former simply because there are relatively few water-miscible vinyl monomers that form water-insoluble polymers, which is a prerequisite for aqueous dispersion polymerisation. Notable exceptions include the preparation of polypyrrole latexes in the presence of polymeric stabilisers such as poly(vinyl alcohol),⁵⁶ poly(ethylene oxide) (PEO)⁵⁷ or poly(*N*-vinyl pyrrolidone) (PNVP).⁵⁷ Although it is not widely recognised, the synthesis of thermoresponsive poly(*N*-isopropylacrylamide) (PNIPAM) microgels involves aqueous dispersion polymerisation.⁵⁸ Of particular relevance to this Thesis, the aqueous dispersion polymerisation of 2-hydroxypropyl methacrylate (HPMA) by FRP was achieved by Ali et al. using PNVP as a steric stabiliser.⁵⁹ This was considered to be a model system for understanding aqueous dispersion polymerisation formulations.

1.4.5. Surface-initiated (SI) polymerisation

1.4.5.1. Polymer brushes

A polymer brush is formed when multiple chains are tethered to either a planar or a colloidal surface, such that the individual chains stretch normal to the surface.⁶⁰ When polymer chains are anchored to an interface in this geometry, their physico-chemical properties can vary considerably to their untethered equivalents. Polymer brushes have been suggested for various applications, ranging from stimulus responsive surfaces for controlled catalysis and biosensing⁶¹ to antifouling surfaces.^{62–64} A key parameter in defining the behaviour and character of brushes is the grafting density, which is the number of bound polymer chains per unit surface area. The grafting density affects the conformation that the polymer chains can adopt at the surface; a lower density results in “mushroom” or “pancake” regimes, while a higher grafting density provides access to the “brush” regime.⁶⁰ Controlling this parameter can improve the suitability of polymer brushes for certain applications.⁶⁵

There are two main approaches for the preparation of polymer brushes: “grafting to” and “grafting from” (Figure 1.7). The “grafting to” approach produces brushes by tethering polymers to a surface using their chain-end functionality.⁶⁶ In contrast, the “grafting from” approach requires attachment of an initiator to the surface with polymer chains subsequently grown from the surface. This is also known as SI polymerisation. The “grafting from” approach enables a much greater chain grafting density to be achieved compared to the “grafting to” approach, where kinetic, steric and entropic factors combine to significantly limit the grafting density.^{60,67} Furthermore, film thickness achieved by “grafting to” approaches are limited by the initial chain length. In principle, the “grafting

from” approach does not have this limitation with thicker films achievable. Hence, the “grafting from” approach has received much more attention in the literature.^{64,65,68–73}

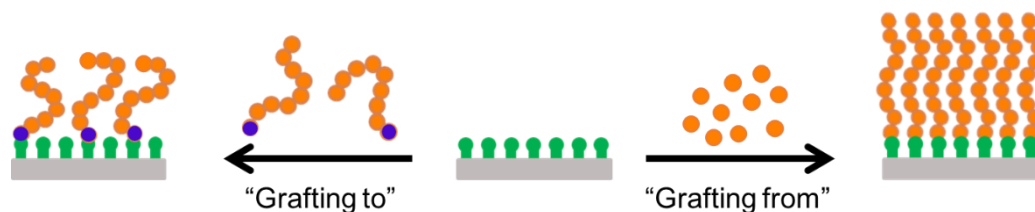


Figure 1.7. Schematic illustration of the preparation of polymer brushes *via* the “grafting to” and “grafting from” approaches.

1.4.5.2. Surface-initiated controlled radical polymerisation (SI-CRP)

SI-CRP (or SI-RDRP) is a versatile technique for the growth of polymer brushes from surfaces. It allows for precise control over polymer architecture, composition, molecular weight, and brush thickness and can be used to functionalise a wide range of substrates. It is tolerant towards many functional groups, resulting in polymers with many potential applications.⁶⁰ There are two main types of SI-CRP: surface RAFT polymerisation and surface-initiated ATRP (SI-ATRP). The mechanism for each of these surface polymerisations is essentially the same as for the corresponding polymerisations in solution.

In surface RAFT polymerisation the radical source (the initiator) is anchored to the surface and the RAFT CTA is present in the reaction solution. This method can lead to controlled polymerisations, whereby the surface initiator density controls the grafting density of the polymer brush, while the solution concentration of the RAFT CTA controls the mean chain length.^{40,45} For example, increasing the RAFT CTA concentration reduces the degree of polymerisation of the brush chains and hence results in thinner films.^{74,75}

Another way to conduct surface RAFT polymerisations involves anchoring the RAFT CTA to the surface by either its R⁷⁶ or Z group,⁷⁷ with the initiator being located in the reaction solution. This approach has been used to produce polymer brushes from planar gold surfaces,⁷⁸ quantum dots,⁷⁹ polymer substrates⁸⁰ and carbon fibres.⁸¹ Anchoring *via* a carboxylic acid located within the R group is particularly popular because many RAFT CTAs offer this possibility.⁶⁰ Indeed, this method is more widely used than surface anchoring of an initiator. For example, Di Carlo et al.⁶⁸ copolymerised *N,N*-dimethylacrylamide and *N*-acryloyloxysuccinimide from glass slides *via* surface RAFT polymerisation (Figure 1.8) to produce bioreactive coatings for use in microarray technologies.

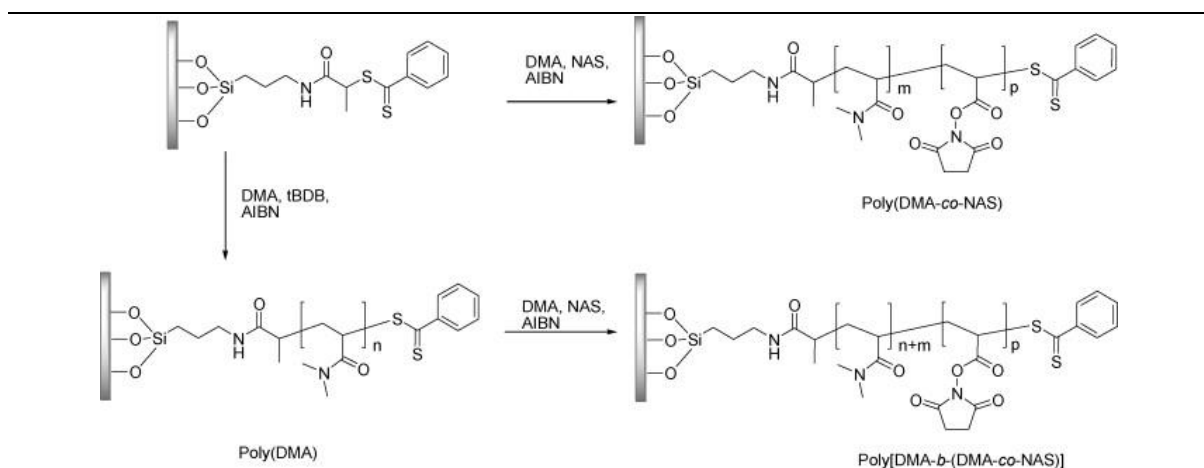


Figure 1.8. Schematic synthesis of the RAFT mediated brush polymers: mono-block and diblock architectures. Reprinted with permission from G. Di Carlo et al., *Appl. Surf. Sci.*, 2012, 258, 3750–3756. Copyright 2011 Elsevier.

However, despite its broad monomer scope and tolerance of functionality, surface RAFT polymerisation is not the most widely used SI-CRP method. This may be because the RAFT agent is relatively expensive, or perhaps because the resulting polymer brushes contain malodorous, coloured organosulfur-based end-groups. Instead, SI-ATRP is much more widely used to prepare polymer brushes from either planar or colloidal surfaces.

1.4.5.3. Surface-initiated atom transfer radical polymerisation (SI-ATRP)

The SI-ATRP mechanism works in essentially the same way as conventional ATRP. However, the initiator is anchored to the underlying substrate e.g., a glass slide or silicon wafer. SI-ATRP offers many benefits, including control over copolymer architecture, molecular weight and brush thickness. It is a highly versatile technique that is compatible with a wide range of monomers and solvents.⁶⁰ Moreover, unlike conventional solution ATRP, removal of the spent catalyst can be easily achieved by simply washing the polymer brush with a good solvent.

The first example of SI-ATRP came from Fukuda et al., who grew poly(methyl methacrylate) (PMMA) brushes from silicon wafers.⁸² The ATRP initiator was immobilised with sacrificial initiator present in the reaction solution, enabling post-polymerisation characterisation of the free polymer chains. These free chains were assumed to have the same molecular weight and MWD as the polymer brush chains.

Owing to the inherently low monomer conversions achieved in polymer brush syntheses, kinetic studies of brush growth involve monitoring the brush thickness over time, rather than the monomer conversion. Provided that the polymerisation is sufficiently living, a linear relationship should be obtained for a brush thickness vs. time plot (Figure 1.9).^{72,73} In principle, the grafted brush chains should continue growing indefinitely. However,

imperfect living character usually leads to a gradual reduction in the rate of polymerisation.⁸²

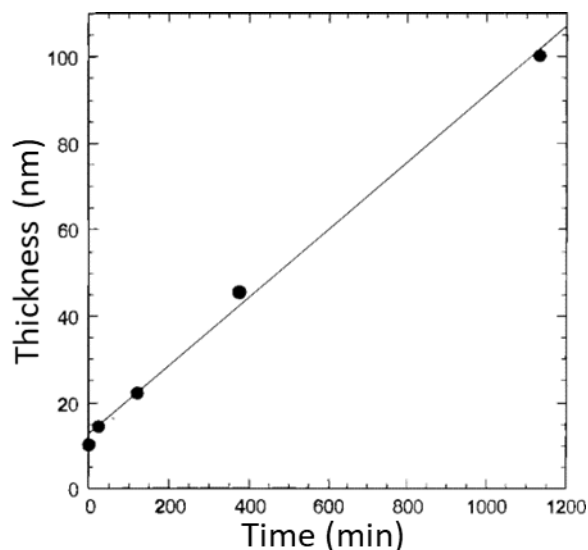


Figure 1.9. Evolution of block copolymer layer thickness from a silicon surface composed of a 12 nm thick polystyrene layer as a function of reaction time. Conditions: methyl acrylate, 1% CuBr(4,4'-di-*n*-nonyl-2,2'-bipyridine)₂, 0.03% CuBr₂(4,4'-di-*n*-nonyl-2,2'-bipyridine)₂, bulk polymerisation in a dry box at 80 °C. A linear fit to the data points is shown. Adapted with permission from K. Matyjaszewski et al., *Macromolecules*, 1999, 32, 8716–8724. Copyright 1999 American Chemical Society.

Since this first start numerous investigations have examined the role of the copper, ligand and solvent and their effects on SI-ATRP. In particular the use of water as a solvent has been found to accelerate SI-ATRP reactions.⁸³ Additionally, to make SI-ATRP reactions more environmentally friendly, the polymerisations can be conducted in water. For example, the Baker group found that the polymerisation of neat 2-hydroxyethyl methacrylate (HEMA) from a planar gold surface gave brushes of 6 nm after 12 h.⁸⁴ Conversely, the same polymerisation conducted in water (50% v/v HEMA) gave polymer brushes with a dry thickness of 700 nm over the same time period.

Other parameters have also been shown to affect the growth of polymer brushes *via* SI-ATRP. For example, reducing the concentration of catalyst should result in an increase in dry brush thickness (Figure 1.10).⁸⁵ This is because a lower catalyst concentration results in a lower radical flux reducing the probability of radical recombination and, hence, premature termination. Additionally, the same authors found that stirring the reaction solution had a negative effect on the growth of PMMA brushes from gold surfaces.

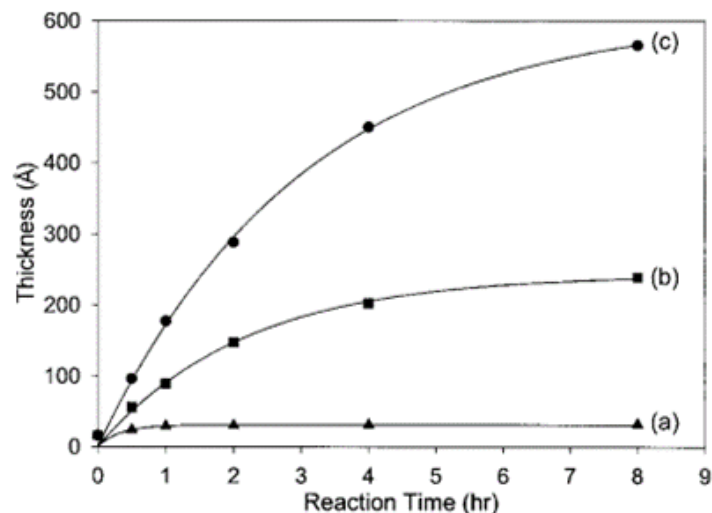
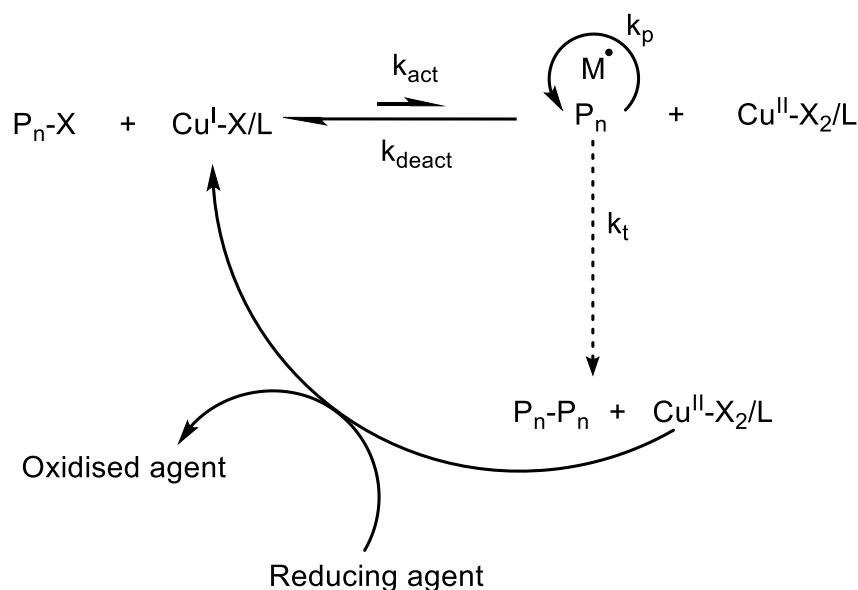


Figure 1.10. Thickness of poly(methyl acrylate) (PMA) films as a function of polymerisation time and catalyst concentration: (a) [MA] = 2 M, [CuCl/tris[2-(dimethylamino)ethyl]amine (Me₆TREN)] = 40 mM, and [CuBr₂/Me₆TREN] = 12 mM; (b) [MA] = 2 M, [CuCl/Me₆TREN] = 2 mM, and [CuBr₂/Me₆TREN] = 0.6 mM and (c) [MA] = 2 M, [CuCl/Me₆TREN] = 0.1 mM, and [CuBr₂/Me₆TREN] = 0.03 mM. SI-ATRP was performed in a 1:1 mixture of acetonitrile and tetrahydrofuran (THF) at 23 °C. The thicknesses of the PMA films were measured by ellipsometry at two different spots on a sample and averaged. The thickness at time zero is that of the initiator layer. Reprinted with permission from J.-B. Kim et al., *J. Polym. Sci. Part A Polym. Chem.*, 2003, **41**, 386–394. Copyright 2003 Wiley Periodicals, Inc.

Although SI-ATRP offers important advantages over other polymerisation techniques (e.g., broad monomer scope and compatibility with various solvents), it suffers from the same problems as conventional solution ATRP, including oxygen sensitivity and the use of relatively large amounts of a toxic copper catalyst. Thus, variations on ATRP have been developed. Matyjaszewski and co-workers have developed many SI-ATRP formulations, including polymerisation in the presence of Cu⁰,^{86,87} electrochemically-mediated ATRP⁸⁸ and light-mediated polymerisations.^{89–91}

Another important formulation is surface-initiated activators regenerated by electron transfer (SI-ARGET) ATRP, which is much more tolerant to air than conventional ATRP.^{39,71} Although originally developed for polymerisation in solution, ARGET ATRP can also be used to prepare polymer brushes.^{71,92,93} One benefit of SI-ARGET ATRP compared to conventional SI-ATRP is that the former approach requires a much lower concentration of copper catalyst.⁹⁴ Cu^{II} is reduced *in situ* to Cu^I by using a reducing agent such as ascorbic acid (Scheme 1.5), which is an environmentally-friendly additive.³⁹ Coupled with a low monomer concentration, this greatly reduces both the cost and environmental impact of SI-ARGET ATRP formulations compared to conventional SI-ATRP. The use of a reducing agent in ARGET ATRP formulations limits the sensitivity of the reaction towards oxygen; indeed, the reaction solution typically does not require deoxygenation prior to

polymerisation. SI-ARGET ATRP conducted in water produces more cost-effective brushes compared to conventional SI-ATRP, which augurs well for potential applications.⁹⁴



Scheme 1.5. Mechanism for ARGET ATRP according to Matyjaszewski and co-workers.

As with traditional SI-ATRP the brush growth kinetics of SI-ARGET ATRP should follow the relationship shown in Figure 1.9, i.e., the brush thickness should increase linearly over time.^{39,92} However it is typical that deviations from linear behaviour are commonly observed (Figure 1.10).^{60,94,95} To highlight this, Dunderdale et al. investigated the SI-ARGET ATRP of 2-(dimethylamino)ethyl methacrylate from planar silicon wafers.⁹⁴ These brush growth experiments were conducted with various concentrations of the reducing agent, ascorbic acid. Less ascorbic acid should mean a slower, more controlled reaction. However, a non-linear brush thickness vs. time plot was obtained even for the lowest amounts of ascorbic acid examined. This was attributed to an imperfectly controlled polymerisation, even under optimised reaction conditions.

1.5. Diblock copolymer nanoparticles

1.5.1. Block copolymer self-assembly

Amphiphiles contain both a hydrophobic and hydrophilic component, which are covalently bonded together. A simple, well known example of an amphiphile is a surfactant, whose self-assembly in aqueous solution has been extensively studied for over a century.⁹⁶ The hydrophobic surfactant tails drive self-assembly *via* the so-called hydrophobic effect.^{97,98} If a molecule is unable to form hydrogen bonds with water, its presence in an aqueous solution necessarily disrupts the hydrogen bond network formed by the water molecules.^{97,99} The self-assembly of amphiphilic diblock copolymer chains involves the same principle operating over a longer length scale.

One important theme in this Thesis is the synthesis and characterisation of aqueous dispersions of amphiphilic diblock copolymers prepared *via* RAFT polymerisation. Such copolymers spontaneously self-assemble in aqueous solution to form sterically stabilised nanoparticles. The copolymer morphology is governed by the packing parameter (p ; Equation 1.1), which depends on the volume of the hydrophobic block (V), the contact area of the hydrophilic block (a_0) and the effective length of the hydrophobic block (l_c).¹⁰⁰

$$p = \frac{V}{a_0 l_c} \quad \text{Equation 1.1}$$

Spherical micelles are typically formed for $p \leq 1/3$. If $1/3 < p \leq 1/2$ then worm-like micelles are formed, and vesicles are formed when $1/2 < p \leq 1$.

1.5.2. Post-polymerisation modification

Traditionally, post-polymerisation modification of block copolymers to form nanoparticles can be achieved by employing a solvent switch,^{101,102} a pH switch, or thin film hydration.¹⁰³ A solvent switch is where the copolymer is dissolved in a good solvent for both blocks followed by the gradual addition of a solvent which is selective for only one of the two blocks.¹⁰¹ This drives microphase separation to produce copolymer micelles. These self-assembled nanoparticles can exhibit various morphologies, including spheres,^{101,104} worm-like micelles,^{105–107} vesicles¹⁰⁸ and toroids (Figure 1.11).¹⁰⁹ The preferred morphology depends on the relative volume fraction occupied by each block, which depends in turn on their mean DP and the mass of the monomer repeat units.^{110,111} However, post-polymerisation processing can be rather laborious and is typically conducted in dilute solution (e.g., < 1% w/w solids).^{101,107,108}

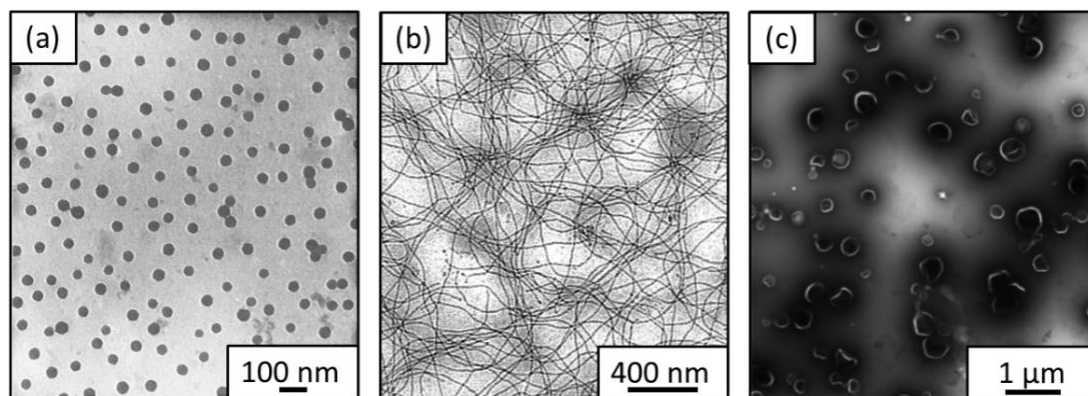


Figure 1.11. Transmission electron microscopy (TEM) images of (a) spherical, (b) worm-like and (c) vesicle nanoparticles prepared by post-polymerisation processing techniques. Adapted with permission from Z. Gao et al., *Macromolecules*, 1994, 27, 7923–7927 and G. Sun et al., *ACS Nano*, 2009, 3, 673–681. Copyright 1994 and 2009 American Chemical Society. From Y.-Y. Won, H. T. Davis and F. S. Bates, *Science*, 1999, 283, 960–963. Adapted with permission from AAAS.

1.5.3. Polymerisation-induced self-assembly (PISA)

PISA has proven to be a convenient method for producing a range of copolymer nanoparticles *in situ* at high solids (up to 50% w/w).¹⁰⁰ Most PISA formulations reported in the literature involve RAFT polymerisation.^{100,112–114} The first step involves the synthesis of a soluble homopolymer (or macro-CTA) *via* RAFT solution polymerisation [or end-group modification of an existing precursor such as a monohydroxy-capped poly(ethylene glycol) (PEG)].^{42,115} This homopolymer acts as a steric stabiliser for the diblock copolymer nanoparticles, so no additional stabiliser (e.g., surfactants) is required for the PISA synthesis (Figure 1.12). In the case of RAFT aqueous dispersion polymerisation, the macro-CTA is chain-extended with a water-miscible monomer to form an amphiphilic diblock copolymer.¹¹⁶ Conversely, the macro-CTA is chain-extended with a water-immiscible monomer in the case of RAFT aqueous emulsion polymerisation.¹¹⁷ The solvent is selected to be a poor solvent for the growing second block. At some critical DP, these chains become insoluble in the solvent, thus driving *in situ* self-assembly to form sterically stabilised diblock copolymer nanoparticles. In principle, PISA syntheses can be conducted in various solvents.¹⁰⁰ However, only aqueous PISA syntheses will be discussed in this Thesis. PISA can be conducted using any type of (pseudo-)living polymerisation.^{118,119} However, in practice most PISA formulations involve RAFT polymerisation, no doubt owing to its applicability to a wide range of vinyl monomers and solvents.

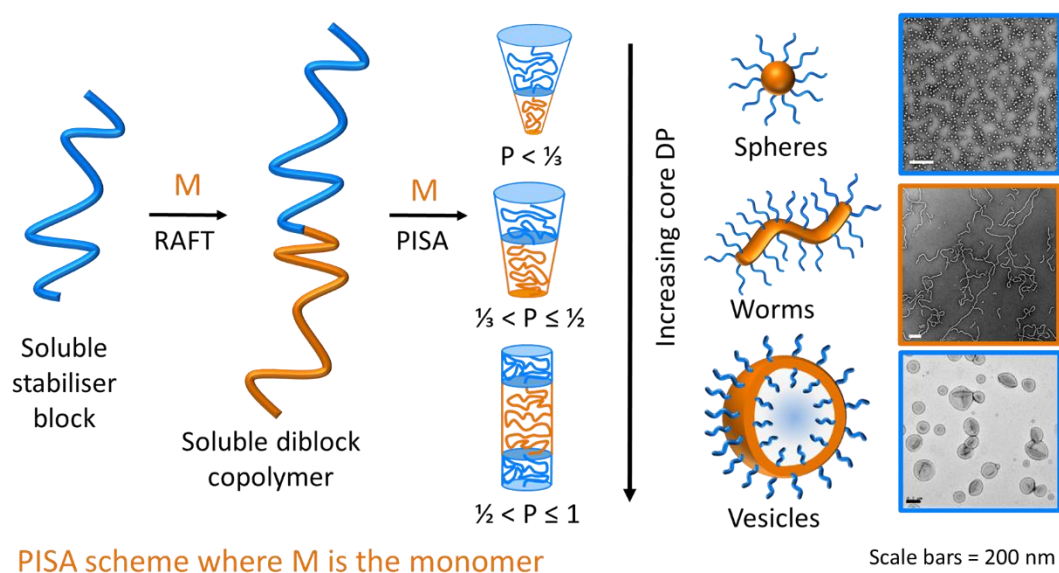


Figure 1.12. Schematic representation of a PISA synthesis *via* dispersion polymerisation, whereby a soluble homopolymer is chain-extended with a soluble monomer. At some critical DP, the second block becomes insoluble, thus driving self-assembly to form sterically stabilised diblock copolymer nanoparticles. The nanoparticle morphology depends on the relative volume fractions of the two blocks.

1.5.3.1. Pseudo-phase diagrams

The final copolymer morphology obtained *via* PISA depends on several parameters, including the mean DP of the core-forming and stabiliser blocks, as indicated by the packing parameter (see section 1.5.1). However, the packing parameter does not account for solvation of the stabiliser chains and the extent of swelling of the core-forming block by solvent and/or unreacted monomer. Consequently, it cannot be used to predict the copolymer morphology for a given PISA formulation.¹²⁰ Instead, pseudo-phase diagrams can be constructed by systematically varying the core-forming block DP and the copolymer concentration for a given stabiliser block DP (Figure 1.13).^{116,121} Such diagrams ensure reproducible targeting of specific morphologies. Typically, higher concentrations favour the formation of worms and vesicles.^{116,117} This is important as worms and vesicles have many interesting properties. For example, worms can be used as thickeners¹²² and typically form soft physical gels in semi-concentrated solution owing to multiple worm-worm interactions,¹²³ while vesicles can be used to encapsulate water-soluble molecules, proteins (e.g., enzymes) or nanoparticles.^{115,124–127} Generally, shorter macro-CTA DPs are employed when targeting copolymer morphologies other than spheres.^{128,129} If this

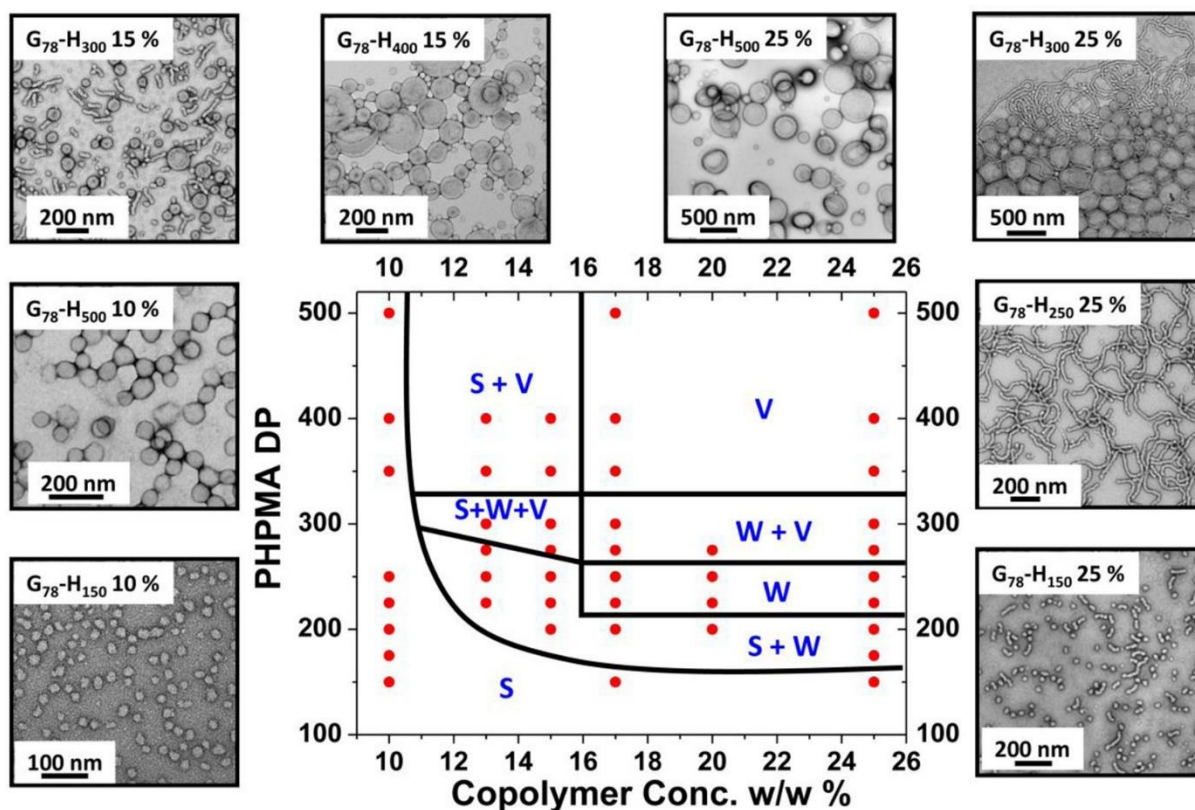


Figure 1.13. Representative TEM images and the corresponding pseudo-phase diagram constructed for a series of PGMA₇₈-PHPMA_x diblock copolymers prepared by RAFT aqueous dispersion polymerisation at copolymer concentrations ranging between 10 and 25% w/w solids (S, W and V denote spheres, worms and vesicles, respectively). Reprinted with permission from A. Blanz, A. J. Ryan and S. P. Armes, *Macromolecules*, 2012, **45**, 5099–5107. Copyright 2012 American Chemical Society.

steric stabiliser block is too long, only kinetically-trapped spheres are obtained.¹¹⁶ This is because the initial spheres cannot undergo sphere-sphere fusion, which is the key first step in the production of worms.

1.5.3.2. Thermoresponsive nanoparticles

Many diblock copolymers can exhibit stimulus-responsive behaviour.¹³⁰ For example, thermoresponsive polymers such as PNIPAM exhibit inverse temperature solubility behaviour on heating an aqueous solution above approximately 32 °C.¹³¹ It is well documented that poly(glycerol monomethacrylate)-poly(2-hydroxypropyl methacrylate) (PGMA-HPMA) worm gels exhibit a fully reversible worm-to-sphere transition on cooling from 22 °C to 4 °C.^{130,132–134} This behaviour differs from that exhibited by PNIPAM because the thermosensitive HPMA block always remains weakly hydrophobic – the change in morphology is driven by a subtle change in its (partial) degree of hydration.¹³⁰ Moreover, a freeze-dried PGMA_x-HPMA_y powder can be redispersed in ice-cold water as a 10% w/w solution prior to warming to 22 °C.¹³⁴ Spherical nanoparticles are formed at sub-ambient temperatures and a free-standing soft worm gel is obtained at 22 °C.¹³⁴ This strongly suggests that the worm morphology is the thermodynamically-preferred structure for this diblock copolymer composition. Similarly, Mable and co-workers exploited the thermoresponsive behaviour exhibited by PGMA₅₈-HPMA₂₅₀ vesicles.^{124,125} The silica-loaded vesicles were cooled to 0 °C to induce a vesicle-to-sphere transition, which led to the release of the silica nanoparticles into the aqueous continuous phase (Figure 1.14).

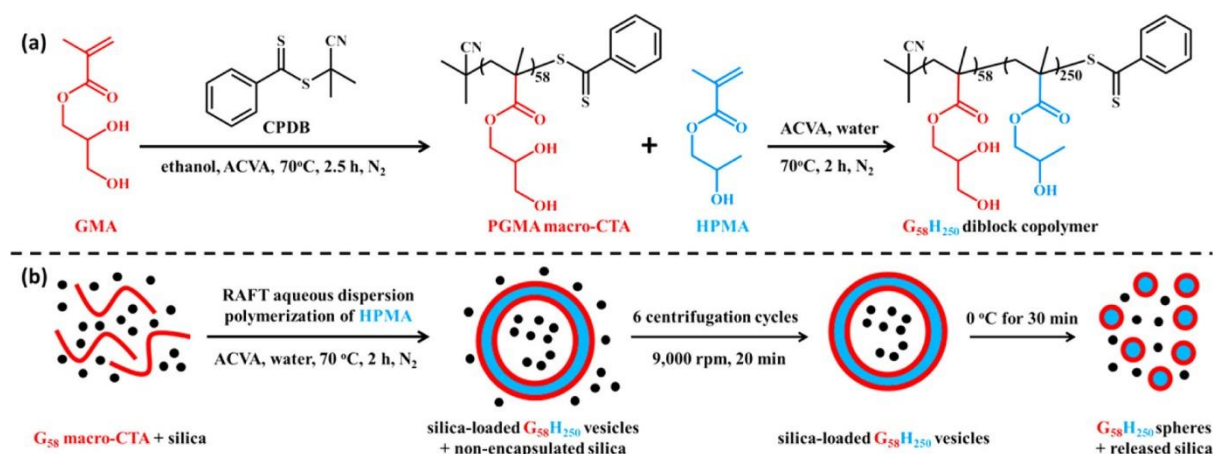


Figure 1.14. (a) Synthesis of a PGMA₅₈ macro-CTA *via* RAFT solution polymerisation and subsequent synthesis of PGMA₅₈-HPMA₂₅₀ diblock copolymer nano-objects *via* RAFT aqueous dispersion polymerisation. (b) Schematic cartoon illustrating *in situ* encapsulation of silica nanoparticles during the synthesis of PGMA₅₈-HPMA₂₅₀ diblock copolymer vesicles *via* RAFT aqueous dispersion polymerisation and subsequent release of such silica nanoparticles on cooling to around 0 °C, which induces vesicle dissociation. Reprinted with permission from C. J. Mable et al., *J. Am. Chem. Soc.*, 2015, 137, 51, 16098–16108. Copyright 2015 American Chemical Society.

Byard et al. synthesised a new amphiphilic diblock copolymer that could form spheres, worms, vesicles or lamellae depending on the aqueous solution temperature.¹³⁵ The steric stabiliser block was poly(*N,N*'-dimethyl acrylamide) and the structure-directing block was a statistical copolymer comprising 80 mol% 4-hydroxybutyl acrylate and 20 mol% diacetone acrylamide. A free-flowing liquid comprising spherical nanoparticles was obtained at 1 °C. Warming this copolymer dispersion up to 25 °C induced a sphere-to-worm transition to generate a free-standing worm gel. The worms were transformed into vesicles at 50 °C and a vesicle-to-lamella transition was observed at 70 °C. Rheological studies indicated that the worm/sphere and vesicle/worm transitions were almost fully reversible, but the lamella/vesicle transition exhibited significant hysteresis.

1.5.3.3. Diblock copolymer worm gels for biological applications

Biocompatible hydrogels have many biomedical applications, ranging from soft contact lenses¹³⁶ to drug delivery.¹³⁷ However, an essential requirement for such applications is rigorous sterilisation. The thermoresponsive nature of PGMA-PHPMA worm gels provides an opportunity in this regard.^{124,125,133,138–141} Thus, Blanazs et al. reported that cooling a PGMA₅₄-PHPMA₁₄₀ diblock copolymer worm gel from 21 °C to 4 °C leads to *in situ* degelation to produce a low-viscosity, free-flowing copolymer dispersion (Figure 1.15).¹³² This was attributed to a worm-to-sphere transition, which was confirmed by small-angle X-ray scattering (SAXS) and TEM studies. Importantly, this morphological transition proved to be fully reversible on returning to room temperature.¹³² This behaviour enables facile sterilisation *via* cold ultrafiltration: the spherical nanoparticles are sufficiently small to pass through 0.45 µm pores, whereas relatively large bacteria (500–600 nm diameter) are unable to do so.¹³² Thus, simply warming the ultrafiltered cold dispersion of spheres to ambient temperature leads to the reconstitution of a sterilised worm gel.¹³² This concept

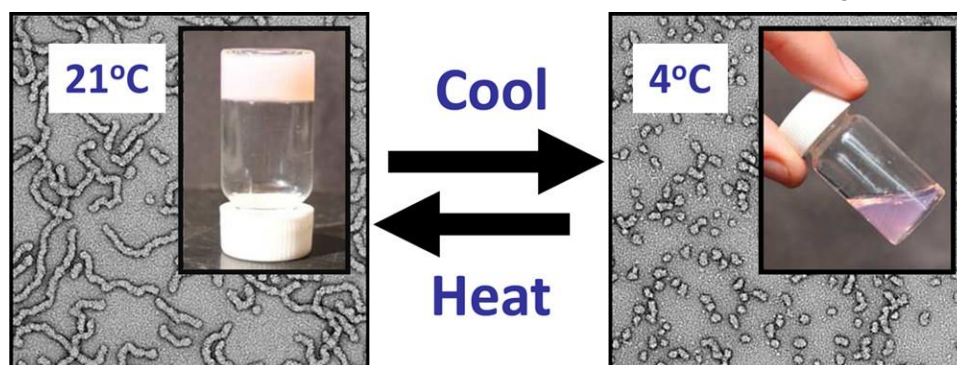


Figure 1.15. Thermoresponsive behaviour of a 10% w/w aqueous dispersion of PGMA₅₄-PHPMA₁₄₀ diblock copolymer nanoparticles. A free-standing gel is formed at 21 °C, which becomes a free-flowing dispersion when cooled to 4 °C. TEM studies of grids prepared from a dilute aqueous dispersion of PGMA₅₄-PHPMA₁₄₀ nanoparticles dried at either 21 or 4 °C provide strong evidence for a reversible worm-to-sphere transition. Reprinted with permission from A. Blanazs et al., *J. Am. Chem. Soc.*, 2012, **134**, 9741–9748. Copyright 2012 American Chemical Society.

was verified by deliberately contaminating a worm gel with fluorescently-labelled bacteria, which were completely removed by a single cold ultrafiltration step.¹³²

Canton et al. investigated the use of PGMA₅₅-PHPMA₁₃₅ worm gels as mimics for natural mucins (Figure 1.16).¹³⁸ Natural mucins are known to induce a state of suspended animation in viable mammalian embryos for weeks/months.¹⁴² The worm gels were cooled to 4 °C to induce a worm-to-sphere transition before being sterilised *via* ultrafiltration. Either human embryonic stem cell colonies or fertilised human embryos were then mixed with the sterile cold aqueous dispersion, which was warmed to 37 °C to reform a worm gel containing cells/embryos. The cell/embryo-loaded gels were stored for up to 3 weeks at 37 °C. The stem cells remained viable after 14 days after immersion within the worm gel and on removal they retained their pluripotency. Moreover, protein assays indicated that the stem cells entered stasis, i.e., the non-proliferative, dormant G₀ state that lies outside of the normal cell cycle. Similarly, the gel-coated human embryos remained intact when stored in such worm gels for up to 8 days at 37 °C, whereas embryos immersed in alternative hydrogels underwent fragmentation under such conditions. Subsequent studies conducted by Sponchioni and co-workers investigated whether stasis induction was simply the result of the relatively soft nature of the worm gel ($G' < 100$ Pa) or whether the hydroxyl functionality on the PGMA block played an important role.¹⁴³ On replacing the PGMA stabiliser chains with an alternative biocompatible polymer (PEG), the stem cells did not enter stasis and instead continued to proliferate. These observations indicated that the hydroxyl functionality is essential for stasis induction.

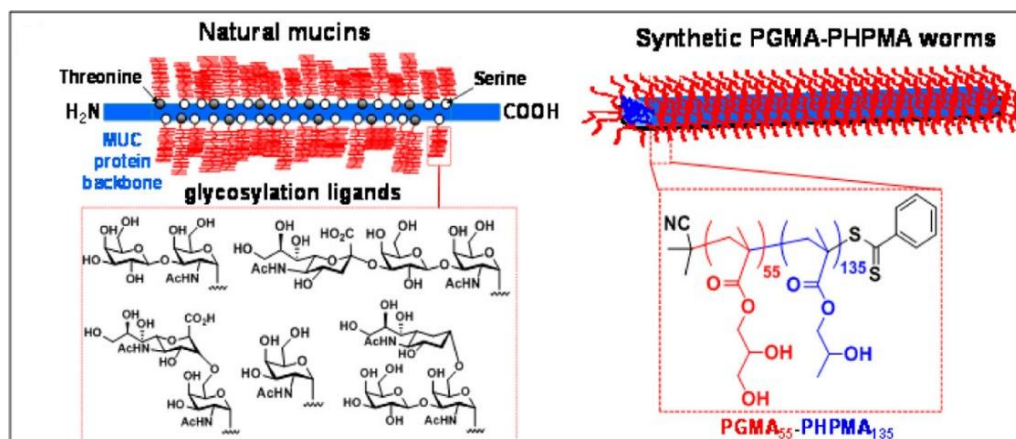


Figure 1.16. Schematic comparison of the similar physical and chemical (hydroxyl-rich) structures of mucin gels and PGMA-PHPMA worm gels. Reprinted with permission from I. Canton et al., *ACS Cent. Sci.*, 2016, 2, 65–74. Copyright 2016 American Chemical Society.

One of the main drawbacks in using RAFT-synthesised polymers for biological applications is that their organosulfur chain-ends are both malodorous and potentially

toxic. Ideally, these groups should be removed prior to bioapplications. Chain-end removal can be performed by ozonolysis,¹⁴⁴ thermolysis¹⁴⁵ or C-S bond cleavage *via* the introduction of excess initiator.^{145,146} Recently, Jesson et al.¹⁴⁷ used H₂O₂ as a cheap and convenient reagent for the removal of either dithiobenzoate- or trithiocarbonate-based RAFT chain-ends from aqueous dispersions of diblock copolymer nanoparticles. Moreover, chain-end removal had minimal impact on the copolymer morphology and small-molecule by-products could be easily removed by dialysis against deionised water.

1.6. Aldehyde-functional polymers

1.6.1. Chemistry of the aldehyde functional group

Aldehyde-based vinyl monomers are of interest owing to the diverse reactivity of this functional group under relatively mild conditions (Figure 1.17).^{148,149} Aldehydes can be readily oxidised to carboxylic acids, reduced to alcohols, undergo nucleophilic substitution *via* the α -carbon to form imine bonds, acetals, hemi-acetals and hydrazine linkages. Aldehydes are also used in Grignard reactions¹⁵⁰ to make chemically complex alcohols, in the Wittig reaction¹⁵¹ to produce substituted alkenes and in aldolisation reactions.¹⁵²

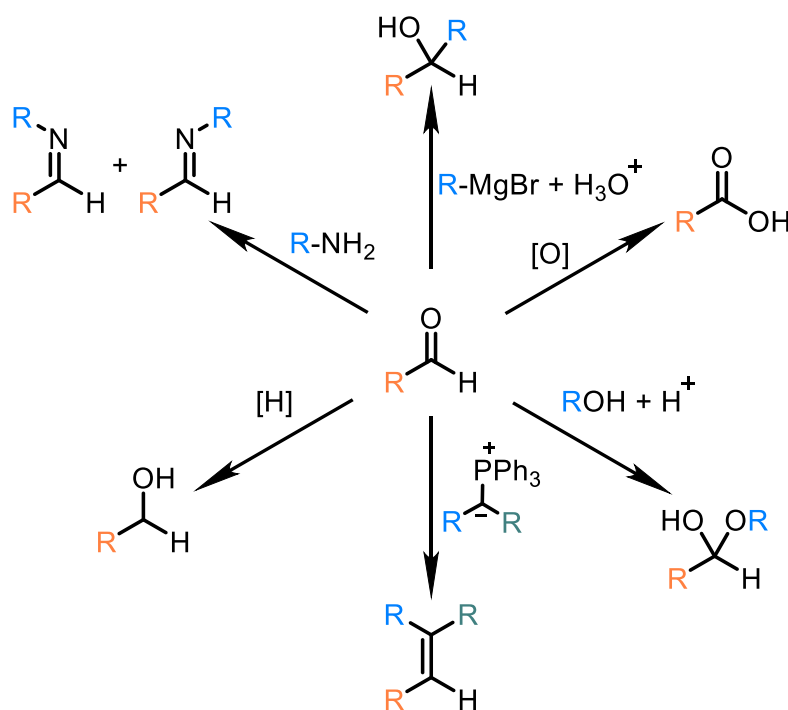


Figure 1.17. Examples of the diverse chemistry based on well-known reactions of aldehyde groups. Clockwise from the top: Grignard reaction to form complex alcohols, oxidation to carboxylic acid, reaction with alcohols to form hemi-acetals, Wittig reaction to form complex alkenes, reduction to alcohol, and reaction with primary amines to form imines.

The reactivity of the aldehyde functional group has also been exploited for polymerisations. For example, a ketone monomer has been reacted with an aldehyde monomer to make aldol polymers.¹⁴⁹ Metal-catalysed polymerisations *via* the aldehyde functional group have been employed to synthesise polyesters.^{153–155} Similarly, Baylis-Hillman polymerisation has been used to prepare functional polyesters using dialdehydes.¹⁵⁶

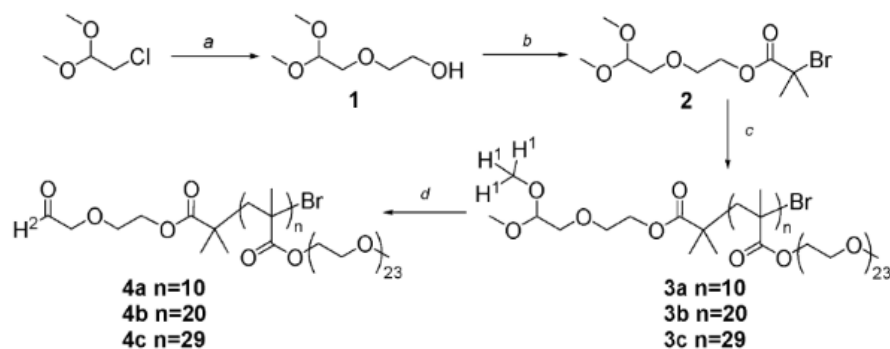
In particular, the reaction of aldehydes with primary amines will be explored in this Thesis. Once an imine bond has been formed *via* such Schiff base chemistry, it can be reduced *in situ* by reductive amination using either sodium cyanoborohydride (NaCNBH_3)¹⁵⁷ or sodium triacetoxyborohydride ($\text{NaBH}(\text{OAc})_3$).¹⁵⁸ One of the main drawbacks of NaCNBH_3 is that it can decompose to produce cyanides. Nevertheless, it is preferred for aqueous syntheses owing to its relatively high stability.

1.6.2. Synthesis of linear aldehyde-functional polymers

Since the 1950s, there have been various studies of the free radical polymerisation of aldehyde-functional monomers.^{159,160} However, typically only ill-defined polymers were obtained.^{31,159,160} Since then, both ionic^{161–163} and RDRP polymerisation techniques have been developed. Owing to the synthetically demanding nature of ionic polymerisation techniques (e.g., intolerance of protic impurities) and the tedious preparation protocols (e.g., protection of the aldehyde monomer and deprotection after polymerisation), RDRP techniques have become preferred. The relatively mild conditions under which these polymerisations can occur has been particularly beneficial.¹⁶⁴ There are many examples of keto/aldehyde polymers prepared *via* RDRP that exhibit narrow MWDs.^{165–167} However, all of these syntheses were conducted in non-aqueous media.^{165,168} This is due to the hydrophobic nature of the keto/aldehyde group in these monomers/polymers. Nevertheless, aqueous syntheses are preferential as water is an inexpensive, non-flammable, environmentally friendly solvent.

1.6.2.1. Synthesis using aldehyde-functional initiators

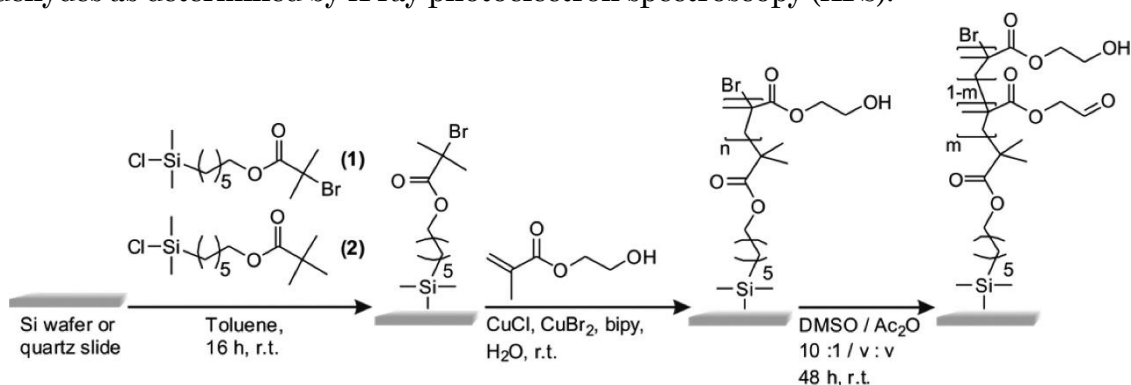
One method to synthesise aldehyde-functional polymers is to use an aldehyde-based initiator to produce aldehyde-capped polymer chains. This synthesis route has been explored by Haddleton et al., who used an acetal-protected ATRP initiator (Scheme 1.6).¹⁶⁹ After polymerisation, acid hydrolysis afforded aldehyde-capped linear or comb PEG-based polymers and poly(oligo(2-ethyl-2-oxazoline)methacrylate) polymers, which were subsequently evaluated for protein conjugation.^{170,171}



Scheme 1.6. Reagents and conditions: (a) ethylene glycol, KOH, 115 °C; (b) 2-bromoisobutyryl bromide, Et₃N, 0 °C; (c) Cu^IX (X=Cl, Br)/N-(ethyl)-2-pyridylmethanimine, methoxyPEG₍₁₁₀₀₎methacrylate, toluene; T=80 °C (X=Cl) or T=50 °C (X=Br); (d) CF₃COOH/H₂O 1:1, room temperature. Reprinted with permission from L. Tao et al., *J. Am. Chem. Soc.*, 2004, **126**, 13220–13221. Copyright 2004 American Chemical Society.

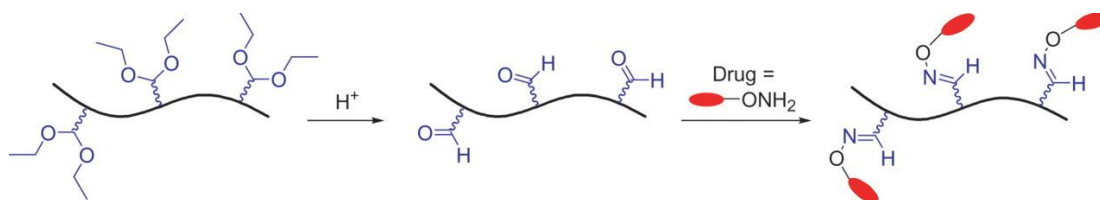
1.6.2.2. Incorporation of aldehyde functionality after polymerisation

Using a protected aldehyde group during polymerisation reduces the possibility of unwanted side reactions. Incorporation of aldehyde functionality after polymerisation has been reported by a few research groups.^{65,172–174} Installation of aldehyde functionality can be achieved by oxidation reactions. For example, the Wooley group incorporated aldehyde groups into a series of polycarbonate-based polymers *via* ozonolysis of the alkene pendent group to produce statistical copolymers comprising both aldehyde and alkene functionality.¹⁷² However, the aldehyde functionality had to be produced *in situ* owing to the limited solubility of the polymer. It was suggested that such aldehyde-functional copolymers should be useful precursors for various oxime, hydrazine and Schiff base compounds. Similarly, Klok et al. prepared polymer brushes by SI-ATRP of HEMA in water, which was followed by post-polymerisation oxidation of the 2-hydroxyethyl group to afford pendent aldehyde groups *via* Albright-Goldman oxidation in DMSO/Ac₂O (Scheme 1.7).⁶⁵ Unfortunately, this method only converted 49% of the hydroxy groups into aldehydes as determined by X-ray photoelectron spectroscopy (XPS).



Scheme 1.7. Preparation of aldehyde-functionalised PHEMA brushes *via* SI-ATRP of HEMA and subsequent post-polymerisation oxidation of the brush side chain hydroxyl groups. Reprinted with permission from T. Bilgic and H.-A. Klok, *Biomacromolecules*, 2015, **16**, 3657–3665. Copyright 2015 American Chemical Society.

Acetal deprotection has also been used to design aldehyde-functional polymers. For example, Frey et al. reported the homopolymerisation or copolymerisation of two epoxide monomers [3,3-dimethoxy-propanyl glycidyl ether (DMPGE) and 3,3-dimethoxy-2,2-dimethylpropanyl glycidyl ether (DDPGE)] with ethylene oxide in DMSO to produce polymers comprising of a PEG backbone with multiple pendent acetal groups.¹⁷³ These acetals were then deprotected under acidic conditions in an acetone/water mixture with minimal effect on the polymer MWD. However, hydrolysis of the (co)polymers of DMPGE produced aldehyde-functional (co)polymers that were no longer soluble in the acetone/water mixture. This was attributed to cross-linking *via* aldol reactions under the acidic reaction conditions. To remove such unwanted side-reactions, (co)polymers with no acidic α -protons were targeted using DDPGE and this approach proved to be much less problematic; acetal deprotection resulted in soluble, well-defined aldehyde-functional (co)polymers. In related work, Maynard and co-workers used ATRP to polymerise 3,3'-diethoxypropyl methacrylate to produce an acetal-protected aldehyde precursor.¹⁷⁴ The aldehyde functionality was generated *in situ* prior to conjugation reactions conducted using model drug compounds (Scheme 1.8). *In situ* generation of the aldehyde was preferred owing to insolubility issues with the purified polymer, which was attributed to crosslinking side-reactions. Nevertheless, the authors concluded that their approach provided a convenient method for the synthesis of polymer-drug conjugates.



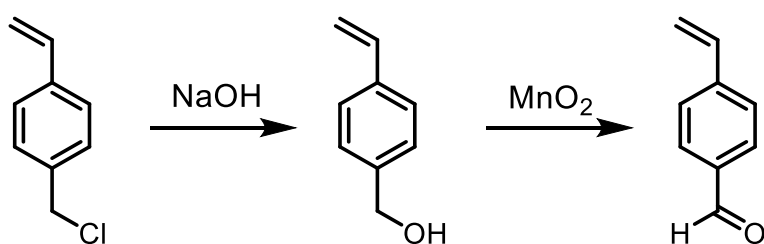
Scheme 1.8. Schematic synthesis of polymer-drug conjugates *via* aldehyde-functional polymers prepared from acetal-protected precursors. Reprinted with permission from C. L. I. Ronald, R. M. Broyer and H. D. Maynard, *J. Polym. Sci. Part A Polym. Chem.*, 2006, **44**, 5004–5013. Copyright 2006 Wiley Periodicals, Inc.

1.6.2.3. Synthesis using aldehyde-functional monomers

In principle, synthesis of aldehyde-functional polymers from aldehyde-functional monomers is preferable to protecting group chemistry since it is inherently more atom-efficient. Moreover, deprotection can result in various unwanted side-reactions, as discussed above. Radical polymerisation has been successfully applied to aldehyde-based vinyl monomers.^{165,175} However, other techniques have also been used.¹⁷⁶

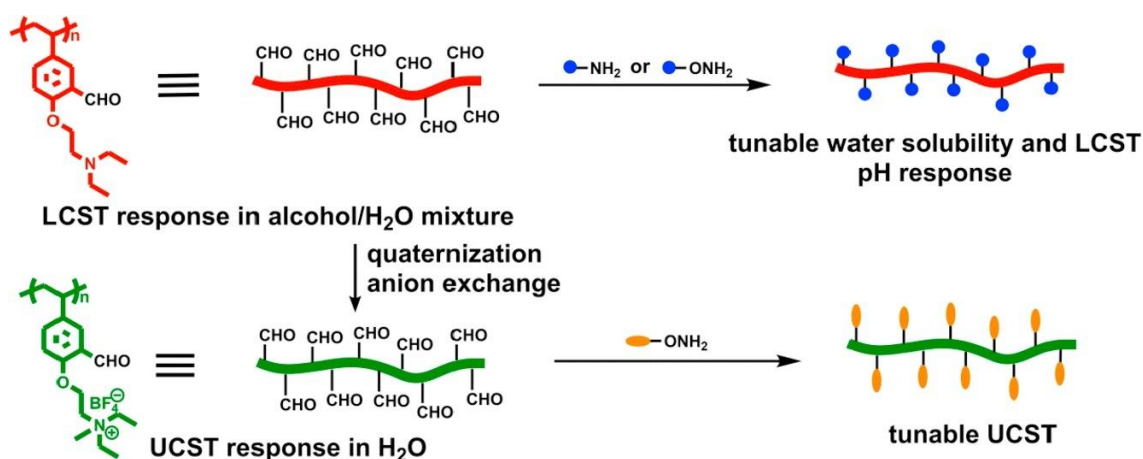
Many examples of the (co)polymerisation of aldehyde-functional monomers involve 4-vinylbenzaldehyde (VBA).^{159,168,175,177–179} For example, RAFT polymerisation has been

employed for the synthesis of poly(4-vinylbenzaldehyde) (PVBA). Wooley et al. found that VBA could be polymerised in either 1,4-dioxane or 2-butanone to give well-defined PVBA polymers ($\bar{D} \leq 1.17$) without any side-reactions.¹⁶⁵ Such PVBA precursors were then chain-extended with styrene to produce the first examples of diblock copolymers bearing multiple aldehyde groups prepared without protecting group chemistry. Boutevin et al. copolymerised VBA with styrene, methyl methacrylate and butyl acrylate *via* FRP in propionitrile.¹⁷⁵ The aldehyde functionality was then used to crosslink the polymer chains to produce coatings with high chemical and thermal stability. One of the main drawbacks of using VBA as an aldehyde-functional monomer is that it is very expensive. Therefore, it is often synthesised in-house for various academic studies (Scheme 1.9).^{168,180,181}



Scheme 1.9. Two-step synthesis of 4-vinylbenzaldehyde monomer.

An alternative aldehyde-functional monomer has been reported by Legros et al., who synthesised aldehyde-functional polymers based on poly(2-oxazoline) prepared by cationic ring-opening polymerisation.¹⁷⁶ These precursors were subsequently used to prepare graft copolymers and crosslinked polymer networks. Hydrogels were obtained by reacting the aldehyde groups with adipic acid dihydrazide. Such networks underwent hydrolytic degradation over several days at physiological pH, with more rapid cleavage occurring at pH 3. Lu et al. have extensively investigated the RAFT polymerisation of aldehyde-functional monomers such as 2-formal-4-vinylphenyl ferrocenecarboxylate, 2-(2-(diethylamino)ethoxy)-5-vinylbenzaldehyde and acrolein.^{166,167,182} Most recently, they functionalised poly(2-(2-(diethylamino)ethoxy)-5-vinylbenzaldehyde) (PDEVB) homopolymers *via* imine or oxime linkages to tune the solubility and thermoresponsive nature of the target polymers (Scheme 1.10) in both water and alcohol/water mixtures.¹⁸³

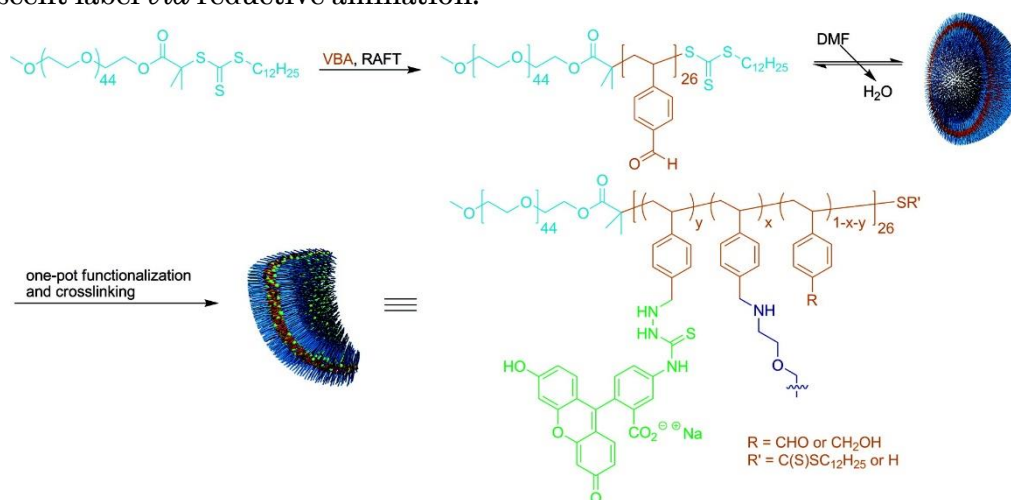


Scheme 1.10. Chemical modification of a thermoresponsive polymer (PDEVB). [Note: lower critical solution temperature (LCST) and upper critical solution temperature (UCST)]. Reprinted with permission from J. Huang et al., *Polymer*, 2019, **160**, 99–106. Copyright 2019 Elsevier.

1.6.3. Synthesis of aldehyde-functional nanoparticles

1.6.3.1. Synthesis by post-polymerisation modification

There are several literature examples of the post-polymerisation modification of aldehyde-functional block copolymers to form nanoparticles. For example, Wooley and co-workers prepared poly(ethylene oxide)-poly(4-vinyl benzaldehyde) (PEO-PVBA) diblock copolymers *via* RAFT polymerisation of VBA (Scheme 1.11) using a PEO macro-CTA.¹⁸⁴ The polymerisation was conducted in dry DMF at 75 °C and the resulting copolymer had a relatively narrow molecular weight distribution ($\mathcal{D} = 1.20$). The solvent was gradually adjusted from DMF to water to induce self-assembly of the amphiphilic diblock copolymers. This post-polymerisation processing strategy produced vesicles, as confirmed by TEM, scanning electron microscopy (SEM) and dynamic light scattering (DLS). The aldehyde groups within the vesicle membranes were subsequently reacted with a fluorescent label *via* reductive amination.



Scheme 1.11. Construction and functionalisation of PEO₄₅-PVBA₂₆ vesicles through reductive amination. Reprinted with permission from G. Sun et al., *ACS Nano*, 2009, **3**, 673–681. Copyright 2009 American Chemical Society.

Nagasaki and co-workers have reported many examples of the synthesis of various aldehyde-functional poly(ethylene glycol)-polylactide (PEG-PLA) nanoparticles (Figure 1.18).^{104,185–187} First, acetal-capped diblock copolymer chains were prepared *via* anionic ring-opening polymerisation in dry THF. These PEG-PLA copolymers were then self-assembled to form spherical micelles by initial dissolution in *N,N'*-dimethylacetamide (a good solvent for both blocks), followed by dialysis against water for 24 h. Then the acetal groups were converted into aldehyde groups by acid hydrolysis. The resulting aldehyde-functional micelles proved to be stable under various conditions, including the presence of surfactants, organic solvents, at elevated temperature and over time.¹⁸⁶ Given the well-known biocompatibility and biodegradability of PEG-PLA diblock copolymers, the authors suggested that such micelles should be suitable for drug delivery and biomedical diagnosis applications.

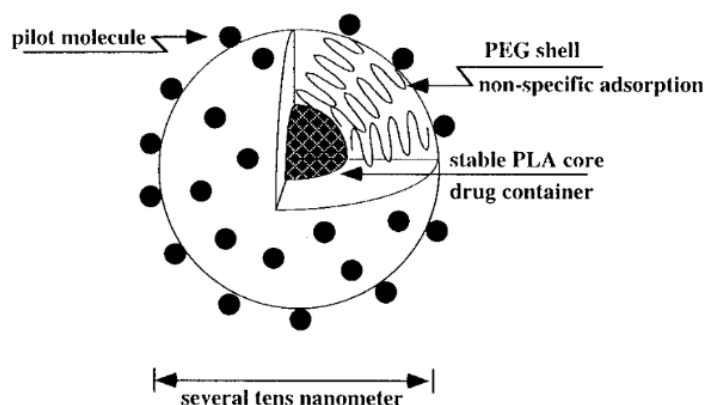
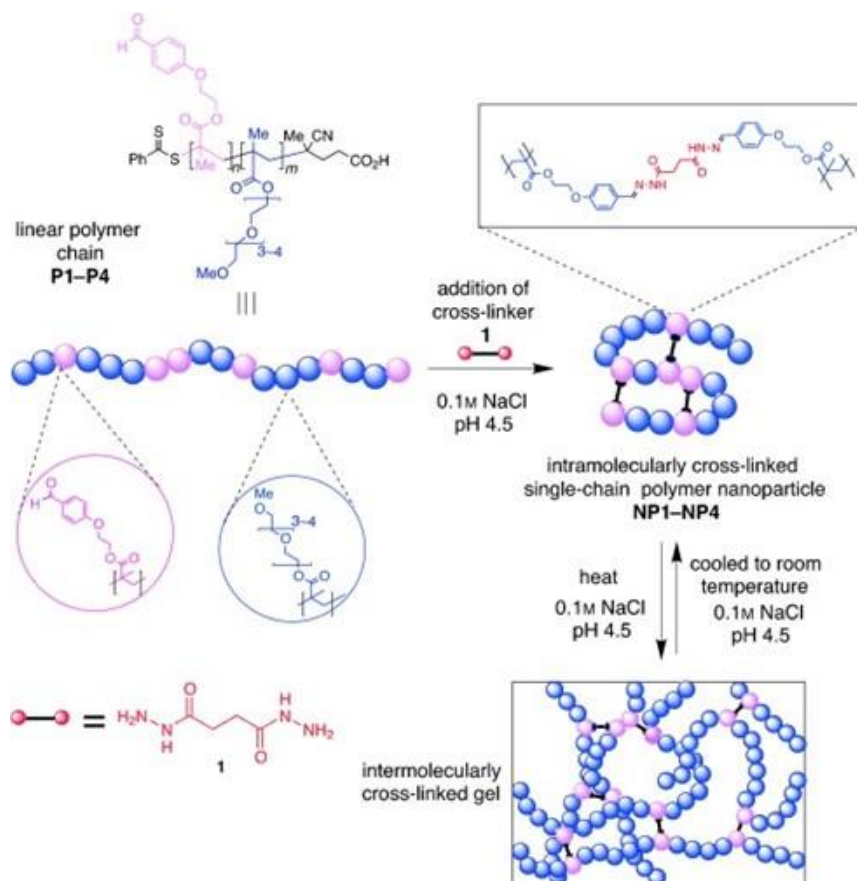


Figure 1.18. Schematic cartoon of aldehyde-decorated PEG-PLA spherical micelles. Reprinted with permission from M. Iijima et al., *Macromolecules*, 1999, 32, 1140–1146. Copyright 1999 American Chemical Society.

Similarly, Lu and co-workers copolymerised 1,2:3,4-di-*O*-isopropylidene-6-*O*-(2'-formyl-4'-vinylphenyl)-D-galactopyranose (IVDG) with 5,6-benzo-2-methylene-1,3-dioxepane (BMDO) at 130 °C in anisole to produce PIVDG-PBMDO statistical copolymers.^{178,179} RAFT polymerisation was used to ensure a relatively narrow MWD. The copolymers were then dissolved in DMSO and self-assembled to produce micelles by dialysis against water. These nanoparticles were then bound to an anti-cancer drug [doxorubicin (DOX)] and the rate of drug release was examined over a 100 h period.

Post-polymerisation modification can also involve crosslinking chemistry. For example, Fulton et al. copolymerised methacrylate *p*-(methacryloxyethoxy)benzaldehyde with (oligo(ethylene glycol) methacrylate) to prepare water-soluble aldehyde-functional statistical copolymers.¹⁸⁸ These copolymers had reasonably low dispersities ($1.34 < D < 1.41$) and no protection of the pendent aldehyde groups was required, making the synthesis

relatively straightforward. Such copolymers were subsequently used to prepare single-chain nanoparticles by exploiting the labile reaction between aldehydes and dihydrazides.¹⁸⁴ Crosslinking between the aldehyde groups in the copolymer and the dihydrazide crosslinker was performed under mildly acidic conditions (pH 4.5). Heating the reaction mixture resulted in further intermolecular interactions and produced a crosslinked hydrogel (Scheme 1.12), which dissolved on cooling to reform the single-chain nanoparticles.



Scheme 1.12. Conjugation of polymer chains P1–P4 with 1 to form intramolecularly crosslinked single-chain polymer nanoparticles NP1–NP4, and their subsequent reversible transformation into an intermolecularly cross-linked hydrogel. Reprinted with permission from D. E. Whitaker, C. S. Mahon and D. A. Fulton, *Angew. Chem. Int. Ed.*, 2013, 52, 956–959. Copyright 2013 Wiley-VCH Verlag GmbH & Co.

1.6.3.2. Synthesis via PISA

PISA can also be employed to produce aldehyde-functional nanoparticles. For example, Boyer et al. used RAFT-mediated PISA to prepare poly(oligo(ethylene glycol) methacrylate)-poly(styrene-co-VBA) nanoparticles (Figure 1.19), which were used to deliver DOX to breast cancer cells (MCF-7).¹⁸⁹ The nanoparticle morphology had a significant effect on cell uptake, with worm-like micelles outperforming spherical micelles. Despite the reactive nature of the aldehyde-functional group, copolymer dispersities were relatively

low ($D \leq 1.21$). This is a good example of how PISA can be used to design novel aldehyde-functional nanoparticles for potential biomedical applications.

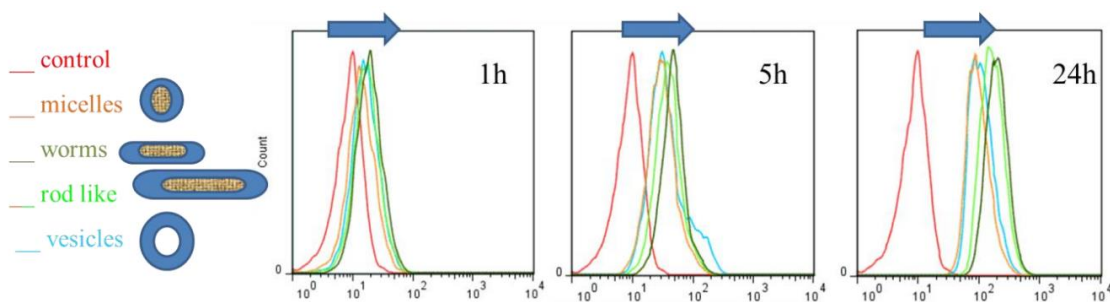
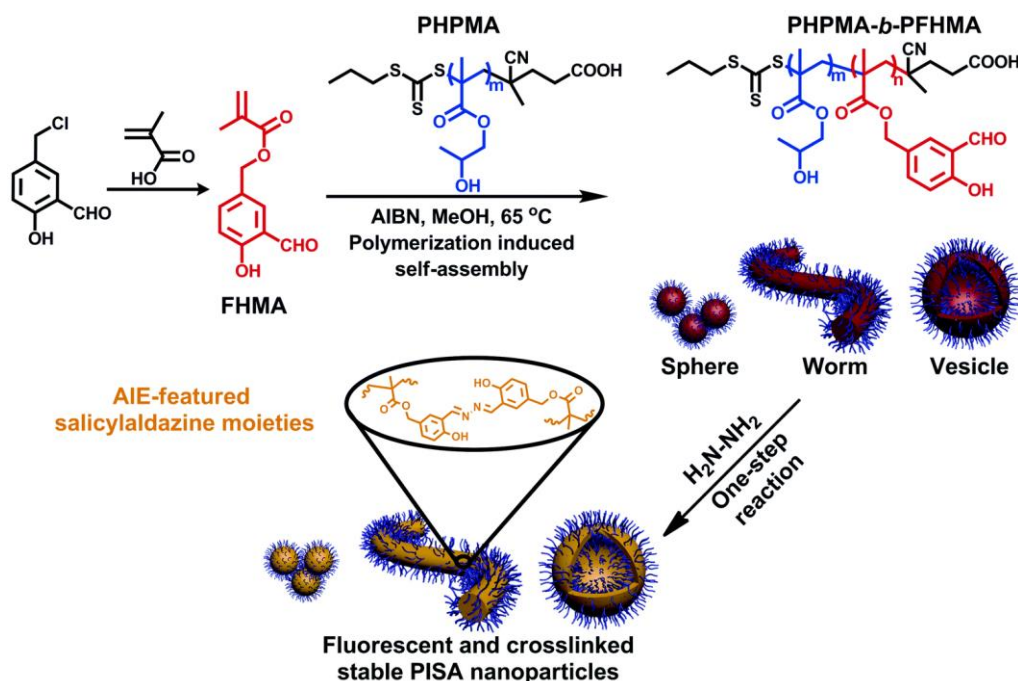


Figure 1.19. Cell uptake of different nanoparticle morphologies using MCF-7 breast cancer cells using flow cytometry at different time points (1, 5 and 24 h). Reproduced from B. Karagoz et al., *Polym. Chem.*, 2014, 5, 350–355 with permission from the Royal Society of Chemistry.

Lu et al. synthesised 3-formyl-4-hydroxybenzyl methacrylate (FHMA) for use as a core-forming block.¹⁹⁰ Accordingly, a PHPMA stabiliser block was chain-extended with FHMA in methanol to produce PHPMA-PFHMA spheres, worms or vesicles depending on the precise PISA formulation (Scheme 1.13). These nano-objects could be readily crosslinked using a hydrazine crosslinker. Furthermore, a fluorescent crosslinker could be incorporated into such nanoparticles. However, the weakly hydrophobic PHPMA stabiliser block means that such nanoparticles cannot be dispersed in aqueous media without loss of colloidal stability.



Scheme 1.13. Synthesis of fluorescent cross-linkable PHPMA-PFHMA diblock copolymer nano-objects. Reproduced from J. Huang et al., *Polym. Chem.*, 2016, 7, 4761–4770 with permission from the Royal Society of Chemistry.

Similarly, the Whittaker group reported the synthesis of fluorine-containing aldehyde-functional nanoparticles comprising poly(oligo(ethylene glycol) methyl ether methacrylate-*co*-2,2,2-trifluoroethyl acrylate)-*block*-poly(styrene-*co*-VBA).¹⁹¹ Spheres, worms and vesicles were prepared *via* RAFT-mediated PISA in isopropanol, as judged by both TEM and DLS. However, the copolymer dispersity increased when targeting a higher DP for the insoluble block ($\bar{D} = 1.61$ at 28.8% VBA and 22.5% styrene conversion), which was attributed to premature chain termination. The aldehyde functionality within the nanoparticle cores was employed to bind dye molecules, which did not induce any change in the copolymer morphology. In principle, such nanoparticles could be used as ¹⁹F MRI agents.

1.6.4. Applications of aldehyde-functional polymers

In principle, the scope of applications for aldehyde-functional polymers includes acrylic coatings,¹⁷⁵ anti-corrosion agents¹⁹² and various biomedical applications.^{65,104,170,171,174,187,193} This Thesis will focus on potential biomedical applications for aldehyde-functional polymers.

1.6.4.1. Aldehyde-functional polymers as drug conjugates

One important application for aldehyde-functional polymers is in the field of drug delivery. This is because many drugs contain amine groups, which can react readily with aldehydes to form labile imine bonds (Figure 1.17, Section 1.6.1). Studies have shown that using polymer-drug conjugates can increase the aqueous solubility of a drug (most small-molecule drugs are hydrophobic) and its mean circulation time within the body, as well as reducing its toxicity.^{174,194,195}

Aldehyde-functional polymers have been utilised as drug delivery systems for DOX by the Davis group,¹⁸⁹ Lu and co-workers,¹⁷⁸ Pan et al.¹⁹⁶ and the Whittaker group.¹⁹¹ For example, Pan et al. investigated how the copolymer morphology influenced the release of DOX from the nanoparticle cores into HeLa cells at pH 5.0, 6.0 or 7.4.¹⁹⁶ Poly(2-(dimethylamino)ethyl methacrylate)-poly(2-(methacryloxy)ethoxybenzaldehyde) (PDMAEMA-PMAEBA) diblock copolymer nanoparticles were prepared *via* RAFT dispersion polymerisation in alcohol (Figure 1.20). Four copolymer morphologies were targeted: spheres, nanorods, larger nanowires and vesicles. The copolymer chains had relatively high dispersities ($\bar{D} \leq 1.60$). Cleavage of the imine bond led to DOX release, which was monitored for each type of nanoparticle. The rate of release was fastest for the DOX-loaded nanorods and was more

rapid at pH 5.0 than at pH 6.0 or 7.4. The larger nanowires could not deliver DOX into the HeLa cells because they were too large to become internalised.



Figure 1.20. Chain extension of a PDMAEMA macro-CTA by RAFT dispersion polymerisation of MAEBA at 70 °C to produce PDMAEMA–PMAEBA diblock copolymer nano-objects. Reprinted with permission from L. Qiu et al., *ACS Appl. Mater. Interfaces*, 2016, 8, 18347–18359. Copyright 2016 American Chemical Society.

Hydrogels are an attractive means of achieving the controlled delivery of specific therapeutic agents. Wu et al. prepared hydrogels based on random copolymers of poly(2-(methacryloyloxy)ethyl phosphorylcholine-co-4-formylbenzoate ethyl methacrylate) (P(MPC-co-FBEMA)), which were reacted *via* their aldehyde-functional groups with primary amine-modified silica nanoparticles (Figure 1.21).¹⁹⁷ These hydrogels proved to be highly stable under neutral physiological conditions but underwent a sharp gel-sol transition at mildly acidic pH. The imine bonds were extremely pH-sensitive, with a pH change of just ~0.2 units causing degelation. The hydrogels were also found to be

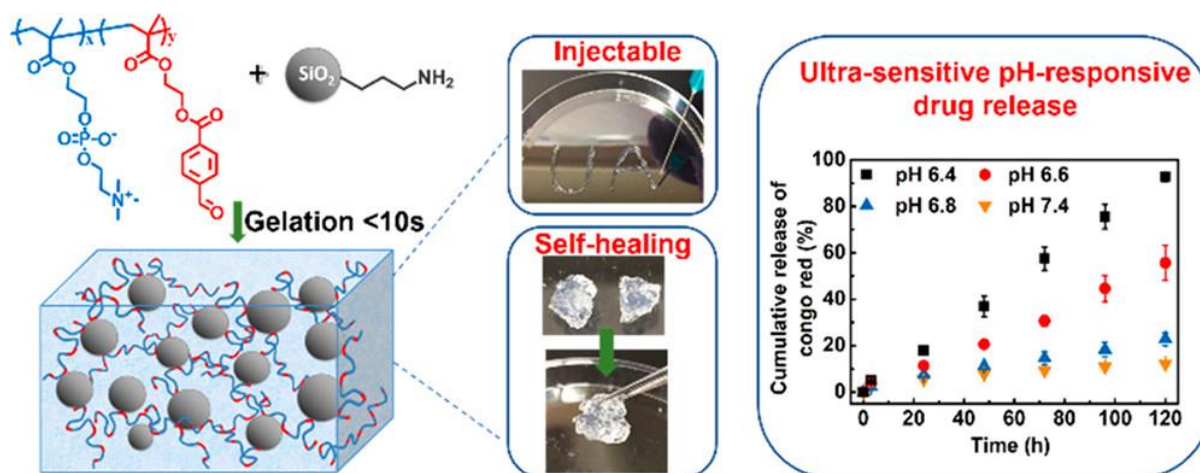
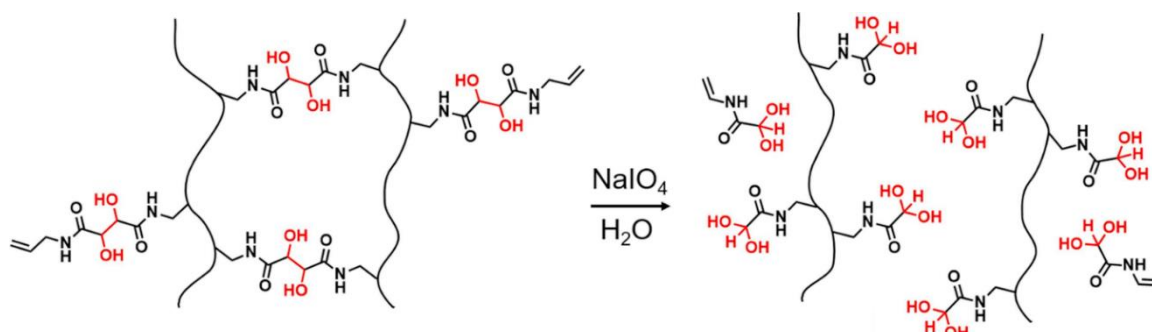


Figure 1.21. Injectable, self-healing P(MPC-co-FBEMA) hydrogels formed by reaction with amine-based silica nanoparticles. Such hydrogels proved to be highly pH-sensitive. Reprinted with permission from M. Wu et al., *Biomacromolecules*, 2020, 21, 2409-2420. Copyright 2020 American Chemical Society.

rapidly self-healing, with regelation occurring within 10 s. The mechanical and pH responses were readily tunable by changing the gel composition. Cytotoxicity studies using human dermal fibroblast cells confirmed that the hydrogels were biocompatible. These hydrogels show considerable promise for cancer therapy, wound healing and infection treatment.

Wolfel et al. synthesised PNIPAM-based α -oxoaldehyde hydrogels using sodium periodate (NaIO_4 ; Scheme 1.14).¹⁹⁸ These hydrogels contain a *cis*-diol-based crosslinker (DAT), which can be cleaved by selective oxidation using NaIO_4 in aqueous solution to produce pendent aldehyde groups. Under such conditions, degelation occurs and the aldehyde group reacts with water to form a geminal diol. The hydrogels could be recrosslinked using adipic acid dihydrazide, which conferred stimulus-responsive behaviour. Crosslinking was favoured at pH 5.3 and on heating above the copolymer LCST. In principle, this strategy could be used to design pH- and thermoresponsive hydrogels for biomedical applications.



Scheme 1.14. Schematic representation of the reaction of PNIPAM-DAT with NaIO_4 to yield PNIPAM- α -oxoaldehyde. Reprinted with permission from A. Wolfel, M. R. Romero and C. I. Alvarez Igarzabal, *Eur. Polym. J.*, 2019, **112**, 389–399. Copyright 2019 Elsevier.

PEG or PEO are widely used as the hydrophilic component of block copolymers owing to their wide availability, aqueous solubility and non-toxicity.^{199,200} Functionalised PEGs are attractive as biocompatible polymer-drug conjugates. Aldehyde-terminated PEGs are considered to be second-generation PEGylation agents.^{201,202} Haddleton et al. have investigated the PEGylation of oxytocin to enhance its stability for transportation and storage.^{170,171} Oxytocin can be bound to either comb or linear polymers *via* a terminal aldehyde end-group. Initially, the oxytocin was irreversibly bound to the polymer chains *via* reductive amination.^{157,203} Binding occurred within 24 h, as confirmed by reverse-phase high performance liquid chromatography (RP-HPLC). Such conjugation increased the high temperature stability of oxytocin. Subsequently, reversible binding of oxytocin was demonstrated by exploiting the labile imine bond that is formed when one of the primary amines on the oxytocin reacts with the aldehyde-functional PEG. The controlled release of

oxytocin from linear PEG was observed at pH 5.0, whereas little oxytocin was recovered after 4 days at pH 7.4 (Figure 1.22). Perhaps surprisingly, relatively little oxytocin was released from the comb PEGs.

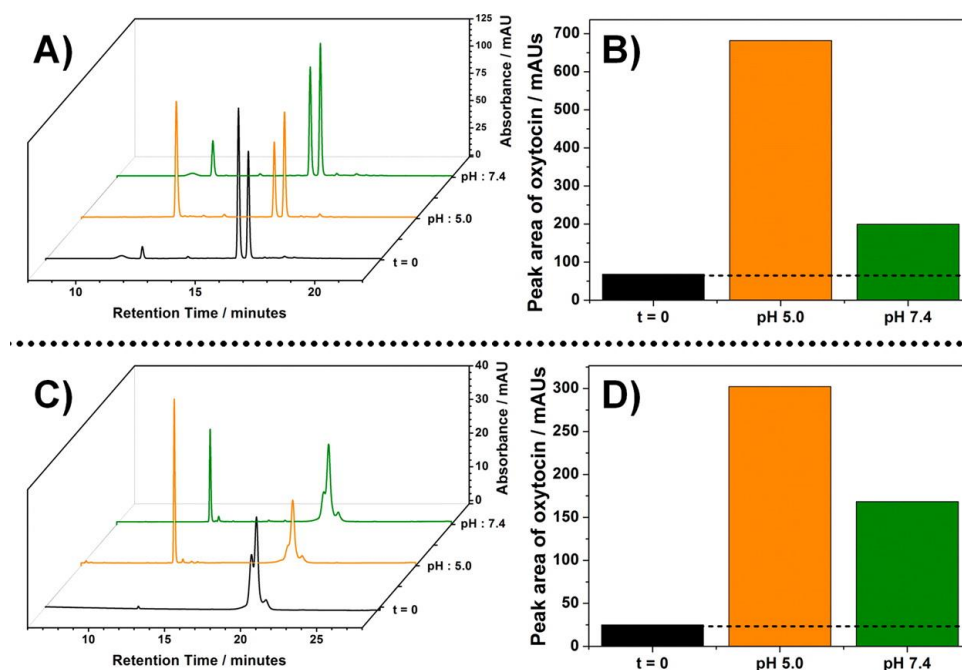
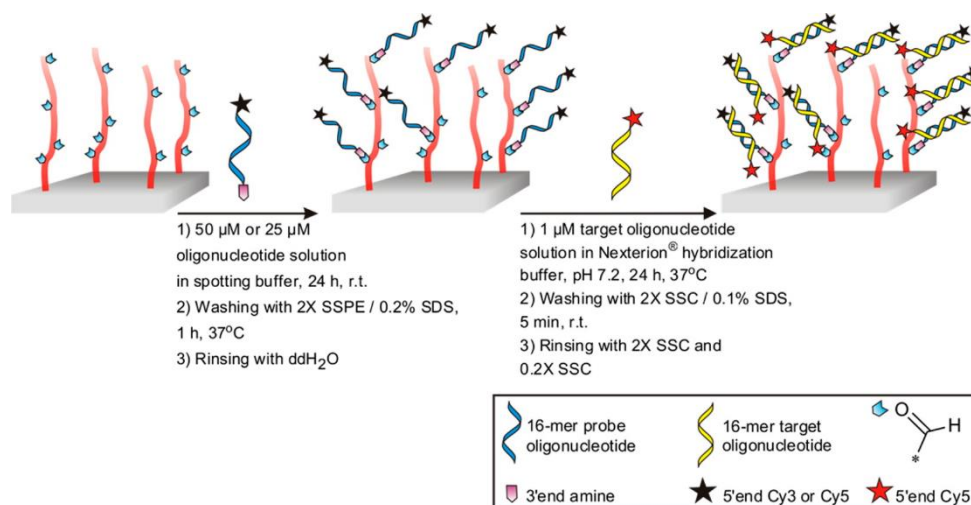


Figure 1.22. (A) RP-HPLC traces and (B) increase in oxytocin observed for hydrolytic cleavage of oxytocin–butyraldehyde conjugates at pH 5.0 and pH 7.4, (C) RP-HPLC traces, and (D) increase in oxytocin observed for hydrolytic cleavage of oxytocin–linear PEG conjugates at pH 5.0 and pH 7.4. Reprinted with permission from J. Collins et al., *Biomacromolecules*, 2016, **17**, 2755–2766. Copyright 2016 American Chemical Society.

1.6.4.2. Aldehyde-functional polymers as biosensors

The use of aldehyde-functional brushes for the construction of biosensors is potentially attractive owing to their highly reactive nature under relatively mild conditions. Furthermore, recent advances in polymer brush synthesis have improved oxygen tolerance and scalability making them ideal candidates.²⁰⁴ The aldehyde group can be utilised to immobilise various species at a surface. For example, Klok et al. investigated oligonucleotide binding to aldehyde-functionalised PHEMA brushes.⁶⁵ As described earlier, such brushes were prepared by SI-ATRP of HEMA in water, followed by Albright-Goldman oxidation. The binding ability of a series of brushes with varying grafting densities and film thicknesses were assessed to determine the optimum parameters required for maximum binding capacity and oligonucleotide hybridisation. XPS was used to confirm both selective oxidation of the PHEMA brushes and their binding to a model amine (benzylamine). Remarkably, densely grafted brushes exhibited the highest binding capacity. However, thicker brushes exhibited lower binding capacities. In contrast, hybridisation efficiencies with the target (yellow) oligonucleotide were as high as 93% for brushes when using lower surface concentrations of the complementary (blue)

oligonucleotide binder (Scheme 1.15). These findings highlight the importance of optimising both the brush grafting density and the concentration of surface functional groups.



Scheme 1.15. Schematic illustration of the immobilisation of amine-modified (blue) oligonucleotides on aldehyde-functionalised PHEMA brushes and subsequent hybridisation with complementary (yellow) oligonucleotides. Reprinted with permission from T. Bilgic and H.-A. Klok, *Biomacromolecules*, 2015, 16, 3657–3665. Copyright 2015 American Chemical Society.

Vardar et al. modified a *cis*-diol containing PEG-based polymer using NaIO₄ to produce a PEG-aldehyde.²⁰⁵ The PEG-aldehyde was bound non-covalently to urease to produce a urease/PEG-aldehyde complex for use as a urea biosensor. Such urease-based assays are commonly used in pharmaceutical applications to detect urea in biological fluids, e.g., blood or urine. The stability of these urease complexes was assessed at various temperatures and solution pH. Urease bound to the PEG-aldehyde had a higher activity between pH 4 and pH 9 than its free counterpart (Figure 1.23). Moreover, these complexes exhibited greater thermal and storage stability and could be reliably used as urea biosensors for real-world biological samples.

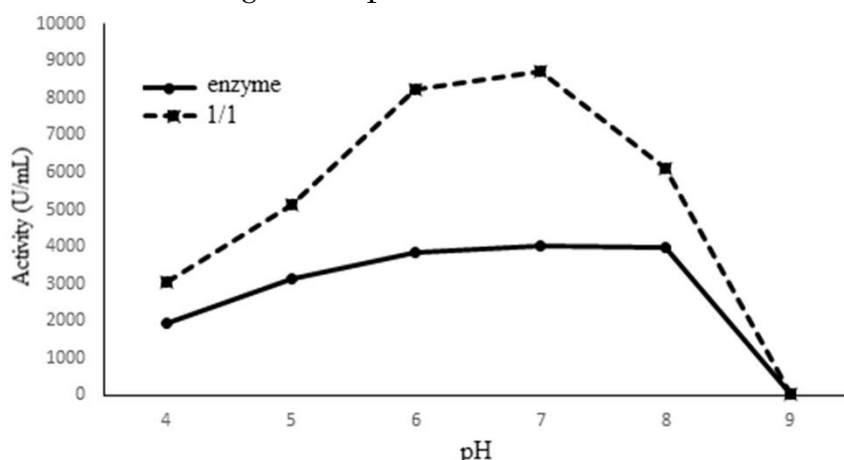


Figure 1.23. Activities of free urease and urease/PEG-aldehyde complex depending on pH, at 25 °C. All data points are averaged over three repeat measurements. Reprinted with permission from G. Vardar et al., *Prep. Biochem. Biotechnol.*, 2019, 49, 868–875.

1.6.4.3. Aldehyde-functional polymers for protein binding

Use of aldehyde-functional polymers for protein binding has been studied for many years.^{166,206,207} For example, Xiao et al. immobilised bovine serum albumin (BSA) as a model protein on aldehyde-functional micelles.¹⁶⁶ The BSA was incubated with the micelles to allow the formation of multiple imine bonds and immobilisation was confirmed by an increase in the mean hydrodynamic particle diameter by DLS.

Zou and co-workers synthesised patterned aldehyde-functional polymer brushes for protein immobilisation.²⁰⁸ The first step was the polymerisation of [(2,2-dimethyl-1,3-dioxolane)methyl]acrylamide (DMDOMA) by SI-ATRP in DMF (Figure 1.24). Then this PDMDOMA brush was deprotected using 10% acetic acid to produce poly-*N*-[(2,3-dihydroxypropyl)acrylamide] (PDHPA) brushes. Lithography was used to create patterns on the brush (Figure 1.24). Finally, the PDHPA-aldehyde was produced by

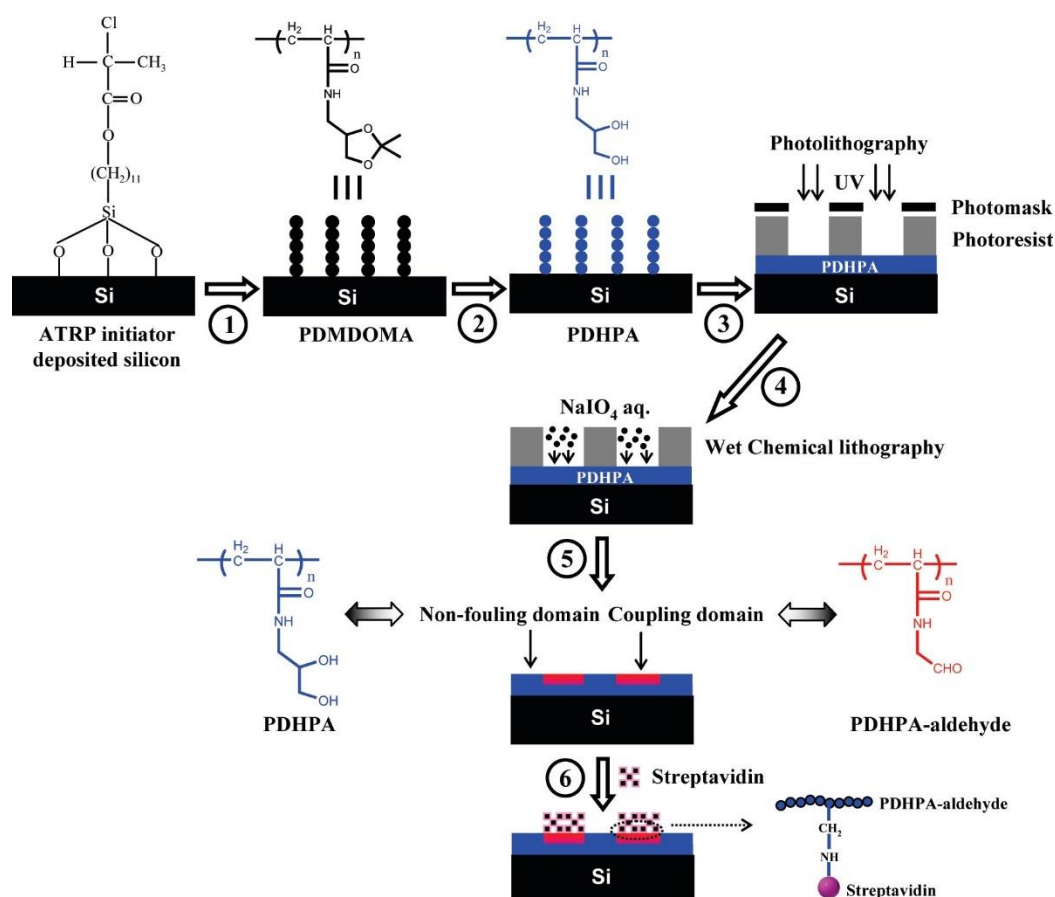


Figure 1.24. Synthetic scheme for preparing a micropatterned protein array using a combination of photolithography and chemical lithography from single, homogeneous polymer brush layer. Step 1: SI-ATRP of DMDOMA from ATRP initiator deposited silicon wafer surface. Step 2: modification of PDMDOMA brush *via* acidic hydrolysis to yield PDHPA brushes. Step 3: deposition of photoresist and generation of micropatterns. Step 4: wet chemical lithography to generate PDHPA/PDHPA-aldehyde binary brush system. Steps 5 and 6: removal of the photoresist and selective coupling of streptavidin onto the patterned substrate. Reprinted with permission from Y. Zou et al., *Biomacromolecules*, 2010, **11**, 284–293. Copyright 2010 American Chemical Society.

immersion of the polymer brush in an aqueous solution of NaIO_4 (3.0 mg mL^{-1}) for 60 min. The PDHPA microdomains were found to be antibiofouling and prevented non-specific binding of proteins such as streptavidin. In contrast, the aldehyde-functional microdomains covalently bound streptavidin.

These literature examples highlight the potential for the use of aldehyde-based hydrophilic polymers as biosensors both in aqueous solution and on surfaces. Nevertheless, more investigation in this field is certainly warranted, not least because the introduction of aldehyde groups invariably involves use of organic solvents, multistep syntheses, and poorly optimised chemistry (e.g., atom-inefficient protecting group chemistry).

1.7. Thesis outline

This Thesis will focus on the synthesis of a new *cis*-diol-functional methacrylic monomer (GEO5MA) and its conversion into a hydrophilic aldehyde-functional monomer (AGEO5MA). Chapter II describes all of the materials and methods used throughout this Thesis. In Chapter III, GEO5MA is polymerised *via* RAFT solution polymerisation and the resulting homopolymer is converted into a water-soluble aldehyde-functional polymer *via* selective oxidation using a stoichiometric amount of aqueous NaIO_4 . Using sub-stoichiometric amounts of periodate yields a series of statistical copolymers, while oxidation of double-hydrophilic PGEO5MA-based diblock copolymers produces aldehyde-functional water-soluble diblock copolymers. In Chapter IV, the RAFT aqueous dispersion polymerisation of HPMA using a PGEO5MA precursor is used to prepare PGEO5MA-PHPMA diblock copolymer nano-objects. Spheres, worms or vesicles can be obtained by targeting a progressively longer PHPMA block. A pseudo-phase diagram is constructed to enable pure copolymer morphologies to be reproducibly targeted. In the case of the PGEO5MA-PHPMA vesicles, periodate oxidation leads to the formation of aldehyde-functional vesicles that can either (i) be reacted with various amino acids or (ii) be decorated with a model protein (BSA). In both cases, the electrophoretic footprint of the vesicles is modified. Moreover, control experiments conducted using the PGEO5MA-PHPMA vesicles confirm that protein adsorption at the vesicle surface does not occur in the absence of any aldehyde groups. In Chapter V, thermoresponsive PGEO5MA-PHPMA worms are prepared using the design rules established in Chapter IV. As expected, these worms form soft hydrogels in aqueous solution owing to multiple inter-worm contacts. Treatment of such PGEO5MA-PHPMA worms with varying amounts

of NaIO₄ produces a small library of aldehyde-functional hydrogels, which were evaluated in the context of mucoadhesion. The latter studies involved an informal collaboration with Prof. V. Khutoryanskiy's team at the University of Reading. In Chapter VI, the synthesis of a hydrophilic aldehyde-functional polymer brush is explored. This is achieved by SI-ARGET ATRP of GEO5MA from a planar surface to produce a PGEO5MA precursor brush, followed by periodate oxidation to introduce the desired aldehyde functionality. Subsequently, the PAGEO5MA brush is reacted with the amino acid histidine, a cationic amine and a semi-fluorinated amine in a series of model reactions. Such brushes are characterised by ellipsometry, surface zeta potential measurements and XPS. Some overall conclusions and suggestions for future work are presented in Chapter VII.

1.8. References

- 1 J. Blumm, A. Lindemann, M. Meyer and C. Strasser, *Int. J. Thermophys.*, 2010, **31**, 1919–1927.
- 2 G. Moad and D. H. Solomon, *The Chemistry of Radical Polymerization*, Elsevier, Oxford, 2nd edn., 2006.
- 3 R. J. Young and P. A. Lovell, *Introduction to Polymers*, CRC Press, Boca Raton, Florida, 3rd edn., 2001.
- 4 J. O. Edwards, *Progress in inorganic chemistry Vol 17: inorganic reaction mechanisms Part 2 - progress in inorganic chemistry*, John Wiley & Sons, Inc., New York, 1972.
- 5 M. P. Stevens, *Polymer Chemistry: An Introduction*, Addison-Wesley Publishing Company, Inc., Reading, MA, 1975.
- 6 L. A. Camacho-Cruz, M. A. Velazco-Medel and E. Bucio, *Green Sustainable Process for Chemical and Environmental Engineering and Science*, Elsevier B.V., Amsterdam, Netherlands, 2020.
- 7 D. M. Kuznetsov, V. V. Tumanov and W. A. Smit, *J. Polym. Res.*, 2013, **20**, 128.
- 8 T. Biedroń and P. Kubisa, *J. Polym. Sci. Part A Polym. Chem.*, 2004, **42**, 3230–3235.
- 9 S. V. Kostjuk, H. Y. Yeong and B. Voit, *J. Polym. Sci. Part A Polym. Chem.*, 2013, **51**, 471–486.
- 10 W. Lang, P. K. Sarker and S. Rimmer, *Macromol. Chem. Phys.*, 2004, **205**, 1011–1020.
- 11 U. Akbulut, S. Eren and L. K. Toppare, *Polymer*, 1984, **25**, 1028–1030.
- 12 T. Higashimura, Y. Ishihama and M. Sawamoto, *Macromolecules*, 1993, **26**, 744–751.
- 13 Y. Tabata, H. Sobue and E. Oda, *J. Phys. Chem.*, 1961, **65**, 1645–1647.
- 14 C. S. Marvel, R. Gilkey, C. R. Morgan, J. F. Noth, R. D. Rands and C. H. Young, *J. Polym. Sci.*, 1951, **6**, 483–502.
- 15 J. Cheng, B. Han, H. Yang, C. He and G. Jin, *Chinese J. Chem. Eng.*, 1999, **7**, 154–160.

-
- 16 X. Chen, I. S. Ke, M. Li, J. Wu and M. A. Rickard, *J. Raman Spectrosc.*, 2017, **48**, 1002–1006.
- 17 M. Szwarc, M. Levy and R. Milkovich, *J. Am. Chem. Soc.*, 1956, **78**, 2656–2657.
- 18 J. C. Saam, D. J. Gordon and S. Lindsey, *Macromolecules*, 1970, **3**, 1–4.
- 19 D. Walton and P. Lorimer, *Polymers*, Oxford University Press, Oxford, 2005.
- 20 M. Morton, *Ind. Eng. Chem. Prod. Res. Dev.*, 1972, **11**, 106.
- 21 C. E. Carraher Jr., *Seymour/Carraher's Polymer Chemistry*, CRC Press, Boca Raton, 7th edn., 2007.
- 22 D. Greszta and K. Matyjaszewski, *Macromolecules*, 1996, **29**, 7661–7670.
- 23 C. J. Hawker and J. L. Hedrick, *Macromolecules*, 1995, **28**, 2993–2995.
- 24 M. K. Georges, R. P. N. Veregin, P. M. Kazmaier and G. K. Hamer, *Macromolecules*, 1993, **26**, 2987–2988.
- 25 D. Benoit, V. Chaplinski, R. Braslau and C. J. Hawker, *J. Am. Chem. Soc.*, 1999, **121**, 3904–3920.
- 26 C. J. Hawker, G. G. Barclay, A. Orellana, J. Dao and W. Devonport, *Macromolecules*, 1996, **29**, 5245–5254.
- 27 C. J. Hawker, A. W. Bosman and E. Harth, *Chem. Rev.*, 2001, **101**, 3661–3688.
- 28 M. Kato, M. Kamigaito, M. Sawamoto and T. Higashimura, *Macromolecules*, 1995, **28**, 1721–1723.
- 29 J.-S. Wang and K. Matyjaszewski, *J. Am. Chem. Soc.*, 1995, **117**, 5614–5615.
- 30 L. Fetzer, V. Toniazzo, D. Ruch and F. di Lena, *Isr. J. Chem.*, 2012, **52**, 221–229.
- 31 G. Odian, *Principles of Polymerisation*, John Wiley & Sons, Inc., Hoboken, New Jersey, 4th edn., 2004.
- 32 K. Matyjaszewski, *Macromolecules*, 2012, **45**, 4015–4039.
- 33 K. Min and K. Matyjaszewski, *Cent. Eur. J. Chem.*, 2009, **7**, 657–674.
- 34 M. Li and K. Matyjaszewski, *Macromolecules*, 2003, **36**, 6028–6035.
- 35 M. Li and K. Matyjaszewski, *J. Polym. Sci. Part A Polym. Chem.*, 2003, **41**, 3606–3614.
- 36 T. Saigal, H. Dong, K. Matyjaszewski and R. D. Tilton, *Langmuir*, 2010, **26**, 15200–15209.
- 37 F. L. Hatton, J. R. Lovett and S. P. Armes, *Polym. Chem.*, 2017, **8**, 4856–4868.
- 38 K. Matyjaszewski, J. Qiu, N. V. Tsarevsky and B. Charleux, *J. Polym. Sci. Part A Polym. Chem.*, 2000, **38**, 4724–4734.
- 39 W. Jakubowski and K. Matyjaszewski, *Angew. Chemie - Int. Ed.*, 2006, **45**, 4482–4486.
- 40 J. Chiefari, Y. K. Chong, F. Ercole, J. Krstina, J. Jeffery, T. P. T Le, R. T. A Mayadunne, G. F. Meijs, C. L. Moad, G. Moad, E. Rizzardo and S. H. Thang, *Macromolecules*, 1998, **31**, 5559–5562.
-

-
- 41 D. J. Keddie, G. Moad, E. Rizzardo and S. H. Thang, *Macromolecules*, 2012, **45**, 5321–5342.
- 42 C. Barner-Kowollik, Ed., *Handbook of RAFT Polymerisation*, John Wiley & Sons, Inc., Weinheim, Germany, 1st edn., 2008.
- 43 W. A. Braunecker and K. Matyjaszewski, *Prog. Polym. Sci.*, 2007, **32**, 93–146.
- 44 A. Favier and M. T. Charreyre, *Macromol. Rapid Commun.*, 2006, **27**, 653–692.
- 45 G. Moad, A. E. Rizzardo and S. H. Thang, *Aust. J. Chem.*, 2005, **58**, 379–410.
- 46 S. Perrier, *Macromolecules*, 2017, **50**, 7433–7447.
- 47 A. J. Bryztwa and J. Johnson, *Polym. Prepr. Am. Chem. Soc. Div. Polym. Chem.*, 2011, **52**, 533–534.
- 48 G. S. Whitby and M. Katz, *Ind. Eng. Chem.*, 2002, **25**, 1338–1348.
- 49 W. P. Hohenstein and H. Mark, *J. Polym. Sci.*, 1946, **1**, 127–145.
- 50 J. Maul, B. G. Frushour, J. R. Kontoff, H. Eichenauer, K.-H. Ott and C. Schade, *Polystyrene and Styrene Copolymers*, John Wiley & Sons, Inc., Weinheim, Germany, 2007.
- 51 C. R. S. Buono and E. Bittencourt, *Chem. Eng. Trans.*, 2009, **17**, 129–134.
- 52 M. Basuni, W. A. Hassan, Y. A. Youssef, S. M. El-Kousy and M. A. Tawila, *Res. J. Pharm. Biol. Chem. Sci.*, 2016, **7**, 2650–2664.
- 53 F. Yilmaz, Ed., *Polymer Science*, InTech, London, 2013.
- 54 R. G. Gilbert, *Emulsion Polymerization: A Mechanistic Approach*, Academic Press, London, 1995.
- 55 D. H. Napper, *Polymeric Stabilization of Colloidal Dispersions*, Academic Press, London, 1983.
- 56 S. P. Armes and B. Vincent, *J. Chem. Soc. Chem. Commun.*, 1987, 288–290.
- 57 S. P. Armes, M. Aldissi, G. C. Idzorek, P. W. Keaton, L. J. Rowton, G. L. Stradling, M. T. Collopy and D. B. McColl, *J. Colloid Interface Sci.*, 1991, **141**, 119–126.
- 58 C. Obeso-Vera, J. M. Cornejo-Bravo, A. Serrano-Medina and A. Licea-Claverie, *Polym. Bull.*, 2013, **70**, 653–664.
- 59 A. M. I. I. Ali, P. Pareek, L. Sewell, A. Schmid, S. Fujii, S. P. Armes and I. M. Shirley, *Soft Matter*, 2007, **3**, 1003–1013.
- 60 J. O. Zoppe, N. C. Ataman, P. Mocny, J. Wang, J. Moraes and H.-A. Klok, *Chem. Rev.*, 2017, **117**, 1105–1318.
- 61 R. Barbey, L. Lavanant, D. Paripovic, N. Schüwer, C. Sugnaux, S. Tugulu and H.-A. Klok, *Chem. Rev.*, 2009, **109**, 5437–5527.
- 62 X. Yang, W. Zhang, X. Qin, M. Cui, Y. Guo and T. Wang, *Biomimetics*, 2022, **7**, 88.
- 63 L. W. Teunissen, A. R. Kuzmyn, F. S. Ruggeri, M. M. J. Smulders and H. Zuilhof, *Adv. Mater. Interfaces*, 2022, **9**, 2101717.
- 64 A. M. Alswieleh, N. Cheng, I. Canton, B. Ustbas, X. Xue, V. Ladmiral, S. Xia, R. E.
-

-
- Ducker, O. El Zubir, M. L. Cartron, C. N. Hunter, G. J. Leggett and S. P. Armes, *J. Am. Chem. Soc.*, 2014, **136**, 9404–9413.
- 65 T. Bilgic and H.-A. Klok, *Biomacromolecules*, 2015, **16**, 3657–3665.
- 66 J. Klobenstein and C. Laub, *Polym. Prepr. (Am. Chem. Soc. Div. Polym. Chem.)*, 1999, **40**, 126.
- 67 A. Balazs and Y. Lyatskaya, *Macromolecules*, 1998, **31**, 6676.
- 68 G. Di Carlo, F. Damin, L. Armelao, C. MacCato, S. Unlu, P. S. Spuhler and M. Chiari, *Appl. Surf. Sci.*, 2012, **258**, 3750–3756.
- 69 S. Tugulu and H.-A. Klok, *Biomacromolecules*, 2008, **9**, 906–912.
- 70 A. Lishchuk, E. Csányi, B. Darroch, C. Wilson, A. Nabok and G. J. Leggett, *Chem. Sci.*, 2022, **13**, 2405–2417.
- 71 K. Matyjaszewski, D. Hongchen, W. Jakubowski, J. Pietrasik and A. Kusumo, *Langmuir*, 2007, **23**, 4528–4531.
- 72 N. Schüwer and H.-A. Klok, *Langmuir*, 2011, **27**, 4789–4796.
- 73 K. Matyjaszewski, P. J. Miller, N. Shukla, B. Immaraporn, A. Gelman, B. B. Luokala, T. M. Siclovan, G. Kickelbick, T. Vallant, H. Hoffmann and T. Pakula, *Macromolecules*, 1999, **32**, 8716–8724.
- 74 E. D. Bain, K. Dawes, A. E. Özçam, X. Hu, C. B. Gorman, J. Šogl and J. Genzer, *Macromolecules*, 2012, **45**, 3802–3815.
- 75 H. Takahashi, M. Nakayama, M. Yamato and T. Okano, *Biomacromolecules*, 2010, **11**, 1991–1999.
- 76 J. Moraes, K. Ohno, T. Maschmeyer and S. Perrier, *Chem. Mater.*, 2013, **25**, 3522–3527.
- 77 M. H. Stenzel, L. Zhang and W. T. S. Huck, *Macromol. Rapid Commun.*, 2006, **27**, 1121–1126.
- 78 C. D. Grande, M. C. Tria, G. Jiang, R. Ponnampati, Y. Park, F. Zuluaga and R. Advincula, *React. Funct. Polym.*, 2011, **71**, 938–942.
- 79 J. Dilag, H. Kobus and A. V. Ellis, *Forensic Sci. Int.*, 2013, **228**, 105–114.
- 80 G. Pan, Y. Ma, Y. Zhang, X. Guo, C. Li and H. Zhang, *Soft Matter*, 2011, **7**, 8428–8439.
- 81 L. Xiong, X. Li, H. Liang and S. Huang, *Asian J. Chem.*, 2013, **25**, 4032–4034.
- 82 M. Ejaz, S. Yamamoto, K. Ohno, Y. Tsujii and T. Fukuda, *Macromolecules*, 1998, **31**, 5934–5936.
- 83 D. M. Jones and W. T. S. Huck, *Adv. Mater.*, 2001, **13**, 1256–1259.
- 84 W. Huang, J. B. Kim, M. L. Bruening and G. L. Baker, *Macromolecules*, 2002, **35**, 1175–1179.
- 85 J. B. Kim, W. Huang, M. D. Miller, G. L. Baker and M. L. Bruening, *J. Polym. Sci. Part A Polym. Chem.*, 2003, **41**, 386–394.
- 86 B. M. Rosen and V. Percec, *Chem. Rev.*, 2009, **109**, 5069–5119.
- 87 V. Percec, T. Guliasvili, J. S. Ladislav, A. Wistrand, A. Stjerndahl, M. J. Sienkowska,
-

-
- M. J. Monteiro and S. Sahoo, *J. Am. Chem. Soc.*, 2006, **128**, 14156–14165.
- 88 A. J. D. Magenau, N. C. Strandwitz, A. Gennaro and K. Matyjaszewski, *Science*, 2011, **332**, 81–84.
- 89 Y. Kwak and K. Matyjaszewski, *Macromolecules*, 2010, **43**, 5180–5183.
- 90 J. Yan, B. Li, F. Zhou and W. Liu, *ACS Macro Lett.*, 2013, **2**, 592–596.
- 91 M. A. Tasdelen, M. Uygun and Y. Yagci, *Macromol. Chem. Phys.*, 2010, **211**, 2271–2275.
- 92 B. T. Cheesman, E. G. Smith, T. J. Murdoch, C. Guibert, G. B. Webber, S. Edmondson and E. J. Wanless, *Phys. Chem. Chem. Phys.*, 2013, **15**, 14502–14510.
- 93 A. Simakova, S. E. Averick, D. Konkolewicz and K. Matyjaszewski, *Macromolecules*, 2012, **45**, 6371–6379.
- 94 G. J. Dunderdale, C. Urata, D. F. Miranda and A. Hozumi, *ACS Appl. Mater. Interfaces*, 2014, **6**, 11864–11868.
- 95 B. T. Cheesman, J. D. Willott, G. B. Webber, S. Edmondson and E. J. Wanless, *ACS Macro Lett.*, 2012, **1**, 1161–1165.
- 96 J. N. Israelachvili, *Intermolecular and surface forces*, Academic Press, London, 3rd edn., 2011.
- 97 C. Tanford, *Science*, 1978, **200**, 1012–1018.
- 98 C. Tanford, *The Hydrophobic effect: Formation of micelles and biological membranes*, Wiley, 2nd edn., 1980.
- 99 D. Chandler, *Nature*, 2005, **437**, 640–647.
- 100 S. L. Canning, G. N. Smith and S. P. Armes, *Macromolecules*, 2016, **49**, 1985–2001.
- 101 Z. Gao, S. K. Varshney, S. Wong and A. Eisenberg, *Macromolecules*, 1994, **27**, 7923–7927.
- 102 A. J. Paine, Y. Deslandes, P. Gerroir and B. Henrissat, *J. Colloid Interface Sci.*, 1990, **138**, 170–181.
- 103 A. P. Richez, H. N. Yow, S. Biggs and O. J. Cayre, *Prog. Polym. Sci.*, 2013, **38**, 897–931.
- 104 C. Scholz, M. Iijima, Y. Nagasaki and K. Kataoka, *Macromolecules*, 1995, **28**, 7295–7297.
- 105 Y. Geng and D. E. Discher, *J. Am. Chem. Soc.*, 2005, **127**, 12780–12781.
- 106 P. Dalhaimer, A. J. Engler, R. Parthasarathy and D. E. Discher, *Biomacromolecules*, 2004, **5**, 1714–1719.
- 107 Y.-Y. Won, H. Ted Davis and F. S. Bates, *Science*, 1999, **283**, 960–963.
- 108 G. Sun, H. Fang, C. Cheng, P. Lu, K. Zang, A. V. Walker, J.-S. A. Taylor and K. L. Wooley, *ACS Nano*, 2009, **3**, 673–681.
- 109 D. J. Pochan, Z. Chen, H. Cui, K. Hales, K. Qi and K. L. Wooley, *Science*, 2004, **306**, 94–97.
- 110 L. Zhang and A. Eisenberg, *Science*, 1995, **268**, 1728–1731.
-

-
- 111 L. Zhang and A. Eisenberg, *J. Am. Chem. Soc.*, 1996, **118**, 3168–3181.
- 112 N. J. Warren and S. P. Armes, *J. Am. Chem. Soc.*, 2014, **136**, 10174–10185.
- 113 J. Rieger, *Macromol. Rapid Commun.*, 2015, **36**, 1458–1471.
- 114 F. D’Agosto, J. Rieger and M. Lansalot, *Angew. Chemie Int. Ed.*, 2019, **59**, 2–27.
- 115 N. J. Warren, O. O. Mykhaylyk, D. Mahmood, A. J. Ryan and S. P. Armes, *J. Am. Chem. Soc.*, 2014, **136**, 1023–1033.
- 116 A. Blanazs, A. J. Ryan and S. P. Armes, *Macromolecules*, 2012, **45**, 5099–5107.
- 117 V. J. Cunningham, A. M. Alswieleh, K. L. Thompson, M. Williams, G. J. Leggett, S. P. Armes and O. M. Musa, *Macromolecules*, 2014, **47**, 5613–5623.
- 118 K. H. Kim, J. Kim and W. H. Jo, *Polymer*, 2005, **46**, 2836–2840.
- 119 G. Delaittre, J. Nicolas, C. Lefay, M. Save and B. Charleux, *Chem. Commun.*, 2005, **2**, 614–616.
- 120 R. Nagarajan, *Langmuir*, 2002, **18**, 31–38.
- 121 A. Blanazs, J. Madsen, G. Battaglia, A. J. Ryan and S. P. Armes, *J. Am. Chem. Soc.*, 2011, **133**, 16581–16587.
- 122 J. W. van Egmond, *Curr. Opin. Colloid Interface Sci.*, 1998, **3**, 385–390.
- 123 J. R. Lovett, M. J. Derry, P. Yang, F. L. Hatton, N. J. Warren, P. W. Fowler and S. P. Armes, *Chem. Sci.*, 2018, **9**, 7138–7144.
- 124 C. J. Mable, R. R. Gibson, S. Prevost, B. E. McKenzie, O. O. Mykhaylyk and S. P. Armes, *J. Am. Chem. Soc.*, 2015, **137**, 16098–16108.
- 125 C. J. Mable, M. J. Derry, K. L. Thompson, L. A. Fielding, O. O. Mykhaylyk and S. P. Armes, *Macromolecules*, 2017, **50**, 4465–4473.
- 126 L. D. Blackman, S. Varlas, M. C. Arno, A. Fayter, M. I. Gibson and R. K. O’Reilly, *ACS Macro Lett.*, 2017, **6**, 1263–1267.
- 127 L. D. Blackman, S. Varlas, M. C. Arno, Z. H. Houston, N. L. Fletcher, K. J. Thurecht, M. Hasan, M. I. Gibson and R. K. O’Reilly, *ACS Cent. Sci.*, 2018, **4**, 718–723.
- 128 C. Gonzato, M. Semsarilar, E. R. Jones, F. Li, G. J. P. Krooshof, P. Wyman, O. O. Mykhaylyk, R. Tuinier and S. P. Armes, *J. Am. Chem. Soc.*, 2014, **136**, 11100–11106.
- 129 D. Zehm, L. P. D. Ratcliffe and S. P. Armes, *Macromolecules*, 2013, **46**, 128–139.
- 130 J. R. Lovett, N. J. Warren, L. P. D. Ratcliffe, M. K. Kocik and S. P. Armes, *Angew. Chemie Int. Ed.*, 2015, **54**, 1279–1283.
- 131 M. Heskins and J. E. Guillet, *J. Macromol. Sci. Part A - Chem.*, 1968, **2**, 1441–1455.
- 132 A. Blanazs, R. Verber, O. O. Mykhaylyk, A. J. Ryan, J. Z. Heath, C. W. I. Douglas and S. P. Armes, *J. Am. Chem. Soc.*, 2012, **134**, 9741–9748.
- 133 R. Verber, A. Blanazs and S. P. Armes, *Soft Matter*, 2012, **8**, 9915–9922.
- 134 M. K. Kocik, O. O. Mykhaylyk and S. P. Armes, *Soft Matter*, 2014, **10**, 3984–3992.
- 135 S. J. Byard, C. T. O’Brien, M. J. Derry, M. Williams, O. O. Mykhaylyk, A. Blanazs and
-

-
- S. P. Armes, *Chem. Sci.*, 2020, **11**, 396–402.
- 136 O. Wichterle and D. Lím, *Nature*, 1960, **185**, 117–118.
- 137 C. He, S. W. Kim and D. S. Lee, *J. Control. Release*, 2008, **127**, 189–207.
- 138 I. Canton, N. J. Warren, A. Chahal, K. Amps, A. Wood, R. Weightman, E. Wang, H. Moore and S. P. Armes, *ACS Cent. Sci.*, 2016, **2**, 65–74.
- 139 R. Deng, Y. Ning, E. R. Jones, V. J. Cunningham, N. J. W. Penfold and S. P. Armes, *Polym. Chem.*, 2017, **8**, 5374–5380.
- 140 R. Deng, M. J. Derry, C. J. Mable, Y. Ning and S. P. Armes, *J. Am. Chem. Soc.*, 2017, **139**, 7616–7623.
- 141 V. J. Cunningham, L. P. D. Ratcliffe, A. Blanazs, N. J. Warren, A. J. Smith, O. O. Mykhaylyk and S. P. Armes, *Polym. Chem.*, 2014, **5**, 6307–6317.
- 142 M. B. Renfree and G. Shaw, *Int. J. Dev. Biol.*, 2014, **58**, 175–181.
- 143 M. Sponchioni, C. T. O'Brien, C. Borchers, E. Wang, M. N. Rivolta, N. J. W. Penfold, I. Canton and S. P. Armes, *Chem. Sci.*, 2020, **11**, 232–240.
- 144 D. Matioszek, P. E. Dufils, J. Vinas and M. Destarac, *Macromol. Rapid Commun.*, 2015, **36**, 1354–1361.
- 145 A. Postma, T. P. Davis, G. Moad and M. S. O'Shea, *Macromolecules*, 2005, **38**, 5371–5374.
- 146 E. J. Cornel, S. Van Meurs, T. Smith, P. S. O'Hora and S. P. Armes, *J. Am. Chem. Soc.*, 2018, **140**, 12980–12988.
- 147 C. P. Jesson, C. M. Pearce, H. Simon, A. Werner, V. J. Cunningham, J. R. Lovett, M. J. Smallridge, N. J. Warren and S. P. Armes, *Macromolecules*, 2017, **50**, 182–191.
- 148 R. C. Larock, *Comprehensive Organic Transformations: A Guide to Functional Group Preparations, 4 Volume Set, 3rd Edition*, John Wiley & Sons, Inc., New York, 3rd edn., 2018.
- 149 M. B. Smith and J. March, *March's advanced organic chemistry: reactions, mechanisms, and structure*, John Wiley & Sons, Inc., Hoboken, NJ, 2007.
- 150 V. Grignard, *Compt. rend. Hebd. Séances Acad. Sci.*, 1900, **130**, 1322.
- 151 G. Wittig and U. Schöllkopf, *Chem. Ber.*, 1954, **87**, 1318.
- 152 N. Liu, A. Martin, F. Robert, J.-M. Vincent, Y. Landais, J. Vignolle, H. Cramail and D. Taton, *Macromolecules*, 2014, **47**, 525–533.
- 153 S. Y. Onozawa, T. Sakakura, M. Tanaka and M. Shiro, *Tetrahedron*, 1996, **52**, 4291–4302.
- 154 I. Yamaguchi, T. Kimishima, K. Osakada and T. Yamamoto, *J. Polym. Sci. Part A Polym. Chem.*, 1997, **35**, 2821–2825.
- 155 I. Yamaguchi, T. Kimishima, K. Osakada and T. Yamamoto, *J. Polym. Sci. Part A Polym. Chem.*, 1997, **35**, 1265–1273.
- 156 S. Ji, B. Bruchmann and H.-A. Klok, *Macromolecules*, 2011, **44**, 5218–5226.
- 157 R. F. Borch, M. D. Bernstein and H. D. Durst, *J. Am. Chem. Soc.*, 1971, **93**, 2897–2904.
-

-
- 158 A. F. Abdel-Magid, K. G. Carson, B. D. Harris, C. A. Maryanoff and R. D. Shah, *J. Org. Chem.*, 1996, **61**, 3849–3862.
- 159 R. H. Wiley and P. H. Hobson, *J. Polym. Sci.*, 1950, **5**, 483–486.
- 160 J. E. Mulvaney and D. M. Chang, *Macromolecules*, 1980, **13**, 240–243.
- 161 O. Vogl and W. M. D. Bryant, *J. Polym. Sci. Part A Gen. Pap.*, 1964, **2**, 4633–4645.
- 162 C. Taubmann, R. Luxenhofer, S. Cesana and R. Jordan, *Macromol. Biosci.*, 2005, **5**, 603–612.
- 163 A. Hirao and S. Nakahama, *Macromolecules*, 1987, **20**, 2968–2972.
- 164 D. A. Shipp, *Polym. Rev.*, 2011, **51**, 99–103.
- 165 C. Cheng, G. Sun, E. Khoshdel and K. L. Wooley, *J. Am. Chem. Soc.*, 2007, **129**, 10086–10087.
- 166 N. Y. Xiao, A. L. Li, H. Liang and J. Lu, *Macromolecules*, 2008, **41**, 2374–2380.
- 167 M. Shi, A. L. Li, H. Liang and J. Lu, *Macromolecules*, 2007, **40**, 1891–1896.
- 168 G. Sun, C. Cheng and K. L. Wooley, *Macromolecules*, 2007, **40**, 793–795.
- 169 L. Tao, G. Mantovani, F. Lecolley and D. M. Haddleton, *J. Am. Chem. Soc.*, 2004, **126**, 13220–13221.
- 170 J. Collins, S. J. Wallis, A. Simula, M. R. Whittaker, M. P. McIntosh, P. Wilson, T. P. Davis, D. M. Haddleton and K. Kempe, *Macromol. Rapid Commun.*, 2017, **38**, 1600534.
- 171 J. Collins, K. Kempe, P. Wilson, C. A. Blindauer, M. P. McIntosh, T. P. Davis, M. R. Whittaker and D. M. Haddleton, *Biomacromolecules*, 2016, **17**, 2755–2766.
- 172 G. S. Heo, S. Cho and K. L. Wooley, *Polym. Chem.*, 2014, **5**, 3555–3558.
- 173 J. Blankenburg, K. Maciol, C. Hahn and H. Frey, *Macromolecules*, 2019, **52**, 1785–1793.
- 174 C. L. I. Ronald, R. M. Broyer and H. D. Maynard, *J. Polym. Sci. Part A Polym. Chem.*, 2006, **44**, 5004–5013.
- 175 G. Foyer, M. Barriol, C. Negrell, S. Caillol, G. David and B. Boutevin, *Prog. Org. Coatings*, 2015, **84**, 1–8.
- 176 C. Legros, M. C. De Pauw-Gillet, K. C. Tam, S. Lecommandoux and D. Taton, *Eur. Polym. J.*, 2015, **62**, 322–330.
- 177 B. S. Murray and D. A. Fulton, *Macromolecules*, 2011, **44**, 7242–7252.
- 178 N. Xiao, H. Liang and J. Lu, *Soft Matter*, 2011, **7**, 10834–10840.
- 179 N.-Y. Xiao, L. Zhong, W.-J. Zhai and W.-D. Bai, *Acta Polym. Sin.*, 2012, **8**, 818–824.
- 180 C. R. Smith and T. V. RajanBabu, *Tetrahedron*, 2010, **66**, 1102–1110.
- 181 F. Wessendorf, B. Grimm, D. M. Guldi and A. Hirsch, *J. Am. Chem. Soc.*, 2010, **132**, 10786–10795.
- 182 J. Huang, Z. Xiao, H. Liang and J. Lu, *Polym. Int.*, 2014, **63**, 1122–1128.
- 183 J. Huang, X. Chen, H. Qin, H. Liang and J. Lu, *Polymer*, 2019, **160**, 99–106.
-

-
- 184 D. E. Whitaker, C. S. Mahon and D. A. Fulton, *Angew. Chemie Int. Ed.*, 2013, **52**, 956–959.
- 185 H. Otsuka, Y. Nagasaki and K. Kataoka, *Biomacromolecules*, 2000, **1**, 39–48.
- 186 M. Iijima, Y. Nagasaki, T. Okada, M. Kato and K. Kataoka, *Macromolecules*, 1999, **32**, 1140–1146.
- 187 Y. Nagasaki, T. Okada, C. Scholz, M. Iijima, M. Kato and K. Kataoka, *Macromolecules*, 1998, **31**, 1473–1479.
- 188 B. S. Murray, A. W. Jackson, C. S. Mahon and D. A. Fulton, *Chem. Commun.*, 2010, **46**, 8651–8653.
- 189 B. Karagoz, L. Esser, H. T. Duong, J. S. Basuki, C. Boyer and T. P. Davis, *Polym. Chem.*, 2014, **5**, 350–355.
- 190 J. Huang, H. Zhu, H. Liang and J. Lu, *Polym. Chem.*, 2016, **7**, 4761–4770.
- 191 W. Zhao, H. T. Ta, C. Zhang and A. K. Whittaker, *Biomacromolecules*, 2017, **18**, 1145–1156.
- 192 F. Seidi, A. Couffon, M. Prawatborisut and D. Crespy, *Macromol. Chem. Phys.*, 2019, **220**, 1900236.
- 193 H. Salo, P. Virta, H. Hakala, T. P. Prakash, A. M. Kawasaki, M. Manoharan and H. Lönnberg, *Bioconjug. Chem.*, 1999, **10**, 815–823.
- 194 A. B. Ebrahim Attia, Z. Y. Ong, J. L. Hedrick, P. P. Lee, P. L. R. Ee, P. T. Hammond and Y. Y. Yang, *Curr. Opin. Colloid Interface Sci.*, 2011, **16**, 182–194.
- 195 N. Wiradharma, Y. Zhang, S. Venkataraman, J. L. Hedrick and Y. Y. Yang, *Nano Today*, 2009, **4**, 302–317.
- 196 L. Qiu, C. R. Xu, F. Zhong, C. Y. Hong and C. Y. Pan, *ACS Appl. Mater. Interfaces*, 2016, **8**, 18347–18359.
- 197 M. Wu, J. Chen, W. Huang, B. Yan, Q. Peng, J. Liu, L. Chen and H. Zeng, *Biomacromolecules*, 2020, **21**, 2409–2420.
- 198 A. Wolfel, M. R. Romero and C. I. Alvarez Igarzabal, *Eur. Polym. J.*, 2019, **112**, 389–399.
- 199 G. S. Kwon and K. Kataoka, *Adv. Drug Deliv. Rev.*, 1995, **16**, 295–309.
- 200 C. Allen, D. Maysinger and A. Eisenberg, *Colloids Surfaces B Biointerfaces*, 1999, **16**, 3–27.
- 201 M. J. Roberts, M. D. Bentley and J. M. Harris, *Adv. Drug Deliv. Rev.*, 2002, **54**, 459–476.
- 202 J. Milton Harris and R. B. Chess, *Nat. Rev. Drug Discov.*, 2003, **2**, 214–221.
- 203 R. F. Borch and A. I. Hassid, *J. Org. Chem.*, 1972, **37**, 1673–1674.
- 204 M. Fromel, E. M. Benetti and C. W. Pester, *ACS Macro Lett.*, 2022, **11**, 415–421.
- 205 G. Vardar, A. Attar and M. A. Yapaoz, *Prep. Biochem. Biotechnol.*, 2019, **49**, 868–875.
- 206 T. Basinska, S. Slomkowski and M. Delamar, *J. Bioact. Compat. Polym.*, 1993, **8**, 205–219.
- 207 X. Mao, J. Huang, M. F. Leung, Z. Du, L. Ma, Z. Huang, P. Li and L. Gu, *Appl. Biochem.*
-

Biotechnol., 2006, **135**, 229–239.

208 Y. Zou, P. Y. J. Yeh, N. A. A. Rossi, D. E. Brooks and J. N. Kizhakkedathu,
Biomacromolecules, 2010, **11**, 284–293.

Chapter II: Materials and methods

Chapter II: Materials and methods

2.1. Materials

All reagents were used as received unless otherwise stated. GEO5MA was synthesised by Dr C. Jesson at GEO Specialty Chemicals (Hythe, UK). Methyl methacrylate, isopropylidene glycerol pentaethylene glycol ether, 4-methoxyphenol (MEHQ), titanate catalyst, ammonium 2-sulfatoethyl methacrylate (SEM; supplied as a 26% w/v aqueous solution) and 2-hydroxypropyl methacrylate (97%) were kindly donated by GEO Specialty Chemicals (Hythe, UK). 4,4'-Azobis(4-cyanopentanoic acid) (>98%), glycine ($\geq 98\%$), lysine ($\geq 98\%$), histidine ($\geq 98\%$), cysteine (97%), sodium periodate ($\geq 99.8\%$), sodium cyanoborohydride (95%), ethylene glycol dimethacrylate (98%), bovine serum albumin (BSA, 98%), tris(hydroxymethyl)aminomethane (TRISMA; $\geq 99.8\%$), sodium nitrate (NaNO_3 ; 99%), tris(hydroxymethyl)aminomethane hydrochloride ($\geq 99\%$), sodium dihydrogen phosphate (NaH_2PO_4 ; $\geq 99\%$), [2-(methacryloyloxy)ethyl] trimethylammonium chloride (METAC; supplied as an 80% w/w aqueous solution), chitosan (low molecular weight), fluorescein methacrylate (95%), fluorescein isothiocyanate (FITC) (isomer 1) and FITC-dextran (MW = 3,000–5,000 Da), (3-aminopropyl)triethoxysilane (99%), α -bromoisobutyryl bromide (98%), 2,2,2-trifluoroethylamine (99.5%), (2-aminoethyl)trimethylammonium chloride hydrochloride (99%), 1,4 dioxane, d_8 -toluene and deuterium oxide (D_2O) were purchased from Sigma-Aldrich, UK. 2,2'-Azobis[2-(2-imidazolin-2-yl)propane]dihydrochloride ($\geq 97\%$) was purchased from Wako Chemicals (Germany). 2-Cyano-2-propyl dithiobenzoate (>97%) was purchased from Strem Chemicals Ltd (Cambridge, UK). Copper (II) chloride (99%) was purchased from Acros Organics. 4-(((2-Carboxyethyl)thio)carbonothioyl)thio-4-cyanopentanoic acid (>95%) was obtained from Boron Molecular. 2-(Methacryloyloxy)ethyl phosphorylcholine (MPC) was kindly provided by Biocompatibles (Farnham, UK). Tetrahydrofuran, dimethylformamide (DMF), methanol, ethanol, dichloromethane, diethyl ether and N,N,N',N'',N'' -pentamethyldiethylenetriamine (98%) were purchased from Fisher Scientific (UK). d_4 -Methanol, d_8 -toluene and d_7 -DMF were purchased from Goss Scientific Instruments Ltd (Cheshire, UK). Deionised water was used for all experiments involving aqueous solutions.

2.2. Methods

¹H nuclear magnetic resonance spectroscopy (NMR). ¹H NMR spectra were recorded in either D₂O, *d*₇-DMF, *d*₈-toluene or *d*₄-methanol using a 400 MHz Bruker Avance-400 spectrometer at 298 K with 16 scans being averaged per spectrum.

¹³C NMR spectroscopy. Broadband ¹H-decoupled ¹³C spectra were acquired at 100 MHz using a Bruker Avance-400 spectrometer operating at 298 K. All spectra were recorded in D₂O with between 128 and 10,240 scans being averaged per spectrum.

Attenuated total reflectance Fourier transform infrared (ATR-FTIR) spectroscopy. Spectra were recorded using a Perkin Elmer FTIR Spectrum Two equipped with UATR Two diamond with 32 scans being averaged per spectrum.

Aqueous electrophoresis. Zeta potentials for diblock copolymer nanoparticles were analysed using a Malvern Zetasizer Nano ZS instrument equipped with a 4 mW He-Ne laser ($\lambda = 633$ nm) operating at a fixed scattering angle of 173°. Samples were diluted to 0.1% w/w using 1 mM KCl, with either dilute NaOH or HCl being used for pH adjustment as required. Zeta potentials were calculated from the Henry equation using the Smoluchowski approximation.

Aqueous gel permeation chromatography (GPC). PGEO5MA₃₇-PMETAC₅₀ and PAGEO5MA₃₇-PMETAC₅₀ diblock copolymers were analysed at 0.5% w/w concentration in an acidic aqueous buffer comprising 0.50 M acetic acid and 0.30 M NaH₂PO₄ adjusted to pH 2 using concentrated HCl. The GPC set-up comprised an Agilent 1260 Infinity series degasser and pump, an 8 μ m Agilent PL Aquagel-OH 30 column and a 5 μ m Agilent PL Aquagel-OH 20 column. A series of ten near-monodisperse poly(ethylene oxide) (PEO) standards ranging from 3.8 to 780.0 kg mol⁻¹ were used for calibration. A refractive index detector was employed at 35 °C and the flow rate was 1.0 mL min⁻¹.

0.5% w/w PGEO5MA₃₇-PMPC₅₀ and PAGEO5MA₃₇-PMPC₅₀ diblock copolymers were analysed using an eluent comprising 0.20 M NaNO₃ and 0.05 M TRISMA buffer adjusted to pH 7 using concentrated HCl. The GPC set-up comprised an Agilent 1260 Infinity series degasser and pump, an 8 μ m Agilent PL Aquagel-OH 30 column and a 5 μ m Agilent PL Aquagel-OH 20 column. A series of ten near-monodisperse PEO standards ranging from 3.8 to 780.0 kg mol⁻¹ were used for calibration. A refractive index detector was employed at 35 °C and the flow rate was 1.0 mL min⁻¹.

0.5% w/w PGEO5MA₃₇-PSEM₅₀ and PAGEO5MA₃₇-PSEM₅₀ diblock copolymers were analysed using an eluent comprising 0.20 M NaNO₃ and 0.05 M TRISMA buffer adjusted to pH 7 using concentrated HCl. The GPC set-up comprised an Agilent 1260 Infinity series degasser and pump, an 8 µm Agilent PL Aquagel-OH 40 column and a 5 µm Agilent PL Aquagel-OH 30 column. A series of ten near-monodisperse PEO standards ranging from 3.8 to 780.0 kg mol⁻¹ were used for calibration. A refractive index detector was employed at 35 °C and the flow rate was 1.0 mL min⁻¹.

Centrifugation. Centrifugation of BSA functionalised vesicles was conducted using a Thermo Heraeus Biofuge Pico centrifuge.

DMF GPC. GPC was used to determine the number-average molecular weights (M_n) and dispersities (\mathcal{D}) of all (co)polymers. The instrument set-up comprised two Agilent PL gel 5 µm Mixed-C columns and a guard column connected in series to an Agilent 1260 Infinity GPC system operating at 60 °C. The GPC eluent was HPLC-grade DMF containing 10 mmol LiBr at a flow rate of 1.0 mL min⁻¹ and calibration was achieved using either a series of ten near-monodisperse poly(methyl methacrylate) (PMMA) standards ranging from 1.0 to 1,020.0 kg mol⁻¹ or a series of ten near-monodisperse PEO standards ranging from 3.8 to 780.0 kg mol⁻¹. Copolymer solutions (1.0% w/w) were prepared in DMF. Chromatograms were analysed using Agilent GPC/SEC software.

Dynamic light scattering (DLS). DLS studies were performed using a Malvern Zetasizer Nano-ZS instrument equipped with a 4 mW He-Ne laser ($\lambda = 633$ nm) operating at a fixed scattering angle of 173°. Copolymer dispersions were diluted to 0.1% w/w in deionised water prior to light scattering studies at 25 °C with 120 s allowed for thermal equilibrium prior to each measurement. The intensity-average hydrodynamic particle diameters were calculated *via* the Stokes-Einstein equation.

Elemental analysis. CHN contents were determined using an Elementar vario MICRO cube analyser.

Flow-through technique for ex vivo mucoadhesion studies. Porcine urinary bladder tissues were received from P.C. Turner Abattoirs (Farnborough, UK) immediately after animal slaughter and used within 24 h. Such bladder tissue was used to evaluate mucosal retention of the worm gels (or chitosan) using an established flow-through method involving fluorescence detection.¹⁻³ Tissues were carefully dissected (avoiding contact with

the internal mucosa) using disposable sharp blades to yield 2 x 2 cm sections, which were then used for the experiments. Dissected bladder tissue was mounted on a glass slide with the mucosal side facing upward and pre-rinsed with 3.0 mL of artificial urine (AU) solution (pH 6.20) before commencing each *ex vivo* mucoadhesion test. Experiments to assess the retention of each worm gel on urinary bladder mucosa were performed at 37 °C and 100% relative humidity within an incubator. Fluorescence images were recorded for the mucosal surface of the bladder using a Leica MZ10F stereomicroscope (Leica Microsystems, UK) equipped with a Leica DFC3000G digital camera fitted with a green fluorescence protein filter at 1.25× magnification using an exposure time of 485 ms and a 2.0× gain. Initially, images of bare bladder tissue (without any test material) were acquired to determine the background fluorescence intensity for each sample.

Aqueous solutions of FITC-chitosan (1.0 mg mL⁻¹ in 0.5% acetic acid) and FITC-dextran (1.0 mg mL⁻¹ in deionised water) were prepared for use as positive and negative controls, respectively. The FITC-chitosan solution was adjusted to pH 6.0 using 0.1 M NaOH. Then a 200 µL aliquot of either a fluorescently-labelled 12% w/w PGE05MA₁₃-P(HPMA₁₅₅-*stat*-FMA_{0.15}) worm gel prepared in deionised water or a control sample was pipetted onto a mucosal surface and repeatedly washed with AU solution at a flow rate of 2.0 mL min⁻¹ using a syringe pump (total washing time was 60 min). A microscopy image of the mucosal surface of each bladder sample was collected at predetermined time points and then analysed with ImageJ software by measuring the pixel intensity after each wash. The pixel intensity of the control samples was subtracted from each measurement to obtain normalised intensities. Images from control samples were collected using an exposure time of 20 ms at 1.0× gain. All measurements were conducted in triplicate.

Liquid chromatography-mass spectrometry (LC-MS). Mass spectrometry analysis was conducted using an Agilent 6530 Accurate-Mass Q-TOF instrument connected to an Agilent 1260 Infinity liquid chromatograph equipped with an Agilent extended C18 2.1 mm x 50 mm column. The mobile phase consisted of solvent A (0.1% aqueous formic acid) and solvent B (acetonitrile with 0.1% formic acid) run as a gradient ranging from 5 to 95% solvent B over a 10 min period. The injection volume was 1.0 µL and the flow rate was 0.40 ml min⁻¹. Samples were analysed using the electrospray ionisation positive mode unless otherwise stated.

4-Methoxyphenol (MEHQ) inhibitor content. The MEHQ content was determined according to ASTM D 3125 using a ThermoScientific Evolution 220 UV-visible spectrophotometer.

OH number and water content. OH numbers were determined by titration according to ASTM E 326 using a Mettler Toledo T70 Titroprocessor. Water contents were determined by titration according to ASTM E 203 using a Metrohm 787 KF Titrator.

Rheology. An AR-G2 rheometer equipped with a variable temperature Peltier plate and a 40 mm 2° aluminum cone was used for all rheological experiments. Preliminary strain sweep experiments were performed on worm gels at 0.1 to 20% strain and a constant angular frequency of 1.0 rad s⁻¹ to assess their gel strength and to identify the linear viscoelastic region. Subsequently, the storage modulus (G'), loss modulus (G'') and complex viscosity ($|\eta^*|$; the resistance to flow as a function of angular frequency, which is calculated by dividing G' by G'' using the rheometer software) were determined as a function of temperature at an applied strain of 1.0% and an angular frequency of 1.0 rad s⁻¹. The gels were initially cooled to 5 °C for 10 min, prior to heating to 37 °C and allowing 10 min for thermal equilibrium at the latter temperature.

Small-angle X-ray scattering (SAXS). SAXS patterns were recorded using a Xeuss 2.0 laboratory beamline (Xenocs, Grenoble, France) equipped with a 2D Pilatus 1M pixel detector (Dectris, Baden-Daettwil, Switzerland) and a MetalJet X-ray source (Ga K α radiation, $\lambda = 1.34 \text{ \AA}$; Excillum, Kista, Sweden). The scattering vector range was $0.006 \text{ \AA}^{-1} < q < 0.2 \text{ \AA}^{-1}$, where $q = \frac{4\pi}{\lambda} \sin\theta$ and θ is half of the scattering angle. Glass capillaries of 2.0 mm diameter were used as a sample holder and the sample temperature was controlled using a HFSX350-CAP heating/cooling stage (Linkam Scientific Instruments Ltd, Tadworth, UK), with 10 min being allowed for thermal equilibration of each capillary prior to data collection. 2D X-ray scattering patterns were reduced using software supplied by the SAXS instrument manufacturer. Background subtraction and further data analysis were performed using Irena SAS macro (version 2.61) for Igor Pro.⁴ The scattering of pure water was used for absolute intensity calibration of the SAXS patterns.

Spectroscopic ellipsometry. Dry ellipsometry measurements were performed on bare silicon wafers, initiator-functionalised silicon wafers or polymer brush-functionalised silicon wafers. Measurements were performed in air and at room temperature using a J. A. Woollman M2000 V ellipsometer at a fixed angle of incidence of 75° to the sample surface normal. Measurements were conducted over a wavelength range of 370 to 1000 nm to

obtain the ellipsometry parameters Ψ and Δ . These parameters were fitted to a 2-layer model consisting of a native oxide layer and Cauchy layer (Equation 2.1). Data analysis and modelling were performed using Woollam CompleteEASE software, which fits the values of Ψ and Δ calculated from this 2-layer model to the experimentally measured values.

$$n(\lambda) = A_n = \frac{B_n}{\lambda^2} + \frac{C_n}{\lambda^4} \quad \text{Equation 2.1}$$

Statistical analysis for ex vivo mucoadhesion studies. Mucoadhesion data (expressed as mean values \pm standard deviations) were calculated and assessed for significance using a two-tailed Student's t-test and a one-way analysis of variance followed by the Bonferroni post hoc test using GraphPad Prism software (version 7.0), where $p < 0.05$ was taken to be significant.

Surface zeta potential measurements via laser Doppler electrophoresis. Surface zeta potentials were calculated for selected polymer brushes from laser Doppler electrophoresis data obtained using Malvern Zetasizer instrument equipped with a Malvern Surface Zeta Potential ZEN1020 dip cell. Polymer brushes grown from planar silicon wafers (4 x 5 mm) were attached to the sample holder using an ethyl cyanoacrylate-based adhesive (Gorilla Super Glue, Gorilla Glue Europe) and the wafer-loaded sample holder was placed into the Malvern ZEN1020 dip cell. The Zetasizer instrument set up detects forward-scattered light at an angle of 13° with the attenuator adjusted to 100% laser transmission (position eleven). Voltage selection was set to automatic (typically 10 V). The dip cell was placed in a cuvette containing 1.0 mL of either 0.003% w/w neutral PGMA₅₈-PBzMA₅₀₀ or cationic PMETAC₄₇-PBzMA₁₀₀ tracer nanoparticles in the presence of 1 mM KCl at 25 °C. This nanoparticle concentration was chosen to provide an optimal derived count rate of 500 kcps under the stated operating conditions.⁵ Five slow-field reversal measurements were performed at four distances from the sample surface (125, 250, 375 and 500 μm), with each measurement comprising 15 sub-runs and a 1 min interval being allowed between measurements. Lastly, three fast-field reversal measurements were performed at a distance of 1000 μm from the sample surface to calculate the electro-osmotic mobility of the tracer nanoparticles. In this case, each measurement consisted of 100 sub-runs with an interval of 20 s being allowed between each measurement. Zeta potentials were calculated *via* the Henry equation using the Smoluchowski approximation.

Transmission electron microscopy (TEM). Copper/palladium TEM grids (Agar Scientific, UK) were coated in-house to yield a thin film of amorphous carbon. The grids were subjected to a glow discharge for 30 s. Aqueous droplets of copolymer dispersions (5.0 μL , 0.1% w/w) were placed on freshly treated grids for 1 min and then carefully blotted with filter paper to remove excess solution. Aqueous droplets of uranyl formate solution (5 μL , 0.75% w/w) were then placed on the sample-loaded grids for 20 s and blotted with filter paper to remove excess stain. This negative staining protocol ensured sufficient electron contrast. Each grid was then dried using a vacuum hose. Imaging was performed at 80 kV using an FEI Tecnai Spirit 2 microscope fitted with an Orius SC1000B camera.

X-ray photoelectron spectroscopy (XPS). Polymer brushes grown from planar silicon wafers were analysed using a Kratos Axis Supra X-ray photoelectron spectrometer. Step sizes of 0.50 and 0.05 eV were used to record survey spectra and high-resolution spectra, respectively. In each case, spectra were recorded from at least two separate areas. The XPS data were analysed using Casa XPS software (UK). All binding energies were calibrated with respect to the C 1s saturated hydrocarbon peak at 285.0 eV.

2.3. References

- 1 E. A. Mun, A. C. Williams and V. V. Khutoryanskiy, *Int. J. Pharm.*, 2016, **512**, 32–38.
- 2 D. B. Kaldybekov, P. Tonglairoum, P. Opanasopit and V. V. Khutoryanskiy, *Eur. J. Pharm. Sci.*, 2018, **111**, 83–90.
- 3 D. B. Kaldybekov, S. K. Filippov, A. Radulescu and V. V. Khutoryanskiy, *Eur. J. Pharm. Biopharm.*, 2019, **143**, 24–34.
- 4 J. Ilavsky and P. R. Jemian, *J. Appl. Crystallogr.*, 2009, **42**, 347–353.
- 5 T. E. Thomas, S. Al Aani, D. L. Oatley-Radcliffe, P. M. Williams and N. Hilal, *J. Memb. Sci.*, 2017, **523**, 524–532.

*Chapter III: New
aldehyde-functional methacrylic
water-soluble polymers*

Reproduced in full with permission from:

E. E. Brotherton, C. P. Jesson, N. J. Warren, M. J. Smallridge and S. P. Armes, *Angew. Chemie Int. Ed.*, 2021, **60**, 12032–12037.

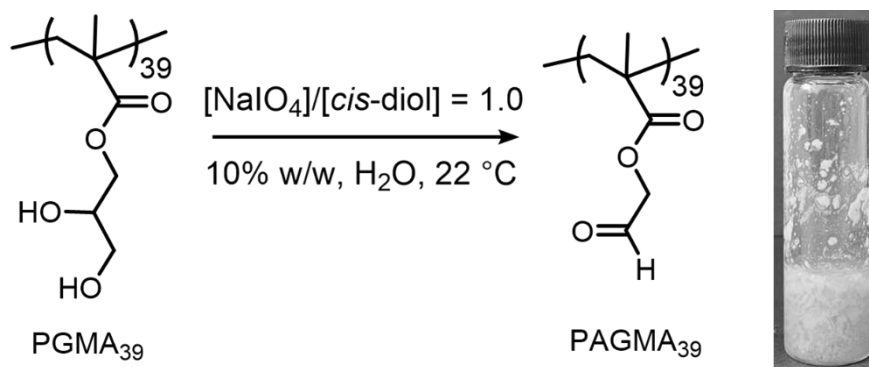
Chapter III: New aldehyde-functional methacrylic water-soluble polymers

3.1. Introduction

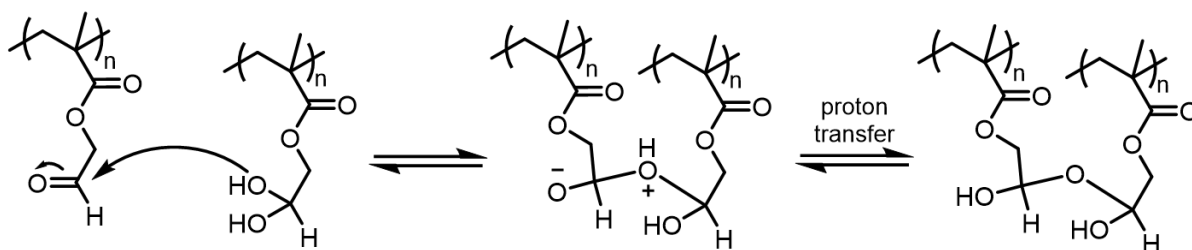
Aldehydes are extremely useful functional groups in synthetic organic chemistry: they can be oxidised to give carboxylic acids, reduced to afford alcohols, undergo Schiff base chemistry and also form (hemi)acetals.¹ In the field of synthetic polymer chemistry, aldehyde-based initiators^{2–8} have been utilised to prepare various types of aldehyde-functional polymers. Alternatively, Bilgic and Klok derivatised poly(2-hydroxyethyl methacrylate) brushes under oxidative conditions in order to introduce aldehyde groups for subsequent oligonucleotide conjugation.⁹ However, surprisingly few aldehyde-functional monomers have been reported in the literature.^{10–25} Most of these examples are hydrophobic (e.g., 4-vinylbenzaldehyde) and hence produce water-insoluble polymers.^{12–15,22,25–32} This is unfortunate, because aldehyde groups enable facile conjugation to peptides/proteins and water-soluble dyes in aqueous solution under mild conditions.^{2–5,10,17,33–38} In principle, this problem can be circumvented by statistical copolymerisation of the hydrophobic aldehyde-functional monomer with a sufficiently hydrophilic comonomer.^{17–19,21,35,39} Alternatively, the incorporation of a terminal protected aldehyde moiety onto a polyethylene glycol (PEG) chain has been utilised to confer aldehyde functionality under aqueous conditions.^{5–8,40,41} Nevertheless, despite the remarkable progress made in synthetic polymer chemistry over the past few decades, there seem to be few, if any, literature examples of *hydrophilic* aldehyde-functional vinyl monomers (and their corresponding water-soluble homopolymers).

One well-known route to aldehyde-terminated water-soluble polymers is the selective oxidation of the minor fraction of *cis*-diol units within poly(vinyl alcohol).⁴² This water-soluble polymer can be obtained *via* hydrolysis of poly(vinyl acetate), which contains defect sites resulting from a small amount of head-to-head coupling during the free radical homopolymerisation of vinyl acetate.⁴³ Such oxidation is readily achieved in aqueous solution under mild conditions using sodium periodate (NaIO₄).⁴⁴ Inspired by this well-established chemistry, the periodate oxidation of poly(glycerol monomethacrylate) (PGMA) to produce an aldehyde-functional methacrylic polymer was investigated (see Scheme 3.1). However, periodate oxidation of a 10% w/w aqueous solution of PGMA₃₉ at 22 °C merely produced a macroscopic precipitate. This suggests that the target

aldehyde-functional methacrylic homopolymer (PAGMA) is actually hydrophobic. In principle, such precipitation could be the result of reaction between the *cis*-diol and aldehyde units at intermediate conversion. However, reaction exotherms (see Appendix 1) and visual inspection of the reaction mixtures suggest that the timescale required for the *cis*-diol oxidation is much shorter than that for precipitation. Thus, it seems more likely that intermolecular crosslinking occurs between geminal diols and aldehydes (Scheme 3.2).



Scheme 3.1. Selective oxidation of a water-soluble PGMA₃₉ homopolymer precursor using a stoichiometric amount of NaIO₄ in aqueous solution at 22 °C affords PAGMA₃₉ as a water-insoluble precipitate.



Scheme 3.2. Crosslinking side reaction that can occur between aldehyde and geminal diol groups on PAGMA.

In view of these problems, a new *cis*-diol-based methacrylic monomer (GEO5MA) was designed. It was envisaged that the pendent oligo(ethylene glycol) moiety in GEO5MA should confer sufficient hydrophilic character to ensure water solubility after converting its terminal *cis*-diol group into an aldehyde *via* periodate oxidation to form either AGE05MA monomer or the corresponding PAGE05MA homopolymer.

3.2. Experimental

3.2.1. Synthesis

Transesterification of isopropylidenglycerol penta(ethylene glycol) ether to afford IPGEO5MA

A 5 L transesterification rig equipped with an air sparge was charged with isopropylidenglycerol penta(ethylene glycol) ether (1500 g, 4.26 mol), methyl methacrylate (MMA) (2300 g, 22.97 mol) and 4-methoxyphenol (MEHQ) (1.30 g, 10.4 mmol). This reaction mixture was heated to 115 °C at a constant air sparge rate of 300 mL min⁻¹. Water/MMA distillate was periodically removed from the still head until the headspace reached a constant temperature (~100 °C) after 2 h. Titanate catalyst (2.0 g) was added by syringe and transesterification was allowed to proceed for 2 h under partial take-off conditions. The reactor was periodically topped up with MMA to maintain a constant reaction volume. Once the head temperature reached 95 °C, the reaction was switched to 'run and bump' conditions. Thus, the still head was allowed to fill up prior to draining in order to concentrate methanol within the distillate. The still head was drained every 20 min for 2 h, after which transesterification was deemed complete. The reaction mixture was allowed to cool overnight. The following day, MMA was stripped from the same rig at 80 °C under vacuum for 2 h. Deionised water (400 g) was added and allowed to react for 1 h at 80 °C in order to deactivate the titanate catalyst. The resulting precipitate was removed by filtration and the water was removed under vacuum at 80 °C for 2 h. The resulting colourless liquid (IPGEO5MA, 1500 g) had a water content of 0.01% w/w and an OH number of 2.63 mg KOH g⁻¹. If full conversion had been achieved, an OH number of 0 mg KOH g⁻¹ would be expected in the absence of any water. Thus, the measured value indicates that high conversion was achieved for this transesterification reaction.

Acidic Deprotection of IPGEO5MA

IPGEO5MA (1500 g) was treated with an Ambersep 900 OH resin (150 g) to remove MEHQ inhibitor. The reaction solution was stirred for 20 min at 22 °C and the resin was removed by filtration. The residual level of MEHQ was determined to be 25 ppm using UV spectroscopy and this was subsequently topped up to 100 ppm by adding fresh MEHQ (0.115 g, 0.92 mmol). The IPGEO5MA was placed in a 3 L flask followed by addition of deionised water (300 g) and concentrated (37%) hydrochloric acid (11 g). This reaction mixture was stirred for 48 h using a 300 mL min⁻¹ air sparge, while water was periodically topped up to maintain a constant reaction volume. The resulting homogeneous solution was neutralised using an ion exchange resin (150 g), which was then removed by filtration.

Finally, water was removed from the reaction solution at 50 °C under vacuum for 4 h prior to analysis. The resulting yellowish liquid had a water content of 0.3 % w/w and an OH number of 289 mg KOH g⁻¹. If full conversion had been achieved, an OH number of 294 mg KOH g⁻¹ would be expected in the absence of any water. Thus, high conversion was achieved for this acid deprotection. Elemental microanalyses: C, 52.59; H, 8.66; N, 0.0%. C₁₇H₃₂O₉ requires C, 52.69; H, 8.22; N, 0.0%; FTIR (ATR ν_{\max} , cm⁻¹): 3442 (-OH, H-bonded), 2870 (C-H stretch), 1716 (C=O ester), 1637 (C=C stretch), 1453 (-CH₃), 1403 (-OH bending, alcohol), 1098 (C-O stretch, aliphatic ether); ¹H NMR (400 MHz; D₂O), *J* values given in Hz, δ = 1.86 (3H, s, CH₃C), 3.39–3.78 (22H, m, CH₂CH₂O), 3.80 (1H, m, CH₂CHOHCH₂OH), 4.26 (2H, t, 4.5 Hz, CH₂CH₂O), 5.66 (1H, s, CH₂CH₂), 6.08 (1H, s, CH₂CH₂); ¹³C NMR (125 MHz, D₂O) δ = 159.56, 135.73, 127.04, 71.75, 70.33, 69.77, 68.63, 64.23, 62.60, 17.45; MS ESI positive m/z (M+H)⁺ requires 381.4, found 381.2.

Oxidation of GEO5MA using NaIO₄ and isolation of AGEO5MA monomer

GEO5MA monomer (10 g, 0.026 mol) and NaIO₄ (5.62 g, 0.026 mol) were dissolved in water (150 g) and stirred in the dark at 22 °C. The extent of oxidation of the *cis*-diol group to afford an aldehyde (or hydrated geminal diol) group was determined to be \geq 99% within 5 min by ¹H NMR spectroscopy. The AGEO5MA monomer was purified by extraction with dichloromethane and excess solvent was removed under reduced pressure to give a yellowish viscous liquid (7.5 g, 82%). ¹H NMR spectroscopy studies in *d*₈-toluene indicated that, after drying, the purified AGEO5MA monomer was predominantly in its aldehyde form (62%) with the remaining 38% corresponding to its hydrated geminal diol form. Elemental microanalyses: 62% C₁₆H₂₈O₈ + 38% C₁₆H₃₀O₉ requires C, 54.13%; H, 8.16%; N, 0.0%. Found: C, 53.97%; H, 7.98%; N, 0.0%. FTIR (ATR ν_{\max} , cm⁻¹): 3425 (-OH, H bonded), 2870 (C-H stretch), 1716 (C=O ester), 1637 (C=C stretch), 1453 (-CH₃), 1404 (-OH bending, alcohol), 1098 (C-O stretch, aliphatic ether); ¹H NMR (400 MHz; D₂O), *J* values given in Hz, δ = 1.87 (3H, s, CH₃C), 3.43 (2H, t, *J* 4.0 Hz, CH₂CH₂O), 3.59–3.69 (18H, m, CH₂CH₂O), 3.76 (2H, t, *J* 4.5 Hz, CH₂CH₂O), 4.27 (2H, m, C(=O)OCH₂CH₂), 5.09 (1H, m, CHC(OH)₂), 5.67 (1H, s, CH₂CH₂), 6.09 (1H, s, CH₂CH₂), 9.52 (1H, s, C(=O)H); ¹³C NMR (125 MHz, D₂O) δ = 202.9, 169.4, 135.8, 126.9, 88.4, 73.5, 69.7, 68.7, 64.2, 17.5. MS ESI positive m/z (M+Na)⁺ requires 389.4, found 389.2.

Synthesis of PAGEO5MA₃₀ homopolymer by reversible addition-fragmentation chain-transfer (RAFT) aqueous solution polymerisation

AGEO5MA monomer (1.50 g, 4.31 mmol), 4-(((2-carboxyethyl)thio)carbonothioyl)thio)-4-cyanopentanoic acid (CECPA) RAFT agent (0.0441 g, 0.14 mmol), 2,2'-azobis[2-(2-imidazolin-2-yl)propane]dihydrochloride (VA-044) initiator (9.3 mg,

29 μmol ; CECPA/VA-044 molar ratio = 5.0) and H_2O (8.8 g) were weighed into a 30 mL sample vial. The reaction solution was degassed *via* N_2 purge for 30 min before placing the sample vial into an oil bath set at 50 $^\circ\text{C}$ for 5 h. The polymerisation was quenched by removing the sample vial from the oil bath and exposing the reaction mixture to air. The AGE05MA conversion was determined to be more than 99% by ^1H NMR spectroscopy by comparing the integrated monomer vinyl signals at 5.69 and 6.11 ppm to the integrated signal assigned to the two oxymethylene protons attached to the ester group for the monomer (4.12 ppm) and polymer (4.38 ppm), respectively.

Synthesis of PGEO5MA₃₇ homopolymer by RAFT solution polymerisation in ethanol

GEO5MA monomer (30.0 g, 0.079 mol), 2-cyano-2-propyl benzodithioate (CPDB) RAFT agent (0.437 g, 1.97 mmol) and 4,4'-azobis(4-cyanovaleric acid) (ACVA) initiator (0.111 g, 0.395 mmol; CPDB/ACVA molar ratio = 5.0) were weighed into a 100 mL round-bottomed flask. Ethanol (20 g) was added and the reaction solution was degassed *via* N_2 purge for 40 min. Then the reaction mixture was heated for 120 min [target degree of polymerisation (DP) of 30 based on the reaction kinetics; Appendix 2] by immersing the flask in an oil bath set at 70 $^\circ\text{C}$. The polymerisation was quenched by removing the flask from the oil bath and exposing the reaction mixture to air. The GEO5MA conversion was 72% as determined by ^1H NMR spectroscopy by comparing the integrated monomer vinyl signals at 5.66 and 6.14 ppm to the integrated signal assigned to the two oxymethylene protons attached to the ester group for the monomer (4.16 ppm) and polymer (4.31 ppm), respectively. The crude PGEO5MA was precipitated into excess diethyl ether to remove unreacted GEO5MA and any other impurities, filtered and redissolved in methanol. After reprecipitation into excess diethyl ether, the product was redissolved in water and freeze-dried to produce a viscous red liquid. The mean DP of the purified PGEO5MA₃₇ was determined to be 37 by end-group analysis using ^1H NMR spectroscopy: the integrated five aromatic protons assigned to the dithiobenzoate chain-end at 7.34–8.03 ppm were compared to the two oxymethylene proton signals attached to the ester group at 4.02–4.34 ppm and also to the five methacrylic backbone signals at 0.78–2.71 ppm.

Oxidation of PGEO5MA₃₇ homopolymer using NaIO_4

The oxidation of PGEO5MA₃₇ using a NaIO_4 /*cis*-diol molar ratio of unity is representative of the general protocol. PGEO5MA₃₇ homopolymer (0.22 g, 15.7 μmol) was added to 2.0 mL of a 0.29 M aqueous solution of NaIO_4 to give a polymer concentration of 10% w/w. This reaction mixture was stirred for 30 min at 22 $^\circ\text{C}$. The extent of oxidation was determined by ^1H NMR spectroscopy by comparing the integrated proton signals assigned to the

aldehyde proton at 9.51 ppm and the proton adjacent to the geminal diols at 5.13 ppm to that of the two oxymethylene protons attached to the ester group at 4.11 ppm. The resulting PAGEO5MA₃₇ solution was purified by dialysis against deionised water for two days (with three changes of water per day). Partial oxidation of PAGEO5MA₃₇ was achieved in essentially the same way. However, a lower NaIO₄/*cis*-diol molar ratio was used in each case.

Synthesis of a PAGEO5MA homopolymer by free-radical polymerisation (FRP) in aqueous solution

GEO5MA monomer (0.5 g, 1.31 mmol), ACVA initiator (9.2 mg, 32.9 μmol) and water (10 g) were weighed into a 27 mL sample vial. The reaction solution was degassed *via* N₂ purge for 30 min. The reaction mixture was then heated for 18 h by immersing the sample vial in an oil bath set at 70 °C. The polymerisation was quenched by removing the vial from the oil bath and exposing the reaction mixture to air. The GEO5MA conversion was more than 99% as determined by ¹H NMR spectroscopy (the integrated monomer vinyl signals at 5.66 and 6.14 ppm were compared to the integrated signal assigned to the two oxymethylene protons attached to the ester group for the monomer (4.16 ppm) and polymer (4.31 ppm), respectively). Selective oxidation of this polydisperse homopolymer [$M_n = 12.4 \text{ kg mol}^{-1}$; $D = 4.55$, as indicated by DMF GPC analysis vs. a series of poly(methyl methacrylate) (PMMA) calibration standards] was achieved under the same conditions as those employed for the near-monodisperse PAGEO5MA₃₇ homopolymer.

Derivatisation of PAGEO5MA₃₇ homopolymer with various amino acids

The following protocol for the reductive amination of PAGEO5MA₃₇ with glycine is representative. PAGEO5MA₃₇ (1.00 g of a 10% w/w aqueous solution), glycine (23.4 mg, 0.31 mmol) and excess sodium cyanoborohydride (NaCNBH₃; 48.1 mg, 0.77 mmol) were weighed into a 15 mL sample vial. A glycine/aldehyde molar ratio of unity was employed in combination with a 2.45-fold excess of NaCNBH₃. The reaction mixture was stirred at 35 °C for 48 h to ensure full conversion of aldehyde to the corresponding secondary amine *via* the imine intermediate. The overall conversion was determined by ¹H NMR spectroscopy by comparing the integrated residual geminal diol signal at 5.10 ppm with the five methacrylic backbone protons at 0.78–2.71 ppm. The resulting aqueous solution of glycine-functionalised PAGEO5MA₃₇ was purified by dialysis against deionised water for two days (with at least three water changes per day). Essentially the same protocol was used for cysteine (37.8 mg, 0.31 mmol) and lysine (45.7 mg, 0.31 mmol) instead of glycine.

Synthesis of PEG₁₁₃-PGEO5MA₅₀ diblock copolymer via RAFT aqueous solution polymerisation of GEO5MA

A trithiocarbonate-capped PEG₁₁₃ macro-CTA (0.281 g, 52.5 μ mol), GEO5MA monomer (1.00 g, 2.62 mmol), VA-044 initiator (3.4 mg, 10.5 μ mol) and water (1.93 g) were weighed into a 15 mL sample vial. A macro-CTA/initiator ratio of 5.0 was employed and a copolymer concentration of 40% w/w was targeted. The reaction solution was degassed for 30 min before placing the sample vial into an oil bath set at 50 °C for 18 h. The polymerisation was quenched by removing the vial from the oil bath and exposing the reaction mixture to air. The GEO5MA monomer conversion was determined to be more than 99% by ¹H NMR spectroscopy (the integrated vinyl monomer signals at 5.66 and 6.08 ppm were compared to that of the two oxymethylene protons attached to the ester group in the GEO5MA repeat units at 4.26 ppm).

Synthesis of PGEO5MA₃₇-PX₅₀ diblock copolymers via RAFT aqueous solution polymerisation

The synthesis of a PGEO5MA₃₇-poly[2-(methacryloyloxy)ethyl phosphorylcholine]₅₀ (PMPC) diblock copolymer is representative and was conducted as follows. PGEO5MA₃₇ macro-CTA (0.241 g, 16.9 μ mol), MPC monomer (0.25 g, 0.847 mmol), ACVA initiator (1.2 mg, 4.23 μ mol) and water (1.97 g) were weighed into a 15 mL sample vial. A total copolymer concentration of 20% w/w was targeted and a macro-CTA/initiator ratio of 4.0 was employed. The reaction solution was degassed for 30 min before placing the sample vial into an oil bath set at 70 °C for 18 h. The MPC conversion was determined to be more than 98% by ¹H NMR spectroscopy (the integrated vinyl monomer signals at 6.56–6.11 ppm were compared to the methacrylic backbone signals at 0.31–2.46 ppm). The other two diblock copolymers were prepared by replacing the MPC monomer with either [2-(methacryloyloxy)ethyl] trimethylammonium chloride (METAC; 0.32 g of an 80% w/w stock solution, 0.12 mmol) or ammonium 2-sulfatoethyl methacrylate (SEM; 0.96 g of a 26% w/w stock solution, 0.11 mmol).

Oxidation of PEG₁₁₃-PGEO5MA₃₇ and PGEO5MA₃₇-PX₅₀ diblock copolymers using NaIO₄

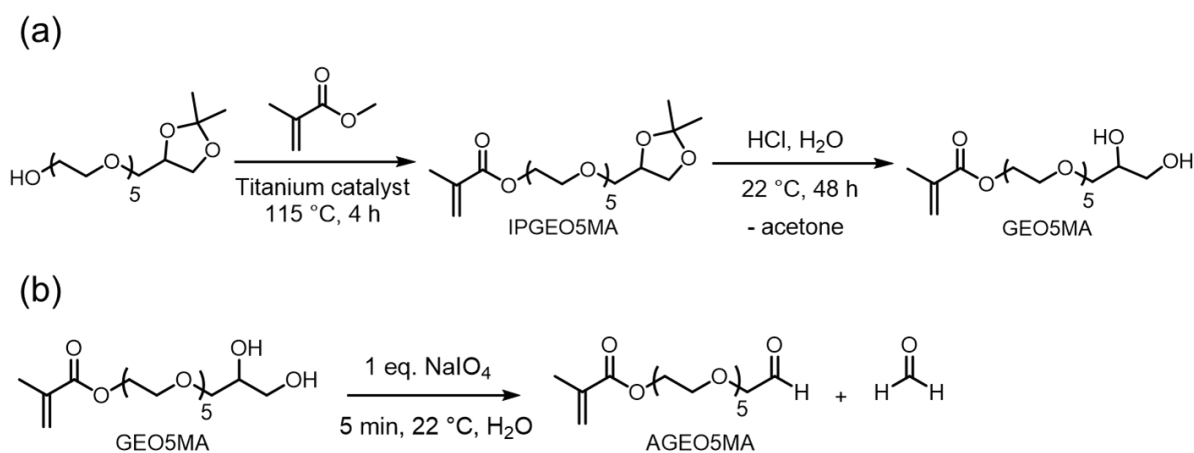
The oxidation of the *cis*-diol units in PEG₁₁₃-PGEO5MA₅₀ is representative of the general protocol. A 40% w/w aqueous PEG₁₁₃-PGEO5MA₅₀ solution (2.60 g, 1.04 g dry weight PEG₁₁₃-PGEO5MA₃₇, 0.11 mmol) was added to 5.6 mL of a 0.38 M aqueous solution of NaIO₄. The resulting ~15% w/w copolymer solution was stirred at 22 °C for 30 min and the extent of oxidation was determined by ¹H NMR spectroscopy (the integrated signals for the aldehyde proton at 9.51 ppm and the proton adjacent to the geminal diol at 5.13 ppm were

compared to that for the signal at 4.11 ppm corresponding to two oxymethylene protons attached to the ester group). The resulting diblock copolymer solution was purified by dialysis against deionised water for two days (with three changes of water per day).

3.3. Results and Discussion

3.3.1. Synthesis of GEO5MA monomer

The two-step synthesis of GEO5MA monomer was conducted on a 1.2 kg scale (by Dr C. P. Jesson at GEO Specialty Chemicals, Hythe) *via* (i) transesterification of isopropylidene glycerol penta(ethylene glycol) using MMA to afford IPGEO5MA (Scheme 3.3a) and (ii) acid hydrolysis to remove the acetone protecting group. The chemical structure of this new methacrylic monomer was confirmed by ^1H and ^{13}C NMR spectroscopy (see Figure 3.1a and Appendix 3), mass spectrometry, elemental microanalysis and FT-IR spectroscopy. The integrated signals in the ^1H NMR spectrum are consistent with the proposed monomer structure. Its ^{13}C NMR spectrum contained ten distinct signals. A characteristic signal at ~ 160 ppm was assigned to the ester carbonyl carbon; its relatively low intensity is attributed to the slow relaxation time for such quaternary carbon atoms.⁴⁵ The presence of a methacrylate group is confirmed by signals at 135 and 127 ppm. Several signals between 62.6 and 71.3 ppm are assigned to the pendent oligo(ethylene glycol) chain and include characteristic signals for the carbons attached to hydroxyl groups. According to mass spectrometry, the number of ethylene glycol units per oligo(ethylene glycol) group ranged from 2 to 7, with a mean value of 5.



Scheme 3.3. (a) Two-step synthesis of GEO5MA monomer starting from a isopropylidene glycerol precursor as a hydroxy-functional initiator. This precursor is then transesterified with MMA to produce IPGEO5MA, before removing the ketal protecting group with acid to afford GEO5MA monomer. (b) Oxidation of GEO5MA in aqueous solution using NaIO_4 at $22\text{ }^\circ\text{C}$ affords AGE5MA with formaldehyde as a by-product. The same selective oxidation can be used to convert PGEO5MA homopolymer into PAGE5MA homopolymer using identical reaction conditions.

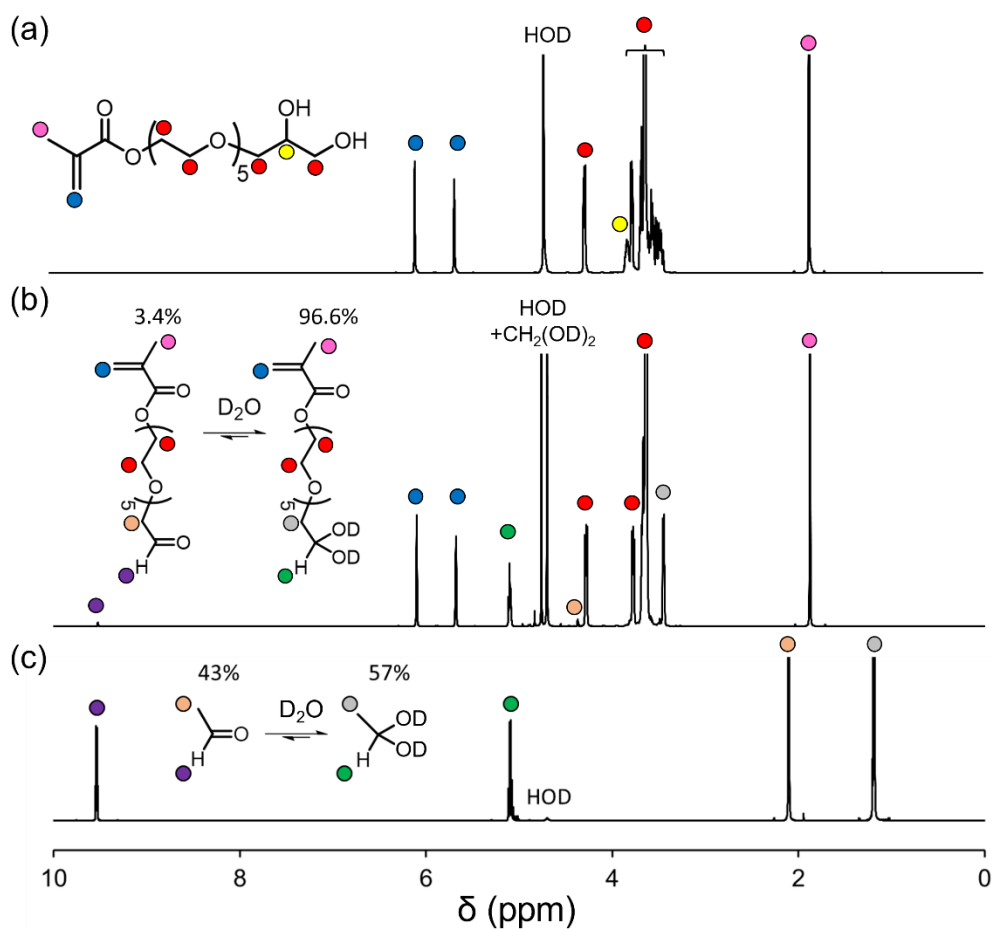


Figure 3.1. ^1H NMR spectra (D_2O) recorded for (a) GEO5MA monomer, (b) AGEO5MA monomer [$\text{CH}_2(\text{OD})_2$ denotes the hydrated form of formaldehyde] and (c) acetaldehyde (used as a reference compound).

3.3.2. Synthesis of AGEO5MA monomer *via* NaIO_4 oxidation

Oxidation of a 10% w/w aqueous solution of GEO5MA using a NaIO_4 /*cis*-diol molar ratio of unity (see Scheme 3.3b) led to essentially complete oxidation of the terminal *cis*-diol units within 5 min at 22 °C, as confirmed by ^1H NMR spectroscopy (see Figure 3.1). The structure of this new AGEO5MA monomer was confirmed by mass spectrometry, elemental microanalysis, ^1H , ^{13}C NMR (Figure 3.1b and Appendix 3) and FT-IR spectroscopy (Appendix 4). Two new signals appear at 9.52 ppm and 5.09 ppm in the ^1H NMR spectrum for AGEO5MA, corresponding to an aldehyde group and a geminal diol, respectively (Figure 3.1b). The aldehyde/geminal diol molar ratio was 0.034, which indicates that AGEO5MA exists primarily in its hydrated geminal diol form in D_2O . Similar observations have been reported for other hydrophilic aldehydes in aqueous solution, such as acetaldehyde (Figure 3.1c).^{46–49} During the periodate oxidation of GEO5MA to form AGEO5MA, the starting material can in principle react with the product to generate dimethacrylate species *via* (hemi)acetal chemistry (Appendix 5).¹ In practice, the final product contains less than 1% dimethacrylate impurity as estimated by ^1H NMR

spectroscopy. The ^{13}C NMR spectrum also shows the appearance of two new signals at 169.5 and 88.0 ppm, which correspond to the aldehyde carbon and the geminal diol carbon, respectively.

3.3.3. Homopolymerisation of GEO5MA and AGEO5MA

After purification by extraction with dichloromethane, the RAFT aqueous solution polymerisation of AGEO5MA was conducted using a dicarboxylic acid-functionalised water-soluble RAFT agent to target a mean DP of 30 (see Figure 3.2a). More than 99% conversion was achieved and the resulting PAGEO5MA₃₀ was relatively well-defined, as indicated by its relatively narrow, unimodal gel permeation chromatography (GPC) trace ($M_n = 11.1 \text{ kg mol}^{-1}$; $D = 1.18$), see Figure 3.2b. ^1H NMR signals for the terminal aldehyde and geminal diol groups were detected for this homopolymer (aldehyde/geminal diol molar ratio = 0.041).

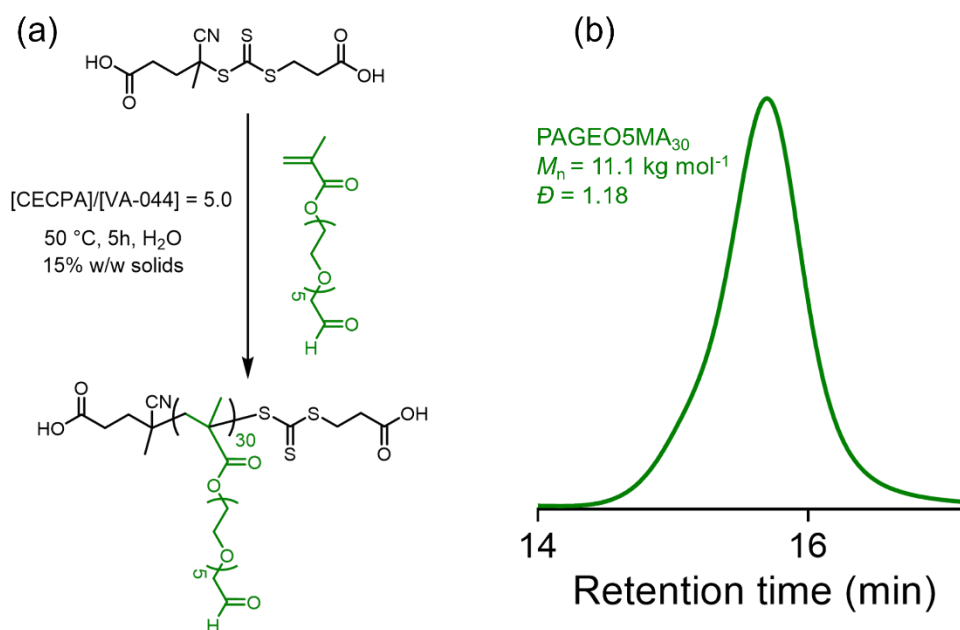


Figure 3.2. (a) Synthesis of PAGEO5MA₃₀ via RAFT aqueous solution polymerisation of AGEO5MA using a water-soluble dicarboxylic acid-functionalised RAFT agent. (b) DMF GPC trace for the resulting PAGEO5MA₃₀ homopolymer (molecular weight data expressed relative to PMMA calibration standards).

Alternatively, RAFT aqueous solution polymerisation of GEO5MA affords a near-monodisperse PGEO5MA₃₇ homopolymer ($M_n = 17.2 \text{ kg mol}^{-1}$; $D = 1.18$). When a NaIO_4 /*cis*-diol molar ratio of unity was used to derivatise this precursor, essentially complete oxidation was achieved to afford PAGEO5MA₃₇ homopolymer within 5 min at 22 °C (see Table 3.1 and Figure 3.3). The latter product proved to be water-soluble at concentrations of up to 15% w/w. In striking contrast, the product of the oxidation of

PGMA₃₉ homopolymer using a stoichiometric amount of periodate, denoted hereafter as PAGMA₃₉, proved to be water-insoluble when prepared at 1.5 to 10% w/w (Table 3.2). The much higher aqueous solubility observed for PAGEO5MA₃₇ is attributed to the hydrophilic oligo(ethylene glycol) units on each repeat unit.

However, only a minor fraction of monomer repeat units may need to be converted into aldehyde groups for certain applications. Thus, partial oxidation of a PGEO5MA₃₇ precursor using sub-stoichiometric quantities of NaIO₄ oxidant relative to its *cis*-diol groups was also investigated (Scheme in Figure 3.3a).

Table 3.1. Extent of oxidation, DMF GPC molecular weight and dispersity data for the selective oxidation of PGEO5MA₃₇ in aqueous solution at 22 °C using (sub-)stoichiometric NaIO₄/*cis*-diol molar ratios ranging between 0.00 and 1.00.

NaIO ₄ / <i>cis</i> -diol molar ratio	Extent of oxidation (%)	M_n (kg mol ⁻¹)	\mathcal{D}
1.00	>99%	16.5	1.22
0.75	78	15.9	1.24
0.50	49	16.8	1.21
0.10	11	17.4	1.22
0.00	0	17.2	1.18

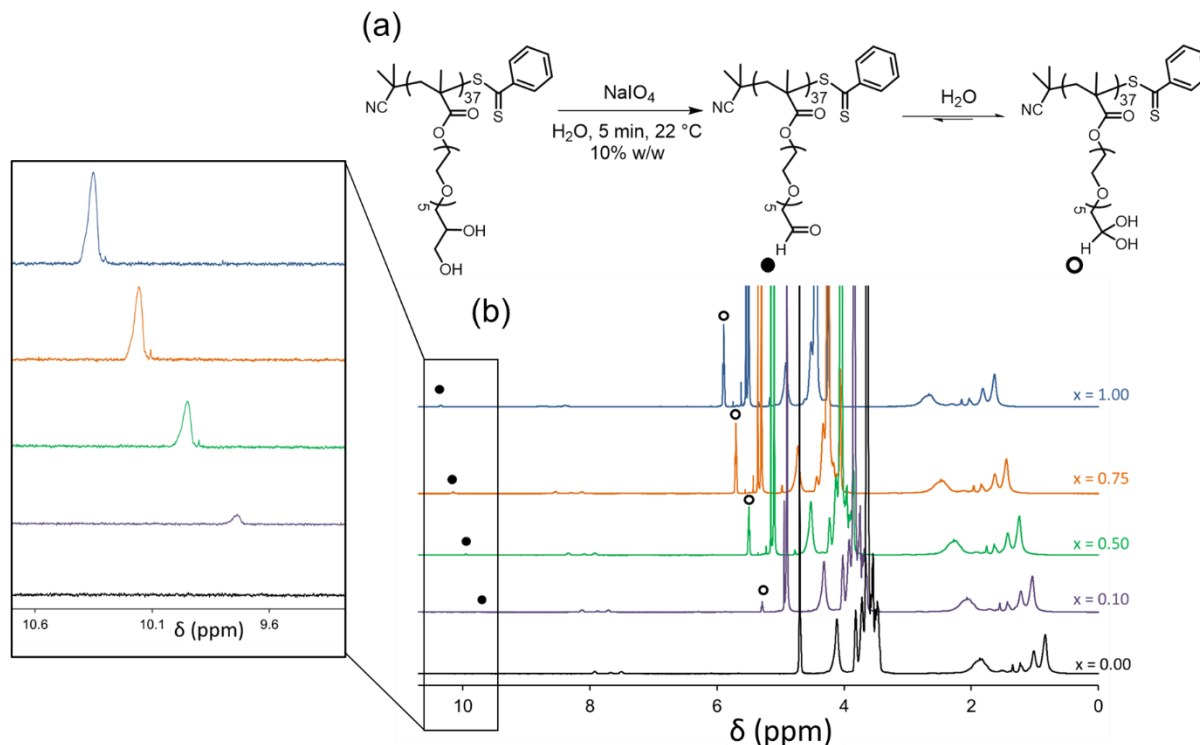


Figure 3.3. (a) Reaction scheme for the (partial) oxidation of a near-monodisperse PGEO5MA₃₇ precursor in aqueous solution using NaIO₄ at 22 °C. Adjusting the NaIO₄/*cis*-diol molar ratio (x) between 0.10 and 1.00 generates a library of aldehyde-functional water-soluble statistical copolymers. (b) Offset ¹H NMR spectra (D₂O) recorded for PAGEO5MA₃₇, P(GEO5MA_{*n*}-stat-AGEO5MA_{*m*})₃₇ (where $m = 0.11, 0.49$ and 0.78), and PGEO5MA₃₇.

Table 3.2. Summary of the aqueous solubilities observed for PAGEO5MA₃₇ and PAGMA₃₉ prepared at various concentrations.

PAGEO5MA ₃₇ concentration		PAGMA ₃₉ concentration		Water soluble?	
% w/w	mol dm ⁻³	% w/w	mol dm ⁻³	PAGEO5MA ₃₇	PAGMA ₃₉
1.5	0.0012	1.5	0.0027	Soluble	Insoluble
2.0	0.0016	2.0	0.0036	Soluble	Insoluble
3.5	0.0027	-	-	Soluble	-
10	0.0079	10	0.0196	Soluble	Insoluble
15	0.0118	-	-	Insoluble	-

All experiments were conducted at 22 °C using a NaIO₄/*cis*-diol molar ratio of unity.

Accordingly, utilising NaIO₄/*cis*-diol molar ratios of 0.10, 0.50 or 0.75 produced a series of water-soluble P(GEO5MA_n-*stat*-AGEO5MA_m)₃₇ statistical copolymers with approximate degrees of aldehyde functionality of 0.11, 0.49 and 0.78, respectively, as estimated from ¹H NMR spectroscopy studies (see Table 3.1 and Figure 3.3). Thus, the target degree of aldehyde functionality is always achieved (within experimental error). DMF GPC analyses confirmed that neither partial nor full oxidation of the PAGEO5MA₃₇ homopolymer had a significant effect on its molecular weight distribution (see Table 3.1 and Figure 3.4).

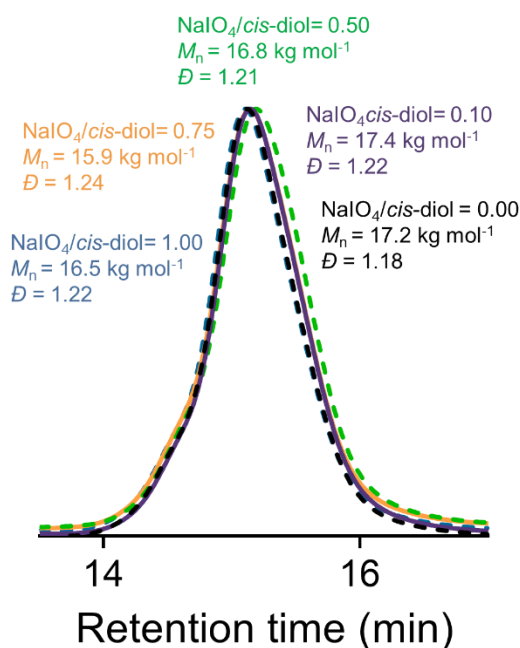


Figure 3.4. DMF GPC traces (vs. PMMA calibration standards) recorded for a PAGEO5MA₃₇ precursor, P(GEO5MA_n-*stat*-AGEO5MA_m)₃₇ statistical copolymers (where $m = 0.11, 0.49$ and 0.78 , when using a NaIO₄/*cis*-diol molar ratio of 0.10, 0.50 or 0.75, respectively) and PAGEO5MA₃₇ (NaIO₄/*cis*-diol molar ratio = 1.00). The desired degree of aldehyde functionality is achieved (within experimental error) when using sub-stoichiometric amounts of periodate and such selective oxidation has essentially no effect on the molecular weight distribution curve of the PAGEO5MA₃₇ precursor.

Moreover, using a slight excess of NaIO_4 relative to the pendent *cis*-diol groups also resulted in partial loss of the dithiobenzoate end-groups. Similarly, a PGE05MA homopolymer ($M_n = 124.1 \text{ kg mol}^{-1}$, $\mathcal{D} = 4.55$) was synthesised *via* FRP in aqueous solution at $70 \text{ }^\circ\text{C}$ for 18 h. Selective oxidation of the *cis*-diol groups on this homopolymer also had minimal effect on its (broad) molecular weight distribution (Figure 3.5 and 3.6).

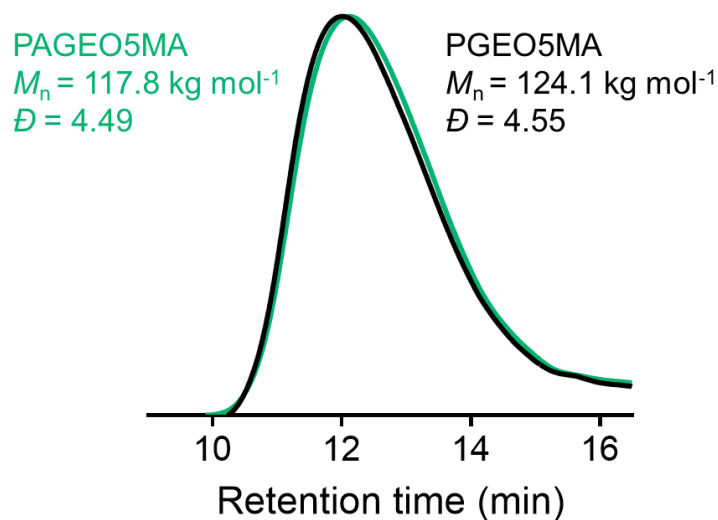


Figure 3.5. DMF GPC traces (vs. PMMA standards) recorded for PGE05MA and PAGE05MA homopolymers synthesised *via* FRP in water.

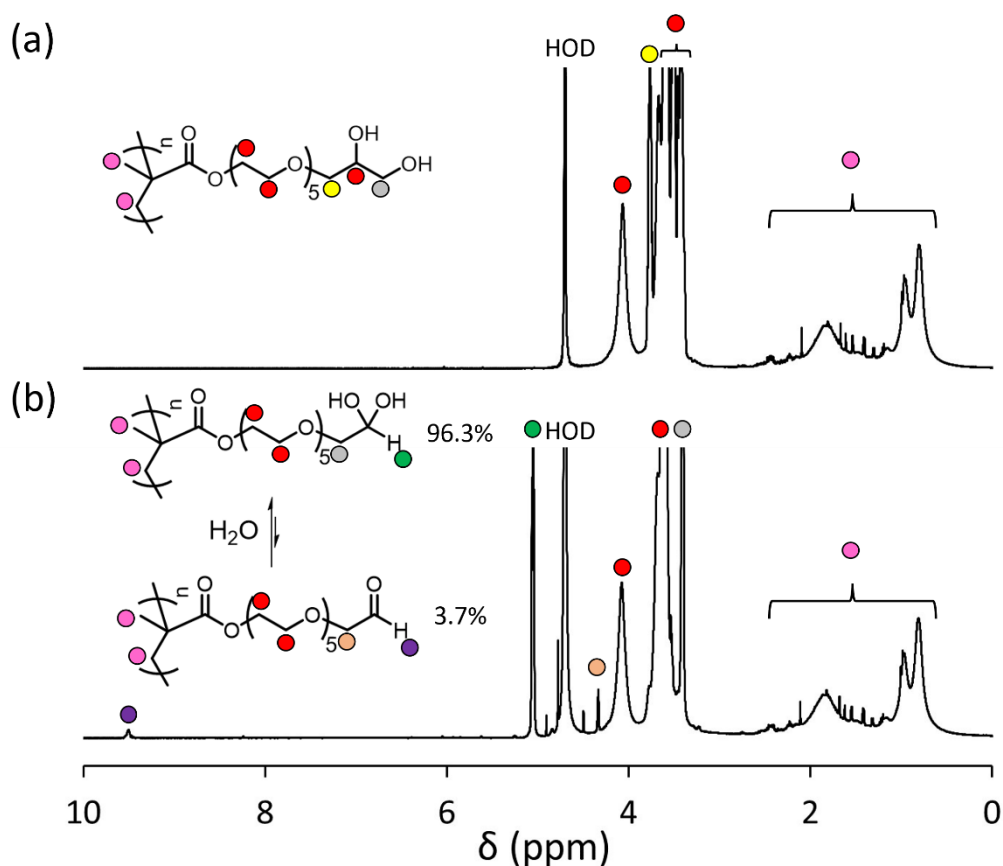
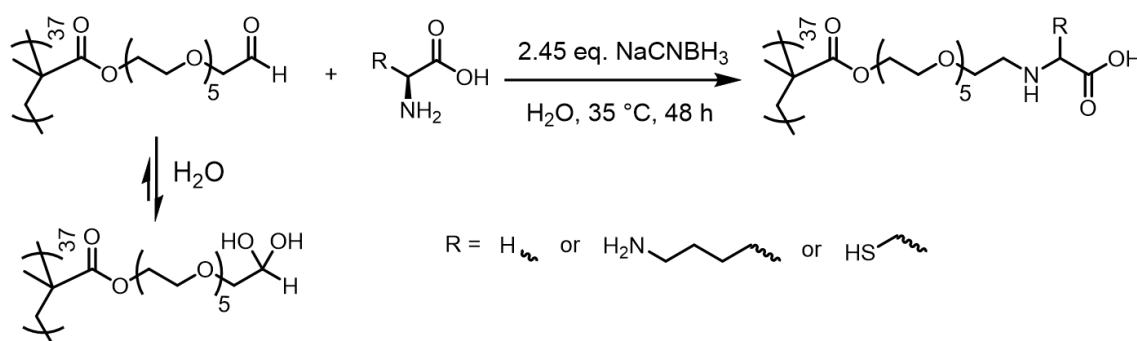


Figure 3.6. Assigned ^1H NMR spectra (D_2O) recorded for (a) PGE05MA synthesised by FRP and (b) PAGE05MA synthesised by oxidising PGE05MA using NaIO_4 .

3.3.4. Functionalisation of PAGEO5MA₃₇ homopolymer *via* reductive amination

To investigate the scope of such new water-soluble aldehyde-functional polymers for conjugation with biologically relevant compounds, PAGEO5MA₃₇ homopolymer was reacted in turn with three amino acids (glycine, lysine or cysteine; amino acid/aldehyde molar ratio = 1.0) to form the corresponding Schiff base, followed by *in situ* reductive amination using excess NaCNBH₃ (see Scheme 3.4). These aqueous reaction mixtures were stirred at 35 °C for 48 h, with ¹H NMR spectroscopy studies indicating very high extents of reaction (>99%) in each case (Appendix 6). It was found that lysine reacted solely *via* the amine group adjacent to the carboxylic acid, which is presumably because this amine group has a lower pK_a than that of the amino acid side-chain. Aqueous GPC analysis of the resulting water-soluble polymers indicated that molecular weight distributions remained relatively narrow after this two-step, one-pot derivatisation (Figure 3.7).



Scheme 3.4. Schiff base reaction of PAGEO5MA₃₇ with an amino acid (e.g., glycine, lysine or cysteine) followed by reductive amination using excess aqueous NaCNBH₃ at 35 °C to afford a series of new zwitterionic homopolymers *via* a two-step, one-pot wholly aqueous protocol.

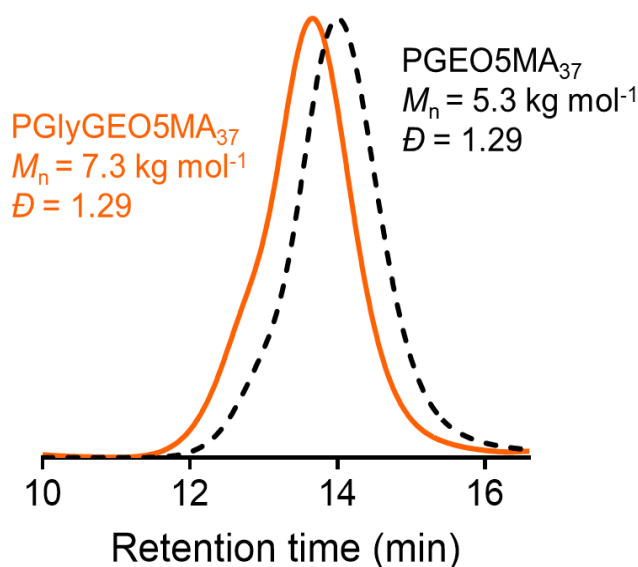
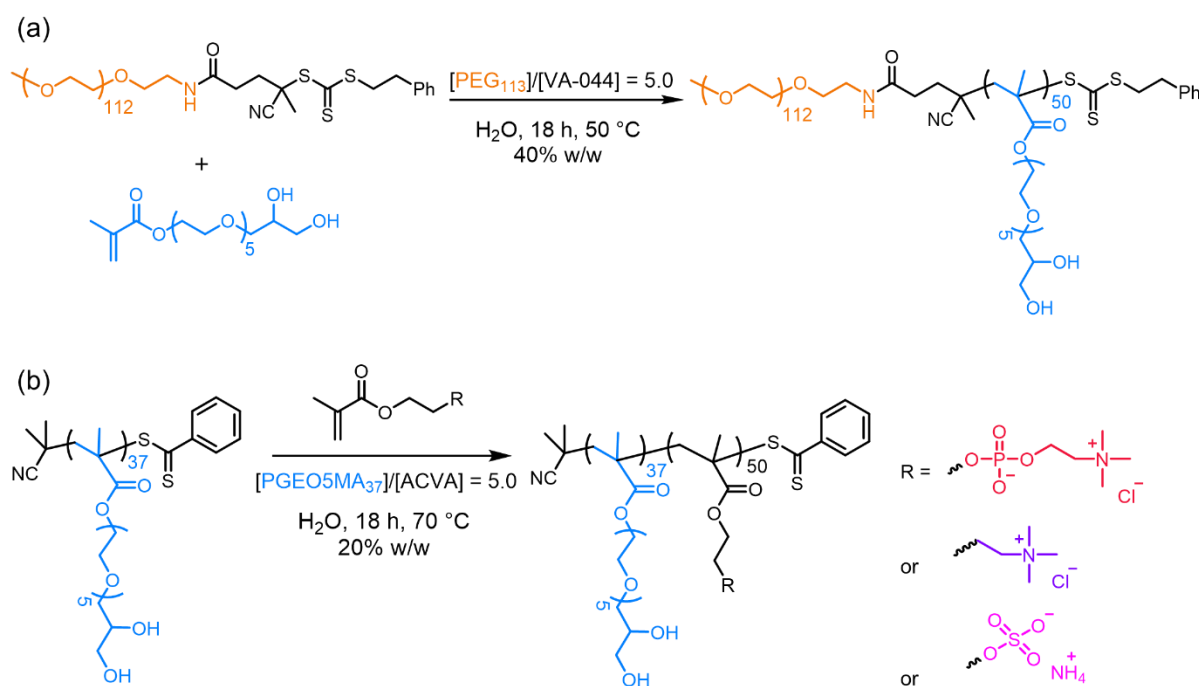


Figure 3.7. Aqueous GPC traces (vs. PEG/PEO calibration standards) recorded for PAGEO5MA₃₇ and poly(glycine-functionalised GEO5MA) (PGlyGEO5MA₃₇). After periodate oxidation, derivatisation with glycine leads to a systematic shift in the molecular weight distribution curve but the dispersity remains narrow.

3.3.5. Synthesis of PAGEO5MA_x-PX_y diblock copolymers

This NaIO₄ oxidation protocol was then extended to a series of diblock copolymers. A series of neutral, zwitterionic, cationic or anionic double-hydrophilic diblock copolymers were targeted in which one of the blocks was PGEO5MA (Scheme 3.5). For the neutral diblock copolymer, a trithiocarbonate-capped PEG₁₁₃ precursor was simply chain-extended *via* RAFT aqueous solution polymerisation of GEO5MA at 50 °C. For the synthesis of the ionic diblock copolymers, a PGEO5MA₃₇ precursor was chain-extended *via* RAFT aqueous solution polymerisation of either MPC, METAC or SEM at 70 °C. Each polymerisation was allowed to proceed overnight to ensure high monomer conversions ($\geq 98\%$ in all cases, as confirmed by ¹H NMR spectroscopy; Table 3.3).



Scheme 3.5. (a) Reaction scheme for the synthesis of PEG₁₁₃-PGEO5MA₅₀ *via* RAFT aqueous solution polymerisation of GEO5MA at 40% w/w solids using a PEG₁₁₃/VA-044 molar ratio of 5.0 at 50 °C. (b) Reaction scheme for the synthesis of PGEO5MA₃₇-PX₅₀ diblock copolymers (where X = MPC, METAC or SEM) at 20% w/w solids using a PGEO5MA₃₇/ACVA molar ratio of 5.0.

DMF GPC indicated a high blocking efficiency for GEO5MA polymerisation using the PEG₁₁₃ macro-CTA and the resulting PEG₁₁₃-PGEO5MA₅₀ diblock copolymer had a relatively low dispersity ($\mathcal{D} = 1.20$), see Table 3.3 and Figure 3.8a). However, aqueous GPC analysis was required to assess the molecular weight distributions of the ionic diblock copolymers (Table 3.3, Figure 3.8b–d). Oxidation of the pendent *cis*-diol groups on the PGEO5MA_x chains was investigated using a NaIO₄/*cis*-diol molar ratio of unity at a diblock copolymer concentration of 15% w/w. According to ¹H NMR analysis, the extent of derivatisation was at least 99% in all cases (Table 3.3). DMF GPC analysis confirmed that periodate oxidation

had minimal effect on the molecular weight distribution ($\bar{D} = 1.22$; Table 3.3 and Figure 3.8a) in the case of the PEG₁₁₃-PGEO5MA₅₀ diblock copolymer. Similar results were obtained for the zwitterionic, cationic and anionic diblock copolymers when using aqueous GPC (Table 3.3, Figure 3.8b–d).

Table 3.3. Summary of monomer conversions, extents of *cis*-diol oxidation and GPC molecular weight data for a series of neutral, zwitterionic, cationic and anionic diblock copolymers (with reference homopolymers included for comparison).

GPC eluent	Polymer composition	Monomer conversion (%)	Extent of <i>cis</i> -diol oxidation (%)	M_n (kg mol ⁻¹) ^c	\bar{D}
DMF	PEG ₁₁₃	-	-	5.0	1.13
DMF	PEG ₁₁₃ -PGEO5MA ₃₇	>99	-	27.7	1.20
DMF	PEG ₁₁₃ -PAGEO5MA ₃₇	-	>99	26.2	1.22
Aqueous ^a	PGEO5MA ₃₇	-	-	5.8	1.29
Aqueous ^a	PGEO5MA ₃₇ -PMPC ₅₀	>99	-	13.1	1.34
Aqueous ^a	PAGEO5MA ₃₇ -PMPC ₅₀	-	99	13.4	1.38
Aqueous ^b	PGEO5MA ₃₇	-	-	-	-
Aqueous ^b	PGEO5MA ₃₇ -PMETAC ₅₀	98	-	23.4	1.12
Aqueous ^b	PAGEO5MA ₃₇ -PMETAC ₅₀	-	>99	23.3	1.11
Aqueous ^a	PGEO5MA ₃₇	-	-	5.7	1.34
Aqueous ^a	PGEO5MA ₃₇ -PSEM ₅₀	>99	-	11.0	1.30
Aqueous ^a	PAGEO5MA ₃₇ -PSEM ₅₀	-	>99	12.7	1.36

^a 0.2 M NaNO₃, 0.05 M TRISMA buffer, pH 7 ^b 0.5 M acetic acid, 0.3 M NaH₂PO₄, pH 2 ^c Relative to PEG/PEO standards

3.4. Conclusion

In summary, the atom-efficient synthesis of a new *cis*-diol-based methacrylic monomer (GEO5MA) that is readily converted into a hydrophilic aldehyde-functional monomer (AGEO5MA) *via* selective oxidation using NaIO₄ in aqueous solution is reported. Unlike almost all other literature examples of aldehyde-based vinyl monomers, this latter monomer is water-soluble and can be polymerised with good control *via* RAFT aqueous solution polymerisation. Alternatively, homopolymerisation of the GEO5MA precursor under similar conditions affords a well-defined water-soluble PGEO5MA precursor that can be converted into PAGEO5MA under mild conditions using a stoichiometric amount of NaIO₄ oxidant. On the other hand, using sub-stoichiometric quantities of NaIO₄ relative to the pendent *cis*-diol units produces a range of water-soluble aldehyde-functional statistical copolymers. New PAGEO5MA-based double-hydrophilic diblock copolymers can be prepared and model Schiff base reactions have been conducted in aqueous solution under mild conditions using various amino acids to introduce zwitterionic groups. It is anticipated that this new hydrophilic aldehydic vinyl monomer and its corresponding

copolymers should offer a range of potential applications in the fields of cell biology and biomaterials.

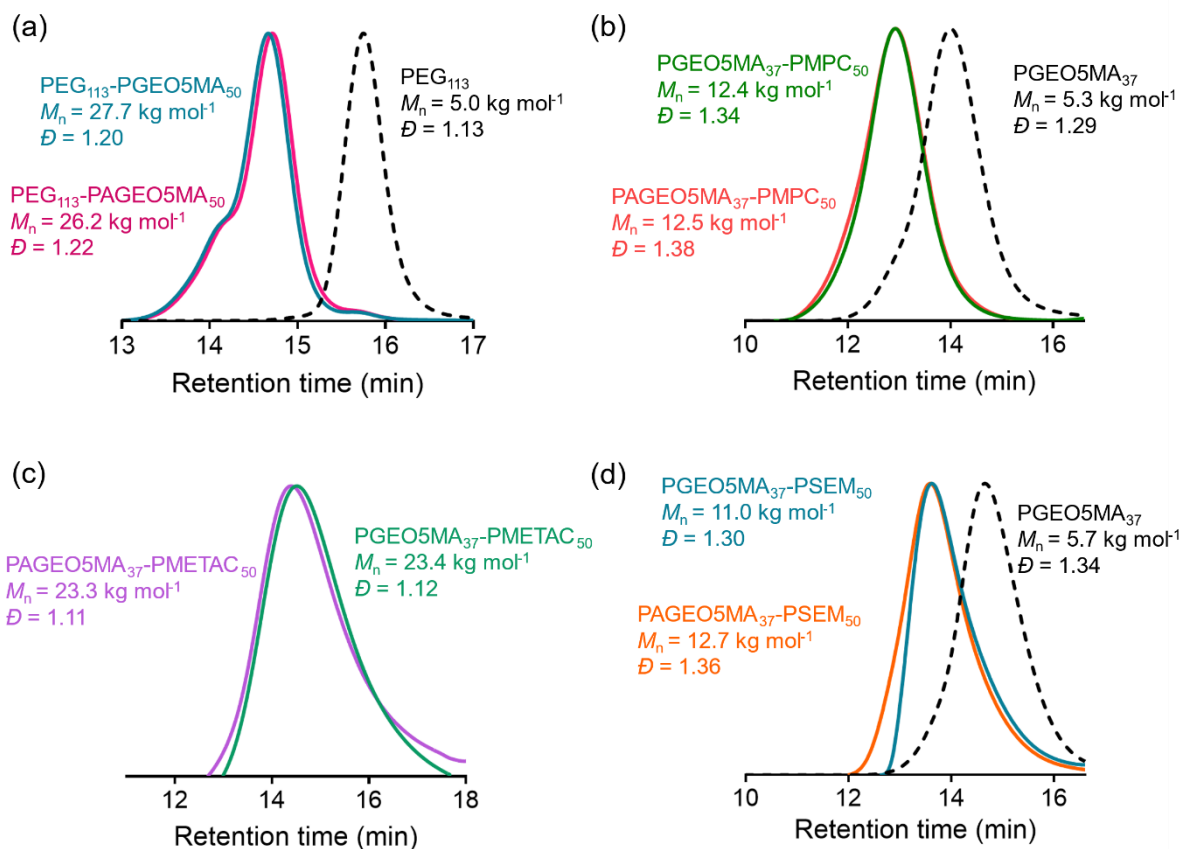


Figure 3.8. DMF GPC traces (vs. PEG/PEO calibration standards) recorded for (a) PEG₁₁₃-PGEO5MA₅₀, PEG₁₁₃-PAGEO5MA₅₀ and PEG₁₁₃ and aqueous GPC traces (vs. PEG/PEO calibration standards) recorded for (b) PGEO5MA₃₇-PMPC₅₀, PAGEO5MA₃₇-PMPC₅₀ and PGEO5MA₃₇, (c) PGEO5MA₃₇-PMETAC₅₀, PAGEO5MA₃₇-PMETAC₅₀ and (d) PGEO5MA₃₇-PSEM₅₀, PAGEO5MA₃₇-PSEM₅₀ and PGEO5MA₃₇. In the case of (a), (b) and (d), there is a substantial shift in molecular weight for the diblock copolymer relative to its corresponding homopolymer. Unfortunately, in (c) it was not possible to record the GPC curve for the PGEO5MA₃₇ precursor using this particular eluent (0.5 M acetic acid, 0.3 M NaH₂PO₄ pH 2). In all four cases, selective oxidation of the pendent *cis*-diol groups using NaIO₄ had minimal effect on the molecular weight distribution.

3.5. References

- 1 M. B. Smith and J. March, *March's advanced organic chemistry: reactions, mechanisms, and structure*, John Wiley & Sons, Inc., Hoboken, NJ, 2007.
- 2 J. Collins, S. J. Wallis, A. Simula, M. R. Whittaker, M. P. McIntosh, P. Wilson, T. P. Davis, D. M. Haddleton and K. Kempe, *Macromol. Rapid Commun.*, 2017, **38**, 1600534.
- 3 J. Collins, K. Kempe, P. Wilson, C. A. Blindauer, M. P. McIntosh, T. P. Davis, M. R. Whittaker and D. M. Haddleton, *Biomacromolecules*, 2016, **17**, 2755–2766.
- 4 L. Tao, G. Mantovani, F. Lecolley and D. M. Haddleton, *J. Am. Chem. Soc.*, 2004, **126**, 13220–13221.
- 5 C. Scholz, M. Iijima, Y. Nagasaki and K. Kataoka, *Macromolecules*, 1995, **28**, 7295–7297.

-
- 6 Y. Nagasaki, T. Okada, C. Scholz, M. Iijima, M. Kato and K. Kataoka, *Macromolecules*, 1998, **31**, 1473–1479.
 - 7 M. Iijima, Y. Nagasaki, T. Okada, M. Kato and K. Kataoka, *Macromolecules*, 1999, **32**, 1140–1146.
 - 8 H. Otsuka, Y. Nagasaki and K. Kataoka, *Biomacromolecules*, 2000, **1**, 39–48.
 - 9 T. Bilgic and H.-A. Klok, *Biomacromolecules*, 2015, **16**, 3657–3665.
 - 10 S. N. S. Alconcel, S. H. Kim, L. Tao and H. D. Maynard, *Macromol. Rapid Commun.*, 2013, **34**, 983–989.
 - 11 A. W. Jackson and D. A. Fulton, *Macromolecules*, 2012, **45**, 2699–2708.
 - 12 B. S. Murray and D. A. Fulton, *Macromolecules*, 2011, **44**, 7242–7252.
 - 13 R. H. Wiley and P. H. Hobson, *J. Polym. Sci.*, 1950, **5**, 483–486.
 - 14 L. Qiu, C. R. Xu, F. Zhong, C. Y. Hong and C. Y. Pan, *Macromol. Chem. Phys.*, 2016, **217**, 1047–1056.
 - 15 N.-Y. Xiao, L. Zhong, W.-J. Zhai and W.-D. Bai, *Acta Polym. Sin.*, 2012, **8**, 818–824.
 - 16 M. E. Wechsler, H. K. H. J. Dang, S. D. Dahlhauser, S. P. Simmonds, J. F. Reuther, J. M. Wyse, A. N. VandeWalle, E. V. Anslyn and N. A. Peppas, *Chem. Commun.*, 2020, **56**, 6141–6144.
 - 17 M. Wu, J. Chen, W. Huang, B. Yan, Q. Peng, J. Liu, L. Chen and H. Zeng, *Biomacromolecules*, 2020, **21**, 2409–2420.
 - 18 C. Cao, K. Yang, F. Wu, X. Wei, L. Lu and Y. Cai, *Macromolecules*, 2010, **43**, 9511–9521.
 - 19 D. E. Whitaker, C. S. Mahon and D. A. Fulton, *Angew. Chemie Int. Ed.*, 2013, **52**, 956–959.
 - 20 J. Huang, X. Chen, H. Qin, H. Liang and J. Lu, *Polymer*, 2019, **160**, 99–106.
 - 21 N. A. A. Rossi, Y. Zou, M. D. Scott and J. N. Kizhakkedathu, *Macromolecules*, 2008, **41**, 5272–5282.
 - 22 G. S. Heo, S. Cho and K. L. Wooley, *Polym. Chem.*, 2014, **5**, 3555–3558.
 - 23 Z. Wu, H. Liang and J. Lu, *Macromolecules*, 2010, **43**, 5699–5705.
 - 24 N. Y. Xiao, A. L. Li, H. Liang and J. Lu, *Macromolecules*, 2008, **41**, 2374–2380.
 - 25 N. Xiao, H. Liang and J. Lu, *Soft Matter*, 2011, **7**, 10834–10840.
 - 26 C. Legros, M. C. De Pauw-Gillet, K. C. Tam, S. Lecommandoux and D. Taton, *Eur. Polym. J.*, 2015, **62**, 322–330.
 - 27 T. Ishizone, A. Hirao, S. Nakahama, T. Kakuchi, K. Yokota and K. Tsuda, *Macromolecules*, 1991, **24**, 5230–5231.
 - 28 J. Hwang, R. C. Li and H. D. Maynard, *J. Control. Release*, 2007, **122**, 279–286.
 - 29 G. Sun, C. Cheng and K. L. Wooley, *Macromolecules*, 2007, **40**, 793–795.
 - 30 G. Foyer, M. Barriol, C. Negrell, S. Caillol, G. David and B. Boutevin, *Prog. Org. Coatings*, 2015, **84**, 1–8.
-

-
- 31 G. Sun, H. Fang, C. Cheng, P. Lu, K. Zang, A. V. Walker, J.-S. A. Taylor and K. L. Wooley, *ACS Nano*, 2009, **3**, 673–681.
- 32 R. H. Wiley and P. H. Hobson, *J. Polym. Sci.*, 1949, **5**, 483–486.
- 33 K. L. Christman and H. D. Maynard, *Langmuir*, 2005, **21**, 8389–8393.
- 34 K. L. Christman, M. V. Requa, V. D. Enriquez-Rios, S. C. Ward, K. A. Bradley, K. L. Turner and H. D. Maynard, *Langmuir*, 2006, **22**, 7444–7450.
- 35 M. Yokoyama, M. Miyauchi, N. Yamada, T. Okano, Y. Sakurai, K. Kataoka and S. Inoue, *Cancer Res.*, 1990, **50**, 1693–1700.
- 36 E. M. Pelegri-O'Day, N. M. Matsumoto, K. Tamshen, E. D. Raftery, U. Y. Lau and H. D. Maynard, *Bioconjug. Chem.*, 2018, **29**, 3739–3745.
- 37 R. M. Broyer, G. N. Grover and H. D. Maynard, *Chem. Commun.*, 2011, **47**, 2212–2226.
- 38 J. M. Stukel, R. C. Li, H. D. Maynard and M. R. Caplan, *Biomacromolecules*, 2010, **11**, 160–167.
- 39 J. Blankenburg, K. Maciol, C. Hahn and H. Frey, *Macromolecules*, 2019, **52**, 1785–1793.
- 40 R. J. Mancini, J. Lee and H. D. Maynard, *J. Am. Chem. Soc.*, 2012, **134**, 8474–8479.
- 41 E. Sawicki, T. R. Hauser, T. W. Stanley and W. Elbert, *Anal. Chem.*, 1961, **33**, 93–96.
- 42 P. J. Flory and F. S. Leutner, *J. Polym. Sci.*, 1948, **3**, 880–890.
- 43 H. W. Melville and P. R. Sewell, *Die Makromol. Chemie*, 1959, **32**, 139–152.
- 44 H. E. Harris and J. G. Pritchard, *J. Polym. Sci. Part A Gen. Pap.*, 1964, **2**, 3673–3679.
- 45 D. H. Williams and I. Fleming, *Spectroscopic methods in organic chemistry*, McGraw-Hill, Oakland, CA, 5th edn., 1995.
- 46 R. Zhao, A. K. Y. Lee, R. Soong, A. J. Simpson and J. P. D. Abbatt, *Atmos. Chem. Phys.*, 2013, **13**, 5857–5872.
- 47 M. Rivlin, U. Eliav and G. Navon, *J. Phys. Chem. B*, 2015, **119**, 4479–4487.
- 48 J. P. Lewicki, C. A. Fox and M. A. Worsley, *Polymer*, 2015, **69**, 45–51.
- 49 A. Wolfel, M. R. Romero and C. I. Alvarez Igarzabal, *Eur. Polym. J.*, 2019, **112**, 389–399.
-

*Chapter IV: Aldehyde-functional diblock
copolymer nano-objects via RAFT
aqueous dispersion polymerisation*

Reproduced in full with permission from:

E. E. Brotherton, M. J. Smallridge and S. P. Armes, *Biomacromolecules*, 2021, **22**, 5382–5389.

Chapter IV: Aldehyde-functional diblock copolymer nano-objects *via* RAFT aqueous dispersion polymerisation

4.1. Introduction

Block copolymer self-assembly in solution has been studied for more than fifty years.¹⁻³ Traditionally, this has been achieved by post-polymerisation processing in dilute solution,^{4,5} but over the past decade, polymerisation-induced self-assembly (PISA) has emerged as a versatile platform technology for the rational synthesis of various block copolymer nano-objects in the form of concentrated colloidal dispersions.⁶⁻⁸ PISA involves growing an insoluble block from a soluble precursor block in a suitable selective solvent to produce sterically-stabilised nanoparticles, with the three most common copolymer morphologies being spheres, worms and vesicles.⁹⁻¹¹ At intermediate conversions, the unreacted monomer effectively acts as a processing aid or co-solvent for the growing insoluble block.⁶ This approach works well in various solvents, including water. In the case of aqueous PISA, there are two possible formulations. Typically, the vinyl monomer used to grow the second block is water-immiscible, which leads to aqueous emulsion polymerisation. On the other hand, if the vinyl monomer is water-miscible, then, this corresponds to aqueous dispersion polymerisation. PISA can be performed using various (pseudo-)living techniques, but the most commonly reported technique in the literature is undoubtedly reversible addition-fragmentation chain transfer (RAFT) polymerisation.¹² This is no doubt because RAFT polymerisation offers excellent tolerance of monomer functionality, can be conducted under a wide range of conditions, and provides the possibility of introducing desirable end-groups by selecting an appropriate RAFT agent.^{13,14}

Aqueous PISA has been used to prepare many examples of functional block copolymer nano-objects. For example, disulfide bonds have been incorporated to prepare thiol-functionalised block copolymer worms and vesicles,^{15,16} while glycidyl methacrylate has been used as a comonomer to introduce epoxy groups into the water-insoluble structure-directing block.¹⁷⁻²¹ Similarly, diacetone acrylamide confers ketone functionality, which has been exploited for both metal complexation²² and post-polymerisation crosslinking.²³ Brendel and co-workers have reported the design of oxidation-sensitive nano-objects based on a thiamorpholine monomer.²⁴ Rieger and

co-workers have demonstrated that using a bisurea-based RAFT agent leads to extensive hydrogen bonding within the core-forming block that strongly favours the formation of the worm morphology.²⁵ Armes and co-workers have shown that using either carboxylic acid-based or tertiary amine-based RAFT agents enables the design of pH-responsive diblock copolymer nano-objects that can switch morphology simply by introducing a single ionic charge at the end of each steric stabiliser chain.^{26,27} If poly(glycerol monomethacrylate) (PGMA) is used as a steric stabiliser block, its pendent *cis*-diol groups can be used to ensure selective adsorption of the resulting nanoparticles onto an appropriately patterned two-dimensional surface.²⁸ Alternatively, binding of water-soluble phenylboronic acid derivatives to diblock copolymer vesicles in alkaline solution can induce a change in copolymer morphology to produce either worms or spheres, thereby releasing any cargo encapsulated within the vesicle lumen.^{29,30} Finally, the highly hydroxylated nature of the PGMA block appears to be essential for inducing stasis in human stem cell colonies immersed within PGMA-based worm gels.³¹

However, as far as we are aware, there have been no reports of aldehyde-functional block copolymer nano-objects prepared by aqueous PISA. This is perhaps surprising because aldehyde chemistry offers many possibilities for derivatisation. In particular, conjugation to amine-functional (macro)molecules *via* Schiff base chemistry³² can be conducted in aqueous solution under mild conditions, which is expected to offer potential biomedical applications.^{33–58} In Chapter III, the synthesis of a new methacrylic monomer (GEO5MA; see Scheme 3.3a) that resembles both glycerol monomethacrylate and oligo(ethylene glycol) methacrylate was reported.⁵⁹ Selective oxidation of the pendent *cis*-diol groups in GEO5MA (or its corresponding PGEO5MA homopolymer) using aqueous sodium periodate (NaIO₄) introduces a geminal diol group, which is simply the hydrated form of an aldehyde group (Scheme 3.3b).

In this Chapter, this chemistry is combined with the RAFT aqueous dispersion polymerisation of 2-hydroxypropyl methacrylate (HPMA) for the rational design of aldehyde-functional diblock copolymer spheres, worms and vesicles. Several model reactions are also conducted on aqueous dispersions of these nano-objects under mild conditions using either amino acids or a common globular protein.

4.2. Experimental

4.2.1. Synthesis

Synthesis of the PGEO5MA₂₆ precursor by RAFT solution polymerisation in ethanol

The GEO5MA monomer (50.0 g, 0.131 mol), 2-cyano-2-propyl benzodithioate (CPDB) RAFT agent (0.882 g, 3.98 mmol), 4,4'-azobis-4-cyanopentanoic acid (ACVA) initiator (0.223 g, 0.797 mmol; CPDB/ACVA molar ratio = 5.0) and ethanol (34 g) were weighed into a 250 mL round-bottomed flask. The reaction mixture was degassed for 40 min using a N₂ purge before being placed into an oil bath set at 70 °C for 110 min [target degree of polymerisation (DP) of 20 based on the reaction kinetics (Appendix 2)]. The polymerisation was quenched by removing the flask from the oil bath and subsequently exposing the reaction mixture to air. The GEO5MA conversion was determined to be 58% by ¹H NMR spectroscopy. The crude PGEO5MA homopolymer was purified by precipitation into diethyl ether (to remove any unreacted monomer and other impurities), before being filtered and redissolved in methanol. This precipitation step was repeated, and the purified homopolymer was dried in a vacuum oven set at 35 °C overnight to produce a viscous red liquid. The mean DP of this PGEO5MA₂₆ precursor was determined by end-group analysis using ¹H NMR spectroscopy. The integrated signals between 7.34 and 8.03 ppm assigned to the five aromatic protons of the dithiobenzoate chain-end were compared to those of the five proton signals assigned to the methacrylate backbone at 0.78–2.71 ppm.

Synthesis of PGEO5MA₂₆-PHPMA_y diblock copolymer nanoparticles by RAFT aqueous dispersion polymerisation of HPMA

The synthesis of PGEO5MA₂₆-PHPMA₁₇₀ spheres at 10% w/w solids is representative of the general protocol. HPMA monomer (0.400 g, 2.77 mmol), PGEO5MA₂₆ precursor (0.165 g, 16.3 μmol; target PHPMA DP = 170), ACVA initiator (1.1 mg, 4.08 μmol; PGEO5MA₂₆/ACVA molar ratio = 4.0) and water (5.10 g; targeting 10% w/w solids) were weighed into a 15 mL glass vial. The reaction mixture was purged using N₂ gas for 30 min and then the vial was placed in an oil bath set at 70 °C. After 4 h, the polymerisation was quenched by removing the vial from the oil bath and exposing its contents to air [polymerisation time determined from the reaction kinetics for the synthesis of PGEO5MA₂₆-PHPMA₃₅₀ diblock copolymer vesicles at 10% w/w solids (Appendix 7)]. The final HPMA conversion was determined to be 99% by ¹H NMR spectroscopy by comparing the integrated vinyl HPMA monomer signals at 5.67 ppm and 6.16 ppm with those assigned to the methacrylate backbone signals at 0.81–2.30 ppm arising from the monomer and polymer.

Synthesis of PGEO5MA₂₆-PHPMA₃₅₀-PEGDMA₂₀ copolymer nanoparticles by RAFT aqueous dispersion polymerisation of HPMA

HPMA monomer (0.600 g, 4.16 mmol), PGEO5MA₂₆ precursor (0.120 g, 11.9 μ mol; target PHPMA DP = 350), ACVA initiator (0.8 mg, 3.0 μ mol; PGEO5MA₂₆/ACVA molar ratio = 4.0) and water (6.49 g; targeting 10% w/w solids) were weighed into a 15 mL glass vial. The reaction mixture was purged using N₂ gas for 30 min and then the vial was placed in an oil bath set at 70 °C. After 4 h, ethylene glycol dimethacrylate (EGDMA) crosslinker (0.047 g, 0.24 mmol) and water (0.42 g) were added to the sample vial *via* a syringe to maintain a copolymer concentration of 10% w/w. The reaction was allowed to proceed for 2 h at 70 °C before quenching by removing the vial from the oil bath and exposing the reaction mixture to air. The final HPMA and EGDMA conversions were determined to be greater than 99% by ¹H NMR spectroscopy by comparing the integrated vinyl HPMA monomer and EGDMA signals at 5.67 and 6.16 ppm with that assigned to the methacrylate backbone signals at 0.81–2.30 ppm arising from the monomer and polymer.

Selective oxidation of PGEO5MA₂₆-PHPMA_y(-PEGDMA₂₀) copolymer nanoparticles using NaIO₄

The general protocol for the oxidation of PGEO5MA₂₆-PHPMA₃₅₀-PEGDMA₂₀ vesicles in aqueous solution was as follows. NaIO₄ (0.014 g, 64 μ mol) was dissolved in a 10% w/w aqueous dispersion of PGEO5MA₂₆-PHPMA₃₅₀-PEGDMA₂₀ vesicles (1.50 g, 2.5 μ mol). A NaIO₄/*cis*-diol molar ratio of unity was used to target 100% oxidation of the PGEO5MA block. The reaction solution was stirred in the dark for 30 min at 22 °C. Degrees of oxidation were determined by ¹H NMR spectroscopy. The oxidation of PGEO5MA₂₆-PHPMA₁₇₀ spheres was also conducted at 10% w/w solids. For the more viscous aqueous dispersion of PGEO5MA₂₆-PHPMA₂₅₀ worms, the periodate oxidation was conducted at 5.0% w/w solids to ensure efficient stirring. Polymers were dialysed against deionised water for two days (with three waters changes per day).

Amino acid conjugation to PAGEO5MA₂₆-PHPMA_y(-PEGDMA₂₀) copolymer nanoparticles via reductive amination

The general protocol used for the reductive amination of PAGEO5MA₂₆-PHPMA_y(-PEGDMA₂₀) block copolymer nanoparticles with either glycine or histidine was conducted as follows. A 10% w/w aqueous dispersion of PAGEO5MA₂₆-PHPMA₃₅₀-PEGDMA₂₀ vesicles (1.00 g, 0.79 μ mol) was weighed into a 15 mL glass vial along with glycine (1.5 mg, 20 μ mol; glycine/aldehyde molar ratio = 1.0). The reaction mixture was adjusted to pH 5–6 by adding either 0.1 M HCl or 0.1 M NaOH. Excess

sodium cyanoborohydride (NaCNBH_3) (3.2 mg, 50 μmol ; 2.45 mol excess) was carefully added to the reaction mixture, which was then stirred at 35 °C for 48 h. The degree of derivatisation was determined by ^1H NMR spectroscopy to be more than 99% by comparing the integrated residual geminal diol signal at 6.09 ppm with that of the five methacrylate backbone protons and three methyl protons belonging to the PHPMA at 0.41–2.35 ppm. Essentially, the same protocol was employed for histidine (3.4 mg, 22 μmol). The reductive amination of PGEO5MA₂₆-PHPMA₁₇₀ spheres was also conducted at 10% w/w solids. For the relatively viscous aqueous dispersion of PGEO5MA₂₆-PHPMA₂₅₀ worms, the reductive amination was conducted at 5.0% w/w solids to ensure efficient stirring.

Functionalisation of PAGEO5MA₂₆-PHPMA₃₅₀-PEGDMA₂₀ block copolymer vesicles with bovine serum albumin (BSA) via reductive amination

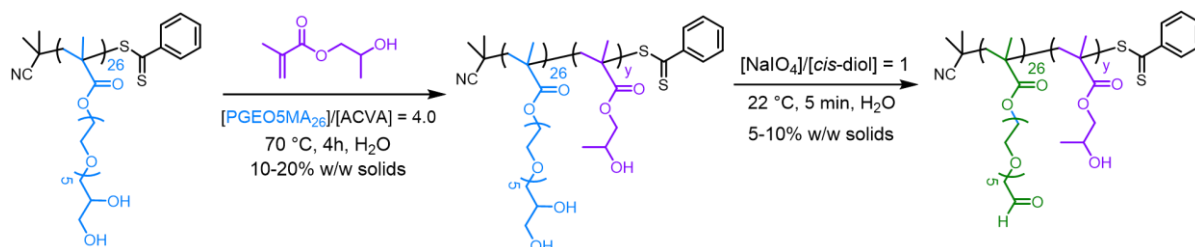
A 10% w/w copolymer dispersion of crosslinked PGEO5MA₂₆-PHPMA₃₅₀-PEGDMA₂₀ vesicles (1.0 g, 26.6 μmol) was weighed into a 15 mL glass vial along with BSA (8.8 mg, 0.13 μmol ; BSA/aldehyde molar ratio = 0.0019). The solution pH was adjusted to pH 5–6 by addition of either 0.1 M HCl or 0.1 M NaOH. NaCNBH_3 (0.2 mg, 0.33 μmol ; 2.45 mol excess) was added to the reaction mixture, which was then stirred at 35 °C for 48 h. The copolymer dispersion was centrifuged at 15,000 rpm for 12 min and then redispersed in deionised water to remove excess BSA remaining in the aqueous phase. This protocol was repeated four times to ensure that all non-adsorbed BSA was removed from the aqueous dispersion.

4.3. Results and Discussion

4.3.1. Synthesis of PGEO5MA₂₆-HPMA_y diblock copolymer nanoparticles *via* RAFT aqueous dispersion polymerisation

A PGEO5MA₂₆ homopolymer was synthesised *via* RAFT solution polymerisation in ethanol. DMF gel permeation chromatography (GPC) confirmed that this precursor had a number-average molecular weight (M_n) of 14.3 kg mol⁻¹ and a relatively narrow molecular weight distribution (\mathcal{D} = 1.18). This PGEO5MA₂₆ was then chain-extended *via* RAFT aqueous dispersion polymerisation of HPMA (Scheme 4.1). The copolymer concentration and the PHPMA target DP were systematically varied to afford a series of nanoparticles exhibiting various copolymer morphologies (Figure 4.1). Transmission electron microscopy (TEM) and dynamic light scattering (DLS) were employed to characterise these nanoparticles. For example, targeting PGEO5MA₂₆-PHPMA₁₇₀ at 10% w/w solids produced spherical nanoparticles as judged by TEM (Figure 4.1a) with a z-average diameter of 31 nm (DLS polydispersity index (PDI) = 0.02). On the other hand, PGEO5MA₂₆-PHPMA₂₄₀ nanoparticles

prepared at 12.5% w/w solids exhibited a highly anisotropic worm-like morphology (Figure 4.1b) with a sphere-equivalent DLS diameter of 504 nm (PDI = 0.38). Targeting PGE05MA₂₆-PHPMA₃₂₀ at 15% w/w solids produced a pure vesicular morphology (Figure 4.1c), with a DLS diameter of 397 nm (PDI = 0.19). Consequently, a PGE05MA₂₆-PHPMA_y pseudo-phase diagram was constructed (Figure 4.1e). This pseudo-phase diagram is similar to that reported by Blanz et al. for a series of PGMA₄₇-PHPMA_y diblock copolymers; in both cases, worms and vesicles are obtained at when targeting higher PHPMA DPs.⁹ Moreover, no concentration dependence is observed for such higher order morphologies. Notably, multilamellar vesicles (MLV; Figure 4.1d) with a DLS diameter of 515 nm (PDI = 0.23) were obtained when targeting PGE05MA₂₆-PHPMA₃₂₀ at 20% w/w solids.



Scheme 4.1. Two-step synthesis of a series of aldehyde-functionalised PGE05MA₂₆-PHPMA_y diblock copolymer nano-objects starting from PGE05MA₂₆ homopolymer. First, this water-soluble precursor is chain-extended *via* RAFT aqueous dispersion polymerisation of HPMA. The second step involves selective oxidation of the PGE05MA₂₆ block using aqueous NaIO₄ at 22 °C.

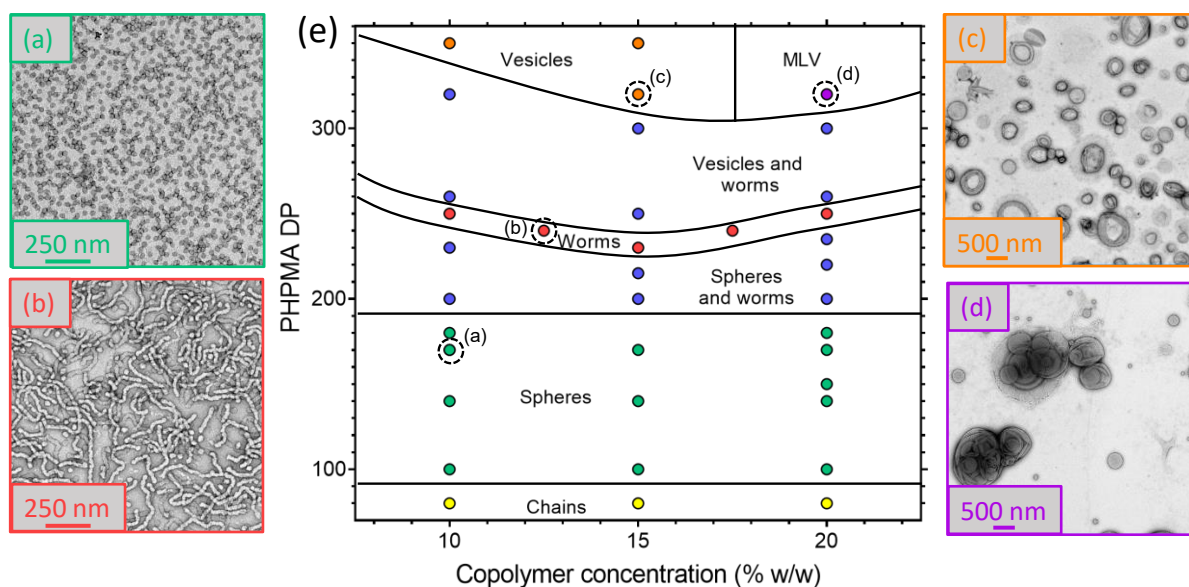


Figure 4.1. TEM images of (a) PGE05MA₂₆-PHPMA₁₇₀ spherical nanoparticles, (b) PGE05MA₂₆-PHPMA₂₄₀ anisotropic worms, (c) PGE05MA₂₆-PHPMA₃₂₀ vesicles, (d) PGE05MA₂₆-PHPMA₃₂₀ MLV, and (e) a PGE05MA₂₆-PHPMA_y diblock copolymer phase diagram showing pure spheres, worms or vesicles could each be obtained under appropriate conditions.

DMF GPC analysis showed that all diblock copolymers exhibited relatively low dispersities ($\mathcal{D} \leq 1.36$, Figure 4.2). However, high molecular weight shoulders can be observed in each

case, which have been previously attributed to dimethacrylate impurities in the HPMA monomer ($\sim 0.20\text{--}0.35\%$).^{60–62}

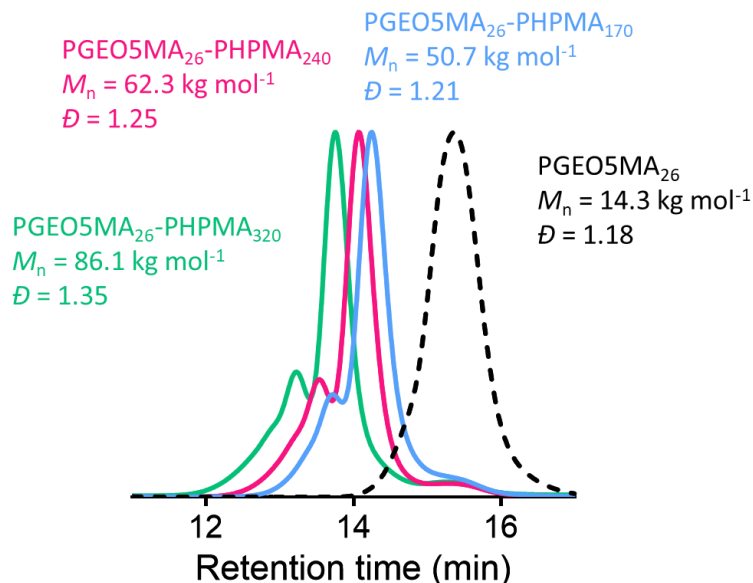


Figure 4.2. DMF GPC curves recorded for PGE05MA₂₆, PGE05MA₂₆-PHPMA₁₇₀, PGE05MA₂₆-PHPMA₂₄₀ and PGE05MA₂₆-PHPMA₃₂₀ diblock copolymers calibrated against a series of near-monodisperse poly(methyl methacrylate) (PMMA) standards.

4.3.2. Oxidation of PGE05MA₂₆-PHPMA_y diblock copolymer nanoparticles using NaIO₄

From this pseudo-phase diagram, three examples of PGE05MA₂₆-PHPMA_y ($y = 170, 250$ and 350) nanoparticles were synthesised at 10% w/w solids. ¹H NMR spectroscopy studies indicated that the HPMA conversion was greater than 99% in each case. TEM analysis indicated a spherical morphology for PGE05MA₂₆-PHPMA₁₇₀ nanoparticles (Figure 4.3a), a worm-like morphology for PGE05MA₂₆-PHPMA₂₅₀ (Figure 4.3c), and a vesicular morphology for PGE05MA₂₆-PHPMA₃₅₀ (Figure 4.4a). Oxidation of the PGE05MA₂₆ block to produce aldehyde-functional PAGE05MA₂₆ stabiliser chains was conducted using NaIO₄ in aqueous solution using the protocol reported in Chapter III.⁵⁹ A NaIO₄/*cis*-diol molar ratio of unity was selected to target oxidation of all of the pendent *cis*-diol groups within the PGE05MA₂₆ block, and the copolymer concentration was 5–10% w/w solids, which ensured efficient stirring. The extent of oxidation was determined to be more than 99% in each case by ¹H NMR spectroscopy as determined by the appearance of two new signals at 6.09 and 9.71 ppm corresponding to the geminal diol and aldehyde, respectively (Appendix 8). For PGE05MA₂₆-PHPMA₁₇₀ spheres, DMF GPC analysis indicated that periodate oxidation had a significant effect on the copolymer molecular weight distribution: the PGE05MA₂₆-PHPMA₁₇₀ precursor had an M_n of 50.7 kg mol⁻¹ and a \mathcal{D} of 1.21, whereas the PAGE05MA₂₆-PHPMA₁₇₀ product had an M_n of 66.0 kg mol⁻¹ and a \mathcal{D} of 1.74 (Figure 4.5a).

This was attributed to crosslinking between the aldehyde-functional group and the hydroxyl group on the HPMA units occurring at intermediate conversions. Perhaps surprisingly, periodate oxidation of the PGEO5MA₂₆-PHPMA₂₅₀ worms led to a relatively modest change in the copolymer molecular weight distribution [$M_n = 71.4 \text{ kg mol}^{-1}$ and $\mathcal{D} = 1.30$ for the precursor vs. $M_n = 71.8 \text{ kg mol}^{-1}$ and $\mathcal{D} = 1.37$ for the product (Figure 4.5b)]. The cause of this increase in dispersity is not currently understood. In both cases, TEM studies indicated that such oxidation did not affect the original copolymer morphology (Figure 4.3b and 4.3d). This suggests that chain transfer to polymer is not the cause of this increase, otherwise the PAGEO5MA₂₆-PHPMA₂₅₀ worms would have a higher degree of branching than the PAGEO5MA₂₆-PHPMA₁₇₀ spheres. Moreover, PGEO5MA₂₆-PHPMA₁₇₀ spheres had a DLS diameter of 31 nm (PDI = 0.02), whereas the PAGEO5MA₂₆-PHPMA₁₇₀ spheres had a DLS diameter of 32 nm (PDI = 0.08). These DLS data indicate that no interparticle crosslinking has occurred, so the increase in copolymer chain dispersity must be associated with intraparticle crosslinking. Further investigation into the underlying reason for the increase in copolymer dispersity is certainly warranted, but is unfortunately beyond the scope of this Thesis. The DLS data for the PGEO5MA₂₆-PHPMA₂₅₀ and PAGEO5MA₂₆-PHPMA₂₅₀ worms showed large apparent particle diameters and high PDIs [409 nm (PDI = 0.44) and 242 nm (PDI = 0.26), respectively]. However, as DLS measurements are based on a spherical model, these values do not correspond to either the worm length or width.

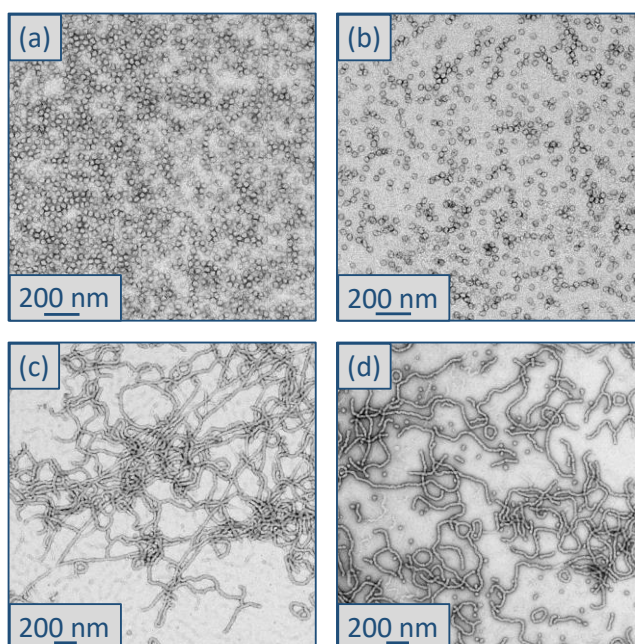


Figure 4.3. TEM images recorded for (a) PGEO5MA₂₆-PHPMA₁₇₀ spheres, (b) PAGEO5MA₂₆-PHPMA₁₇₀ spheres, (c) PGEO5MA₂₆-PHPMA₂₅₀ worms and (d) PAGEO5MA₂₆-PHPMA₂₅₀ worms.

In contrast, DLS analysis suggested a modest reduction in the z-average vesicle diameter for the periodate-treated PGEO5MA₂₆-PHPMA₃₅₀ vesicles [231 nm diameter (PDI = 0.04) vs. 219 nm diameter (PDI = 0.09)], while GPC studies indicated a significantly broader molecular weight distribution ($\mathcal{D} = 1.41$ vs. $\mathcal{D} = 2.09$ for PGEO5MA₂₆-PHPMA₃₅₀ and PAGEO5MA₂₆-PHPMA₃₅₀, respectively). More importantly, TEM studies revealed a minor worm population in addition to the oxidised vesicles (Figure 4.4b). These differences in copolymer morphology observed after periodate treatment are not currently understood and further studies are clearly warranted. For example, a series of systematic experiments should enable the minimum degree of oxidation of the PGEO5MA stabiliser chains required to induce vesicle instability to be identified. Similarly, it would be interesting to examine whether vesicles with thicker membranes also suffered from this problem.

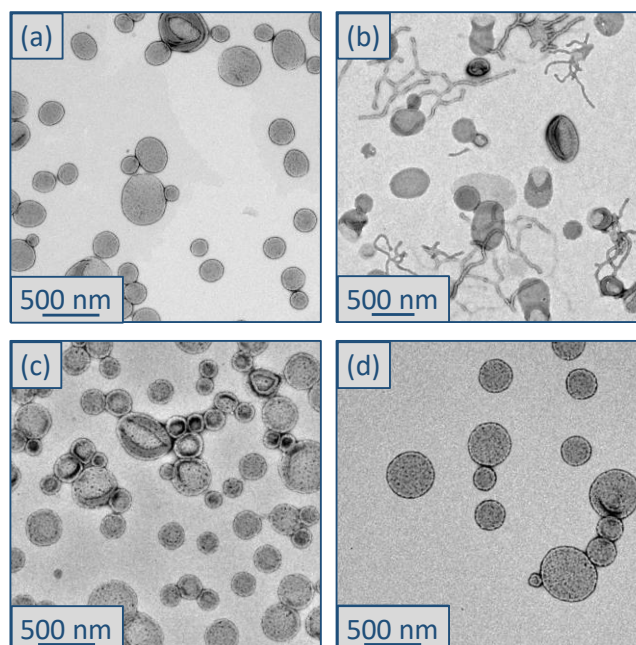


Figure 4.4. TEM images recorded for (a) PGEO5MA₂₆-PHPMA₃₅₀, (b) PAGEO5MA₂₆-PHPMA₃₅₀, (c) PGEO5MA₂₆-PHPMA₃₅₀-PEGDMA₂₀ and (d) PAGEO5MA₂₆-PHPMA₃₅₀-PEGDMA₂₀ vesicles.

To prevent the partial loss of the original vesicular morphology, 20 units of EGDMA crosslinker were added as a third block to crosslink the membrane-forming chains prior to periodate oxidation (Scheme 4.2).²⁰ The resulting covalently-stabilised vesicles (see Figure 4.4c) had a slightly smaller z-average diameter (214 nm, PDI = 0.11) than the original linear vesicles (231 nm, PDI = 0.04). To confirm successful crosslinking, further DLS studies were conducted in ethanol, which is a good solvent for both blocks. Addition of ethanol to the linear vesicles led to a derived count rate (or scattered light intensity) that was two orders of magnitude lower than that observed in water (Table 4.1). In contrast, the derived count rate was reduced by only a factor of two for the crosslinked vesicles dispersed in ethanol, indicating successful crosslinking of the membrane-forming chains. The

crosslinked vesicles were treated with periodate in aqueous solution. Unlike the linear vesicles, there was no TEM evidence for a worm population in this case (Figure 4.4d). Hence covalent stabilisation is sufficient to prevent degradation of the original vesicle morphology during oxidation of the PGE05MA stabiliser chains.

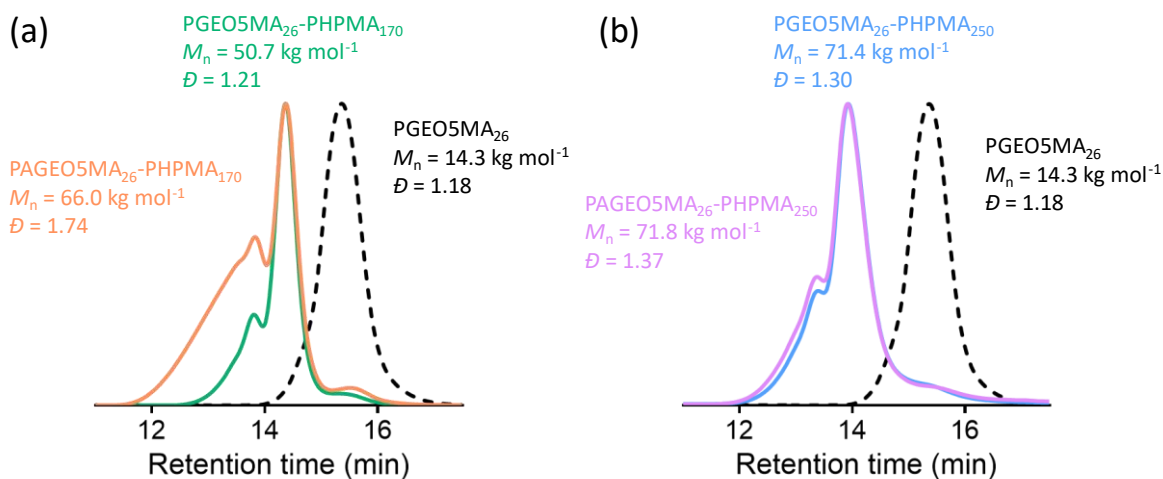
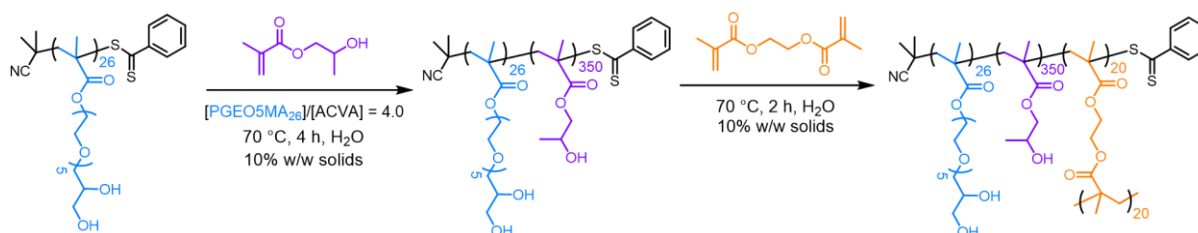


Figure 4.5. DMF GPC curves recorded for (a) PGE05MA₂₆, PGE05MA₂₆-PHPMA₁₇₀ and PAGE05MA₂₆-PHPMA₁₇₀ and (b) PGE05MA₂₆, PGE05MA₂₆-PHPMA₂₅₀ and PAGE05MA₂₆-PHPMA₂₅₀ diblock copolymers calibrated against a series of near-monodisperse PMMA standards.



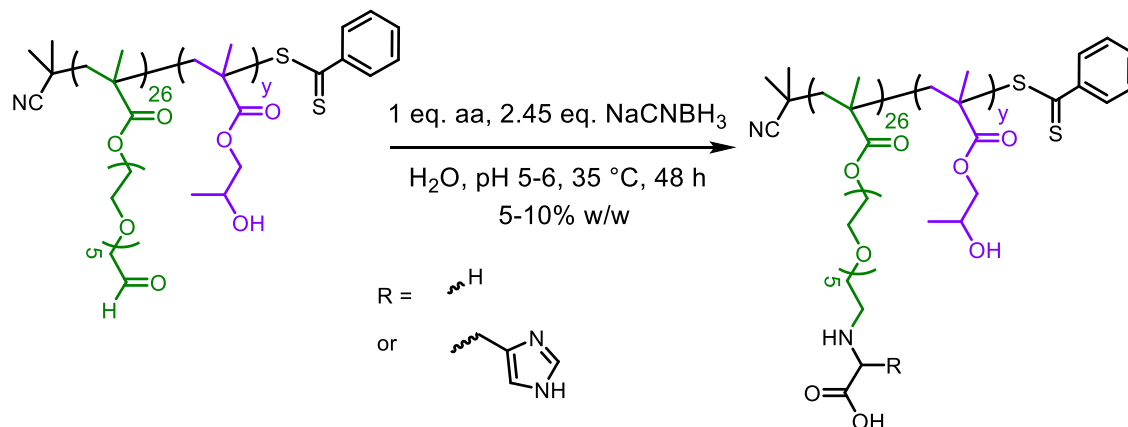
Scheme 4.2. Two-step, one-pot synthesis of membrane-crosslinked PGE05MA₂₆-PHPMA₃₅₀-PEGDMA₂₀ copolymer vesicles. The first step involves the chain extension of a PGE05MA₂₆ precursor by RAFT aqueous dispersion polymerisation of HPMA. The second step is the addition of EGDMA as a third block to crosslink the vesicle membrane.

Table 4.1. Summary of DLS data obtained for linear PGE05MA₂₆-PHPMA₃₅₀ and membrane-crosslinked PGE05MA₂₆-PHPMA₃₅₀-PEGDMA₂₀ copolymer vesicles dispersed in either water or ethanol.

Polymer composition	Solvent	DLS diameter (nm)	DLS PDI	Derived count rate (kcps)
PGE05MA ₂₆ -PHPMA ₃₅₀	Water	231	0.04	85976
PGE05MA ₂₆ -PHPMA ₃₅₀ -PEGDMA ₂₀	Water	214	0.11	93896
PGE05MA ₂₆ -PHPMA ₃₅₀	Ethanol	18	0.15	680
PGE05MA ₂₆ -PHPMA ₃₅₀ -PEGDMA ₂₀	Ethanol	549	0.14	41095

4.3.3. Functionalisation of PAGEO5MA₂₆-PHPMA_y(-PEGDMA₂₀) block copolymer nanoparticles *via* reductive amination

PAGEO5MA₂₆-PHPMA₁₇₀ spheres, PAGEO5MA₂₆-PHPMA₂₅₀ worms and PAGEO5MA₂₆-PHPMA₃₅₀-PEGDMA₂₀ vesicles were purified by dialysis against water and then reacted with either glycine or histidine *via* reductive amination (to produce PGlyGEO5MA₂₆-PHPMA_y(-PEGDMA₂₀) and PHisGEO5MA₂₆-PHPMA_y(-PEGDMA₂₀), respectively; Scheme 4.3). An amino acid/aldehyde molar ratio of unity was used for the initial Schiff base reaction, with a 2.45 excess of NaCNBH₃ being employed as the reducing agent. ¹H NMR spectroscopy studies confirmed the mean degree of amino acid functionalisation to be greater than 99% in each case (Appendix 8). Given the zwitterionic nature of the stabiliser block and the weakly hydrophobic character of the core-forming block, no GPC eluent was found to be suitable for the linear diblock copolymer chains. DLS studies indicated that the z-average particle diameter remained essentially unchanged after amino acid functionalisation (Table 4.2) while TEM analysis confirmed that such derivatisation led to no change in the copolymer morphology (Figure 4.6). This is not unexpected, as it has been shown that zwitterionic PMPC can be utilised as the stabiliser block for the synthesis of PMPC-PHPMA worms.⁶³



Scheme 4.3. Schiff base reaction of PAGEO5MA₂₆-PHPMA_y with an amino acid (e.g., glycine or histidine) followed by reductive amination using excess aqueous NaCNBH₃ at 35 °C to afford new amino acid-based diblock copolymers *via* a two-step, one-pot wholly aqueous protocol.

Aqueous electrophoresis studies were conducted to obtain zeta potential vs. pH curves. For *cis*-diol functionalised linear PAGEO5MA₂₆-PHPMA₁₇₀ spheres (Figure 4.7a), linear PAGEO5MA₂₆-PHPMA₂₅₀ worms (Figure 4.8a), and crosslinked PAGEO5MA₂₆-PHPMA₃₅₀-PEGDMA₂₀ vesicles (Figure 4.9a), and also the corresponding aldehyde-functionalised nano-objects obtained after NaIO₄ oxidation (Figure 4.7b, 4.8b and 4.9b), zeta potentials always remained close to zero over the whole pH range.

Table 4.2. DLS diameters and PDIs recorded for *cis*-diol-functionalised PGEO5MA₂₆-PHPMA_y(-PEGDMA₂₀), aldehyde-functionalised PAGEO5MA₂₆-PHPMA_y(-PEGDMA₂₀), glycine-functionalised PGlyGEO5MA₂₆-PHPMA_y(-PEGDMA₂₀), and histidine-functionalised PHisGEO5MA₂₆-PHPMA_y(-PEGDMA₂₀) spheres ($y = 170$), worms ($y = 250$) and vesicles ($y = 350$).

Polymer composition	DLS diameter (nm)	DLS PDI
PGEO5MA ₂₆ -PHPMA ₁₇₀	31	0.02
PAGEO5MA ₂₆ -PHPMA ₁₇₀	32	0.08
PGlyGEO5MA ₂₆ -PHPMA ₁₇₀	26	0.08
PHisGEO5MA ₂₆ -PHPMA ₁₇₀	32	0.08
PGEO5MA ₂₆ -PHPMA ₂₅₀	409	0.44
PAGEO5MA ₂₆ -PHPMA ₂₅₀	242	0.26
PGlyGEO5MA ₂₆ -PHPMA ₂₅₀	146	0.26
PHisGEO5MA ₂₆ -PHPMA ₂₅₀	320	0.48
PGEO5MA ₂₆ -PHPMA ₃₅₀ -PEGDMA ₂₀	214	0.11
PAGEO5MA ₂₆ -PHPMA ₃₅₀ -PEGDMA ₂₀	210	0.10
PGlyGEO5MA ₂₆ -PHPMA ₃₅₀ -PEGDMA ₂₀	216	0.08
PHisGEO5MA ₂₆ -PHPMA ₃₅₀ -PEGDMA ₂₀	212	0.10

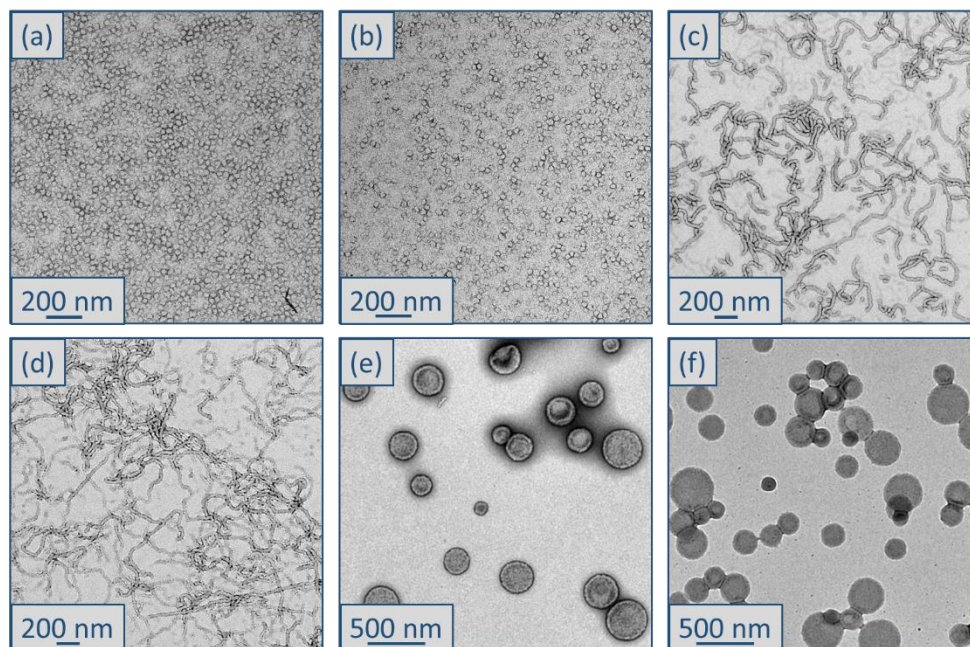


Figure 4.6. TEM images for (a) PGlyGEO5MA₂₆-PHPMA₁₇₀ spheres, (b) PHisGEO5MA₂₆-PHPMA₁₇₀ spheres, (c) PGlyGEO5MA₂₆-PHPMA₂₅₀ worms, (d) PHisGEO5MA₂₆-PHPMA₂₅₀ worms, (e) PGlyGEO5MA₂₆-PHPMA₃₅₀-PEGDMA₂₀ vesicles and (f) PHisGEO5MA₂₆-PHPMA₃₅₀-PEGDMA₂₀ vesicles.

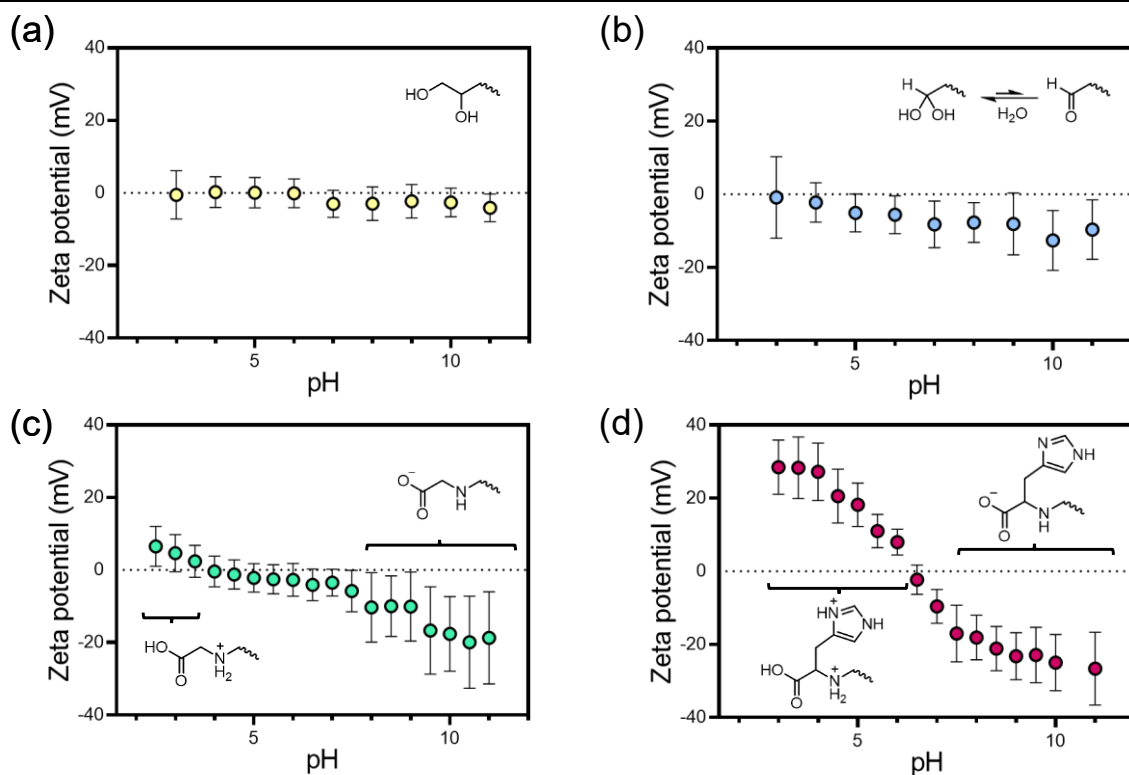


Figure 4.7. Zeta potential vs. pH curves obtained for (a) PGE05MA₂₆-PHPMA₁₇₀, (b) PAGE05MA₂₆-PHPMA₁₇₀, (c) PGlyGEO5MA₂₆-PHPMA₁₇₀, and (d) PHisGEO5MA₂₆-PHPMA₁₇₀ spheres.

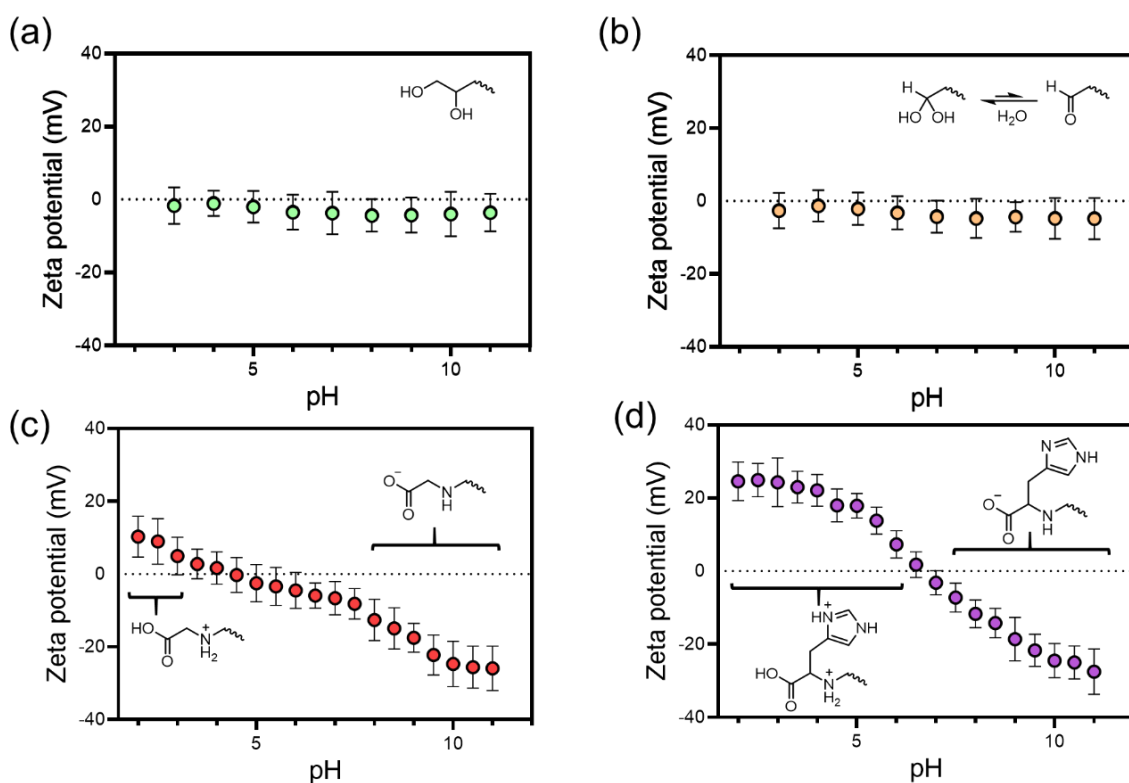


Figure 4.8. Zeta potential vs. pH curves obtained for (a) PGE05MA₂₆-PHPMA₂₅₀, (b) PAGE05MA₂₆-PHPMA₂₅₀, (c) PGlyGEO5MA₂₆-PHPMA₂₅₀, and (d) PHisGEO5MA₂₆-PHPMA₂₅₀ worms.

In contrast, glycine-functionalised copolymer nano-objects [e.g., PGlyGEO5MA₂₆-PHPMA₁₇₀ (Figure 4.7c), PGlyGEO5MA₂₆-PHPMA₂₅₀ (Figure 4.8c) and PGlyGEO5MA₂₆-PHPMA₃₅₀-PEGDMA₂₀ (Figure 4.9c)] exhibited positive zeta potentials

between pH 3 and pH 4.5 owing to protonation of both the carboxylic acid and the secondary amine groups. An isoelectric point (IEP) was observed at around pH 5, as expected for the zwitterionic form of the pendent amino acid. At higher pH, increasingly negative zeta potentials are obtained as the protonated secondary amine group is gradually converted into its neutral form.

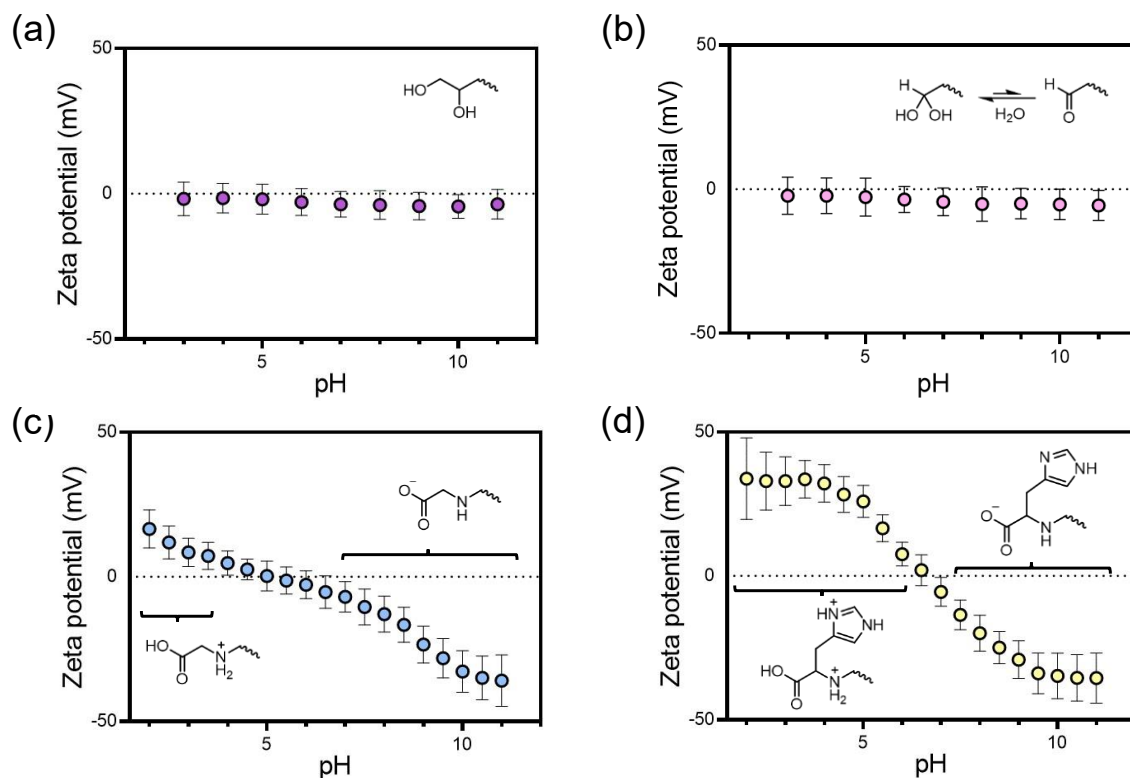


Figure 4.9. Zeta potential vs. pH curves obtained for (a) PGE05MA₂₆-PHPMA₃₅₀-PEGDMA₂₀ vesicles, (b) PAGE05MA₂₆-PHPMA₃₅₀-PEGDMA₂₀ vesicles, (c) PGlyGEO5MA₂₆-PHPMA₃₅₀-PEGDMA₂₀ vesicles, and (d) PHisGEO5MA₂₆-PHPMA₃₅₀-PEGDMA₂₀ vesicles.

Similarly, histidine-functionalised PHisGEO5MA₂₆-PHPMA₁₇₀ spheres (Figure 4.7d), PHisGEO5MA₂₆-PHPMA₂₅₀ worms (Figure 4.8d) and PHisGEO5MA₂₆-PHPMA₃₅₀-PEGDMA₂₀ vesicles (Figure 4.9d) each exhibited positive zeta potentials at low pH, indicating protonation of the pendent imidazole ring. An IEP is observed at around pH 6.5 in each case. Above pH 6.5, zeta potentials became progressively more negative as the protonated secondary amine groups revert to their neutral form. These aqueous electrophoresis studies demonstrate how the electrophoretic footprint of such nano-objects can be tuned by amino acid functionalisation.

The crosslinked PAGE05MA₂₆-PHPMA₃₅₀-PEGDMA₂₀ vesicles were also reacted with a model globular protein, BSA, *via* reductive amination using excess NaCNBH₃ as the reducing agent (Figure 4.10a–b). In this case, the surface amine groups on the protein react with the pendent aldehyde groups located on the outer surface of the vesicles.

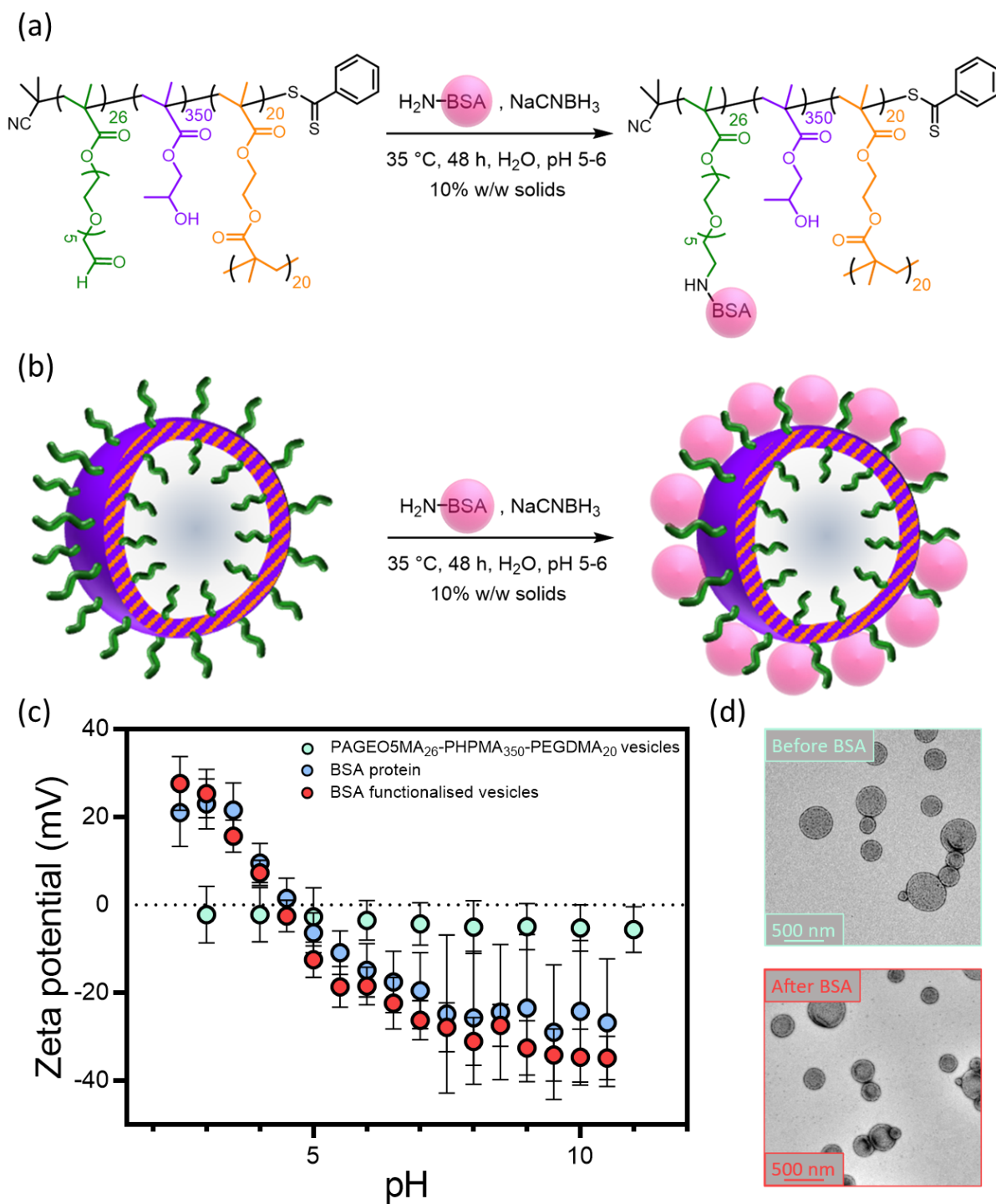


Figure 4.10. (a) Reductive amination of crosslinked PAGEO5MA₂₆-PHPMA₃₅₀-PEGDMA₂₀ vesicles with BSA protein, (b) schematic representation of the reaction of crosslinked PAGEO5MA₂₆-PHPMA₃₅₀-PEGDMA₂₀ vesicles with BSA *via* reductive amination (N.B. BSA is not shown to scale relative to the vesicles), (c) zeta potential vs. pH curves obtained for the original aldehyde-functionalised PAGEO5MA₂₆-PHPMA₃₅₀-PEGDMA₂₀ vesicles, BSA alone, and the final BSA-functionalised PAGEO5MA₂₆-PHPMA₃₅₀-PEGDMA₂₀ vesicles. (d) TEM analysis confirms that BSA functionalisation did not affect the original vesicle morphology.

The maximum number of BSA molecules adsorbed onto each vesicle was calculated using the approach reported by Balmer and co-workers, which calculates how many smaller spheres can be packed around a larger central sphere on the basis of geometric considerations.⁶⁴ The functionalised vesicles were then centrifuged and redispersed five times to ensure that any unbound BSA was removed from the aqueous dispersion. TEM analysis confirmed that the original vesicle morphology remained intact after exposure to BSA (Figure 4.10d). In order to determine whether the BSA had been successfully grafted onto the surface of the vesicles, aqueous electrophoresis studies were conducted (Figure 4.10c). The zeta potential vs. pH curve obtained for BSA alone indicated an IEP at pH 4.5, which is in good agreement with the literature.⁶⁵ In contrast, the aldehyde-functionalised vesicles exhibited approximately neutral character over the whole pH range. In principle, the BSA-grafted vesicles should exhibit a comparable electrophoretic footprint to that of the BSA alone. Indeed, a very similar zeta potential vs. pH curve was obtained, with essentially the same IEP being observed at around pH 4.5.

As a control experiment, the *cis*-diol-functionalised PGE05MA₂₆-PHPMA₃₅₀-EGDMA₂₀ precursor vesicles were also exposed to BSA under the same conditions, followed by purification *via* five centrifugation-redispersion cycles (Figure 4.11). In this case, no change in the electrophoretic footprint was observed relative to the original vesicles (Figure 4.12). This confirms that surface aldehyde groups are required to ensure that the BSA molecules adsorb onto the vesicles.

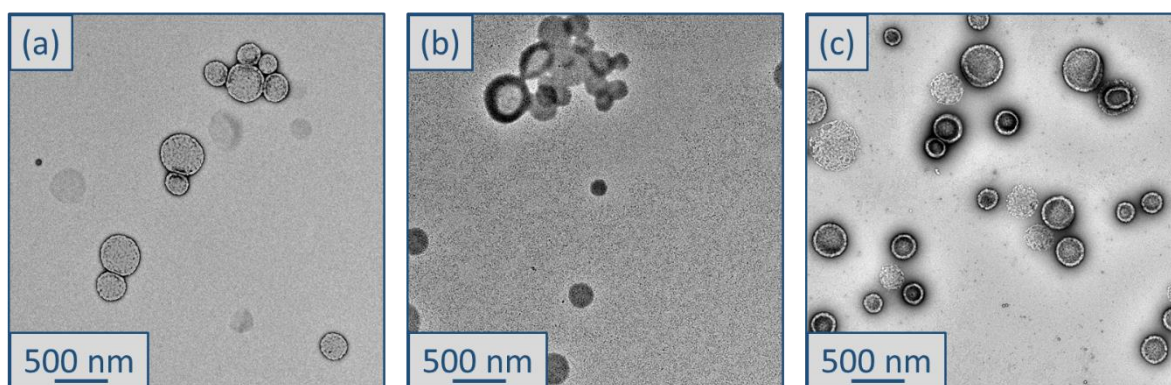


Figure 4.11. Transmission electron microscopy images obtained for (a) PGE05MA₂₆-PHPMA₃₅₀-PEGDMA₂₀ vesicles before attempted reaction with BSA, (b) PGE05MA₂₆-PHPMA₃₅₀-PEGDMA₂₀ vesicles directly after attempted reaction with BSA and (c) PGE05MA₂₆-PHPMA₃₅₀-PEGDMA₂₀ vesicles after attempted reaction with BSA and subsequent purification *via* five centrifugation and redispersion cycles.

4.4. Conclusion

The synthesis of a series of new diblock copolymer nano-objects *via* RAFT aqueous dispersion polymerisation of HPMA using a new methacrylic monomer, GEO5MA, to

prepare the water-soluble precursor block is reported. The pendent *cis*-diol groups located within the PGEO5MA steric stabiliser chains can be selectively oxidised using NaIO₄ to afford aldehyde-functional PAGEO5MA-PHPMA nano-objects without loss of colloidal stability. In the case of PAGEO5MA-PHPMA spheres or worms, periodate treatment does not affect the original copolymer morphology. In contrast, TEM studies indicate that periodate oxidation of the vesicles generates a minor population of worms. Fortunately, this undesirable partial loss of the original vesicular morphology can be prevented by introducing EGDMA as a third block to crosslink the membrane-forming copolymer chains. Such covalently-stabilised PAGEO5MA-PHPMA-PEGDMA vesicles can be reacted with either an amino acid or a model globular protein (BSA) to form Schiff base linkages under mild conditions. In both cases, this leads to a significant change in the electrophoretic footprint of the vesicles. Such facile conjugation chemistry should offer potential bio-applications. For example, the BSA-functionalised vesicles should exhibit excellent stealth-like behaviour in either *in vitro* or *in vivo* experiments.

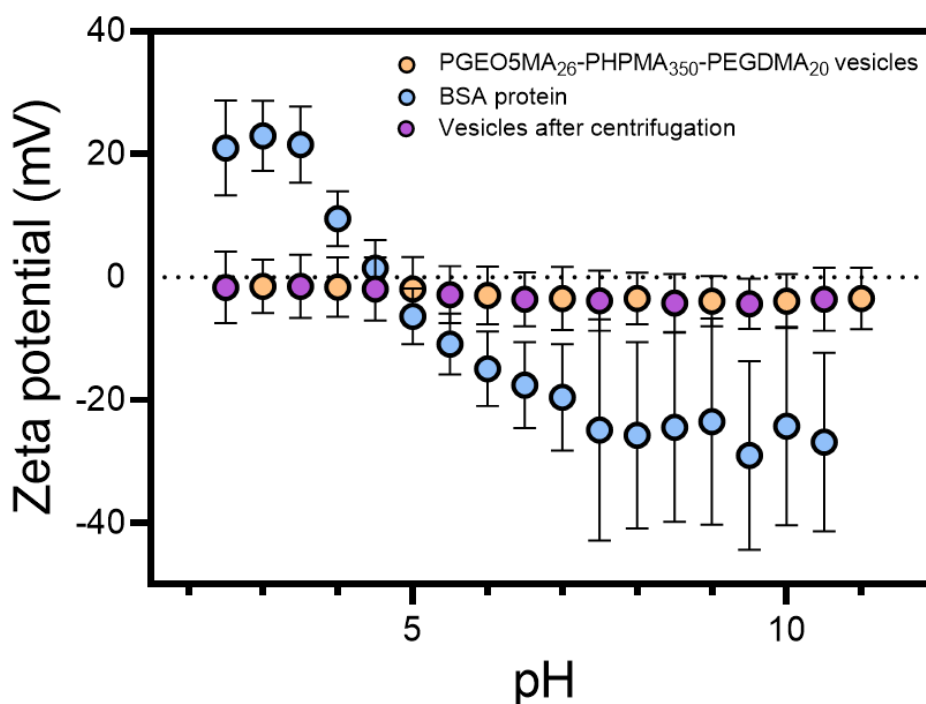


Figure 4.12. Zeta potential vs. pH curves obtained for crosslinked PGEO5MA₂₆-PHPMA₃₅₀-PEGDMA₂₀ vesicles, BSA protein alone and crosslinked PGEO5MA₂₆-PHPMA₃₅₀-PEGDMA₂₀ vesicles after exposure to BSA followed by five centrifugation and redispersion cycles. The unchanged electrophoretic data observed for the vesicles confirms that there is no BSA adsorption in this case.

4.5. References

- 1 S. Newman, *J. Appl. Polym. Sci.*, 1962, **6**, S15–S16.
- 2 G. M. Burnett, P. Mears and C. Paton, *Trans. Faraday Soc.*, 1962, **58**, 737–746.

- 3 S. Krause, *J. Phys. Chem.*, 1964, **68**, 1948–1955.
 - 4 Z. Gao, S. K. Varshney, S. Wong and A. Eisenberg, *Macromolecules*, 1994, **27**, 7923–7927.
 - 5 L. Zhang and A. Eisenberg, *Science*, 1995, **268**, 1728–1731.
 - 6 S. L. Canning, G. N. Smith and S. P. Armes, *Macromolecules*, 2016, **49**, 1985–2001.
 - 7 B. Charleux, G. Delaittre, J. Rieger and F. D'Agosto, *Macromolecules*, 2012, **45**, 6753–6765.
 - 8 F. D'Agosto, J. Rieger and M. Lansalot, *Angew. Chemie Int. Ed.*, 2019, **59**, 2–27.
 - 9 A. Blanazs, A. J. Ryan and S. P. Armes, *Macromolecules*, 2012, **45**, 5099–5107.
 - 10 L. D. Blackman, K. E. B. Doncom, M. I. Gibson and R. K. O'Reilly, *Polym. Chem.*, 2017, **8**, 2860–2871.
 - 11 E. R. Jones, M. Semsarilar, P. Wyman, M. Boerakker and S. P. Armes, *Polym. Chem.*, 2016, **7**, 851–859.
 - 12 J. Chiefari, Y. K. Chong, F. Ercole, J. Krstina, J. Jeffery, T. P. T Le, R. T. A Mayadunne, G. F. Meijs, C. L. Moad, G. Moad, E. Rizzardo and S. H. Thang, *Macromolecules*, 1998, **31**, 5559–5562.
 - 13 D. J. Keddie, G. Moad, E. Rizzardo and S. H. Thang, *Macromolecules*, 2012, **45**, 5321–5342.
 - 14 Y. Du, S. Jia, Y. Chen, L. Zhang and J. Tan, *ACS Macro Lett.*, 2021, **10**, 297–306.
 - 15 J. Rosselgong, A. Blanazs, P. Chambon, M. Williams, M. Semsarilar, J. Madsen, G. Battaglia and S. P. Armes, *ACS Macro Lett.*, 2012, **1**, 1041–1045.
 - 16 K. A. Simon, N. J. Warren, B. Mosadegh, M. R. Mohammady, G. M. Whitesides and S. P. Armes, *Biomacromolecules*, 2015, **16**, 3952–3958.
 - 17 F. L. Hatton, J. R. Lovett and S. P. Armes, *Polym. Chem.*, 2017, **8**, 4856–4868.
 - 18 F. L. Hatton, A. M. Park, Y. Zhang, G. D. Fuchs, C. K. Ober and S. P. Armes, *Polym. Chem.*, 2019, **10**, 194–200.
 - 19 F. L. Hatton, M. J. Derry and S. P. Armes, *Polym. Chem.*, 2020, **11**, 6343–6355.
 - 20 P. Chambon, A. Blanazs, G. Battaglia and S. P. Armes, *Macromolecules*, 2012, **45**, 5081–5090.
 - 21 X. Dai, L. Yu, Y. Zhang, L. Zhang and J. Tan, *Macromolecules*, 2019, **52**, 7468–7476.
 - 22 Z. Cui, H. Cao, Y. Ding, P. Gao, X. Lu and Y. Cai, *Polym. Chem.*, 2017, **8**, 3755–3763.
 - 23 S. J. Byard, M. Williams, B. E. McKenzie, A. Blanazs and S. P. Armes, *Macromolecules*, 2017, **50**, 1482–1493.
 - 24 F. H. Sobotta, F. Hausig, D. O. Harz, S. Hoepfner, U. S. Schubert and J. C. Brendel, *Polym. Chem.*, 2018, **9**, 1593–1602.
 - 25 G. Mellot, J.-M. Guigner, L. Bouteiller, F. Stoffelbach and J. Rieger, *Angew. Chemie Int. Ed.*, 2019, **58**, 3173–3177.
-

-
- 26 J. R. Lovett, N. J. Warren, S. P. Armes, M. J. Smallridge and R. B. Cracknell, *Macromolecules*, 2016, **49**, 1016–1025.
- 27 J. R. Lovett, N. J. Warren, L. P. D. Ratcliffe, M. K. Kocik and S. P. Armes, *Angew. Chemie Int. Ed.*, 2015, **54**, 1279–1283.
- 28 V. J. Cunningham, A. M. Alswieleh, K. L. Thompson, M. Williams, G. J. Leggett, S. P. Armes and O. M. Musa, *Macromolecules*, 2014, **47**, 5613–5623.
- 29 R. Deng, Y. Ning, E. R. Jones, V. J. Cunningham, N. J. W. Penfold and S. P. Armes, *Polym. Chem.*, 2017, **8**, 5374–5380.
- 30 R. Deng, M. J. Derry, C. J. Mable, Y. Ning and S. P. Armes, *J. Am. Chem. Soc.*, 2017, **139**, 7616–7623.
- 31 I. Canton, N. J. Warren, A. Chahal, K. Amps, A. Wood, R. Weightman, E. Wang, H. Moore and S. P. Armes, *ACS Cent. Sci.*, 2016, **2**, 65–74.
- 32 M. B. Smith and J. March, *March's advanced organic chemistry: reactions, mechanisms, and structure*, John Wiley & Sons, Inc., Hoboken, NJ, 2007.
- 33 J. Collins, K. Kempe, P. Wilson, C. A. Blindauer, M. P. McIntosh, T. P. Davis, M. R. Whittaker and D. M. Haddleton, *Biomacromolecules*, 2016, **17**, 2755–2766.
- 34 J. Collins, S. J. Wallis, A. Simula, M. R. Whittaker, M. P. McIntosh, P. Wilson, T. P. Davis, D. M. Haddleton and K. Kempe, *Macromol. Rapid Commun.*, 2017, **38**, 1600534.
- 35 A. W. Jackson and D. A. Fulton, *Macromolecules*, 2012, **45**, 2699–2708.
- 36 G. Sun, H. Fang, C. Cheng, P. Lu, K. Zang, A. V. Walker, J.-S. A. Taylor and K. L. Wooley, *ACS Nano*, 2009, **3**, 673–681.
- 37 G. S. Heo, S. Cho and K. L. Wooley, *Polym. Chem.*, 2014, **5**, 3555–3558.
- 38 G. Sun, C. Cheng and K. L. Wooley, *Macromolecules*, 2007, **40**, 793–795.
- 39 S. N. S. Alconcel, S. H. Kim, L. Tao and H. D. Maynard, *Macromol. Rapid Commun.*, 2013, **34**, 983–989.
- 40 J. Hwang, R. C. Li and H. D. Maynard, *J. Control. Release*, 2007, **122**, 279–286.
- 41 C. L. I. Ronald, R. M. Broyer and H. D. Maynard, *J. Polym. Sci. Part A Polym. Chem.*, 2006, **44**, 5004–5013.
- 42 T. Bilgic and H.-A. Klok, *Biomacromolecules*, 2015, **16**, 3657–3665.
- 43 M. A. Gauthier and H.-A. Klok, *Biomacromolecules*, 2011, **12**, 482–493.
- 44 J. Wang, P. Karami, N. C. Ataman, D. P. Pioletti, T. W. J. Steele and H.-A. Klok, *Biomacromolecules*, 2020, **21**, 240–249.
- 45 C. Scholz, M. Iijima, Y. Nagasaki and K. Kataoka, *Macromolecules*, 1995, **28**, 7295–7297.
- 46 M. A. Gauthier, M. Ayer, J. Kowal, F. R. Wurm and H. A. Klok, *Polym. Chem.*, 2011, **2**, 1490–1498.
- 47 L. Tao, G. Mantovani, F. Lecolley and D. M. Haddleton, *J. Am. Chem. Soc.*, 2004, **126**, 13220–13221.
-

- 48 B. S. Murray and D. A. Fulton, *Macromolecules*, 2011, **44**, 7242–7252.
- 49 D. E. Whitaker, C. S. Mahon and D. A. Fulton, *Angew. Chemie Int. Ed.*, 2013, **52**, 956–959.
- 50 B. S. Murray, A. W. Jackson, C. S. Mahon and D. A. Fulton, *Chem. Commun.*, 2010, **46**, 8651–8653.
- 51 H. Otsuka, Y. Nagasaki and K. Kataoka, *Biomacromolecules*, 2000, **1**, 39–48.
- 52 Y. Nagasaki, T. Okada, C. Scholz, M. Iijima, M. Kato and K. Kataoka, *Macromolecules*, 1998, **31**, 1473–1479.
- 53 M. Iijima, Y. Nagasaki, T. Okada, M. Kato and K. Kataoka, *Macromolecules*, 1999, **32**, 1140–1146.
- 54 R. J. Mancini, J. Lee and H. D. Maynard, *J. Am. Chem. Soc.*, 2012, **134**, 8474–8479.
- 55 B. Karagoz, L. Esser, H. T. Duong, J. S. Basuki, C. Boyer and T. P. Davis, *Polym. Chem.*, 2014, **5**, 350–355.
- 56 J. Liu, H. Duong, M. R. Whittaker, T. P. Davis and C. Boyer, *Macromol. Rapid Commun.*, 2012, **33**, 760–766.
- 57 L. Qiu, C. R. Xu, F. Zhong, C. Y. Hong and C. Y. Pan, *ACS Appl. Mater. Interfaces*, 2016, **8**, 18347–18359.
- 58 L. Qiu, C. R. Xu, F. Zhong, C. Y. Hong and C. Y. Pan, *Macromol. Chem. Phys.*, 2016, **217**, 1047–1056.
- 59 E. E. Brotherton, C. P. Jesson, N. J. Warren, M. J. Smallridge and S. P. Armes, *Angew. Chemie Int. Ed.*, 2021, **60**, 12032–12037.
- 60 Y. Li and S. P. Armes, *Angew. Chemie*, 2010, **122**, 4136–4140.
- 61 I. Bannister, N. C. Billingham, S. P. Armes, S. P. Rannard and P. Findlay, *Macromolecules*, 2006, **39**, 7483–7492.
- 62 A. Blanz, J. Madsen, G. Battaglia, A. J. Ryan and S. P. Armes, *J. Am. Chem. Soc.*, 2011, **133**, 16581–16587.
- 63 D. L. Beattie, O. O. Mykhaylyk, A. J. Ryan and S. P. Armes, *Soft Matter*, 2021, **17**, 5602–5612.
- 64 J. A. Balmer, S. P. Armes, P. W. Fowler, T. Tarnai, Z. Gáspár, K. A. Murray and N. S. J. Williams, *Langmuir*, 2009, **25**, 5339–5347.
- 65 K. M. Au and S. P. Armes, *ACS Nano*, 2012, **6**, 8261–8279.

*Chapter V: Aldehyde-functional
thermoreponsive diblock copolymer
worm gels exhibit strong mucoadhesion*

Reproduced in full with permission from:

E. E. Brotherton, T. J. Neal, D. B. Kaldybekov, M. J. Smallridge, V. V. Khutoryanskiy and S. P. Armes, *Chem. Sci.*, 2022, **13**, 6888–6898.

Chapter V: Aldehyde-functional thermoresponsive diblock copolymer worm gels exhibit strong mucoadhesion

5.1. Introduction

It is well known that amphiphilic diblock copolymers undergo spontaneous self-assembly in aqueous solution to form a wide range of nano-objects, including spheres, worms, vesicles or lamellae.¹⁻⁷ Typically, such copolymer morphologies are accessed through post-polymerisation processing *via* initial copolymer dissolution in a suitable water-miscible solvent such as tetrahydrofuran or dimethylformamide (DMF), followed by dilution *via* slow addition of water.⁸ Under such near-equilibrium conditions, the precise copolymer morphology usually depends solely on the relative volume fraction of each block, as indicated by the fractional packing parameter originally introduced for conventional small molecule surfactants.⁸⁻¹⁰

Over the past decade or so, the development of polymerisation-induced self-assembly (PISA) has provided convenient access to pure copolymer morphologies.¹¹⁻²² Unlike spheres or vesicles, diblock copolymer worms usually occupy relatively narrow phase space. Nevertheless, it has been shown that the construction of pseudo-phase diagrams facilitates the reproducible synthesis of worms, which are usually well-defined in terms of their mean cross-sectional area but typically somewhat polydisperse in terms of their length.^{12,18,20,23-31}

Such worms typically form 3D networks in semi-concentrated solution, which leads to macroscopic gelation under zero shear at ambient temperature.^{25,26} In particular, the reversible addition-fragmentation chain transfer (RAFT) aqueous dispersion polymerisation of 2-hydroxypropyl methacrylate (HPMA) provides access to thermoresponsive worms that exhibit a worm-to-sphere transition on cooling to sub-ambient temperature.^{27,32-35} This morphological transition is reversible and is accompanied by degelation.³⁶ This is important in the context of potential cell biology applications because it enables the media to be sterilised *via* ultrafiltration and for the cells to be readily harvested after cell culture studies.^{34,37-40}

Polymeric hydrogels have many applications in biomedical research, ranging from soft contact lenses to gel electrophoresis.^{41,42} In principle, hydrogels bearing appropriate chemical functionality can adhere to biological surfaces. This is likely to be particularly important for mucosal drug delivery, for which therapeutic efficiency is often substantially reduced by the continuous production and flow of biological fluids.^{43,44} This can result in drug leakage from the site of administration, which prevents effective localised delivery. For example, poor retention on mucosal surfaces is a common problem in delivering drugs to the eye, where the continuous production of tear fluid causes rapid removal of the active pharmaceutical ingredient from ocular surfaces.^{45,46} Similar problems are well-documented for the nasal cavity: the generation of mucus and the protective function afforded by mucociliary clearance does not allow drug molecules to be retained on the olfactory epithelium, which potentially offers efficient nasal delivery to the brain.^{47,48} Similarly, drugs administered by catheter to treat bladder cancer also suffer from short residence times owing to the continuous production of urine and the periodic need for organ voiding.^{49,50}

In principle, more effective drug delivery *via* mucosal surfaces should be feasible by designing mucoadhesive hydrogels. Various strategies to enhance mucoadhesion have been reported, including the design of copolymers containing thiol,^{51,52} acryloyl,^{53,54} methacryloyl^{55,56} or maleimide groups.^{57,58} These reactive moieties can form covalent bonds with the thiol group in cysteine, which is one of the amino acid building blocks present within mucins. Another strategy is the introduction of phenylboronic acid groups, which can form dynamic covalent bonds with the 1,2-diol-functional sugar groups expressed by mucins.^{59,60} Alternatively, catechol-based mucoadhesive polymers have been evaluated owing to their ability to form catechol-thiol or catechol-amine adducts with mucins.^{61,62} More recently, Bernkop-Schnürch and co-workers reported the synthesis of polymers functionalised with *N*-hydroxy(sulfo)succinimide esters that form amide bonds with mucins.^{63,64}

In Chapter III, the use of RAFT polymerisation^{65–67} for the synthesis of a new water-soluble methacrylic polymer (denoted as PGEO5MA) that contains pendent *cis*-diol groups was reported.⁶⁸ This precursor can be oxidised under mild conditions in aqueous solution using sodium periodate (NaIO₄) to produce the corresponding aldehyde-functionalised water-soluble polymer. Subsequently, in Chapter IV, a PGEO5MA precursor was employed for the RAFT aqueous dispersion polymerisation of HPMA to prepare a series of well-defined diblock copolymer spheres, worms or vesicles.⁶⁹ In particular, it was shown

that a model globular protein could be chemically adsorbed onto PGEO5MA-PHPMA vesicles *via* Schiff base chemistry (followed by *in situ* reduction of the initial labile imine linkages to produce hydrolytically stable amine bonds). In this Chapter, this aqueous PISA formulation is revisited to prepare well-defined aldehyde-functional diblock copolymer worm gels and examine whether such materials offer any potential use in the context of mucoadhesion (*via* Schiff base chemistry) using porcine urinary bladder mucosa as a model system.

5.2. Experimental

5.2.1. Synthesis

Synthesis of PGEO5MA_x precursors by RAFT solution polymerisation in ethanol

A PGEO5MA₁₃ and a PGEO5MA₁₆ precursor were prepared in this study. The synthesis of PGEO5MA₁₃ is representative of the general protocol. GEO5MA monomer (25.0 g, 65.7 mmol), 2-cyano-2-propyl dithiobenzoate (CPDB) RAFT agent (1.45 g, 6.57 mmol), 4,4'-azobis(4-cyanopentanoic acid) (ACVA) initiator (0.368 g, 1.31 mmol; RAFT agent/initiator molar ratio = 5.0) and ethanol (17.9 g) were weighed into a 100 mL round-bottomed flask. The reaction mixture was deoxygenated for 40 min using a stream of N₂ gas before immersing the flask in an oil bath set at 70 °C for 180 min. The polymerisation was quenched by removing the flask from the oil bath and cooling to 20 °C while simultaneously exposing the reaction mixture to air. The GEO5MA conversion was determined to be 85% by ¹H NMR spectroscopy (by comparing the residual monomer vinyl signals at 5.61–6.18 ppm to the five methacrylic backbone protons at 0.78–2.71 ppm). The crude precursor was purified by precipitation into excess diethyl ether to remove any unreacted monomer and other impurities, followed by filtration and redissolution in methanol. This precipitation step was repeated and the purified homopolymer was dried in a vacuum oven set at 35 °C overnight to produce a red viscous liquid. The mean degree of polymerisation (DP) of this precursor was determined to be 13 by end-group analysis using ¹H NMR spectroscopy (the five aromatic protons of the dithiobenzoate chain-end at 7.34–8.03 ppm were compared to the five methacrylic backbone protons at 0.78–2.71 ppm).

Synthesis of PGEO5MA_x-PHPMA_y diblock copolymer nanoparticles by RAFT aqueous dispersion polymerisation of HPMA

PGEO5MA₁₃-PHPMA_y and PGEO5MA₁₆-PHPMA_y nanoparticles were prepared at 10% w/w solids. The synthesis of PGEO5MA₁₃-PHPMA₁₅₀ is representative of the general protocol. HPMA monomer (0.500 g, 3.47 mmol), PGEO5MA₁₃ precursor (120 mg, 23.1 μmol; target

PHPMA DP = 150), ACVA initiator (2.2 mg, 7.71 μmol ; PGEO5MA₁₃/initiator molar ratio = 3.0) and water (5.59 g) were weighed into a 15 mL sample vial. The reaction mixture was deoxygenated using a stream of N₂ gas for 30 min and the sample vial was placed into an oil bath set at 70 °C. After 4 h, the vial was removed from the oil bath and the polymerisation was quenched by cooling to 20 °C while exposing the contents of the vial to air. The final HPMA conversion was determined to be 99% by ¹H NMR spectroscopy (the residual monomer vinyl signals at 5.61–6.18 ppm were compared to the integrated methacrylic backbone signals at 0.81–2.30 ppm).

Synthesis of PGEO5MA₁₃-P(HPMA₁₅₅-stat-FMA_{0.15}) diblock copolymer nanoparticles by RAFT aqueous dispersion copolymerisation of HPMA with fluorescein methacrylate (FMA)

Fluorescently-labelled PGEO5MA₁₃-P(HPMA₁₅₅-stat-FMA_{0.15}) nanoparticles were prepared at 10% w/w solids. HPMA monomer (3.00 g, 20.8 mmol), FMA (8.30 mg, 20.8 μmol) and PGEO5MA₁₃ precursor (0.694 g, 134 μmol ; target PHPMA DP = 155) were added in turn to a 100 mL round-bottomed flask and stirred until a homogeneous solution was obtained. Then ACVA initiator (7.5 mg, 26.9 μmol ; PGEO5MA₁₃/ACVA molar ratio = 5.0) and water (27.2 g) were added to the flask and the reaction mixture was deoxygenated using a stream of N₂ gas for 30 min prior to immersing the flask in an oil bath set at 70 °C. After 4 h, the copolymerisation was quenched by cooling the flask to 20 °C while simultaneously exposing the contents of the flask to air. The final HPMA conversion was determined to be 99% by ¹H NMR spectroscopy (the integrated monomer vinyl signals at 5.67–6.16 ppm were compared to the methacrylic backbone protons at 0.81–2.30 ppm). Copolymers were dialysed against methanol for 24 h and then deionised water for two days.

Selective oxidation of PGEO5MA₁₃-P(HPMA₁₅₅-stat-FMA_{0.15}) diblock copolymer nanoparticles using NaIO₄

The synthesis of PGEO5MA₁₃-P(HPMA₁₅₅-stat-FMA_{0.15}) nanoparticles with 10% aldehyde functionality in aqueous solution is representative of the general protocol. NaIO₄ (1.5 mg, 7.14 μmol) was dissolved in a 12% w/w aqueous dispersion of PGEO5MA₁₃-P(HPMA₁₅₅-stat-FMA_{0.15}) nanoparticles (3.00 g, 0.11 mmol) that had been pre-cooled to 5 °C. A NaIO₄/*cis*-diol molar ratio of 0.10 was used to target a degree of aldehyde functionality of 10%. The periodate oxidation reaction was conducted in the dark at 5 °C for 30 min with continuous stirring [N.B. Under such conditions, the PGEO5MA₁₃-P(HPMA₁₅₅-stat-FMA_{0.15}) chains form spherical nanoparticles as opposed to worms, which is beneficial for efficient stirring]. The degree of aldehyde functionality was determined to be approximately 10% by ¹H NMR spectroscopy (the geminal diol signal

assigned to the AGEO5MA units at 5.13 ppm was compared to the five methacrylic backbone protons at 0.81–2.30 ppm). Other degrees of aldehyde functionality were targeted by adjusting the NaIO₄/*cis*-diol molar ratio as required. Periodate-treated copolymers were dialysed against deionised water for two days (with three water changes per day).

Synthesis of fluorescein isothiocyanate (FITC)-labelled chitosan

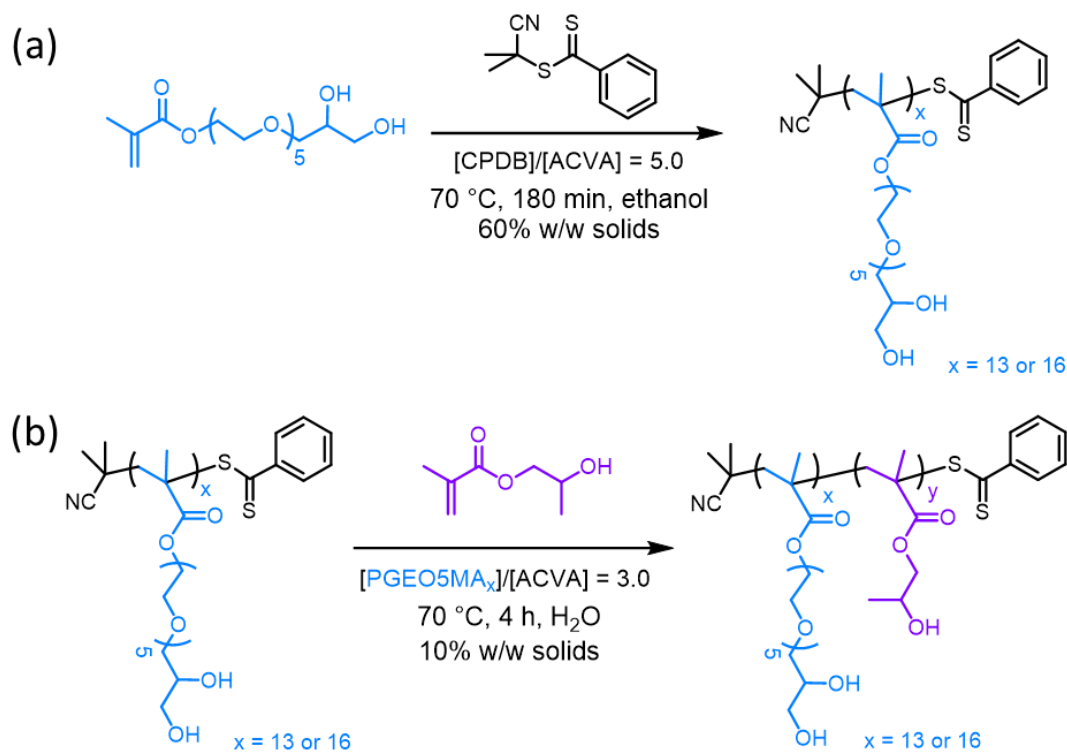
Chitosan was labelled with FITC using a previously reported protocol.^{70,71} First, chitosan (1.00 g) was dissolved in 0.10 M acetic acid (100 mL), stirred overnight and vacuum-filtered to remove any undissolved chitin particles. Then FITC (100 mg) dissolved in methanol (50 mL) was added to the remaining aqueous acidic solution of chitosan and the resulting reaction mixture was stirred in the dark at 20 °C for 3 h. The FITC-labelled chitosan was then precipitated into 0.10 M NaOH. The insoluble product was isolated by filtration, redissolved in water and purified by dialysis against deionised water (5 L; nine changes) in the dark to remove any unreacted FITC. Finally, the dialysed product was lyophilised overnight. The resulting FITC-chitosan was stored in an amber vial wrapped with aluminium foil to exclude light and stored in a refrigerator prior to use.

5.3. Results and Discussion

5.3.1. Synthesis of PGEO5MA_x-PHPMA_y diblock copolymer worms

Water-soluble PGEO5MA₁₃ and PGEO5MA₁₆ precursors were prepared *via* RAFT solution polymerisation of GEO5MA in ethanol (Scheme 5.1a). DMF gel permeation chromatography (GPC) analysis [vs. a series of poly(methyl methacrylate) (PMMA) calibration standards] indicated that these homopolymers had M_n values of 9.7 and 11.5 kg mol⁻¹, respectively, and relatively narrow molecular weight distributions (\mathcal{D} = 1.19 and 1.18, respectively; Figure 5.1). Each PGEO5MA precursor was then chain-extended *via* RAFT aqueous dispersion polymerisation of HPMA at 10% w/w solids (Scheme 5.1b). A series of PGEO5MA₁₃-PHPMA_y (y = 120–200) and PGEO5MA₁₆-PHPMA_y (y = 140–220) diblock copolymer nanoparticles were prepared in order to identify a pure worm phase. All polymerisations had high HPMA conversions (>99%) as determined by ¹H NMR spectroscopy while DMF GPC analysis indicated reasonably good RAFT control (\mathcal{D} ≤ 1.25; Figure 5.2). A high molecular weight shoulder can be observed in each chromatogram, which has been previously attributed to dimethacrylate impurities in the HPMA monomer (<0.30 mol%).^{72,73} In particular, PGEO5MA₁₃-PHPMA_{150–190} formed soft, thermoresponsive free-standing gels and a pure worm morphology was confirmed by transmission electron microscopy (TEM) studies

(Figure 5.3a–b). Similarly, a pure worm phase was obtained for PGEO5MA₁₆-PHPMA_{170–200} as judged by TEM studies (Figure 5.3c–d).



Scheme 5.1. (a) Synthesis of PGEO5MA_x ($x = 13$ or 16) homopolymer by solution polymerisation in ethanol and (b) synthesis of PGEO5MA_x-PPHMA_y diblock copolymer nanoparticles *via* RAFT aqueous dispersion polymerisation.

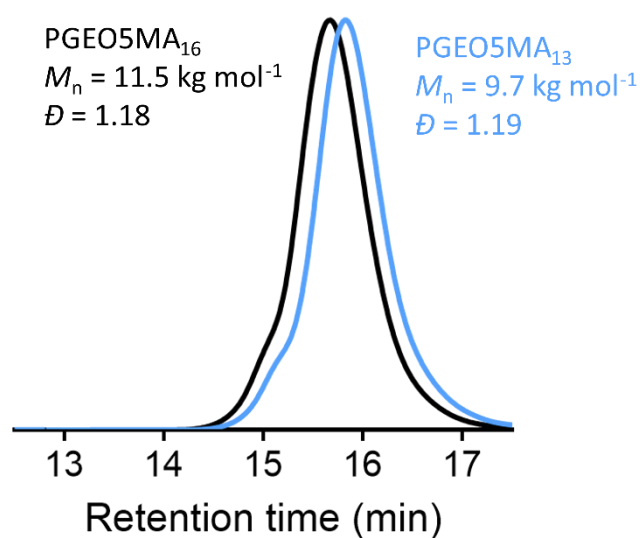


Figure 5.1. DMF gel permeation chromatograms for PGEO5MA₁₃ and PGEO5MA₁₆ relative to PMMA calibration standards.

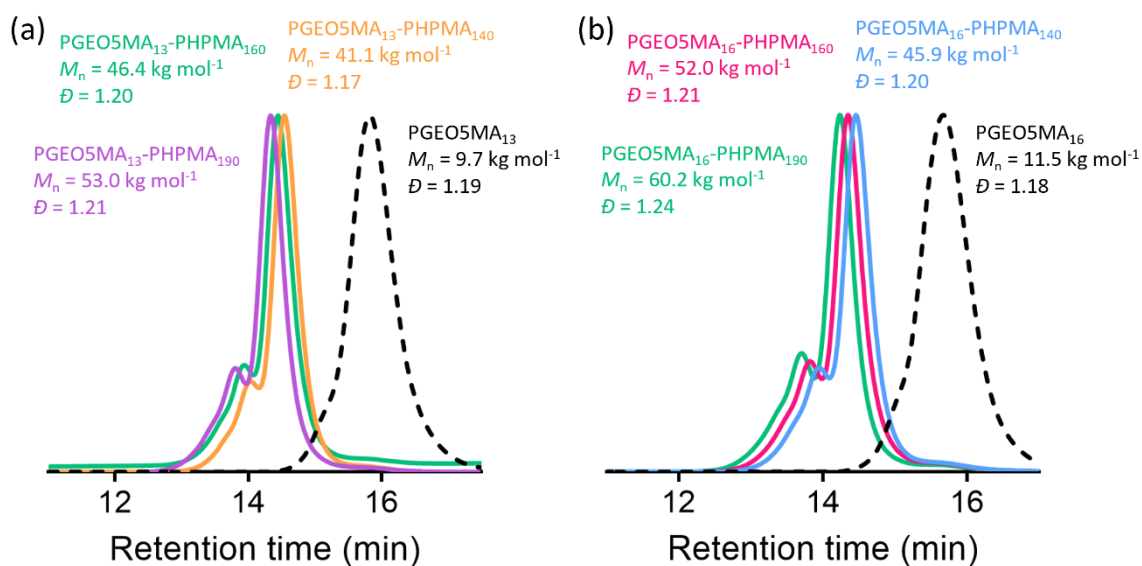


Figure 5.2. DMF gel permeation chromatograms for (a) PGE05MA₁₃, PGE05MA₁₃-PHPMA₁₄₀, PGE05MA₁₃-PHPMA₁₆₀ and PGE05MA₁₃-PHPMA₁₉₀ and (b) PGE05MA₁₆, PGE05MA₁₆-PHPMA₁₄₀, PGE05MA₁₆-PHPMA₁₆₀ and PGE05MA₁₆-PHPMA₁₉₀ relative to PMMA calibration standards.

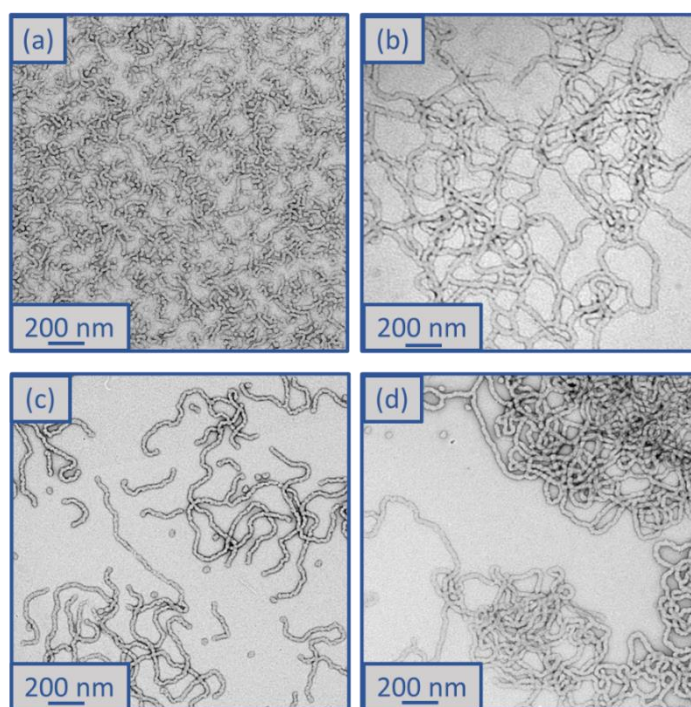


Figure 5.3. TEM images of (a) PGE05MA₁₃-PHPMA₁₅₀, (b) PGE05MA₁₃-PHPMA₁₉₀, (c) PGE05MA₁₆-PHPMA₁₇₀ and (d) PGE05MA₁₆-PHPMA₂₀₀ worm-like nanoparticles.

5.3.2. Investigating the thermoresponsive nature of PGEO5MA_x-PHPMA_y worms

The thermoresponsive nature of a PGEO5MA₁₃-PHPMA₁₅₅ and a PGEO5MA₁₆-PHPMA₂₀₀ worm gel was initially confirmed by visual inspection. A 10% w/w aqueous copolymer dispersion of each sample formed a soft, free-standing gel at 22 °C, see Figure 5.4a and 5.5a. On cooling to 5 °C, degelation occurred to afford free-flowing liquids in both cases, with TEM analysis indicating a concomitant worm-to-sphere transition (Figure 5.4b). On returning to 22 °C, regelation was observed for PGEO5MA₁₃-PHPMA₁₅₅ owing to a sphere-to-worm transition (Figure 5.4c). However, no regelation was observed for PGEO5MA₁₆-PHPMA₂₀₀ (Figure 5.5b), and TEM analysis indicated the presence of kinetically-trapped spheres and short worms in this case (Figure 5.5c). Fully reversible thermoresponsive behaviour is highly desirable for biomedical applications since this enables facile sterilisation *via* cold ultrafiltration.³⁸ Thus, only the PGEO5MA₁₃-PHPMA₁₅₅ worm gel was selected for the subsequent mucoadhesion studies.

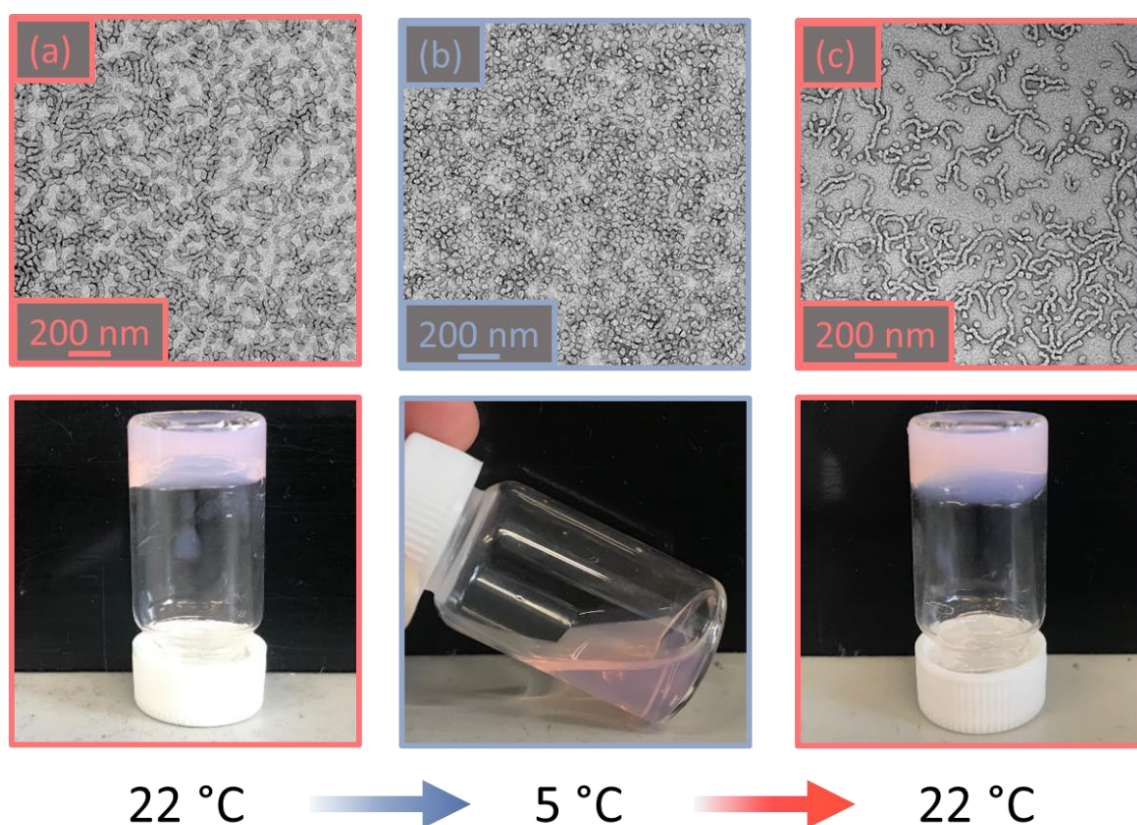


Figure 5.4. TEM images and corresponding digital photographs recorded for a 10% w/w aqueous dispersion of PGEO5MA₁₃-PHPMA₁₅₅ nano-objects: (a) soft, free-standing gel formed at 22 °C, (b) free-flowing fluid obtained on cooling to 5 °C and (c) the reconstituted gel formed after returning to 22 °C. [N.B. The pink coloration is conferred by the dithiobenzoate-based RAFT chain-ends].

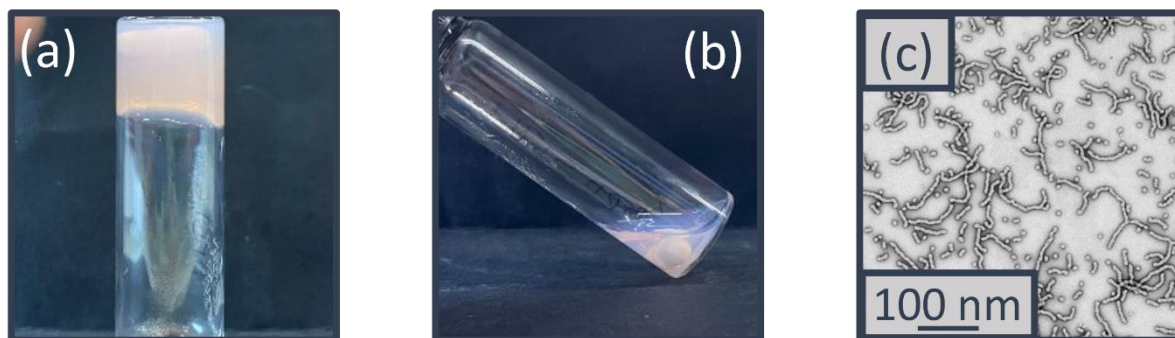


Figure 5.5. Digital photographs recorded for (a) a free-standing PGE05MA₁₆-PHPMA₂₀₀ worm gel at 22 °C, (b) the same PGE05MA₁₆-PHPMA₂₀₀ dispersion after cooling to 5 °C and then warming to 22 °C and (c) TEM image recorded for PGE05MA₁₆-PHPMA₂₀₀ after a 22 °C to 5 °C to 22 °C thermal cycle.

This thermally-induced morphological transition was further characterised using small-angle X-ray scattering (SAXS). A 1.0% w/w aqueous dispersion of PGE05MA₁₃-PHPMA₁₅₅ worms was studied at 37 °C and 5 °C. At 37 °C, a gradient of -1 was observed in the Guinier region (low q) of the SAXS pattern (Figure 5.6a), which is consistent with the highly anisotropic worms observed by TEM (Figure 5.4a). However, a gradient of zero is observed in the same low q region on cooling to 5 °C (Figure 5.6a). This indicates the presence of spherical nanoparticles, which agrees with the TEM image recorded at the same temperature (Figure 5.4b). Finally, the 1.0% w/w dispersion was warmed to 37 °C and allowed to equilibrate at this temperature for 1 h. The SAXS pattern recorded after equilibration is almost identical to the original pattern acquired at 37 °C (Figure 5.6a). This demonstrates that these PGE05MA₁₃-PHPMA₁₅₅ nano-objects exhibit thermoreversible behaviour with minimal hysteresis. Additionally, the core radii for the worms (r_w) and the spheres (r_s) can be approximated using $r_w = 3.83/q$ and $r_s = 4.49/q$ respectively, where q corresponds to the intensity minimum. The approximate core radii for the initial worm gel, the cold spheres, and the reconstituted worm gel are calculated to be 11, 10 and 12 nm, respectively. These values are comparable with core radii estimated by TEM analysis (counting at least 100 nanoparticles per sample).

The PGE05MA₁₃-PHPMA₁₅₅ worm gel was lyophilised to produce a freeze-dried powder. Redispersion of this copolymer powder in ice-cold deionised water (which ensures near-molecular dissolution of the amphiphilic copolymer chains)⁷⁴ followed by warming to 22 °C produced a soft, free-standing worm gel. Empirically, it was found that redispersion at 12% w/w solids produced longer, more linear worms than redispersion at 10% w/w solids. Thus, all subsequent experiments were conducted at 12% w/w solids.

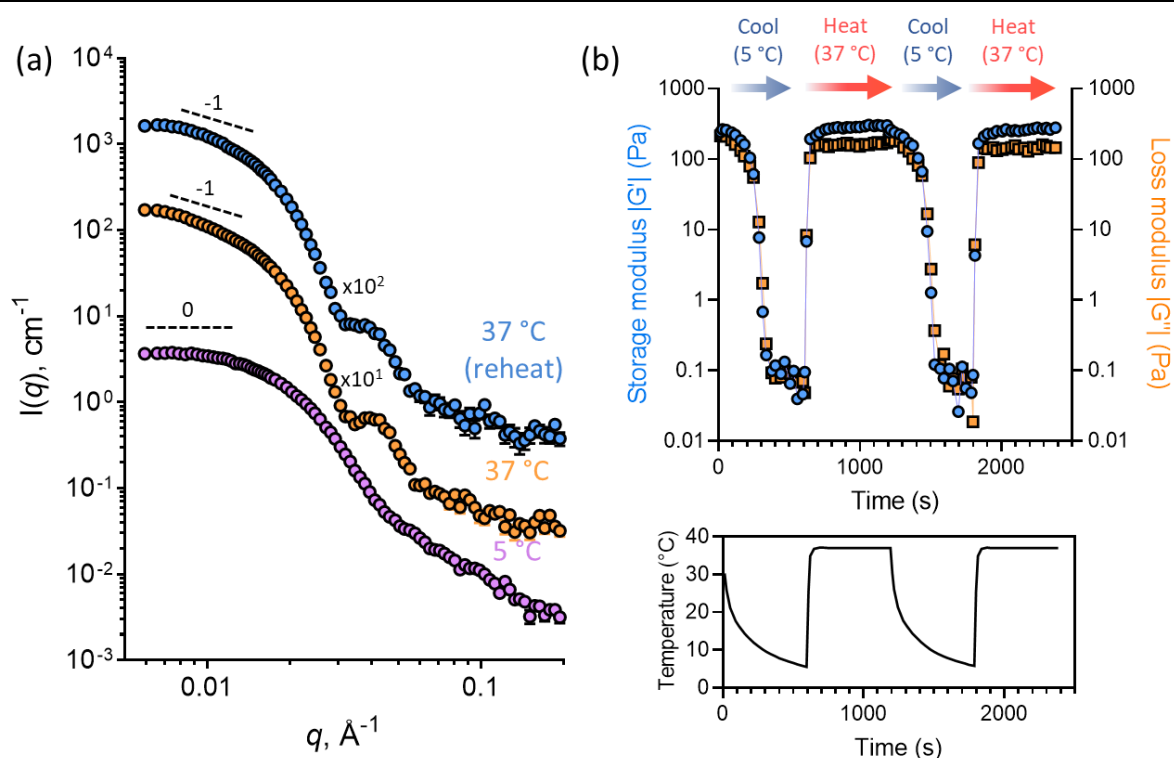


Figure 5.6. (a) SAXS patterns obtained for a 1.0% w/w aqueous dispersion of PGE05MA₁₃-PHPMA₁₅₅ nano-objects initially at 37 °C (orange circles), after cooling to 5 °C (purple circles), and after returning to 37 °C (blue circles) [N.B. The two upper patterns are offset by the stated numerical factors to aid clarity]. Dashed lines indicate low q gradients of 0 and -1 as guidance for the eye, where such gradients indicate the presence of spheres and worms, respectively. (b) Storage and loss moduli (G' and G'' , respectively) recorded for a 12% w/w aqueous dispersion of PGE05MA₁₃-PHPMA₁₅₅ nano-objects over two 37 °C to 5 °C to 37 °C thermal cycles using oscillatory rheology. A temperature-time profile for such experiments is also displayed.

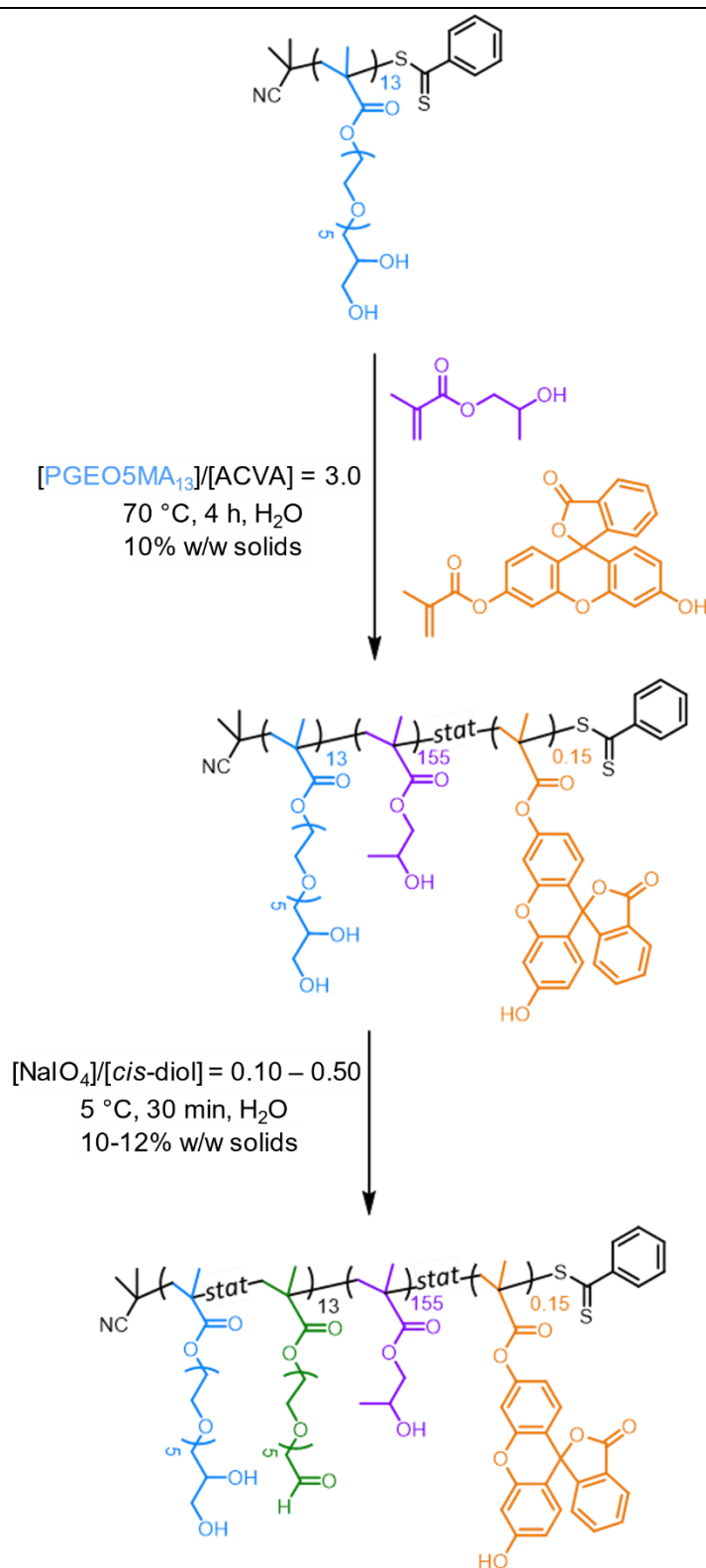
Oscillatory rheology (conducted by Dr T. J. Neal) was used to characterise the thermoresponsive behaviour of a 12% w/w aqueous dispersion of PGE05MA₁₃-PHPMA₁₅₅ nano-objects. This sample was subjected to shear (1.0% strain at an angular frequency of 1 rad s⁻¹; Figure 5.6b) over two thermal cycles (from 5 °C to 37 °C to 5 °C). On cooling to 5 °C the initial worms are converted into spheres, which causes *in situ* degelation ($G'' > G'$; Figure 5.6b) and a significant reduction in the complex viscosity ($|\eta^*|$; from 345 Pa s at 37 °C to 0.09 Pa s at 5 °C). On warming to 37 °C, worms are reformed and regelation occurs ($G'' < G'$; Figure 5.6b), with the complex viscosity increasing to 347 Pa s. Essentially the same (de)gelation behaviour was observed during the second thermal cycle, which indicates excellent thermoreversibility.

5.3.3. Synthesis and oxidation of PGE05MA₁₃-P(HPMA₁₅₅-*stat*-FMA_{0.15}) copolymer worms

Importantly, the pendent *cis*-diol units on these copolymer worms can be selectively oxidised using NaIO₄ in aqueous solution under mild conditions to introduce aldehyde

groups within the steric stabiliser chains.^{68,69} In principle, such derivatisation might be expected to produce mucoadhesive worm gels since it is well-known that aldehydes can react readily with amines *via* Schiff base chemistry.⁷⁵ However, fluorescence labelling is normally required for mucoadhesion flow-through assays.^{76,77} Therefore, HPMA and FMA were statistically copolymerised to produce fluorescein-tagged worms (Scheme 5.2). A FMA content of 0.1 mol% was targeted and the overall comonomer conversion was more than 99% as indicated by ¹H NMR spectroscopy. The initial pink worm gel formed a bright yellow worm gel on adjusting the solution pH to pH 9 with NaOH, indicating that the FMA was incorporated within the core-forming block (Figure 5.7a). Moreover, UV GPC studies performed at $\lambda = 495$ nm (which corresponds to the maximum absorbance for the FMA repeat units when they are in their anionic carboxylate form) observed a similar molecular weight chromatogram (Figure 5.7b).⁷⁸ Additionally, TEM analysis confirmed that there was no discernible difference between the fluorescently-labelled PGEO5MA₁₃-P(HPMA₁₅₅-*stat*-FMA_{0.15}) worms and the non-fluorescent PGEO5MA₁₃-PHPMA₁₅₅ worms (Figure 5.8a–b).

The former worms were subsequently oxidised with NaIO₄ targeting NaIO₄/*cis*-diol molar ratios of 0.10, 0.20, 0.30 or 0.50 using the protocol developed for PGEO5MA homopolymer in Chapter III and crosslinked PGEO5MA₂₆-PHPMA₃₅₀-PEGDMA₂₀ vesicles reported in Chapter IV.⁶⁹ In each case, the extent of oxidation was determined by ¹H NMR spectroscopy (Appendix 9). The periodate oxidation was conducted on the final diblock copolymer nanoparticles rather than the PGEO5MA precursor. This approach means that the same *cis*-diol-functional worm gel precursor is used to produce each aldehyde-functional worm gel examined in this study, which eliminates batch-to-batch variability. Moreover, ¹H NMR spectroscopy studies (data not shown) confirm that a sample of 100% aldehyde-functional PAGEO5MA₂₆-PHPMA₂₅₀ worms, reported in Chapter IV,⁶⁹ remained stable with respect to aerial oxidation for at least one year when stored at ambient temperature. TEM studies confirmed that there was no discernible change in morphology after oxidation (Figure 5.8c–f). Furthermore, oscillatory strain sweeps (from 0.1% to 20%) were performed on these partially oxidised worm gels to assess how the degree of aldehyde functionality affected the gel properties (Figure 5.9a and Appendix 10). It was found that a higher degree of oxidation led to a lower strain being required for degelation ($G'' > G'$). For example, degelation of the *cis*-diol functional precursor worm gel required an applied strain of 16.8%, whereas the 50% aldehyde-functionalised worm gel underwent degelation at 1.1% strain (Figure 5.9a). Moreover, higher degrees of aldehyde functionalisation led to higher gel



Scheme 5.2. Two-step synthesis of fluorescently-labelled aldehyde-functional PAGEO5MA₁₃-P(HPMA₁₅₅-*stat*-FMA_{0.15}) worms. First, a water-soluble PAGEO5MA₁₃ precursor is chain-extended *via* RAFT aqueous dispersion statistical copolymerisation of HPMA with 0.1 mol% FMA. In the second step, the pendant *cis*-diol groups on the PAGEO5MA₁₃ stabiliser chains are selectively oxidised using a sub-stoichiometric amount of NaIO₄ at 22 °C (NaIO₄/*cis*-diol molar ratios = 0.10 to 0.50).

viscosities (Figure 5.9b and Appendix 11). For example, the gel viscosity of the *cis*-diol functional precursor worm gel was 72 Pa s at an applied strain of 1.0% when equilibrated at ambient temperature, whereas the 50% aldehyde-functionalised worm gel exhibited a gel viscosity of 263 Pa s (Figure 5.9b). This indicates that the introduction of aldehyde groups produces stronger (but more fragile/brittle) gels. There are multiple explanations for why the gels become stronger with increased aldehyde content. In principle, the pendent aldehyde groups can react with the remaining *cis*-diols to form hemiacetal bonds between neighbouring worms, thus leading to stronger gels. However, GPC analysis (see Figure 5.10) of the aldehyde-functional diblock copolymer chains provides no evidence for inter-chain crosslinking, which should produce a high molecular weight shoulder. Alternatively, the higher storage moduli observed for the aldehyde-functional worm gels may be related to the formation of stronger hydrogen bonds between the hydroxyl (or ester carbonyl) groups on the remaining *cis*-diol repeat units and the aldehyde groups (or geminal diol) groups. Further studies (perhaps with model compounds) are required to answer this question, but this is beyond the scope of the present study.

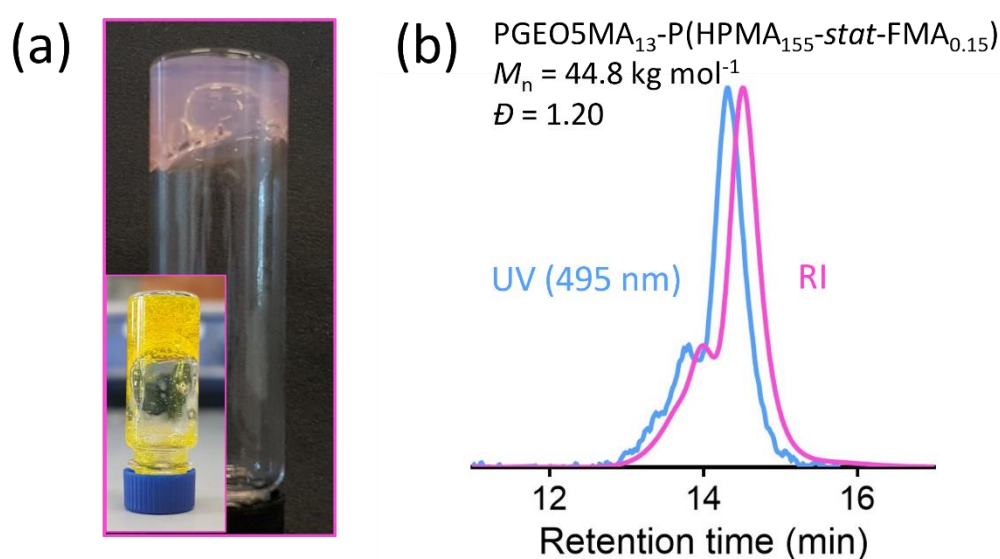


Figure 5.7. (a) Digital photographs recorded for $\text{PGE05MA}_{13}\text{-P(HPMA}_{155}\text{-stat-FMA}_{0.15})$ diblock copolymer worms at pH 4 (pink) and pH 9 (yellow). (b) DMF GPC curves recorded using a refractive index (RI) detector (pink curve) and UV detector (wavelength set at 495 nm; blue curve) for $\text{PGE05MA}_{13}\text{-P(HPMA}_{155}\text{-stat-FMA}_{0.15})$.

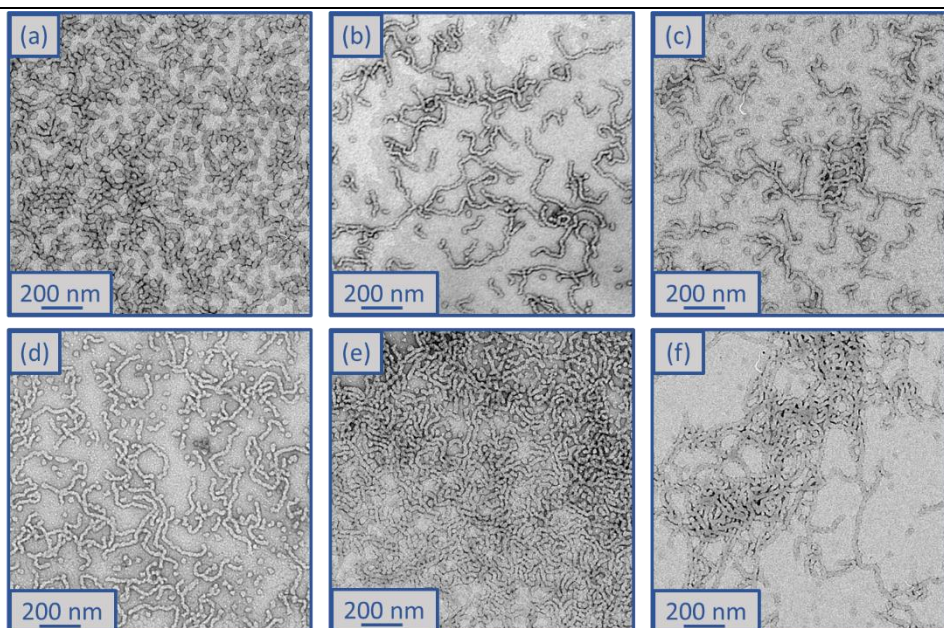


Figure 5.8. TEM images recorded for (a) PGEO5MA₁₃-PHPMA₁₅₅ diblock copolymer worms and fluorescently-labelled PGEO5MA₁₃-P(HPMA₁₅₅-*stat*-FMA_{0.15}) copolymer worms containing (b) 0%, (c) 10%, (d) 20%, (e) 30% or (f) 50% aldehyde functionality.

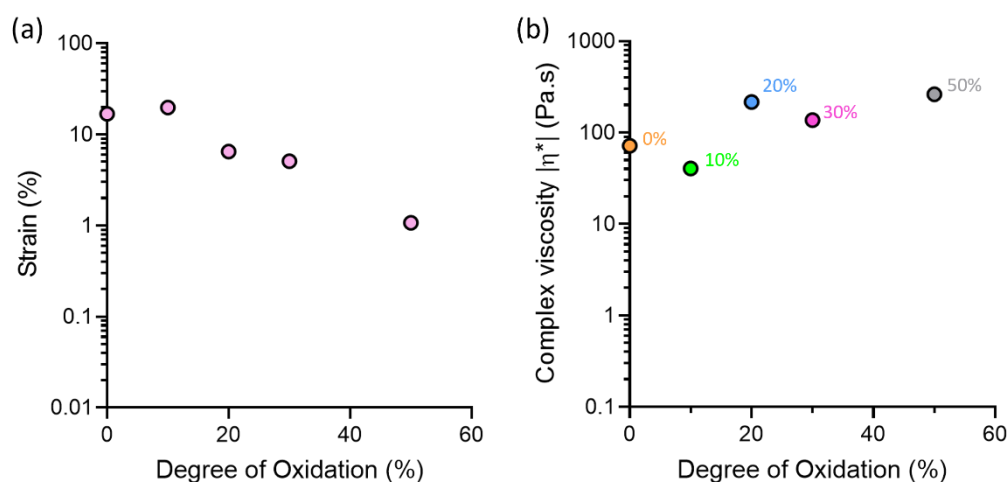


Figure 5.9. (a) Plot of degelation strain against the mean degree of oxidation for PGEO5MA₁₃-P(HPMA₁₅₅-*stat*-FMA_{0.15}) worms and (b) plot of complex viscosity against mean degree of PGEO5MA₁₃-P(HPMA₁₅₅-*stat*-FMA_{0.15}) oxidation recorded at 1.0% strain.

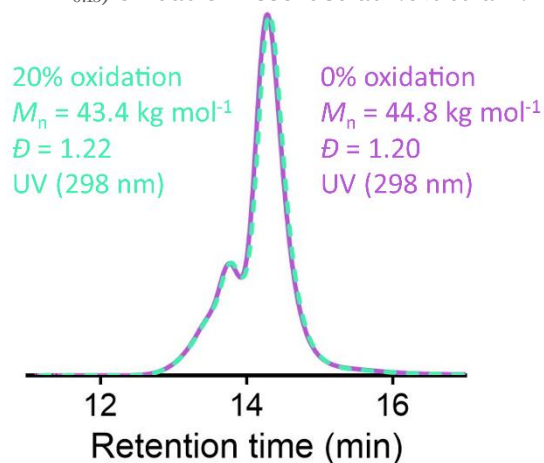


Figure 5.10. DMF UV GPC curves (UV detector wavelength set at 298 nm) for PGEO5MA₁₃-P(HPMA₁₅₅-*stat*-FMA_{0.15}) worms with either 0% or 20% aldehyde functionality.

Further variable temperature oscillatory rheology experiments were performed on the oxidised worm gels, whereby samples were first cooled to 5 °C and subsequently heated to 37 °C under an applied shear (Figure 5.11a and Appendix 12). Thermoreversible degelation was observed in most cases but the rate of degelation was slower for gels with higher degrees of aldehyde functionality. Such thermoresponsive behaviour was confirmed by visual inspection: free-standing gels became free-flowing liquids after cooling from 22 °C to 5 °C for 50 min and reformed free-standing gels on returning to ambient temperature (Appendix 13). These observations were consistent with TEM studies, which indicated the presence of spheres at 5 °C and worms at 22 °C (Figure 5.11b). However, the 50% aldehyde-functional worm gel did not undergo degelation at all on the timescale of the rheology experiments (Appendix 12). Thus, the highest degree of aldehyde functionality that can be incorporated into the PGE05MA₁₃-P(HPMA₁₅₅-*stat*-FMA_{0.15}) worm gel precursor without significantly affecting its thermoresponsive behaviour is 30%. It was noted that the worm gels remained pink after oxidation indicating the retention of RAFT character (Appendix 13). This was further confirmed by UV GPC, performed at a wavelength of 298 nm, which indicated that the UV active dithiocarbonate group was present after oxidation (Figure 5.10).

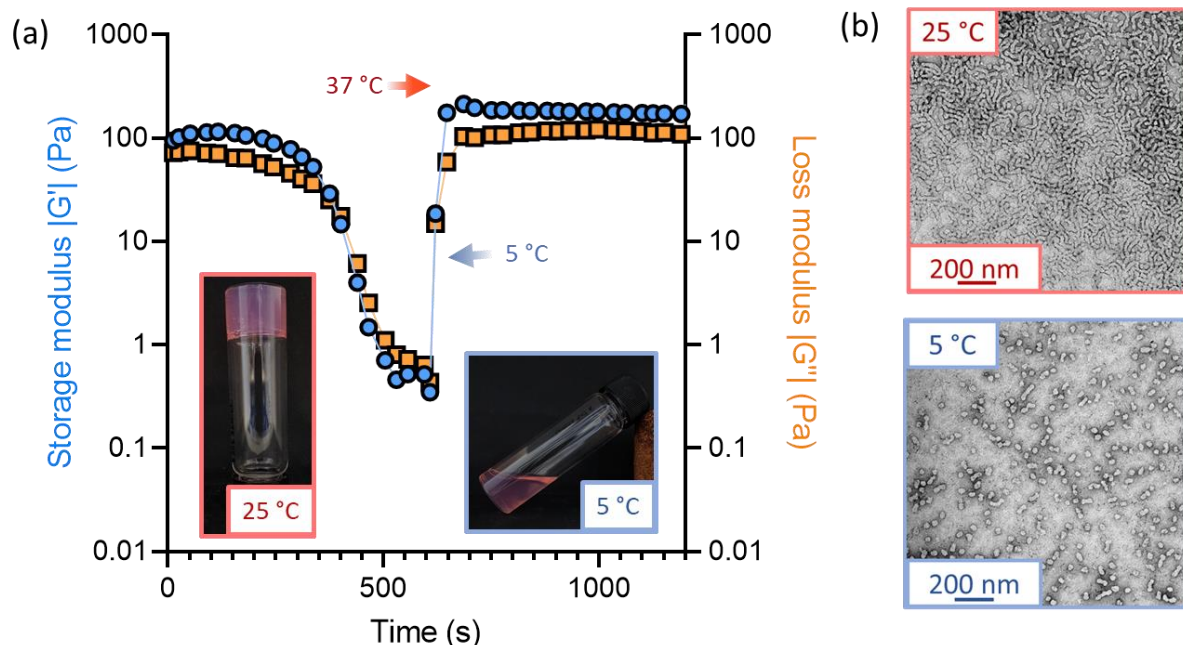


Figure 5.11. (a) Variable temperature oscillatory rheology monitoring the storage and loss modulus (G' and G'' , respectively) at both 5 °C and 37 °C for PGE05MA₁₃-P(HPMA₁₅₅-*stat*-FMA_{0.15}) worms with 30% aldehyde functionality. (b) TEM images for PGE05MA₁₃-P(HPMA₁₅₅-*stat*-FMA_{0.15}) with 30% aldehyde at 25 °C and the spherical nanoparticles at 5 °C.

5.3.4. Investigating the mucoadhesive properties of PGEO5MA₁₃-P(HPMA₁₅₅-*stat*-FMA_{0.15}) based worms

The retention of such worm gels on mucosal surfaces was studied using a porcine urinary bladder mucosa model under a constant flow of artificial urine (AU) by our collaborators at the University of Reading. This model mimics the physiologically relevant conditions within the urinary bladder following the intravesical administration of therapeutic agents for the treatment of bladder cancer or interstitial cystitis. Figure 5.12 shows fluorescence images recorded for urinary bladder tissue when using a series of fluorescently-labelled worm gels plus two control samples after washing with varying volumes of AU. FITC-chitosan and FITC-dextran were used as positive and negative controls owing to their excellent and weak adhesion to mucosal tissues, respectively.⁷⁹ Worm gels bearing 0, 10, 20, 30 or 50 mol% aldehyde functionality (of the PGEO5MA block) were evaluated in these experiments. Visual inspection of these images indicates that the incorporation of aldehyde groups within such worm gels clearly improves their retention on mucosal tissue. All images were then analysed using ImageJ software to determine fluorescence intensities, which were then converted into % mucosal retention (Figure 5.13). This approach enables quantitative interpretation of the wash-off experiments. The worm gel containing no aldehyde groups exhibited relatively weak adhesion to the mucosa, which is initially comparable to that for FITC-dextran. However, unlike this negative control, these worm gels are still retained on mucosal surface to some extent even after washing with up to 120 mL of AU. This may be related to their favourable rheological characteristics relative to non-gelling FITC-dextran. The worm gel containing 10% aldehyde groups exhibits substantially improved retention with around 20% remaining on the bladder mucosa after washing with 120 mL of AU. Further increasing the aldehyde content in the worm gels up to either 20 or 30% leads to progressively stronger mucoadhesion. Most notably, the worm gel bearing 50% aldehyde groups exhibits comparable mucoadhesion to that of chitosan, which is widely considered to be a ‘gold standard’ mucoadhesive polymer.⁸⁰ It is perhaps worth emphasising that such polyelectrolytes usually exhibit superior mucoadhesive properties compared to non-ionic polymers.⁸⁰ In contrast, the hydroxyl-rich worm gels examined in this study exhibit solely non-ionic character.

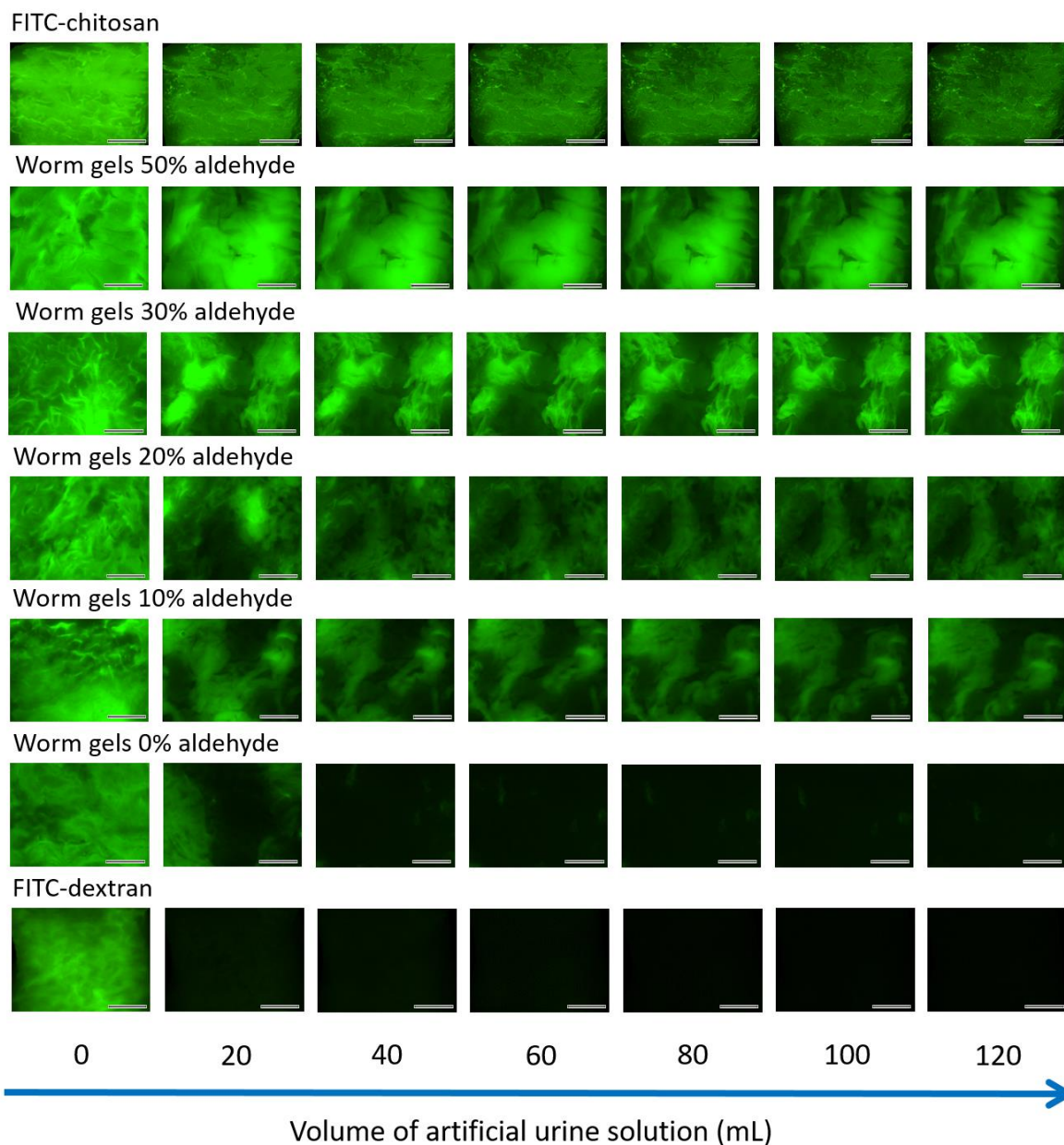


Figure 5.12. Representative fluorescence images of freshly-dissected porcine urinary bladder mucosa illustrating the retention of fluorescently-labelled PGE05MA₁₃-P(HPMA₁₅₅-*stat*-FMA_{0.15}) worm gels bearing varying degrees of aldehyde functionality after irrigation with varying volumes of AU solution at a flow rate of 2.0 mL min⁻¹, plus positive and negative controls. Scale bars correspond to 6 mm.

5.4. Conclusion

The synthesis of thermoresponsive diblock copolymer worm gels *via* RAFT aqueous dispersion polymerisation of HPMA using a water-soluble methacrylic precursor bearing pendent *cis*-diol groups is reported. Selective oxidation using aqueous NaIO₄ introduces aldehyde groups within the steric stabiliser chains and the aldehyde content can be adjusted by varying the NaIO₄/*cis*-diol molar ratio. A series of such aldehyde-functional worm gels are evaluated in the context of mucoadhesion using porcine urinary bladder as a model substrate. A bespoke fluorescence microscopy assay demonstrates that such worm

gels can offer similar performance as that afforded by chitosan, which is widely employed as a ‘gold standard’ positive control in this field. One potentially important advantage of these worm gels over chitosan is their non-ionic character, which should enable potential compatibility problems owing to complexation with anionic drugs to be avoided. The optimum degree of aldehyde functionality is approximately 30%: lower degrees of functionalisation lead to significantly weaker mucoadhesion, whereas higher values compromise the desirable thermoresponsive behaviour of these worm gels. In summary, aldehyde-functionalised worm gels represent a new family of strongly mucoadhesive polymers that can form dynamic covalent bonds with mucosal membranes under physiological conditions.

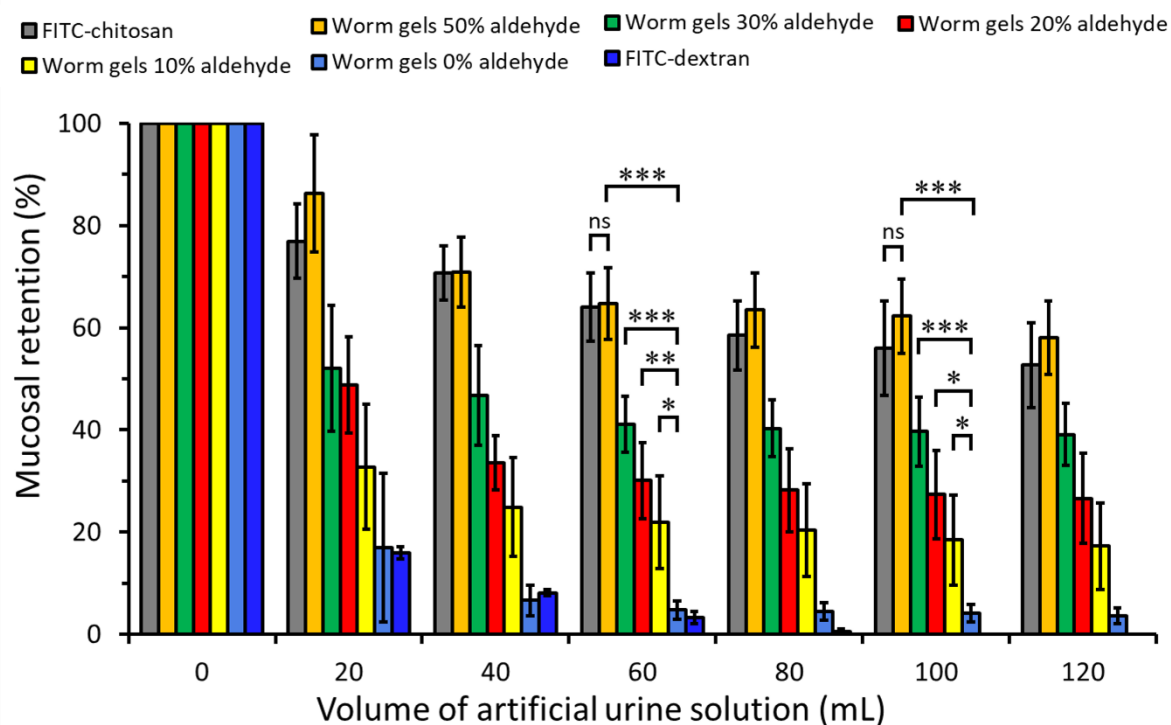


Figure 5.13. Percentage retention for fluorescently-labelled $\text{PGE05MA}_{13}\text{-P(HPMA}_{155}\text{-stat-FMA}_{0.15})$ worm gels with differing degrees of aldehyde functionality on freshly dissected porcine urinary bladder mucosa after irrigating with varying volumes of AU solution at a flow rate of 2.0 mL min^{-1} , plus positive and negative controls. Data are expressed as mean values \pm standard deviations ($n = 3$). Statistically significant differences are given as: * = $p < 0.05$; ** = $p < 0.01$; *** = $p < 0.001$; ns denotes no significance.

5.5. References

- 1 L. Zhang and A. Eisenberg, *Science*, 1995, **268**, 1728–1731.
- 2 L. Zhang, K. Yu and A. Eisenberg, *Science*, 1996, **272**, 1777–1779.
- 3 G. Riess, *Prog. Polym. Sci.*, 2003, **28**, 1107–1170.
- 4 X. Wang, G. Guerin, H. Wang, Y. Wang, I. Manners and M. A. Winnik, *Science*, 2007, **317**, 644–647.

- 5 L. Zhang and A. Eisenberg, *Macromolecules*, 1996, **29**, 8805–8815.
 - 6 H. Shen and A. Eisenberg, *Angew. Chemie Int. Ed.*, 2000, **39**, 3310–3312.
 - 7 Z. Gao, S. K. Varshney, S. Wong and A. Eisenberg, *Macromolecules*, 1994, **27**, 7923–7927.
 - 8 Y. Mai and A. Eisenberg, *Chem. Soc. Rev.*, 2012, **41**, 5969–5985.
 - 9 J. N. Israelachvili, D. J. Mitchell and B. W. Ninham, *J. Chem. Soc. Faraday Trans. 2 Mol. Chem. Phys.*, 1976, **72**, 1525–1568.
 - 10 M. Antonietti and S. Förster, *Adv. Mater.*, 2003, **15**, 1323–1333.
 - 11 N. J. Warren and S. P. Armes, *J. Am. Chem. Soc.*, 2014, **136**, 10174–10185.
 - 12 S. Boissé, J. Rieger, K. Belal, A. Di-Cicco, P. Beaunier, M.-H. Li and B. Charleux, *Chem. Commun.*, 2010, **46**, 1950–1952.
 - 13 C. J. Ferguson, R. J. Hughes, B. T. T. Pham, B. S. Hawkett, R. G. Gilbert, A. K. Serelis and C. H. Such, *Macromolecules*, 2002, **35**, 9243–9245.
 - 14 C. J. Ferguson, R. J. Hughes, D. Nguyen, B. T. T. Pham, R. G. Gilbert, A. K. Serelis, C. H. Such and B. S. Hawkett, *Macromolecules*, 2005, **38**, 2191–2204.
 - 15 P. Yang, Y. Ning, T. J. Neal, E. R. Jones, B. R. Parker and S. P. Armes, *Chem. Sci.*, 2019, **10**, 4200–4208.
 - 16 J. Rieger, *Macromol. Rapid Commun.*, 2015, **36**, 1458–1471.
 - 17 C. E. Boott, J. Gwyther, R. L. Harniman, D. W. Hayward and I. Manners, *Nat. Chem.*, 2017, **9**, 785–792.
 - 18 G. Mellot, J.-M. Guigner, L. Bouteiller, F. Stoffelbach and J. Rieger, *Angew. Chemie Int. Ed.*, 2019, **58**, 3173–3177.
 - 19 E. Vergari, J. G. Knudsen, R. Ramracheya, A. Salehi, Q. Zhang, J. Adam, I. W. Asterholm, A. Benrick, L. J. B. Briant, M. V. Chibalina, F. M. Gribble, A. Hamilton, B. Hastoy, F. Reimann, N. J. G. Rorsman, I. I. Spiliotis, A. Tarasov, Y. Wu, F. M. Ashcroft and P. Rorsman, *Nat. Commun.*, 2019, **10**, 139.
 - 20 A. Blanazs, A. J. Ryan and S. P. Armes, *Macromolecules*, 2012, **45**, 5099–5107.
 - 21 C. J. Mable, N. J. Warren, K. L. Thompson, O. O. Mykhaylyk and S. P. Armes, *Chem. Sci.*, 2015, **6**, 6179–6188.
 - 22 C. J. Mable, I. Canton, O. O. Mykhaylyk, B. Ustbas Gul, P. Chambon, E. Themistou and S. P. Armes, *Chem. Sci.*, 2019, **10**, 4811–4821.
 - 23 O. J. Deane, J. Jennings, T. J. Neal, O. M. Musa, A. Fernyhough and S. P. Armes, *Chem. Mater.*, 2021, **33**, 7767–7779.
 - 24 O. J. Deane, J. Jennings and S. P. Armes, *Chem. Sci.*, 2021, **12**, 13719–13729.
 - 25 W. Zhang, B. Charleux and P. Cassagnau, *Macromolecules*, 2012, **45**, 5273–5280.
 - 26 J. R. Lovett, M. J. Derry, P. Yang, F. L. Hatton, N. J. Warren, P. W. Fowler and S. P. Armes, *Chem. Sci.*, 2018, **9**, 7138–7144.
 - 27 A. Blanazs, R. Verber, O. O. Mykhaylyk, A. J. Ryan, J. Z. Heath, C. W. I. Douglas and
-

-
- S. P. Armes, *J. Am. Chem. Soc.*, 2012, **134**, 9741–9748.
- 28 X. Zhang, S. Boissé, W. Zhang, P. Beaunier, F. D’Agosto, J. Rieger and B. Charleux, *Macromolecules*, 2011, **44**, 4149–4158.
- 29 W. Zhang, F. D’Agosto, O. Boyron, J. Rieger and B. Charleux, *Macromolecules*, 2012, **45**, 4075–4084.
- 30 N. J. Warren, M. J. Derry, O. O. Mykhaylyk, J. R. Lovett, L. P. D. Ratcliffe, V. Ladmiral, A. Blanazs, L. A. Fielding and S. P. Armes, *Macromolecules*, 2018, **51**, 8357–8371.
- 31 A. Czajka and S. P. Armes, *Chem. Sci.*, 2020, **11**, 11443–11454.
- 32 N. J. Warren, O. O. Mykhaylyk, D. Mahmood, A. J. Ryan and S. P. Armes, *J. Am. Chem. Soc.*, 2014, **136**, 1023–1033.
- 33 L. P. D. Ratcliffe, M. J. Derry, A. Ianiro, R. Tuinier and S. P. Armes, *Angew. Chemie Int. Ed.*, 2019, **58**, 18964–18970.
- 34 M. Sponchioni, C. T. O’Brien, C. Borchers, E. Wang, M. N. Rivolta, N. J. W. Penfold, I. Canton and S. P. Armes, *Chem. Sci.*, 2020, **11**, 232–240.
- 35 D. L. Beattie, O. O. Mykhaylyk, A. J. Ryan and S. P. Armes, *Soft Matter*, 2021, **17**, 5602–5612.
- 36 R. Verber, A. Blanazs and S. P. Armes, *Soft Matter*, 2012, **8**, 9915–9922.
- 37 K. A. Simon, N. J. Warren, B. Mosadegh, M. R. Mohammady, G. M. Whitesides and S. P. Armes, *Biomacromolecules*, 2015, **16**, 3952–3958.
- 38 I. Canton, N. J. Warren, A. Chahal, K. Amps, A. Wood, R. Weightman, E. Wang, H. Moore and S. P. Armes, *ACS Cent. Sci.*, 2016, **2**, 65–74.
- 39 R. Spelat, F. Ferro, P. Contessotto, N. J. Warren, G. Marsico, S. P. Armes and A. Pandit, *Mater. Today Bio*, 2020, **5**, 100040.
- 40 A. L. A. Binch, L. P. D. Ratcliffe, A. H. Milani, B. R. Saunders, S. P. Armes and J. A. Hoyland, *Biomacromolecules*, 2021, **22**, 837–845.
- 41 O. Wichterle and D. Lím, *Nature*, 1960, **185**, 117–118.
- 42 P. H. O’Farrell, *J. Biol. Chem.*, 1975, **250**, 4007–4021.
- 43 B. Vignani, S. Rossi, G. Sandri, M. C. Bonferoni, C. M. Caramella and F. Ferrari, *Pharmaceutics*, 2020, **12**, 859.
- 44 F. Zahir-Jouzdani, J. D. Wolf, F. Atyabi and A. Bernkop-Schnürch, *Expert Opin. Drug Deliv.*, 2018, **15**, 1007–1019.
- 45 A. Ludwig, *Adv. Drug Deliv. Rev.*, 2005, **57**, 1595–1639.
- 46 J. L. Greaves and C. G. Wilson, *Adv. Drug Deliv. Rev.*, 1993, **11**, 349–383.
- 47 V. Bourganis, O. Kammona, A. Alexopoulos and C. Kiparissides, *Eur. J. Pharm. Biopharm.*, 2018, **128**, 337–362.
- 48 M. I. Ugwoke, R. U. Agu, N. Verbeke and R. Kinget, *Adv. Drug Deliv. Rev.*, 2005, **57**, 1640–1665.
- 49 S. GuhaSarkar and R. Banerjee, *J. Control. Release*, 2010, **148**, 147–159.
-

-
- 50 O. M. Kolawole, W. M. Lau, H. Mostafid and V. V. Khutoryanskiy, *Int. J. Pharm.*, 2017, **532**, 105–117.
- 51 A. Bernkop-Schnürch, *Adv. Drug Deliv. Rev.*, 2005, **57**, 1569–1582.
- 52 F. Laffleur and A. Bernkop-Schnürch, *Future Med. Chem.*, 2012, **4**, 2205–2216.
- 53 J. Lenoir, I. Claerhout, P. Kestelyn, A. Klomp, J. P. Remon and E. Adriaens, *Toxicol. Vitr.*, 2011, **25**, 1919–1925.
- 54 T. Eshel-Green and H. Bianco-Peled, *Colloids Surfaces B Biointerfaces*, 2016, **139**, 42–51.
- 55 X. Shan, S. Aspinall, D. B. Kaldybekov, F. Buang, A. C. Williams and V. V. Khutoryanskiy, *ACS Appl. Polym. Mater.*, 2021, **3**, 5882–5892.
- 56 O. M. Kolawole, W. M. Lau and V. V. Khutoryanskiy, *Int. J. Pharm.*, 2018, **550**, 123–129.
- 57 P. Tonglairoum, R. P. Brannigan, P. Opanasopit and V. V. Khutoryanskiy, *J. Mater. Chem. B*, 2016, **4**, 6581–6587.
- 58 Y. Shtenberg, M. Goldfeder, A. Schroeder and H. Bianco-Peled, *Carbohydr. Polym.*, 2017, **175**, 337–346.
- 59 O. M. Kolawole, W. M. Lau and V. V. Khutoryanskiy, *J. Pharm. Sci.*, 2019, **108**, 3046–3053.
- 60 G. Prospero-Porta, S. Kedzior, B. Muirhead and H. Sheardown, *Biomacromolecules*, 2016, **17**, 1449–1457.
- 61 S. Hu, X. Pei, L. Duan, Z. Zhu, Y. Liu, J. Chen, T. Chen, P. Ji, Q. Wan and J. Wang, *Nat. Commun.*, 2021, **12**, 1689.
- 62 K. Kim, K. Kim, J. H. Ryu and H. Lee, *Biomaterials*, 2015, **52**, 161–170.
- 63 C. Lechner, P. Wulz, R. A. Baus, C. Menzel, S. K. Götzfried, R. Gust and A. Bernkop-Schnürch, *Mol. Pharm.*, 2019, **16**, 1211–1219.
- 64 C. Menzel, M. Hauser, A. Frey, M. Jelkmann, F. Laffleur, S. K. Götzfried, R. Gust and A. Bernkop-Schnürch, *Eur. J. Pharm. Biopharm.*, 2019, **139**, 161–167.
- 65 J. Chiefari, Y. K. Chong, F. Ercole, J. Krstina, J. Jeffery, T. P. T Le, R. T. A Mayadunne, G. F. Meijs, C. L. Moad, G. Moad, E. Rizzardo and S. H. Thang, *Macromolecules*, 1998, **31**, 5559–5562.
- 66 G. Moad, A. E. Rizzardo and S. H. Thang, *Aust. J. Chem.*, 2005, **58**, 379–410.
- 67 G. Moad, *Polym. Chem.*, 2017, **8**, 177–219.
- 68 E. E. Brotherton, C. P. Jesson, N. J. Warren, M. J. Smallridge and S. P. Armes, *Angew. Chemie Int. Ed.*, 2021, **60**, 12032–12037.
- 69 E. E. Brotherton, M. J. Smallridge and S. P. Armes, *Biomacromolecules*, 2021, **22**, 5382–5389.
- 70 M. T. Cook, G. Tzortzis, D. Charalampopoulos and V. V. Khutoryanskiy, *Biomacromolecules*, 2011, **12**, 2834–2840.
- 71 B. L. Symonds, C. I. Lindsay, N. R. Thomson and V. V. Khutoryanskiy, *RSC Adv.*, 2016,
-

- 6, 102206–102213.
- 72 Y. Li and S. P. Armes, *Angew. Chemie*, 2010, **122**, 4136–4140.
- 73 I. Bannister, N. C. Billingham, S. P. Armes, S. P. Rannard and P. Findlay, *Macromolecules*, 2006, **39**, 7483–7492.
- 74 M. K. Kocik, O. O. Mykhaylyk and S. P. Armes, *Soft Matter*, 2014, **10**, 3984–3992.
- 75 M. B. Smith and J. March, *March's advanced organic chemistry: reactions, mechanisms, and structure*, John Wiley & Sons, Inc., Hoboken, NJ, 2007.
- 76 E. A. Mun, A. C. Williams and V. V. Khutoryanskiy, *Int. J. Pharm.*, 2016, **512**, 32–38.
- 77 C. A. Withers, M. T. Cook, L. Methven, M. A. Gosney and V. V. Khutoryanskiy, *Food Funct.*, 2013, **4**, 1668–1674.
- 78 S. L. Canning, T. J. Neal and S. P. Armes, *Macromolecules*, 2017, **50**, 6108–6116.
- 79 D. B. Kaldybekov, P. Tonglairoum, P. Opanasopit and V. V. Khutoryanskiy, *Eur. J. Pharm. Sci.*, 2018, **111**, 83–90.
- 80 V. V. Khutoryanskiy, *Macromol. Biosci.*, 2011, **11**, 748–764.

*Chapter VI: New hydrophilic
aldehyde-functional polymer brushes:
synthesis, characterisation and
potential bioapplications*

Chapter VI: New hydrophilic aldehyde-functional polymer brushes: synthesis, characterisation and potential bioapplications

6.1. Introduction

When polymer chains are tethered to a surface at a sufficiently high concentration they extend away from the surface and are known as ‘polymer brushes’.^{1,2} Such systems have been extensively explored in the context of surface lubrication,³⁻⁵ the design of high performance anti-biofouling surfaces,⁶⁻⁹ the production of anti-bacterial surfaces¹⁰ and as integral components of (bio)sensors.¹¹⁻¹⁵ The development of copper-catalysed atom transfer radical polymerisation (ATRP) by Matyjaszewski and co-workers¹⁶ has stimulated this field as it enabled the convenient synthesis of a wide range of polymer brushes of controllable thickness from a monolayer of surface initiator sites on a planar substrate using the so-called ‘grafting from’ approach.¹⁷ Early studies involved hydrophobic brushes comprising poly(methyl methacrylate),¹⁸ or poly(*n*-butyl acrylate).¹⁹ However, various examples of hydrophilic brushes quickly became the focus of considerable attention, not least because they provide access to stimulus-responsive brushes.²⁰ Examples include thermoresponsive brushes based on poly(*N*-isopropyl acrylamide)²¹⁻²⁴ or poly(sulfopropylbetaines)²⁵ and pH-responsive brushes based on various tertiary amine methacrylates,²⁶⁻²⁹ or poly(methacrylic acid).³⁰⁻³²

There have been various studies of the chemical derivatisation of polymer brushes.^{33,34} For example, poly(2-hydroxyethyl methacrylate) (PHEMA) brushes can be either esterified³⁵ or oxidised to introduce desired functionality.³⁶ Similarly, the pendent epoxy groups within poly(glycidyl methacrylate) brushes can be reacted with *n*-octylamine³⁷ or *n*-propylamine³⁸ and the tertiary amine groups in poly[(2-dimethylamino)ethyl methacrylate] can be quaternised using various alkyl halides.^{39,40} Zou et al. investigated the functionalisation of oxidised poly-*N*-[(2,3-dihydroxypropyl)acrylamide] (PDHPA) brushes with bovine serum albumin *via* reductive amination.⁴¹ However, brush derivatisation protocols almost invariably involve the use of organic solvents and are often incomplete.

In Chapter III, the synthesis of a new hydrophilic methacrylic monomer, GEO5MA, was reported (see Scheme 3.3a).⁴² The pendent *cis*-diol group on this monomer can be selectively oxidised using sodium periodate (NaIO₄) to afford a rare example of an aldehyde-functional water-soluble monomer, AGEO5MA. Alternatively, GEO5MA can be homopolymerised and the resulting PGEO5MA can be readily converted into PAGEO5MA by treatment with an aqueous solution of NaIO₄ under mild conditions (see Figure 3.3a). Herein this chemistry is exploited to prepare new examples of *hydrophilic aldehyde-functional polymer brushes*. According to the literature, such brushes are expected to be of considerable interest for various bio-applications.^{36,43–46} This is because they should enable facile conjugation of proteins or enzymes in aqueous solution at ambient temperature. In this Chapter, the derivatisation of these aldehyde-functional brushes is investigated using two primary amines and an amino acid (histidine) as model compounds *via* Schiff base chemistry.

6.2. Experimental

6.2.1. Synthesis

Preparation of silane initiator silicon wafers

Silicon (100) wafers were cut into small pieces (~1 x 1 cm³) before being UV-ozone cleaned for 60 min at 10³ Pa using a Bioforce Nanosciences ProCleaner. These wafers were then placed in test tubes along with a 3 mL glass sample vial containing ~100 µL (3-aminopropyl)triethoxysilane (APTES) and the test tubes were sealed with a rubber septum before being placed in a 100 °C oven for 60 min. The resulting APTES-functionalised silicon wafers were then removed from the oven and excess APTES was allowed to evaporate before washing the wafers with tetrahydrofuran (THF) and drying them under a stream of compressed air. The wafers were then functionalised by immersion in a 0.1 M α-bromoisobutyryl bromide (BiBB) solution in 1,4-dioxane for 18 h at 22 °C. Finally, the wafers were rinsed with THF and water before being dried using a stream of compressed air.

Synthesis of PGEO5MA brushes by surface-initiated activator regenerated by electron transfer atom transfer radical polymerisation (SI-ARGET ATRP)

PGEO5MA brushes prepared at an aqueous GEO5MA concentration of 45% v/v in the presence of ascorbic acid is representative of the general protocol. GEO5MA (2.67 mL, 8.44 mmol), water (2.70 mL), copper(II) chloride (CuCl₂; 0.92 mg, 6.84 µmol) and *N,N,N',N',N''*-pentamethyldiethylenetriamine (PMDETA; 50 µL) were added to a 7 mL glass

sample vial. This aqueous solution was stirred for 10 min to ensure thorough mixing before adding the ascorbic acid (3.0 mg, 17 μmol , 1.02 mM) and immersing the silicon wafer. Each sample vial contained roughly 1 cm^3 of air and the SI-ARGET ATRP of GEO5MA was allowed to proceed for up to 2 h at 22 °C. Each polymerisation was quenched by removal of the silicon wafer from the reaction mixture, extensive washing with deionised water and then drying using a stream of compressed air.

Selective oxidation of PGEO5MA brushes using NaIO₄

PGEO5MA brush-functionalised silicon wafers were immersed in a 3.0 mg mL^{-1} aqueous solution of NaIO₄ for 30 min at 22 °C. Each wafer was then rinsed extensively with water and dried using a stream of compressed air.

Synthesis of the PAGEO5MA reference brush by SI-ARGET ATRP

PAGEO5MA reference brushes prepared at an AGEO5MA concentration of 15% v/v in the presence of ascorbic acid is representative of the general protocol. AGEO5MA (0.87 mL, 3.1 mmol), water (4.79 mL), CuCl₂ (0.92 mg, 6.84 μmol) and PMDETA (50 μL) were added to a 7 mL sample vial. This reaction solution was stirred for 2 min to ensure thorough mixing before addition of the ascorbic acid (0.15 mg, 0.85 μmol , 0.42 mM) and immersion of the silicon wafer. Each sample vial contained roughly 1 cm^3 of air and the SI-ARGET ATRP of AGEO5MA was allowed to proceed for 1–2 h at 22 °C. Each polymerisation was quenched by removal of the silicon wafer from the reaction mixture, extensive washing with deionised water and then drying using a stream of compressed air.

Functionalisation of PAGEO5MA brushes with primary amines via reductive amination

An aqueous solution containing 3.0 mg mL^{-1} primary amine [(2-aminoethyl)trimethylammonium chloride hydrochloride (AETMA), histidine or 2,2,2-trifluoroethylamine (TFEA)] and 7.0 mg mL^{-1} sodium cyanoborohydride (NaCNBH₃) was adjusted to pH 5–6. PAGEO5MA brush-functionalised silicon wafers were immersed in this aqueous solution for 48 h at 35 °C. Each wafer was then removed, extensively rinsed with deionised water and dried under a stream of compressed air.

Kinetics of polymerisation studies

Protocol 1. SI-ARGET ATRP was used to grow PGEO5MA brushes from initiator-functionalised silicon wafers at an aqueous GEO5MA concentration of 45% v/v using GEO5MA: CuCl₂: PMDETA: ascorbic acid molar ratios of 1000: 1: 5: 3.

The catalyst, ligand, monomer and water were weighed in turn into a 50 mL round-bottom flask containing a magnetic flea. The resulting solution was stirred for 10 min prior to

addition of the ascorbic acid. The reaction mixture was then stirred for a further 10 min to ensure formation of the active catalyst. Each initiator-functionalised silicon wafer was placed in a sealable 1.5 mL vial before being filled with the reaction mixture such that the volume of air remaining in each sealed vial was less than 0.1 cm³. Each wafer was removed from the reaction mixture after the desired polymerisation time and rinsed extensively with ethanol and deionised water prior to drying under a stream of compressed air for ellipsometry studies.

Protocol 2. SI-ARGET ATRP was used to grow PGEO5MA brushes from initiator-functionalised silicon wafers at an aqueous GEO5MA concentration of 45% v/v using GEO5MA: CuCl₂: PMDETA: ascorbic acid molar ratios of 1000: 1: 5: 3.

The catalyst, ligand, monomer and water were pipetted into a 7 mL sample vial. The reaction mixture was stirred for 10 min followed by addition of ascorbic acid. The polymerisation mixture was then stirred for an additional 10 min. An initiator-functionalised silicon wafer was placed in the sample vial. The volume of air remaining in the vial was ~1 cm³. After 10 min, the wafer was removed from the reaction mixture, washed extensively with deionised water and dried using a stream of compressed air. The dry thickness of the brush was determined using ellipsometry and then the wafer was reimmersed in the reaction mixture. This protocol was repeated five times over a total 'brush immersion' reaction time of 60 min.

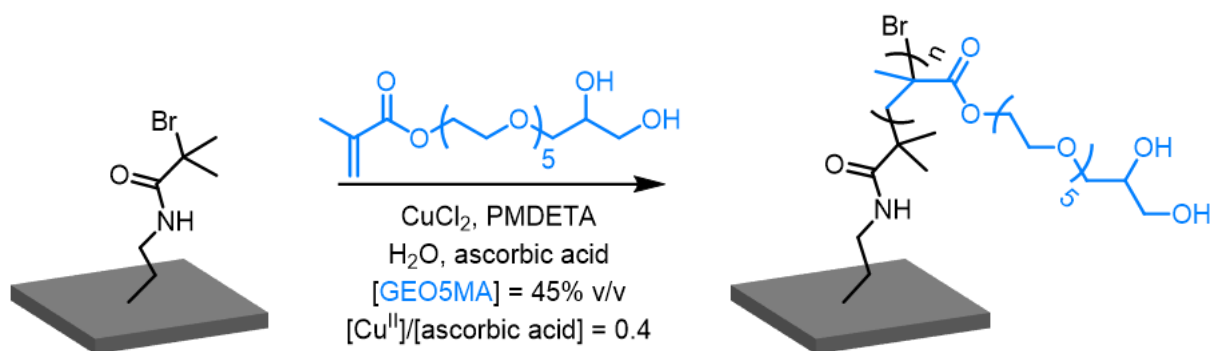
The kinetics of surface-initiated polymerisations differ from that for the analogous solution polymerisation, which makes a direct comparison somewhat problematic.^{47,48} Moreover, determination of the molecular weight of the brush chains *via* degrafting is not feasible for the planar silicon wafers employed in this study owing to the very small mass of grafted polymer (5 µg cm⁻²). Thus, the brush grafting density is simply assumed to be comparable to brushes prepared using similar synthesis protocols.⁴⁹⁻⁵¹

6.3. Results and Discussion

6.3.1. Kinetics of PGEO5MA brush synthesis

PGEO5MA brushes were grown from a planar surface *via* SI-ARGET ATRP. More specifically, an aqueous CuCl₂/PMDETA catalyst was used to grow brushes from 3-(2-bromoisobutyramido)-propyl triethoxysilane (BiBB-APTES) coated silicon wafers at 22 °C using a GEO5MA concentration of 45% v/v and ascorbic acid as the reducing agent ([Cu^{II}]/[ascorbic acid] molar ratio = 0.40), see Scheme 6.1. The polymerisation kinetics were monitored using two different synthesis protocols. **Protocol 1** involved placing individual

wafers in each of five reaction vessels and immersing each wafer in the same stock reaction solution. Each wafer was then removed from its vial at a different time point during the polymerisation followed by copious rinsing (using ethanol and deionised water) and air-drying (yellow points, Figure 6.1). **Protocol 2** involved immersing one wafer in a single reaction vial and immersing the wafer in the reaction solution. During the polymerisation, this wafer was periodically withdrawn (at 10 min intervals), rinsed and air-dried to enable its dry brush thickness to be determined by spectroscopic ellipsometry *prior to its reimmersion in the original reaction solution*; the overall reaction time for this latter protocol was typically 60 min (green points, Figure 6.1). Both protocols enable the polymerisation kinetics to be monitored in order to assess the pseudo-living character of the growing brush chains. In principle, a linear evolution in dry brush thickness over time indicates a well-controlled polymerisation.⁵²



Scheme 6.1. Reaction scheme for the synthesis of PGE05MA brushes *via* SI-ARGET ATRP.

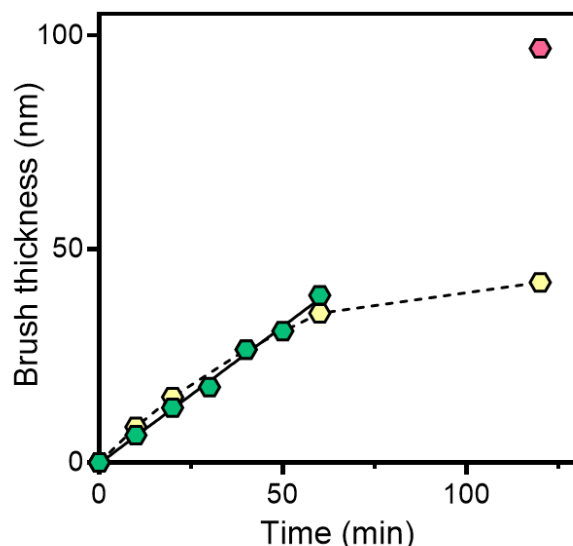


Figure 6.1. Evolution in dry brush thickness determined by ellipsometry during the SI-ARGET ATRP of GEO5MA at 22 °C using **Protocol 1** (yellow data points; individual initiator-functionalised wafers immersed within the same reaction solution in separate sample vials are periodically removed in turn) and **Protocol 2** (green data points; a single initiator-functionalised silicon wafer (re)immersed multiple times into the same reaction mixture). Further formulation details are provided in the Experimental section. Alternatively, significantly thicker brushes could be grown *via* **Protocol 2** in the absence of periodic removal of the silicon wafer from the reaction mixture (see pink data point).

Ellipsometry data was modelled using a single polymer Cauchy layer on native silicon dioxide with good fits being achieved in all cases (Figure 6.2). For **Protocol 1**, a highly linear increase in dry brush thickness with time was observed over ~45 min, suggesting a well-controlled pseudo-living polymerisation with minimal termination (yellow points, Figure 6.1).^{17,52} PGEO5MA brush thicknesses of up to ~36 nm were obtained within 60 min at 22 °C. However, deviation from linearity is observed over longer polymerisation times (>60 min), which suggests premature chain termination. Similar kinetic data were reported by Edmondson and co-workers for the growth of a closely related *cis*-diol-functional methacrylic polymer brush [i.e., poly(glycerol monomethacrylate) (PGMA)].²⁶ In this prior study, surface ATRP was conducted at ambient temperature using an anionic macroinitiator and a 1:1 v/v methanol/water mixture. PGMA brush growth was initially linear over the first 200 min, but slower kinetics and premature chain termination resulted in a dry brush thickness of only 17 nm after 21 h.

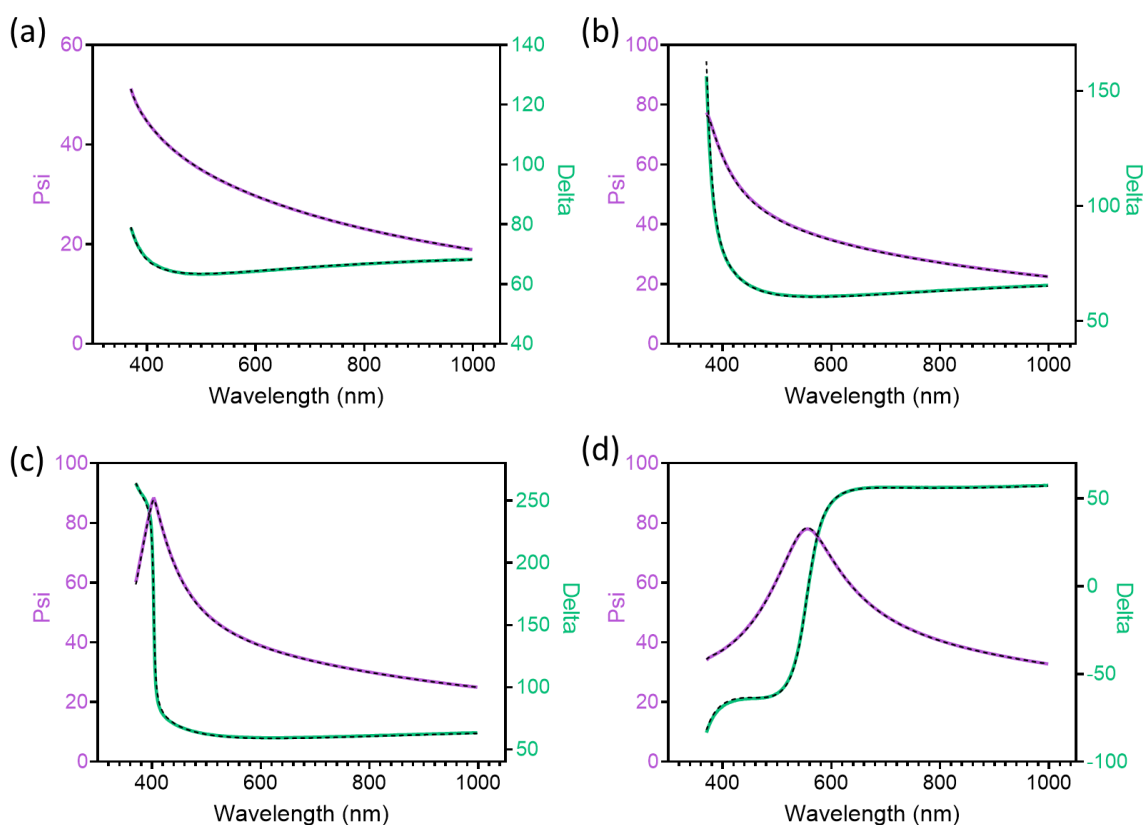


Figure 6.2. Ellipsometry fits for a selection of PGEO5MA polymer brushes. (a) A 66 nm, (b) a 74 nm, (c) a 84 nm and (d) a 120 nm brush.

When using **Protocol 2**, comparable dry brush thicknesses to **Protocol 1** were obtained for polymerisation times of up to 60 min (green data points, Figure 6.1). The exceptionally linear plot observed using **Protocol 2** suggests remarkably high reinitiation efficiency in this case. However, periodic removal/reimmersion of the silicon wafer eventually led to gelation of the reaction solution over longer time scales, which precluded further kinetic

measurements. Importantly, if the initiator-functionalised silicon wafer was simply allowed to remain within the reaction solution (rather than being periodically removed, rinsed and dried for ellipsometry studies), then gelation did not occur and significantly thicker brushes could be grown (see pink data point in Figure 6.1). Accordingly, the latter protocol was used for some of the brushes described below.

6.3.2. X-ray photoelectron spectroscopy (XPS) studies of PGEO5MA brush oxidation

XPS was used to analyse the surface composition of an initiator-functionalised wafer and a PGEO5MA brush with a dry thickness of 97 nm (obtained using **Protocol 2** after 120 min at 22 °C). Comparison of the high-resolution N 1s and Br 3d signals recorded for the initiator-functionalised wafer indicated a Br 3d/N 1s atomic ratio of ~ 0.50 , which suggests that approximately half of the primary amine groups on the initial APTES-treated wafer reacted with the BiBB (Figure 6.3a and 6.3b). Similar results were reported by Morse and co-workers for initiator-functionalised quartz fibres prepared using a similar protocol and the same reagents.⁵³

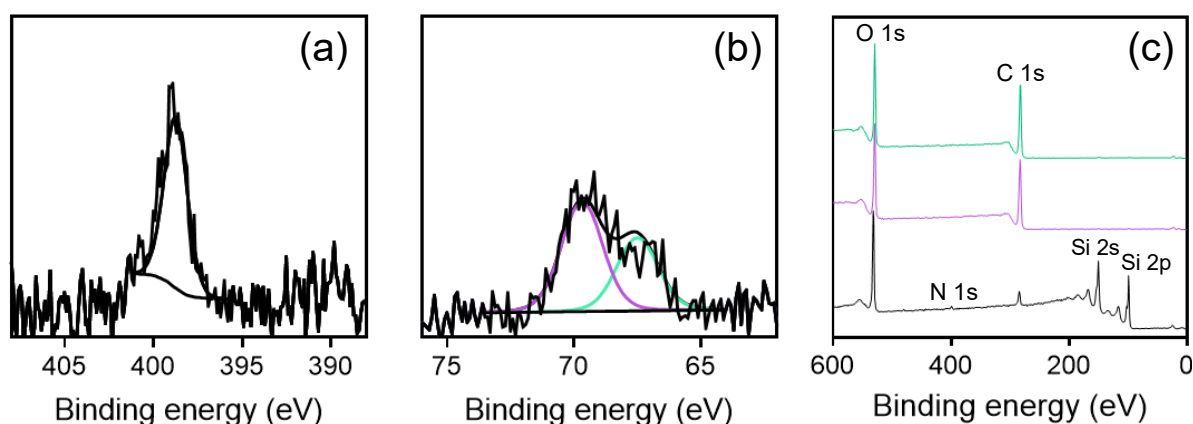


Figure 6.3. High resolution (a) N 1s and (b) Br 3d spectra for a BiBB-APTES coated silicon wafer. (c) XPS survey spectra recorded for initiator-functionalised silicon wafer (black spectrum), a PGEO5MA polymer brush (purple spectrum) and the corresponding PAGEO5MA polymer brush (green spectrum).

Inspecting the survey spectra, the Si 2s and Si 2p signals corresponding to the underlying silicon wafer are clearly evident for the initiator-functionalised wafer but are absent for the PGEO5MA brush-coated wafer (Figure 6.3c). Given the relatively shallow XPS sampling depth,⁵⁴ this indicates uniform coverage of the silicon wafer by the brush chains (i.e., no bare patches). This is consistent with the relatively uniform dry brush thickness indicated by ellipsometry measurements. A high-resolution C 1s spectrum was acquired for the PGEO5MA brush (Figure 6.4a). The C 1s signal was fitted using three components with binding energies of 285.0, 286.5 and 288.9 eV, which correspond to C-C, C-O and O=C-O,

respectively. The experimental atomic ratios for these components were 3.5:12:1.5, close to the theoretical ratios of 3:13:1.

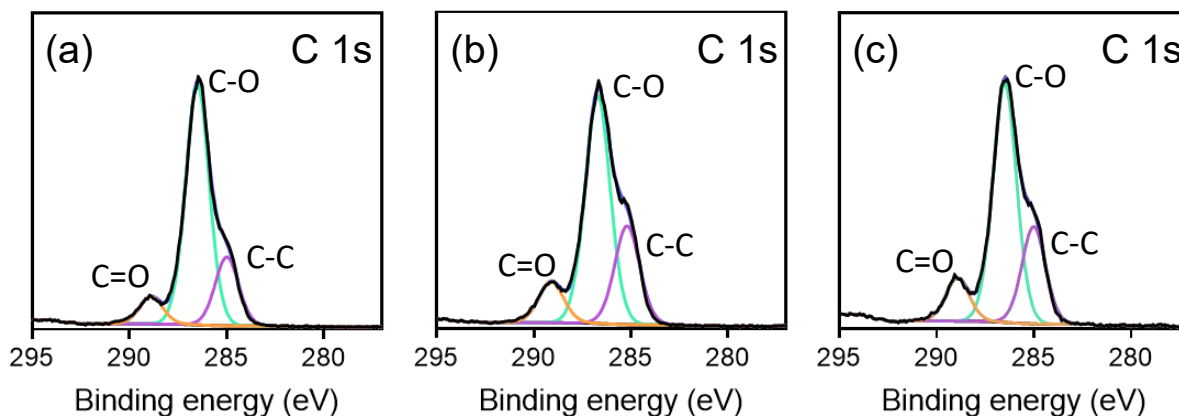
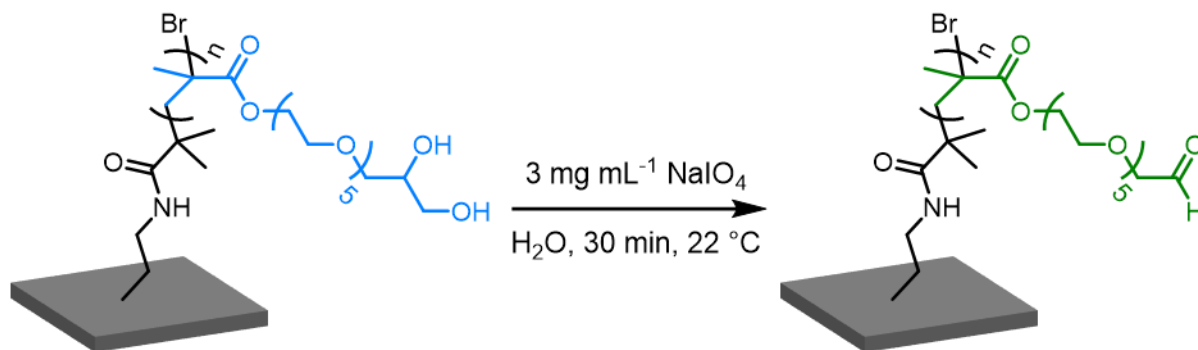


Figure 6.4. High resolution C 1s spectra obtained by XPS for (a) a PGEO5MA brush, (b) the corresponding NaIO₄-oxidised PGEO5MA brush (30 min oxidation time) and (c) a PAGEO5MA brush grown using AGEO5MA monomer.

PGEO5MA brushes were immersed in an aqueous solution of NaIO₄ at 22 °C to produce the corresponding hydrophilic aldehyde-functional PAGEO5MA brushes (Scheme 6.2). In Chapter III, it was reported that a NaIO₄/*cis*-diol molar ratio of unity was required to achieve complete oxidation of the pendent *cis*-diol groups on a PGEO5MA homopolymer dissolved in aqueous solution.⁴² In contrast, oxidation of PGEO5MA brushes necessarily involves a large excess of periodate owing to the relatively low mass of the grafted chains (estimated to be approximately 5 μg cm⁻²). In this case, the extent of oxidation of the PGEO5MA brush was monitored over time using ellipsometry (Figure 6.5a) and XPS (Figure 6.6). In this context, Zou et al. found that a 3.0 mg mL⁻¹ aqueous solution of NaIO₄ was sufficient to fully oxidise a *cis*-diol-functional PDHPA brush (dry brush thickness = 32 nm) within 60 min at ambient temperature,^{41,55} so similar conditions were employed in the present study. The optimum oxidation time was empirically determined to be 30 min since this led to a reduction in dry brush thickness by approximately 8.5%,⁵⁶ which corresponds to the loss of one formaldehyde per *cis*-diol repeat unit as the latter moiety is oxidised to produce a pendent aldehyde group (Scheme 6.2). Longer reaction times led to a progressive further reduction in the brush thickness, indicating chemical degradation. Moreover, preliminary experiments confirmed that employing higher periodate concentrations also led to brush degradation (Figure 6.5b). Indeed, significant brush degrafting was observed in extreme cases (>0.5 M NaIO₄ for 24 h). PGEO5MA brushes (initial dry thickness = 74 to 120 nm) were immersed in turn into a 3.0 mg mL⁻¹ aqueous solution of NaIO₄ for 30 min at 22 °C prior to rinsing with deionised water and air-drying. As expected, a monotonic reduction in dry brush thickness was observed by ellipsometry

(Table 6.1). This was consistent across brushes with different thicknesses and always resulted in a thickness reduction of approximately 8.5%.



Scheme 6.2. Reaction scheme for the oxidation of PGE05MA brushes using aqueous NaIO_4 .

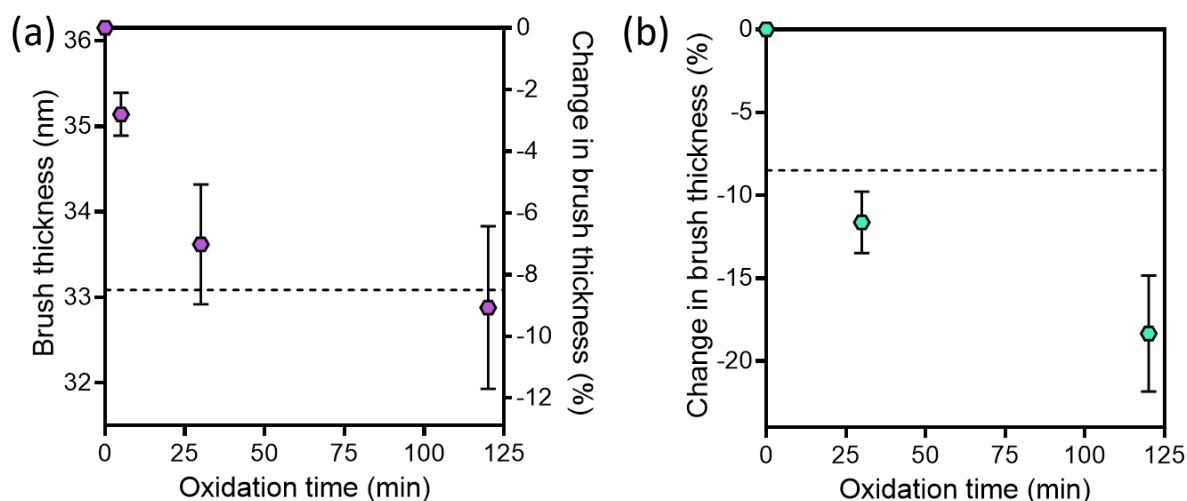


Figure 6.5. (a) Absolute (left-hand axis) and relative (right-hand axis) change in the ellipsometric dry brush thickness observed for a PGE05MA brush exposed to a 3.0 mg mL^{-1} NaIO_4 solution at 22°C . Under such relatively mild conditions, the change in brush thickness is solely due to selective oxidation (i.e., loss of formaldehyde). (b) Reduction in dry brush thickness (initial dry brush thickness = 41 nm) after exposure to a 65 mg mL^{-1} NaIO_4 solution for up to 2 h at 22°C . The initial change in brush thickness observed is attributed to the loss of formaldehyde during selective oxidation (complete oxidation should produce an 8.5% mass loss; dotted black line). The subsequent further reduction in brush thickness observed after 2 h indicates chemical degradation and/or partial degrafting of brush chains from the planar silicon wafer at this higher periodate concentration.

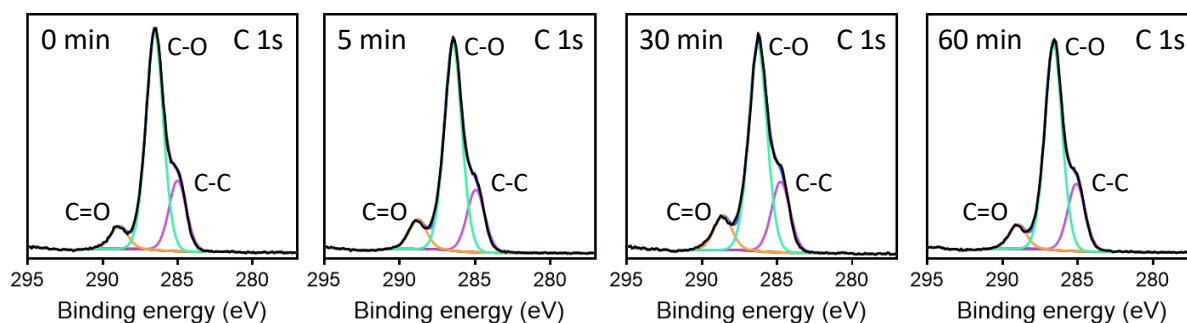
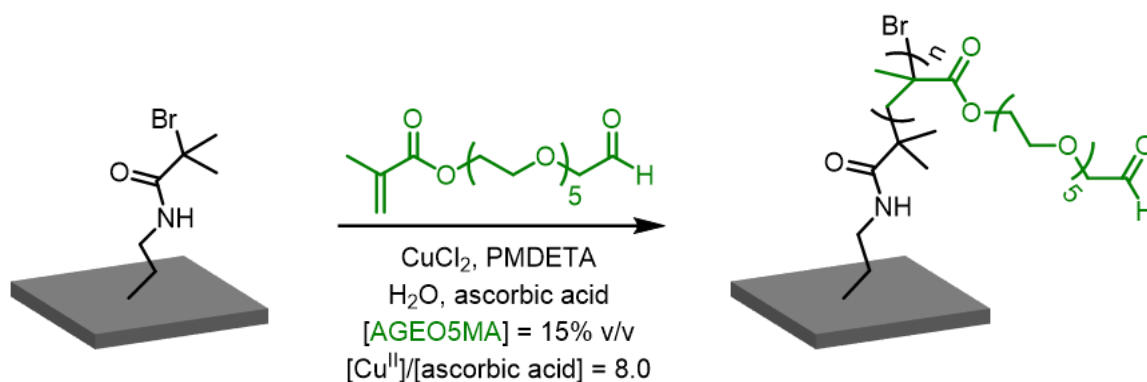


Figure 6.6. Change in the XPS C 1s high-resolution spectrum observed for a PGE05MA brush on exposure to a 3.0 mg mL^{-1} aqueous solution of NaIO_4 for up to 60 min at 22°C .

Table 6.1. Ellipsometry data obtained for six PGEO5MA brushes of varying dry brush thickness and the corresponding NaIO₄-oxidised PGEO5MA brushes. The observed reduction in brush thickness is attributed to the loss of one molecule of formaldehyde per GEO5MA repeat unit.

Thickness before oxidation (nm)	Thickness after oxidation (nm)
74	70
84	79
94	84
109	100
118	109
120	114

The extent of oxidation of the pendent *cis*-diol groups was confirmed by XPS. As the extent of oxidation increased, more C=O was present in the high-resolution C 1s spectra (Figure 6.6). As ellipsometry indicated that 30 min oxidation was sufficient to produce fully oxidised PAGEO5MA brushes, it is sensible to compare the high-resolution C 1s spectra recorded for the PGEO5MA and 30 min NaIO₄-oxidised PGEO5MA brushes as well as a PAGEO5MA reference brush grown using the AGEO5MA monomer (Figure 6.4). The 37 nm dry thickness PAGEO5MA reference brush was prepared by polymerising AGEO5MA monomer (synthesised as reported in Chapter III)⁴² from an initiator-functionalised silicon wafer *via* SI-ARGET ATRP (Scheme 6.3). The C 1s spectrum for the NaIO₄-oxidised PGEO5MA brush reveals a C-C/C-O/C=O atomic ratio of approximately 4:10:2, identical to the 4:10:2 atomic ratio obtained for the PAGEO5MA reference brush (Table 6.2).



Scheme 6.3. Reaction scheme for the synthesis of PAGEO5MA brushes *via* SI-ARGET ATRP.

In summary, the combined XPS and ellipsometry data indicate that essentially full oxidation of the *cis*-diol groups – and hence a very high degree of aldehyde functionality (ca. 99%) – can be achieved within 30 min using 3.0 mg mL⁻¹ NaIO₄ at 22 °C. This is significantly higher than the degree of aldehyde functionality of approximately 49% reported by Klok et al., who used Albright-Goldman oxidation to derivatise a PHEMA

Inspecting the N 1s high resolution spectra recorded for each brush (Figure 6.7), no signal is observed for the PGEO5MA precursor brush (Figure 6.7a). As the brush thickness (97 nm) is much greater than the XPS sampling depth, the amines on the APTES group are not seen. However, a very weak N 1s signal (around 0.1 atom%) is unexpectedly observed for the NaIO₄-oxidised PAGEO5MA brush (Figure 6.7b). This suggests a modest reduction in brush surface density resulting from cleavage of a minor fraction of oxidised brush chains, thus partially exposing the underlying initiator sites. Much stronger N 1s signals are observed for the AETMA-functionalised PGEO5MA brush (PAmGEO5MA; Figure 6.7c), the histidine-functionalised PGEO5MA brush (PHisGEO5MA; Figure 6.7d) and the TFEA-functionalised PGEO5MA brush (PTriFGEO5MA; Figure 6.7e), confirming that conjugation was successful in each case. Moreover, the high-resolution N 1s spectrum recorded for the PAmGEO5MA brush contains two signals of approximately equal intensity, which corresponds to the quaternary amine and secondary amine species that are present after reductive amination of the AETMA-conjugated PAGEO5MA brush (Figure 6.7c). It is expected that the N 1s spectrum for the PHisGEO5MA brush should be fitted with five unique peaks/signals. However, due to the low signal to noise ratio for this spectrum, only three peaks could be fitted (Figure 6.7d). A single N 1s signal is observed for the PTriFGEO5MA brush (Figure 6.7e). Furthermore, a strong F 1s signal is observed for

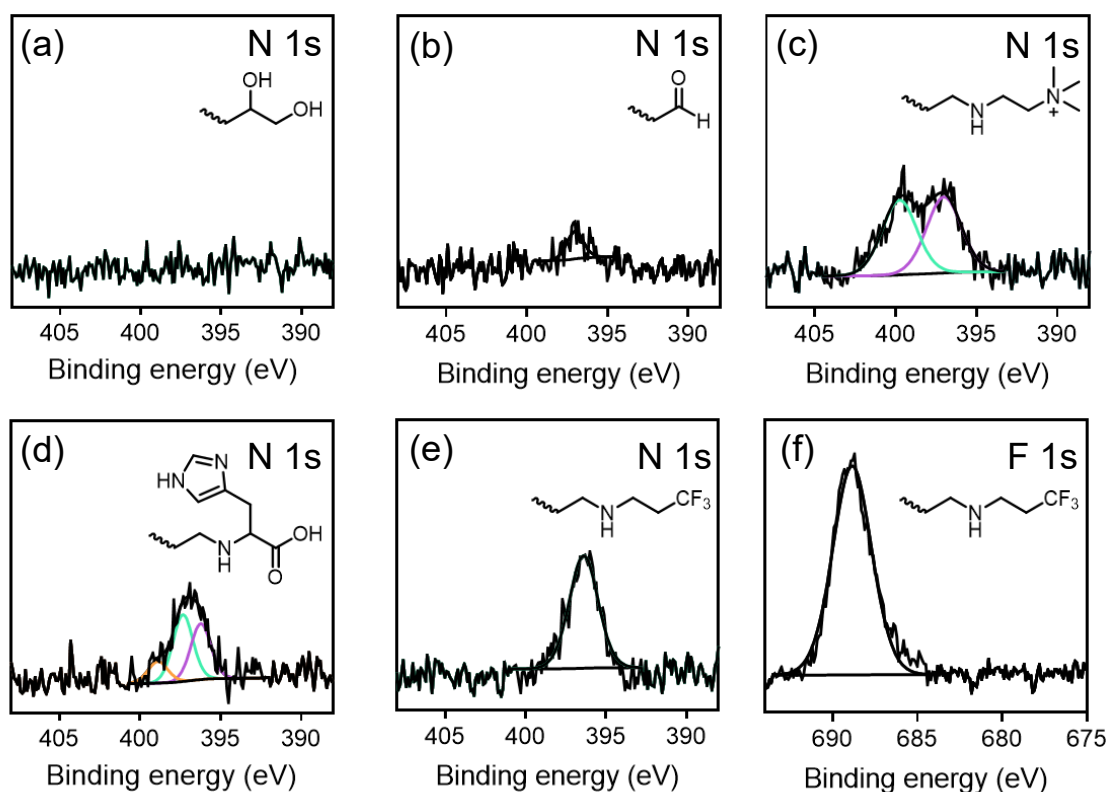


Figure 6.7. High resolution N 1s spectra recorded for (a) PGEO5MA, (b) PAGEO5MA, (c) PAmGEO5MA, (d) PHisGEO5MA and (e) PTriFGEO5MA brushes. (f) High resolution F 1s spectrum recorded for the PTriFGEO5MA brush.

PTriFGEO5MA (Figure 6.7f) and the corresponding F 1s/N 1s atomic ratio is 3.1, which is close to the theoretical value of 3.0 (Figure 6.7e and 6.7f).

The degree of functionalisation for each derivatised brush was calculated using XPS from the respective N 1s/O 1s atomic ratios. By comparing the experimental N 1s/O 1s atomic ratio to its maximum theoretical value (corresponding to 100% functionalisation), the degree of functionalisation was determined as 20% for PAmGEO5MA, 13% for PHisGEO5MA and 29% for PTriFGEO5MA brushes. This is lower than that reported by Klok et al., who achieved degrees of functionalisation of up to 79% for oxidised PHEMA brushes reacted with benzylamine, as calculated using N 1s/C 1s atomic ratios.³⁶ However, given that only ~49% of the PHEMA brush was oxidised to the aldehyde, this suggests an overall degree of functionalisation of ~39%. The reactions of Klok et al. were also performed in non-aqueous solvents. In contrast, these extents of functionalisation are comparable to those reported by Madsen et al. for the functionalisation of glutaraldehyde-treated poly(cysteine methacrylate) with TFEA. It was reported that less than 25% of the aldehyde-functional groups were reacted with the TFEA. The degree of functionalisation of PAGEO5MA *brushes* is also significantly reduced compared to *untethered* polymers where conjugation to amino acids resulted in >98% functionalisation, as reported in Chapters III and IV.^{42,58} The difference in the extent of brush functionalisation to the untethered polymer can be attributed to steric and entropic barriers present in the brush system, where the inclusion of additional mass within the brush reduces the ability for further conjugation reactions. As the degree of functionalisation increases, steric crowding also increases, which makes further reactions entropically unfavourable.

6.3.4. Characterisation of PGEO5MA, PAmGEO5MA and PHisGEO5MA polymer brushes using surface zeta potential measurements

As a result of its dual carboxylic acid and amine functionality, histidine exhibits pH-dependent zwitterionic character in aqueous solution. In contrast, AETMA possesses a quaternary ammonium group that confers cationic character over a wide pH range. Functionalisation of the non-ionic PAGEO5MA brush with either of these amines should introduce ionic character. A related study demonstrated that adjusting the solution pH leads to a substantial change in the surface zeta potential of a zwitterionic poly(cysteine methacrylate) brush.⁷ Therefore, surface zeta potential studies were conducted to further characterise the NaIO₄-oxidised PGEO5MA brushes after conjugation with either histidine or AETMA. Surface zeta potential measurements were recorded using a Malvern Nanosizer instrument and a Malvern Surface Zeta Potential ZEN1020 dip cell. In essence, the zeta

potential of tracer nanoparticles [non-ionic PGMA₅₈-PBzMA₅₀₀ [139 nm by dynamic light scattering (DLS)] and cationic PMETAC₄₇-PBzMA₁₀₀ (34 nm by DLS)] is measured at varying distances from the surface of interest. For cationic surfaces, cationic tracer nanoparticles were used to ensure that no nanoparticle adsorption occurred. Similarly, non-ionic tracer nanoparticles were used to characterise either neutral or anionic surfaces.^{7,59} By monitoring the change in the apparent zeta potential of the tracer nanoparticles, the surface zeta potential of each brush could be determined at a given pH (Figure 6.8).

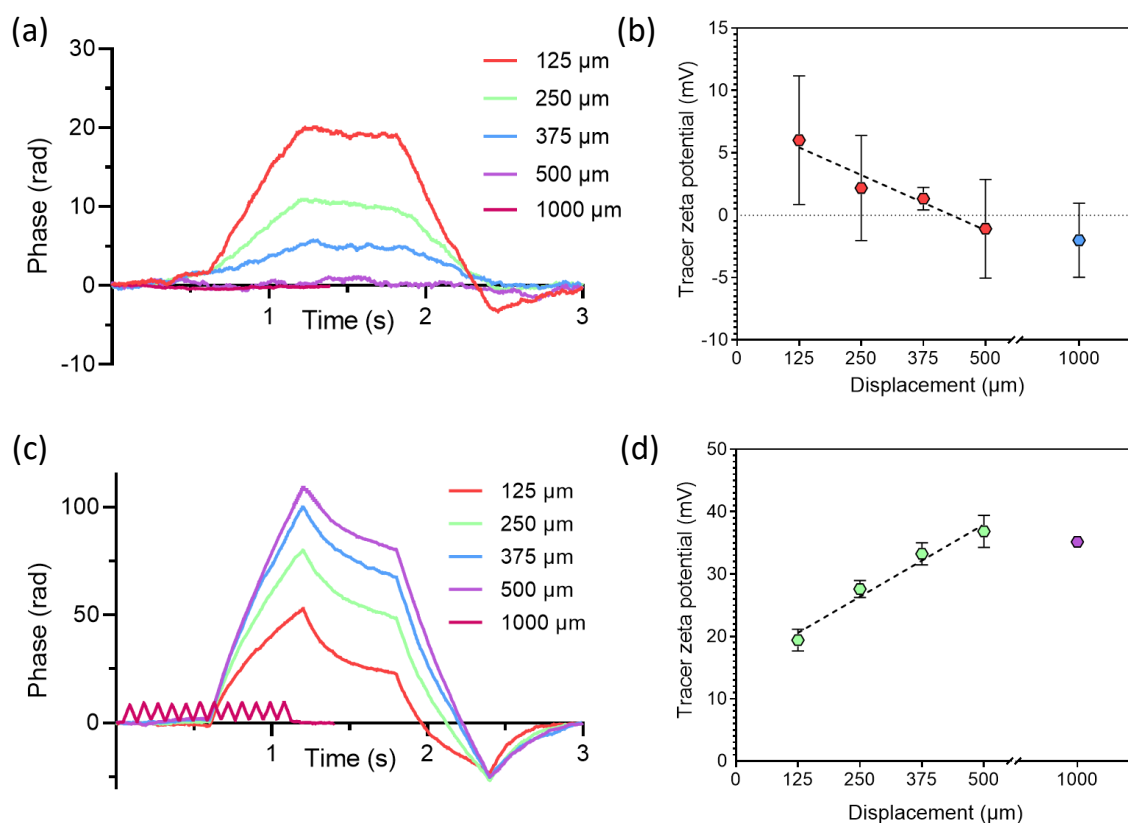


Figure 6.8. (a) Raw phase plot and (b) relationship between tracer particle zeta potential and displacement for a PGEO5MA brush immersed in a 0.003% w/w aqueous dispersion of PGMA₅₈-PzMA₅₀₀ tracer particles in 1 mM KCl at pH 3. (c) Raw phase plot and (d) relationship between tracer particle zeta potential and displacement for a PHisGEO5MA brush immersed in a 0.003% w/w aqueous dispersion of PMETAC₄₇-PBzMA₁₀₀ tracer particles at pH 4.75. [Note: slow field reversal measurements were performed at displacements 125, 250, 375 and 500 μm from the polymer brush surface. A fast field reversal measurement was performed at 1000 μm from the polymer brush surface.]

As expected, the surface zeta potential of a 97 nm neutral PGEO5MA brush remained approximately neutral over a wide range of solution pH (Figure 6.9a). In contrast, the AETMA-functionalised brush exhibits cationic behaviour across the entire pH range (Figure 6.9b.). These observations support the XPS data and confirm successful functionalisation of the PAGEO5MA brush with AETMA. For the PHisGEO5MA brush, strongly positive zeta potentials are observed at low pH owing to protonation of the imidazole ring, the secondary amine linkage and the pendent carboxylic acid group on

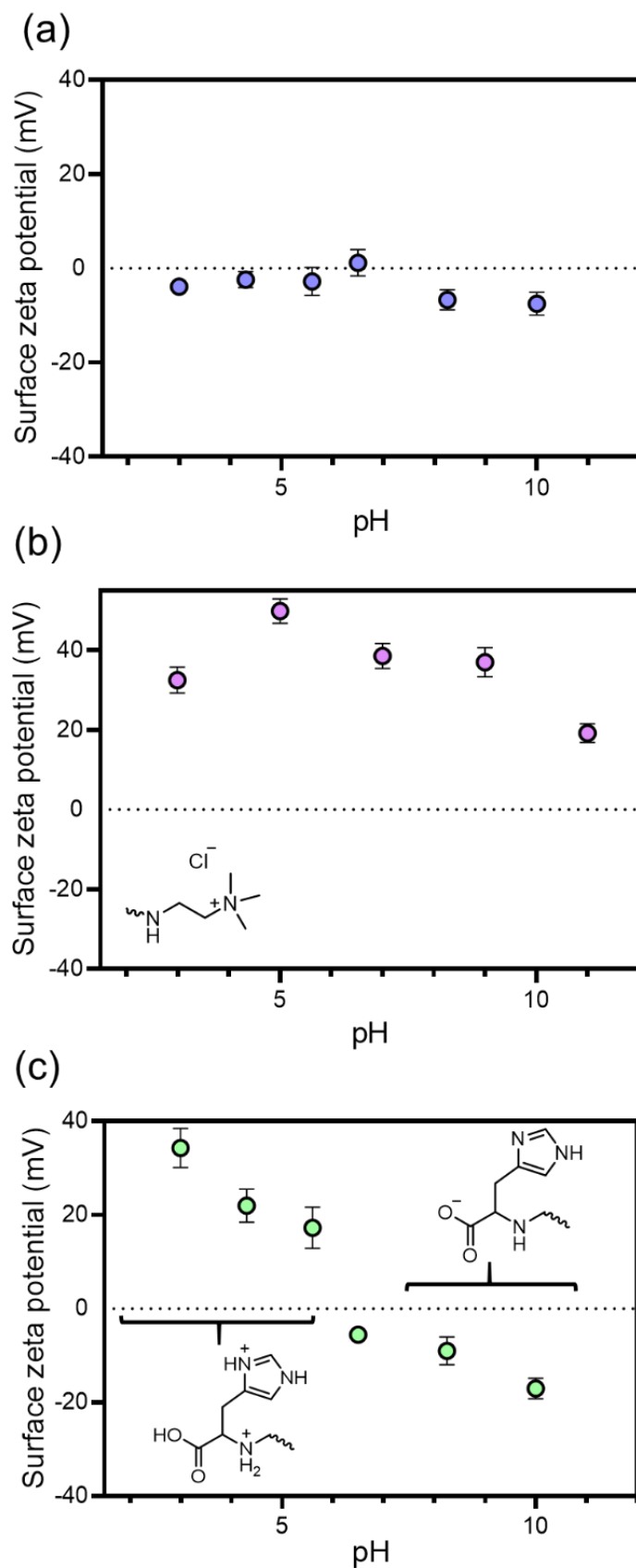
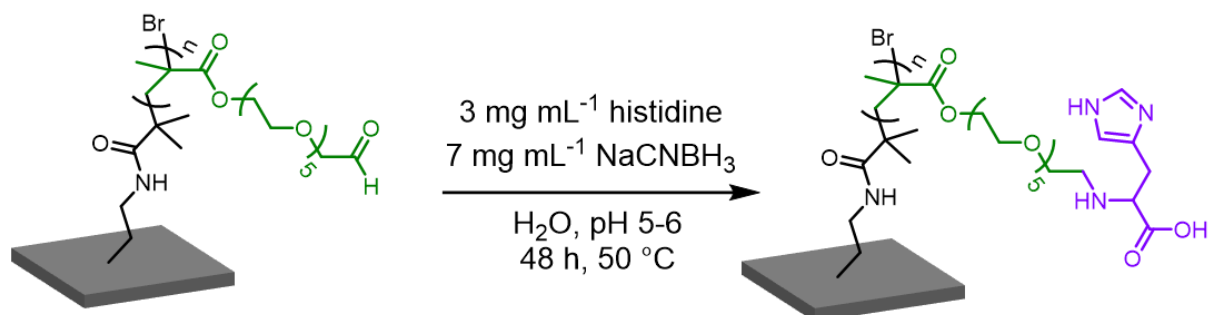


Figure 6.9. Surface zeta potential vs. pH curves recorded for (a) a PGE05MA brush of 97 nm dry thickness, (b) a PAmGEO5MA brush of 88 nm dry thickness and (c) a PHisGEO5MA brush of 91 nm dry thickness.

each histidine repeat unit (Figure 6.9c). However, negative zeta potentials are observed at high pH owing to deprotonation of the imidazole rings and the secondary amine linkages, while the carboxylic acid groups are ionised. An isoelectric point (corresponding to net charge on the brush chains) is observed at around pH 6. As a comparison, in Chapter IV the aqueous electrophoresis behaviour of PHisGEO5MA₂₆-PHPMA_y nanoparticles in 1 mM KCl was reported.⁵⁸ In this case, the isoelectric point occurred at pH 6.5 and similarly positive and negative zeta potentials were observed at low and high pH, respectively. It is worth noting that significant changes in the surface charge can be achieved despite the relatively low extents of brush functionalisation. This highlights the potential of PAGEO5MA brushes to act as hydrophilic scaffolds to which amine functional molecules can be anchored at interfaces.

6.3.5. The effect of temperature on extent of functionalisation for the reductive amination of NaIO₄-oxidised PAGEO5MA polymer brushes

In Chapter III it was reported that reaction of PAGEO5MA₃₇ homopolymer with several amino acids at 35 °C resulted in very high extents of functionalisation (>99% by ¹H NMR spectroscopy). In comparison, the extent of functionalisation for the reaction of a NaIO₄-oxidised PAGEO5MA brush with histidine at 35 °C resulted in functionalisations of 13% as determined by XPS. This low extent of functionalisation could be due to the relatively low mass of the grafted chains (estimated to be approximately 5 ng cm⁻²) with respect to the other reagents. Increasing the temperature of the reductive amination should increase the rate of reaction and, thus, increase the extent of functionalisation. Therefore, a NaIO₄-oxidised PAGEO5MA brush was functionalised in a 3 mg mL⁻¹ aqueous solution of histidine at 50 °C (Scheme 6.5). A NaCNBH₃ concentration of 7 mg mL⁻¹ was maintained as with the reactions conducted at 35 °C. The degree of functionalisation was again calculated by using the N 1s/O 1s atomic ratios obtained from XPS (Table 6.3 and Figure 6.10). A degree of functionalisation of approximately 82% was achieved for the



Scheme 6.5. Reaction scheme for the functionalisation of PAGEO5MA with histidine *via* reductive amination at 50 °C.

PHisGEO5MA brush synthesised at 50 °C as determined by XPS. This is significantly higher than that of the PHisGEO5MA brush synthesised at 35 °C (Table 6.3) indicating that the reaction temperature has a significant impact on the degree on functionalisation. This should allow for tuning the extent of functionalisation of such NaIO₄-oxidised PGE05MA brushes. The ability to tune the extent of functionalisation is desirable as different applications may require different levels of conjugation. For example, high levels of histidine functionality will have a significant impact on the structure and character of the PAGE05MA brush, while lower levels of functionalisation may allow the original structure to be retained. Furthermore, limited functionalisation may open up the possibility of functionalisation with multiple molecules.

Table 6.3. Summary of the wide-angle data obtained by XPS analysis of a PHisGEO5MA brush synthesised at 35 °C and a PHisGEO5MA brush synthesised at 50 °C indicating the relative amounts of each of the N 1s, O 1s and N 1s/O 1s atomic ratio, respectively, and the degree of functionalisation.

Temperature of reductive amination (°C)	Surface composition from wide angle spectra (%)		N 1s/O 1s atomic ratio	Degree of functionalisation (%)
	N1s	O1s		
35 °C	1.1	27.9	0.04	13
50 °C	6.8	25.0	0.27	82

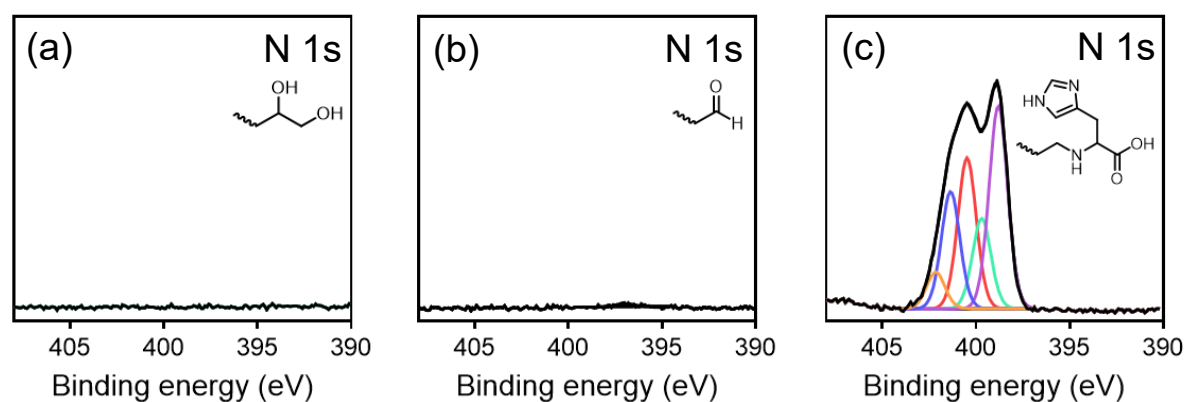


Figure 6.10. High resolution N 1s spectra recorded for (a) PGE05MA, (b) PAGE05MA and (c) PHisGEO5MA synthesised at 50 °C.

6.4. Conclusion

The synthesis of new aldehyde-functional hydrophilic polymer brushes is reported. SI-ARGET ATRP is used to polymerise GEO5MA from a planar silicon wafer followed by selective oxidation of the pendent *cis*-diols using an aqueous solution of NaIO₄ under mild conditions (22 °C). Employing a reference brush prepared using an analogous aldehyde-functional methacrylic monomer, XPS analysis confirmed that the degree of aldehyde functionalisation of such brushes was at least 99% within 30 min of their exposure to NaIO₄. The resulting PAGE05MA brushes were subsequently functionalised in

turn using AETMA, histidine or TFEA *via* Schiff base chemistry followed by reductive amination using NaCNBH₃. By comparing N 1s/O 1s atomic ratios, XPS analysis indicated that the mean degree of functionalisation achieved for each derivatised brush was approximately 20, 13 and 29%, respectively. Nevertheless, surface zeta potential measurements indicated a significant change in the apparent surface charge of each brush relative to that of the neutral PGEO5MA precursor brush. For example, the zwitterionic PHisGEO5MA brush exhibited cationic character at low pH and anionic character at high pH, with an isoelectric point observed at ~pH 6. Functionalisation studies conducted at 50 °C found that the extent of functionalisation using histidine could be increased from 13 to 82%, which should increase the potential applications for such polymer brushes.

6.5. References

- 1 M. Husseman, E. E. Malmström, M. McNamara, M. Mate, D. Mecerreyes, D. G. Benoit, J. L. Hedrick, P. Mansky, E. Huang, T. P. Russell and C. J. Hawker, *Macromolecules*, 1999, **32**, 1424–1431.
- 2 T. Wu, K. Efimenko and J. Genzer, *J. Am. Chem. Soc.*, 2002, **124**, 9394–9395.
- 3 M. Chen, W. H. Briscoe, S. P. Armes and J. Klein, *Science*, 2009, **323**, 1698–1701.
- 4 U. Raviv, S. Giasson, N. Kampf, J. F. Gohy, R. Jérôme and J. Klein, *Nature*, 2003, **425**, 163–165.
- 5 R. M. Bielecki, E. M. Benetti, D. Kumar and N. D. Spencer, *Tribol. Lett.*, 2012, **45**, 477–487.
- 6 W. Feng, J. L. Brash and S. Zhu, *Biomaterials*, 2006, **27**, 847–855.
- 7 A. M. Alswieleh, N. Cheng, I. Canton, B. Ustbas, X. Xue, V. Ladmiral, S. Xia, R. E. Ducker, O. El Zubir, M. L. Cartron, C. N. Hunter, G. J. Leggett and S. P. Armes, *J. Am. Chem. Soc.*, 2014, **136**, 9404–9413.
- 8 C. Rodriguez-Emmenegger, E. Brynda, T. Riedel, M. Houska, V. Šubr, A. B. Alles, E. Hasan, J. E. Gautrot and W. T. S. Huck, *Macromol. Rapid Commun.*, 2011, **32**, 952–957.
- 9 S. Tugulu and H.-A. Klok, *Biomacromolecules*, 2008, **9**, 906–912.
- 10 H. Murata, R. R. Koepsel, K. Matyjaszewski and A. J. Russell, *Biomaterials*, 2007, **28**, 4870–4879.
- 11 N. Schüwer and H. A. Klok, *Adv. Mater.*, 2010, **22**, 3251–3255.
- 12 M. Welch, A. Rastogi and C. Ober, *Soft Matter*, 2011, **7**, 297–302.
- 13 K. Takasu, K. Kushiro, K. Hayashi, Y. Iwasaki, S. Inoue, E. Tamechika and M. Takai, *Sensors Actuators, B Chem.*, 2015, **216**, 428–433.
- 14 M. Badoux, M. Billing and H.-A. Klok, *Polym. Chem.*, 2019, **10**, 2925–2951.
- 15 M. E. Welch, T. Doublet, C. Bernard, G. G. Malliaras and C. K. Ober, *J. Polym. Sci. Part A Polym. Chem.*, 2015, **53**, 372–377.

- 16 K. Matyjaszewski and J. Xia, *Chem. Rev.*, 2001, **101**, 2921–2990.
 - 17 S. Edmondson, V. L. Osborne and W. T. S. Huck, *Chem. Soc. Rev.*, 2004, **33**, 14–22.
 - 18 R. R. Shah, D. Merreceyes, M. Husemann, I. Rees, N. L. Abbott, C. J. Hawker and J. L. Hedrick, *Macromolecules*, 2000, **33**, 597–605.
 - 19 K. Matyjaszewski, P. J. Miller, N. Shukla, B. Immaraporn, A. Gelman, B. B. Luokala, T. M. Siclovan, G. Kickelbick, T. Vallant, H. Hoffmann and T. Pakula, *Macromolecules*, 1999, **32**, 8716–8724.
 - 20 H. Lee, J. Pietrasik, S. S. Sheiko and K. Matyjaszewski, *Prog. Polym. Sci.*, 2010, **35**, 24–44.
 - 21 D. M. Jones, J. R. Smith, W. T. S. Huck and C. Alexander, *Adv. Mater.*, 2002, **14**, 1130–1134.
 - 22 N. Ishida and S. Biggs, *Langmuir*, 2007, **23**, 11083–11088.
 - 23 A. M. Jonas, K. Glinel, R. Oren, B. Nysten and W. T. S. Huck, *Macromolecules*, 2007, **40**, 4403–4405.
 - 24 I. J. Gresham, B. A. Humphreys, J. D. Willott, E. C. Johnson, T. J. Murdoch, G. B. Webber, E. J. Wanless, A. R. J. Nelson and S. W. Prescott, *Macromolecules*, 2021, **54**, 2541–2550.
 - 25 O. Azzaroni, A. A. Brown and W. T. S. Huck, *Angew. Chemie - Int. Ed.*, 2006, **45**, 1770–1774.
 - 26 S. Edmondson, C.-D. Vo, G.-F. Unali and S. P. Armes, *Macromolecules*, 2007, **40**, 5271–5278.
 - 27 L. A. Fielding, S. Edmondson and S. P. Armes, *J. Mater. Chem.*, 2011, **21**, 11773–11780.
 - 28 J. D. Willott, B. A. Humphreys, T. J. Murdoch, S. Edmondson, G. B. Webber and E. J. Wanless, *Phys. Chem. Chem. Phys.*, 2015, **17**, 3880–3890.
 - 29 A. M. Alswieleh, N. Cheng, G. J. Leggett and S. P. Armes, *Langmuir*, 2014, **30**, 1391–1400.
 - 30 S. Tugulu, R. Barbey, M. Harms, M. Fricke, D. Volkmer, A. Rossi and H.-A. Klok, *Macromolecules*, 2007, **40**, 168–177.
 - 31 N. Schüwer and H.-A. Klok, *Langmuir*, 2011, **27**, 4789–4796.
 - 32 A. J. Parnell, S. J. Martin, C. C. Dang, M. Geoghegan, R. A. L. Jones, C. J. Crook, J. R. Howse and A. J. Ryan, *Polymer*, 2009, **50**, 1005–1014.
 - 33 C. J. Galvin and J. Genzer, *Prog. Polym. Sci.*, 2012, **37**, 871–906.
 - 34 H. Jiang and F.-J. Xu, *Chem. Soc. Rev.*, 2013, **42**, 3394.
 - 35 C. P. Radano, G. L. Baker and M. R. Smith, *J. Am. Chem. Soc.*, 2000, **122**, 1552–1553.
 - 36 T. Bilgic and H.-A. Klok, *Biomacromolecules*, 2015, **16**, 3657–3665.
 - 37 S. Edmondson and W. T. S. Huck, *J. Mater. Chem.*, 2004, **14**, 730–734.
 - 38 R. Barbey and H.-A. Klok, *Langmuir*, 2010, **26**, 18219–18230.
 - 39 S. B. Lee, R. R. Koepsel, S. W. Morley, K. Matyjaszewski, Y. Sun and A. J. Russell,
-

- Biomacromolecules*, 2004, **5**, 877–882.
- 40 N. Cheng, P. Bao, S. D. Evans, G. J. Leggett and S. P. Armes, *Macromolecules*, 2015, **48**, 3095–3103.
- 41 Y. Zou, P. Y. J. Yeh, N. A. A. Rossi, D. E. Brooks and J. N. Kizhakkedathu, *Biomacromolecules*, 2010, **11**, 284–293.
- 42 E. E. Brotherton, C. P. Jesson, N. J. Warren, M. J. Smallridge and S. P. Armes, *Angew. Chemie Int. Ed.*, 2021, **60**, 12032–12037.
- 43 S. Tugulu, A. Arnold, I. Sielaff, K. Johnsson and H.-A. Klok, *Biomacromolecules*, 2005, **6**, 1602–1607.
- 44 S. Tugulu, P. Silacci, N. Stergiopoulos and H.-A. Klok, *Biomaterials*, 2007, **28**, 2536–2546.
- 45 K. Glinel, A. M. Jonas, T. Jouenne, J. Leprince, L. Galas and W. T. S. Huck, *Bioconjug. Chem.*, 2009, **20**, 71–77.
- 46 R. Barbey, E. Kauffmann, M. Ehrat and H.-A. Klok, *Biomacromolecules*, 2010, **11**, 3467–3479.
- 47 C. B. Gorman, R. J. Petrie and J. Genzer, *Macromolecules*, 2008, **41**, 4856–4865.
- 48 J. Genzer, *Macromolecules*, 2006, **39**, 7157–7169.
- 49 T. J. Murdoch, B. A. Humphreys, J. D. Willott, S. W. Prescott, A. Nelson, G. B. Webber and E. J. Wanless, *J. Colloid Interface Sci.*, 2017, **490**, 869–878.
- 50 J. D. Willott, T. J. Murdoch, G. B. Webber and E. J. Wanless, *Macromolecules*, 2016, **49**, 2327–2338.
- 51 T. J. Murdoch, B. A. Humphreys, E. C. Johnson, S. W. Prescott, A. Nelson, E. J. Wanless and G. B. Webber, *Polymer*, 2018, **138**, 229–241.
- 52 J. O. Zoppe, N. C. Ataman, P. Mocny, J. Wang, J. Moraes and H.-A. Klok, *Chem. Rev.*, 2017, **117**, 1105–1318.
- 53 A. J. Morse, S. Edmondson, D. Dupin, S. P. Armes, Z. Zhang, G. J. Leggett, R. L. Thompson and A. L. Lewis, *Soft Matter*, 2010, **6**, 1571.
- 54 J. F. Watts and J. Wolstenholme, *An introduction to surface analysis by XPS and AES*, John Wiley & Sons, Inc., Hoboken, New Jersey, 2003.
- 55 Y. Zou, D. E. Brooks and J. N. Kizhakkedathu, *Macromolecules*, 2008, **41**, 5393–5405.
- 56 W. J. Brittain and S. Minko, *J. Polym. Sci. Part A Polym. Chem.*, 2007, **45**, 3505–3512.
- 57 J. Madsen, R. E. Ducker, O. Al Jaf, M. L. Cartron, A. M. Alswieleh, C. H. Smith, C. N. Hunter, S. P. Armes and G. J. Leggett, *Chem. Sci.*, 2018, **9**, 2238–2251.
- 58 E. E. Brotherton, M. J. Smallridge and S. P. Armes, *Biomacromolecules*, 2021, **22**, 5382–5389.
- 59 N. J. W. Penfold, A. J. Parnell, M. Molina, P. Verstraete, J. Smets and S. P. Armes, *Langmuir*, 2017, **33**, 14425–14436.
-

*Chapter VII: Conclusions and
outlook*

Chapter VII: Conclusions and outlook

This Thesis explores the synthesis of a *hydrophilic* aldehyde-functional monomer, AGE05MA, and its corresponding (co)polymers. This new methacrylic monomer can be readily prepared under relatively mild conditions from a precursor *cis*-diol based monomer, GEO5MA, by selective oxidation using an aqueous solution of sodium periodate (NaIO_4). Unlike most literature examples of aldehyde-functional vinyl monomers, AGE05MA is water-soluble. Although the synthesis of AGE05MA is atom-efficient, it is not particularly cost-effective. Its *cis*-diol functional GEO5MA precursor is not yet available on an industrial scale: it is currently manufactured on a 5 L scale *via* transesterification of methyl methacrylate with isopropylidenglycerol penta(ethylene glycol)ether, followed by deprotection using aqueous acid. This GEO5MA monomer is then oxidised using the aforementioned aqueous NaIO_4 solution to afford AGE05MA. In principle, a potentially attractive alternative route to the synthesis of AGE05MA might involve the TEMPO-catalysed oxidation of hydroxy-capped poly(ethylene glycol) monomethacrylate.¹⁻
⁴ This precursor monomer is already commercially available. Optimisation of this method would make AGE05MA much more commercially viable. One possibility could involve using TEMPO-functionalised silica particles. This heterogeneous catalyst would enable facile regeneration and hence make the process more cost-effective.⁵⁻⁷

NaIO_4 can also be employed for the selective oxidation of either PGEO5MA homopolymer or water-soluble diblock copolymers comprising PGEO5MA-PX (where PX is a second hydrophilic polymer). This oxidation proved to be selective for the PGEO5MA block in the case of non-ionic, cationic, anionic and zwitterionic copolymers. Furthermore, NaIO_4 oxidation of PGEO5MA did not result in any discernible change in the molecular weight distribution. PGEO5MA₂₆-PHPMA_y nanoparticles were prepared *via* RAFT aqueous dispersion polymerisation of 2-hydroxypropyl methacrylate (HPMA) targeting spheres, worms or vesicles. In each case, the PGEO5MA block was then selectively oxidised to form the corresponding PAGE05MA₂₆-PHPMA_y nanoparticles. For PGEO5MA₂₆-PHPMA_y spheres and worms, no change in the nanoparticle morphology was observed after NaIO_4 treatment. However, oxidation of PGEO5MA₂₆-PHPMA₃₅₀ vesicles unexpectedly led to a mixed morphology of vesicles and worms. In view of this problem, the linear PGEO5MA-based vesicles were crosslinked using 20 units of ethylene glycol dimethacrylate (EGDMA) as a third block to ensure that the vesicle morphology was maintained during NaIO_4 oxidation. For linear spherical nanoparticles oxidation led to an increase in the copolymer dispersity, suggesting that partial crosslinking had occurred. In

contrast, only a modest change in copolymer dispersity was observed for the worm-like nanoparticles. The reason for these observations is currently not known and further studies are warranted. In principle, aldehydes can be further oxidised to carboxylic acids. However, long-term stability studies of these aldehyde-functional PAGEO5MA₂₆-PHPMA_y nanoparticles indicated that they remained stable towards oxidation for at least one year when stored as a 10% w/w aqueous solution at ambient temperature.

Synthesis of charged polymers is of interest for potential bio-applications. Aldehydes react readily with primary amines *via* Schiff base chemistry to produce an imine bond.⁸ This can be reduced *in situ* using a mild reducing agent, e.g., sodium cyanoborohydride (NaCNBH₃), to produce a secondary amine. Thus, functionalisation of PAGEO5MA homopolymers *via* reductive amination was investigated using several amino acids. High extents of functionalisation were achieved (>99% as judged by ¹H NMR spectroscopy). Thus, this approach was extended to include diblock copolymer nanoparticles. PAGEO5MA₂₆-PHPMA_y-(PEGDMA₂₀) block copolymer spheres, worms and vesicles were each functionalised in turn using two different amino acids as model compounds. Again, very high extents of functionalisation were achieved in each case. The electrophoretic behaviour of these nanoparticles was investigated as a function of pH. For the PAGEO5MA₂₆-PHPMA_y-(EGDMA₂₀) and PAGEO5MA₂₆-PHPMA_y-(PEGDMA₂₀) nanoparticles, zeta potentials remained close to neutral across the whole pH range. In contrast, the zeta potential of the amino acid-functionalised nanoparticles changed dramatically with pH. Characteristic isoelectric points (IEPs) were observed for each type of amino acid-functionalised nanoparticles and these were consistent for each copolymer morphology. These results indicate that amino acids can be incorporated into such polymers while retaining their zwitterionic character. Interestingly, reacting PAGEO5MA₂₆-PHPMA₃₅₀-PEGDMA₂₀ vesicles with a model globular protein (bovine serum albumin, BSA) profoundly affected their electrophoretic behaviour. After functionalisation, the zeta potential vs. pH curve became comparable to that observed for BSA alone. In contrast, the zeta potential vs. pH curve obtained for the *cis*-diol functionalised PAGEO5MA₂₆-PHPMA₃₅₀-PEGDMA₂₀ vesicles remained unchanged after attempted functionalisation with BSA, highlighting that surface aldehyde groups are essential for successful protein conjugation. One of the drawbacks with reductive amination using NaCNBH₃ is that it can decompose to produce toxic cyanides. To make this process safer and more industrially relevant, immobilisation of the cyanoborohydride on a suitable resin could be of interest.^{9,10} This should prevent decomposition of the

cyanoborohydride and minimise the formation of toxic side-products. Alternatively, functionalisation of polymers/nanoparticles without employing a reductive amination step could be explored. Although the imine bond is relatively labile, it may be sufficiently stable for certain applications. This may be particularly true for protein-functionalised nanoparticles because multiple imine bonds should be formed when each protein reacts at the nanoparticle surface. Such multiple imine bonds should make the protein-polymer conjugates much more stable towards hydrolysis. These protein-polymer conjugates could have potential applications. For example, Maynard et al. synthesised protein-polymer conjugates using thiol chemistry to stabilise lysozyme.¹¹ Upon attachment of this protein to a trehalose-based polymer, its stability toward both lyophilisation and thermally-induced denaturation was enhanced.

This reductive amination chemistry was also employed to functionalise PGEO5MA brushes grown from planar substrates. In contrast to the solution oxidation of PGEO5MA-based (co)polymers, a large excess of NaIO₄ was used for the brush oxidation owing to the relatively small mass of brush chains (estimated to be approximately 5 µg cm⁻²). X-ray photoelectron spectroscopy (XPS) studies confirmed that full conversion of *cis*-diols to aldehyde groups could be achieved within 30 min at 22 °C. These PAGEO5MA brushes were then functionalised *via* reductive amination with 2,2,2-trifluoroethylamine, (2-aminoethyl)trimethylammonium chloride hydrochloride (AETMA) or histidine. XPS was used to confirm the mean extent of functionalisation in each case. Compared to the reactions in solution, much lower extents of functionalisation were achieved for these brushes. However, these results were comparable to other brush studies.^{12,13} Surface zeta potential vs. pH measurements were conducted on PGEO5MA, AETMA- and histidine-functionalised brushes. As expected, the non-ionic PGEO5MA brush exhibited surface zeta potentials of almost zero across the whole pH range. In contrast, the surface zeta potential of the AETMA-functionalised brush remained highly cationic regardless of the solution pH. Interestingly, the surface zeta potential vs. pH curve obtained for the histidine-functionalised brush was comparable to that observed for histidine-functionalised PHisGEO5MA₂₆-PHPMA_y nanoparticles, despite the much lower degree of functionalisation achieved in the former case. More specifically, the surface zeta potential was cationic at low pH and an IEP was observed at around pH 6. At high pH, the surface zeta potential became negative as the carboxylic acid groups underwent ionisation and the amine groups are gradually deprotonated. Importantly, increasing the reaction temperature for reductive amination from 35 °C to 50 °C for the synthesis of PHisGEO5MA

brushes increased the mean extent of functionalisation from 13 to 82%. Thus, adjusting the temperature could be a useful way to control the degree of brush functionalisation. Such brushes offer various potential applications including useful scaffolds for small molecules,¹⁴ dye functionalisation¹⁵ or biosensing.^{12,16} Further optimisation of the functionalisation conditions should be undertaken and covalent binding of enzymes onto these brushes could be explored. In principle, enzyme immobilisation should enhance their long-term stability as well as enabling their facile recovery from reaction mixtures.^{17,18} This approach is of interest for applications ranging from biocatalysts to sensors. In principle, the kinetics and extent of enzyme binding could be monitored by flow-through ellipsometry since this should result in an increase in the wet brush thickness. However, covalent binding of enzymes may reduce their activity so this would need to be investigated using appropriate enzyme activity assays.

For many biological applications, ultrafiltration of nanoparticle dispersions is an attractive means of removing bacteria.¹⁹ For PHPMA-based thermoresponsive worms, this can be achieved by cooling from 22 to 5 °C to induce a worm-to-sphere transition.^{19,20} This causes the initial worm gel to become a free-flowing, low-viscosity liquid, which can be easily ultrafiltered to remove bacteria. This cold dispersion of spheres can then be returned to 22 °C to reconstitute the original worm gel. According to Warren et al., PHPMA exhibits an upper limit degree of polymerisation (DP) above which its thermoresponsive character is lost.²¹ Therefore, several PGEO5MA stabiliser blocks were employed to determine the optimum PHPMA DP to produce thermoresponsive PGEO5MA-PHPMA worms. Initially, it was found that PGEO5MA₂₆-PHPMA₂₅₀ worms were not thermoresponsive so two further PGEO5MA precursors with a mean DP of either 13 or 16 were prepared for evaluation. Both PGEO5MA₁₆-PHPMA₂₀₀ and PGEO5MA₁₃-PHPMA₁₅₅ worm gels underwent degelation on cooling from 22 °C to 5 °C. However, cold PGEO5MA₁₆-PHPMA₂₀₀ spheres did not reform a worm gel on returning to 22 °C. In contrast, the cold PGEO5MA₁₃-PHPMA₁₅₅ spheres reformed a worm gel with comparable rheological properties to that of the original gel. This suggests potential biomedical applications for this PGEO5MA₁₃-PHPMA₁₅₅ hydrogel.²²

In principle, hydrogels bearing appropriate chemical functionality can adhere to biological substrates. This is likely to be particularly important for mucosal drug delivery, for which therapeutic efficiency is often substantially reduced by the continuous production and flow of biological fluids.^{23,24} This can result in drug leakage from the site of administration, which prevents effective localised delivery. Thus, designing mucoadhesive

hydrogels should enable more effective drug delivery. For mucoadhesion applications, a high degree of aldehyde functionality may not be desirable. This is not least because aldehyde groups can confer toxicity.²⁵ Hence, selective oxidation of PGEO5MA homopolymers was investigated using sub-stoichiometric amounts of NaIO₄ relative to the pendent *cis*-diol groups. It was found that the extent of oxidation could be selectively tuned, so this approach was employed for the partial oxidation of thermoresponsive PGEO5MA₁₃-PHPMA₁₅₅ diblock copolymer worms. The PGEO5MA block could be oxidised to give worm gels bearing 10, 20, 30 or 50% aldehyde functionality. Mucoadhesion studies were conducted on porcine urinary bladder mucosa subjected to a constant flow of artificial urine by our collaborators at the University of Reading to assess the properties of these worm gels using chitosan as a positive control. Worm gels containing no aldehyde functionality exhibited minimal adhesion to the mucosal substrate. In contrast, worm gels bearing 50% aldehyde functionality resulted in their strong retention (comparable to that observed for chitosan). However, such 50% aldehyde-functionalised worm gels proved to be insufficiently thermoresponsive to enable their convenient purification by ultrafiltration. Instead, the 30% aldehyde-functionalised worm gel was identified as offering a suitable compromise in physical properties because this hydrogel exhibited relatively strong mucoadhesion while also exhibiting relatively fast thermoresponsive behaviour. Cytotoxicity studies are a critical next step for such systems. It has already been shown that PGMA-PHPMA worm gels are highly biocompatible.²⁰ Given the similar chemical structures of PGMA and PGEO5MA, it is anticipated that the PGEO5MA-PHPMA worm gels should also be biocompatible. In principle, cytotoxicity could be assessed by loading mammalian cells into a cold dispersion of these particles and then warming this dispersion up to 37 °C to allow the worm gel to reform. Monitoring cell death within these gels would then determine whether they were cytotoxic or biocompatible. Alternatively, certain organisms such as slugs can be used to evaluate toxicity.²⁶ Slugs release mucus when they come into contact with toxic materials in order to protect themselves. Thus, slugs could be placed onto aldehyde-functional PGEO5MA-PHPMA worm gels and the volume of mucus subsequently released could be monitored gravimetrically and compared to that observed for known cytotoxic and biocompatible substrates. Drug loading studies for such worm gels is also desirable. Thus, an inherently fluorescent drug such as doxorubicin could be encapsulated within a worm gel, which could then be covered with further deionised water (or a pH 7 buffer solution). Fluorescence spectroscopy could then be used to assess how much of the drug is released from the worm gel over a given time period.

This Thesis has highlighted the versatility of this aldehyde-functional AGE05MA monomer for the synthesis of ionic and non-ionic *hydrophilic* diblock copolymers, *hydrophilic* statistical copolymers and various types of diblock copolymer nanoparticles. The aldehyde-functionalised block can be readily derivatised with various amines, amino acids or proteins, which suggests potential bio-applications. Finally, aldehyde-functionalised diblock copolymer worm gels exhibit mucoadhesive behaviour that is comparable to that of chitosan, which is a widely recognised ‘gold standard’ in this context. Further investigation in this particular area appears to be warranted.

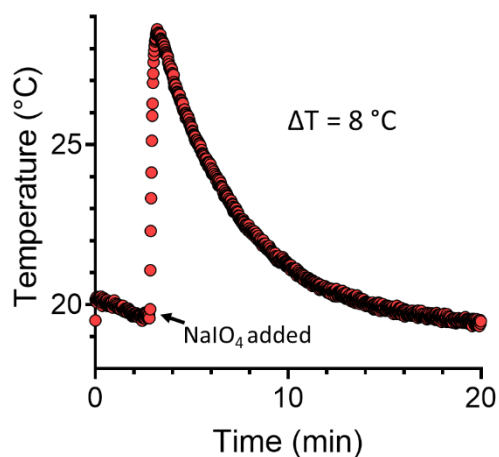
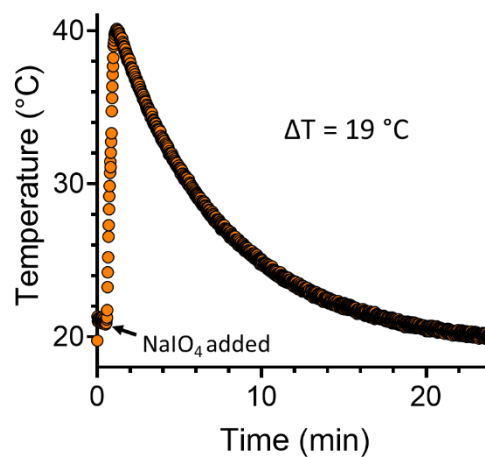
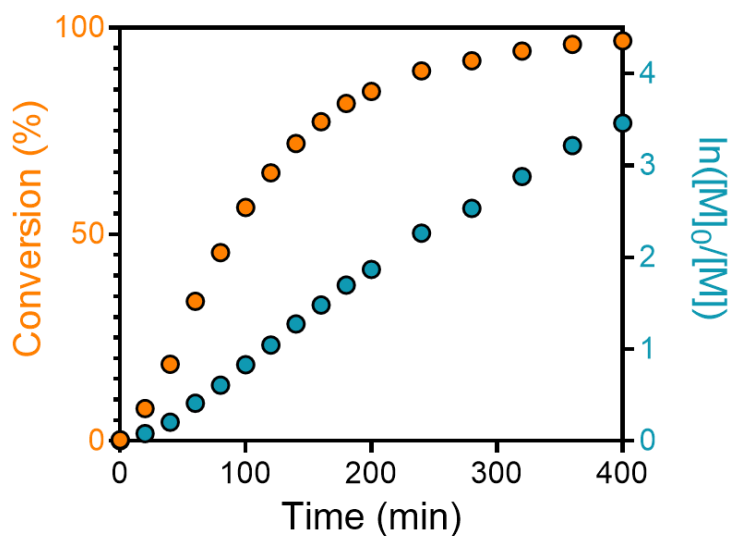
7.1. References

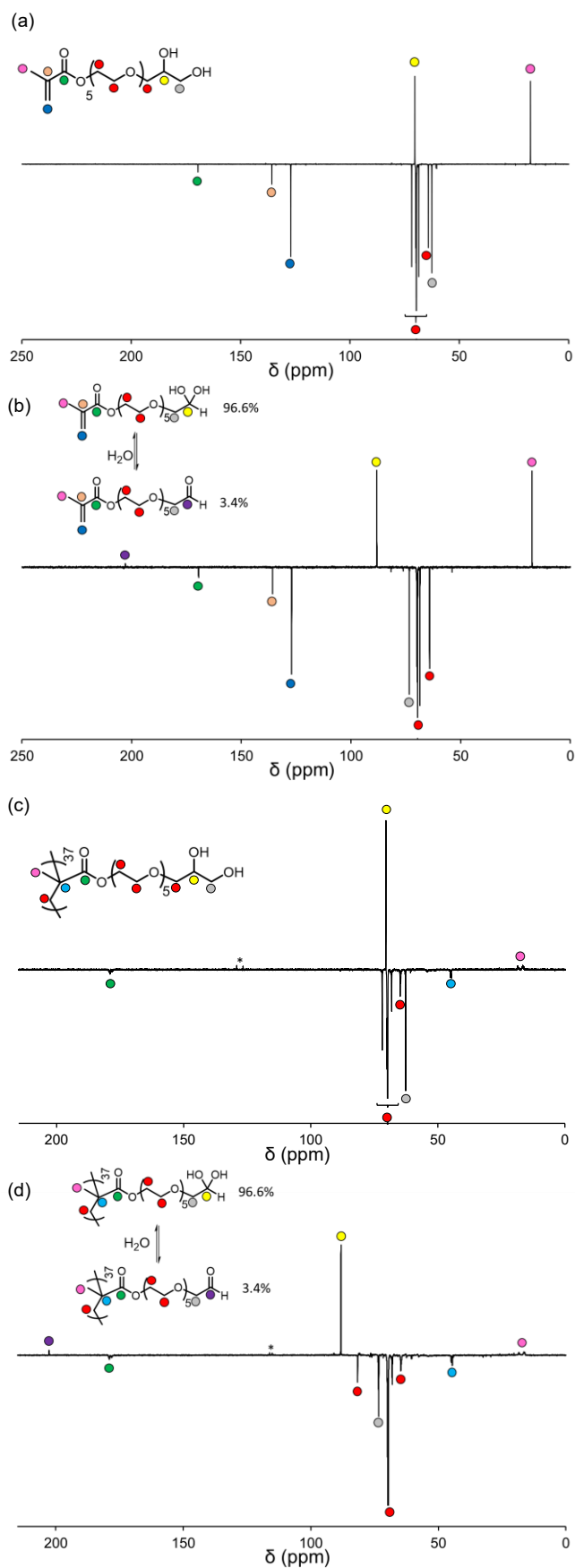
- 1 R. Ciriminna and M. Pagliaro, *Org. Process Res. Dev.*, 2010, **14**, 245–251.
 - 2 A. Zanka, *Chem. Pharm. Bull.*, 2003, **51**, 888–889.
 - 3 A. Hinzmann, M. Stricker, J. Busch, S. Glinski, K. Oike and H. Gröger, *European J. Org. Chem.*, 2020, **2020**, 2399–2408.
 - 4 P. L. Anelli, C. Biffi, F. Montanari and S. Quici, *J. Org. Chem.*, 1987, **52**, 2559–2562.
 - 5 A. Dijkman, I. W. C. E. Arends and R. A. Sheldon, *Chem. Commun.*, 2000, **66**, 271–272.
 - 6 T. Fey, H. Fischer, S. Bachmann, K. Albert and C. Bolm, *J. Org. Chem.*, 2001, **66**, 8154–8159.
 - 7 R. Ciriminna, C. Bolm, T. Fey and M. Pagliaro, *Adv. Synth. Catal.*, 2002, **344**, 159–163.
 - 8 M. B. Smith and J. March, *March’s advanced organic chemistry: reactions, mechanisms, and structure*, John Wiley & Sons, Inc., Hoboken, NJ, 2007.
 - 9 N. M. Yoon, E. G. Kim, H. S. Son and J. Choi, *Synth. Commun.*, 1993, **23**, 1595–1599.
 - 10 R. O. Hutchins, N. R. Natale and I. M. Taffer, *J. Chem. Soc. Chem. Commun.*, 1978, 1088–1089.
 - 11 R. J. Mancini, J. Lee and H. D. Maynard, *J. Am. Chem. Soc.*, 2012, **134**, 8474–8479.
 - 12 T. Bilgic and H.-A. Klok, *Biomacromolecules*, 2015, **16**, 3657–3665.
 - 13 J. Madsen, R. E. Ducker, O. Al Jaf, M. L. Cartron, A. M. Alswieleh, C. H. Smith, C. N. Hunter, S. P. Armes and G. J. Leggett, *Chem. Sci.*, 2018, **9**, 2238–2251.
 - 14 A. Lishchuk, E. Csányi, B. Darroch, C. Wilson, A. Nabok and G. J. Leggett, *Chem. Sci.*, 2022, **13**, 2405–2417.
 - 15 Y. Zou, P. Y. J. Yeh, N. A. A. Rossi, D. E. Brooks and J. N. Kizhakkedathu, *Biomacromolecules*, 2010, **11**, 284–293.
 - 16 M. Badoux, M. Billing and H.-A. Klok, *Polym. Chem.*, 2019, **10**, 2925–2951.
 - 17 R. A. Sheldon and S. van Pelt, *Chem. Soc. Rev.*, 2013, **42**, 6223–6235.
 - 18 J. Zdarta, A. S. Meyer, T. Jesionowski and M. Pinelo, *Catalysts*, 2018, **8**, 92.
 - 19 A. Blanz, R. Verber, O. O. Mykhaylyk, A. J. Ryan, J. Z. Heath, C. W. I. Douglas and
-

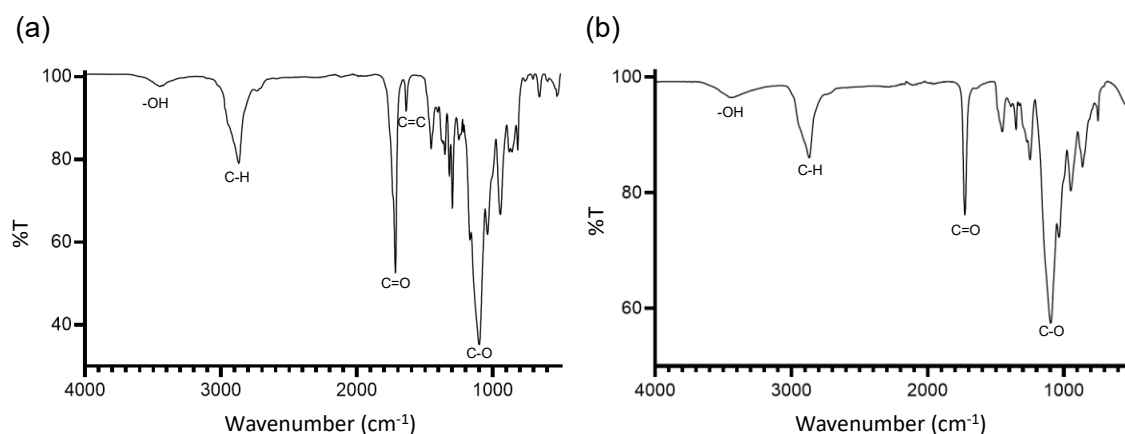
-
- S. P. Armes, *J. Am. Chem. Soc.*, 2012, **134**, 9741–9748.
- 20 I. Canton, N. J. Warren, A. Chahal, K. Amps, A. Wood, R. Weightman, E. Wang, H. Moore and S. P. Armes, *ACS Cent. Sci.*, 2016, **2**, 65–74.
- 21 N. J. Warren, M. J. Derry, O. O. Mykhaylyk, J. R. Lovett, L. P. D. Ratcliffe, V. Ladmiral, A. Blanazs, L. A. Fielding and S. P. Armes, *Macromolecules*, 2018, **51**, 8357–8371.
- 22 O. M. Kolawole, W. M. Lau, H. Mostafid and V. V. Khutoryanskiy, *Int. J. Pharm.*, 2017, **532**, 105–117.
- 23 B. Vigani, S. Rossi, G. Sandri, M. C. Bonferoni, C. M. Caramella and F. Ferrari, *Pharmaceutics*, 2020, **12**, 859.
- 24 F. Zahir-Jouzdani, J. D. Wolf, F. Atyabi and A. Bernkop-Schnürch, *Expert Opin. Drug Deliv.*, 2018, **15**, 1007–1019.
- 25 P. O'Brien, A. Siraki and N. Shangari, *Crit. Rev. Toxicol.*, 2005, **35**, 609–662.
- 26 J. Lenoir, I. Claerhout, P. Kestelyn, A. Klomp, J. P. Remon and E. Adriaens, *Toxicol. Vitr.*, 2011, **25**, 1919–1925.

Chapter VIII: Appendix

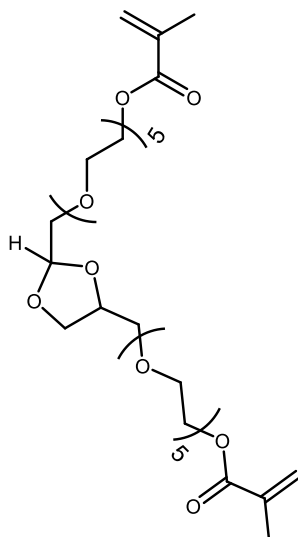
Chapter VIII: Appendix

PGE05MA₃₇ at 10% w/wPGMA₃₉ at 10% w/wAppendix 1. Reaction exotherms for the oxidation of PGE05MA and PGMA using NaIO_4 .Appendix 2. Conversion vs. time and $\ln([M]_0/[M])$ vs. time plots obtained the RAFT solution polymerisation of GEO5MA in ethanol at 70°C.

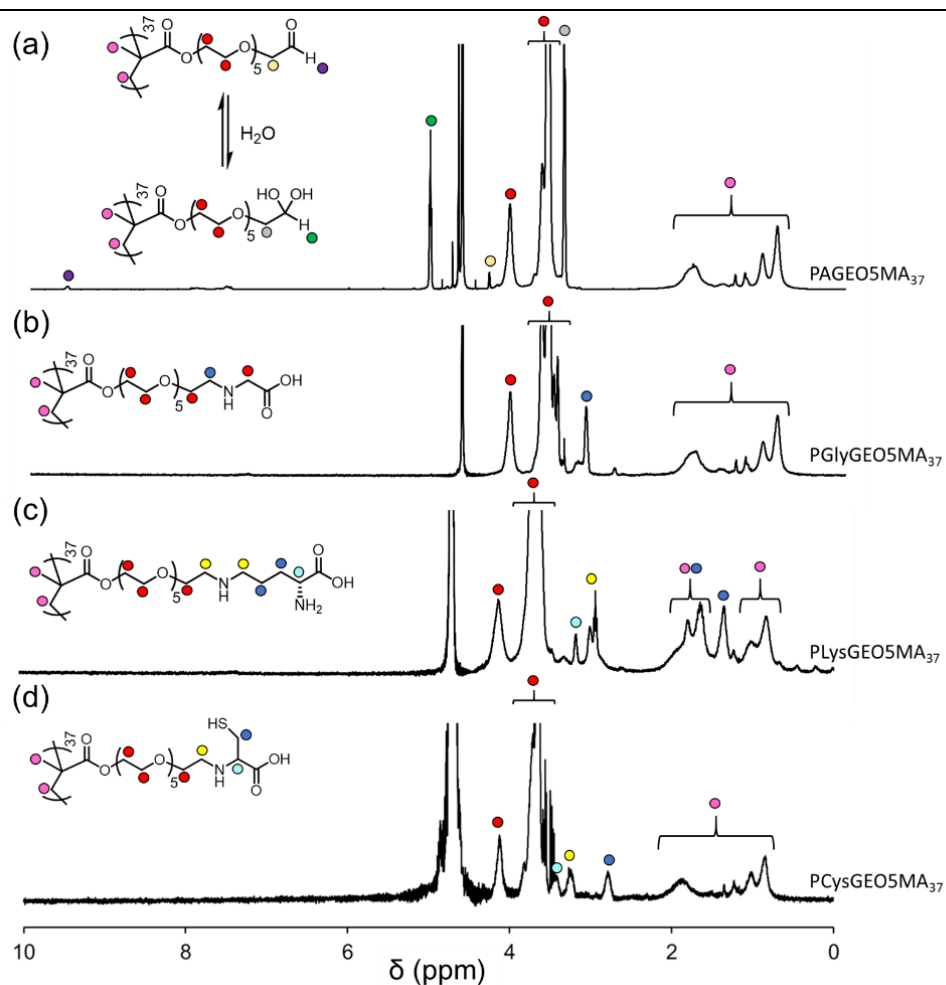




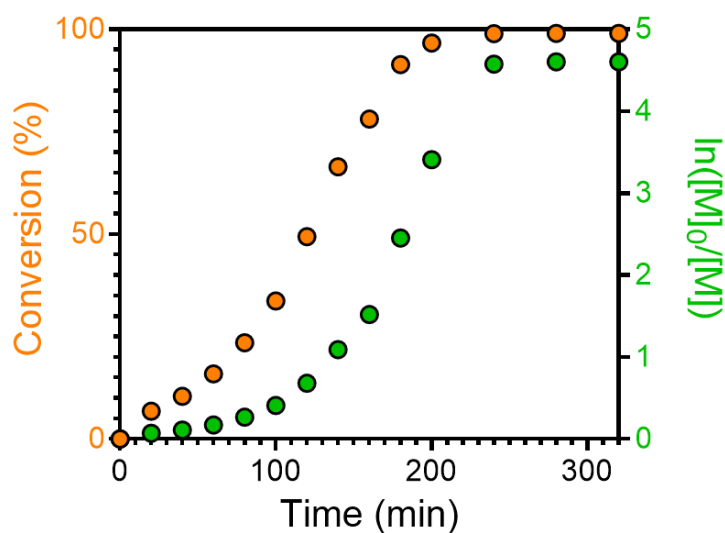
Appendix 4. FT-IR spectra recorded at 22 °C for (a) AGE05MA monomer and (b) PAGE05MA homopolymer. [N.B. There is no detectable aldehyde carbonyl band in these spectra. This is because this group is mainly present in its hydrated geminal diol form. The relatively small number of aldehyde groups indicated by ^1H NMR spectroscopy studies (see Figure 3.1b in Chapter III) would only be expected to produce a very weak band, which is dominated by the strong *methacrylic ester* band that absorbs at a very similar wavenumber (1716 cm^{-1})].



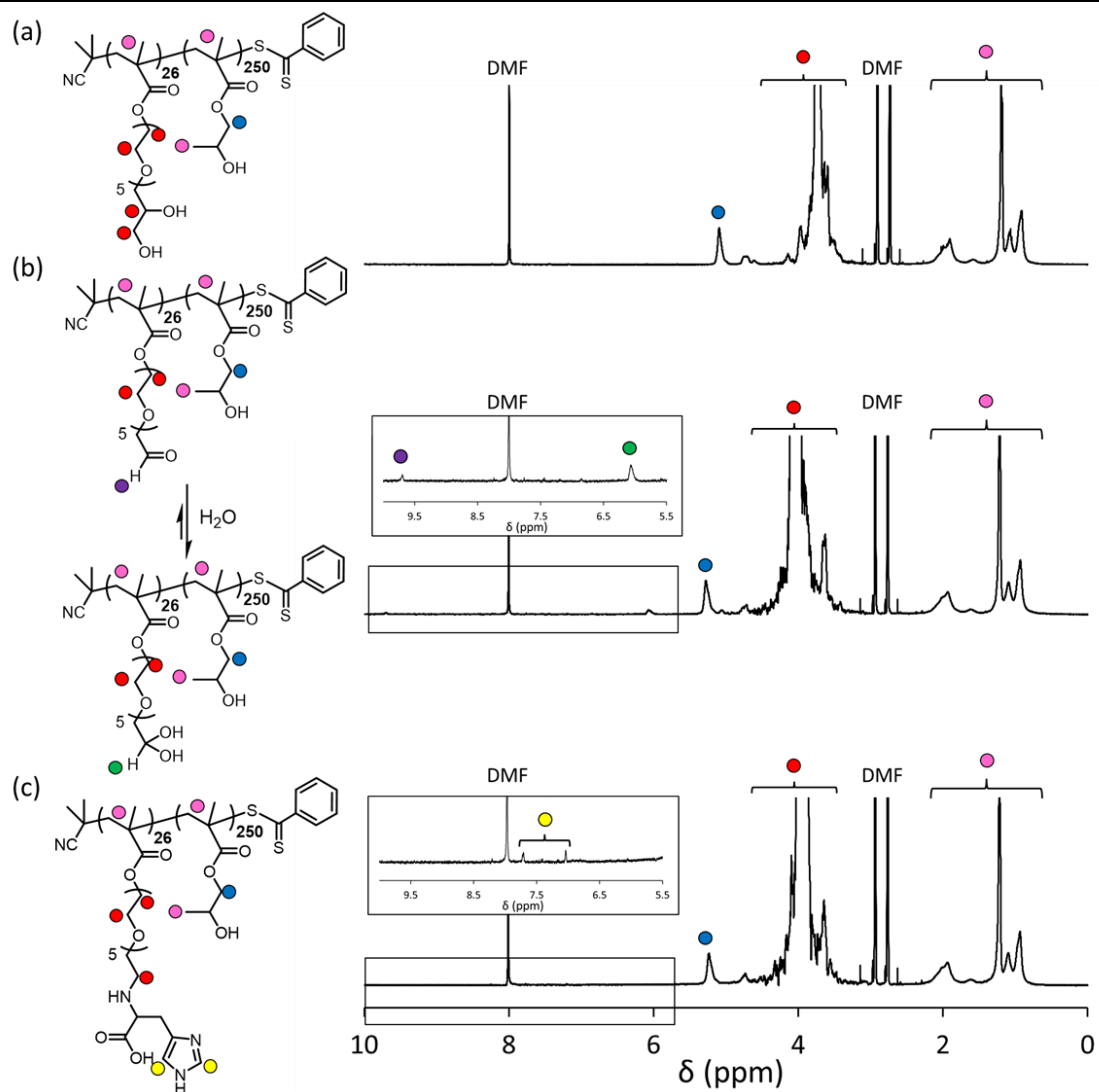
Appendix 5. Proposed structure of unwanted dimethacrylate impurity in AGE05MA monomer formed *via* (hemi)acetal chemistry.



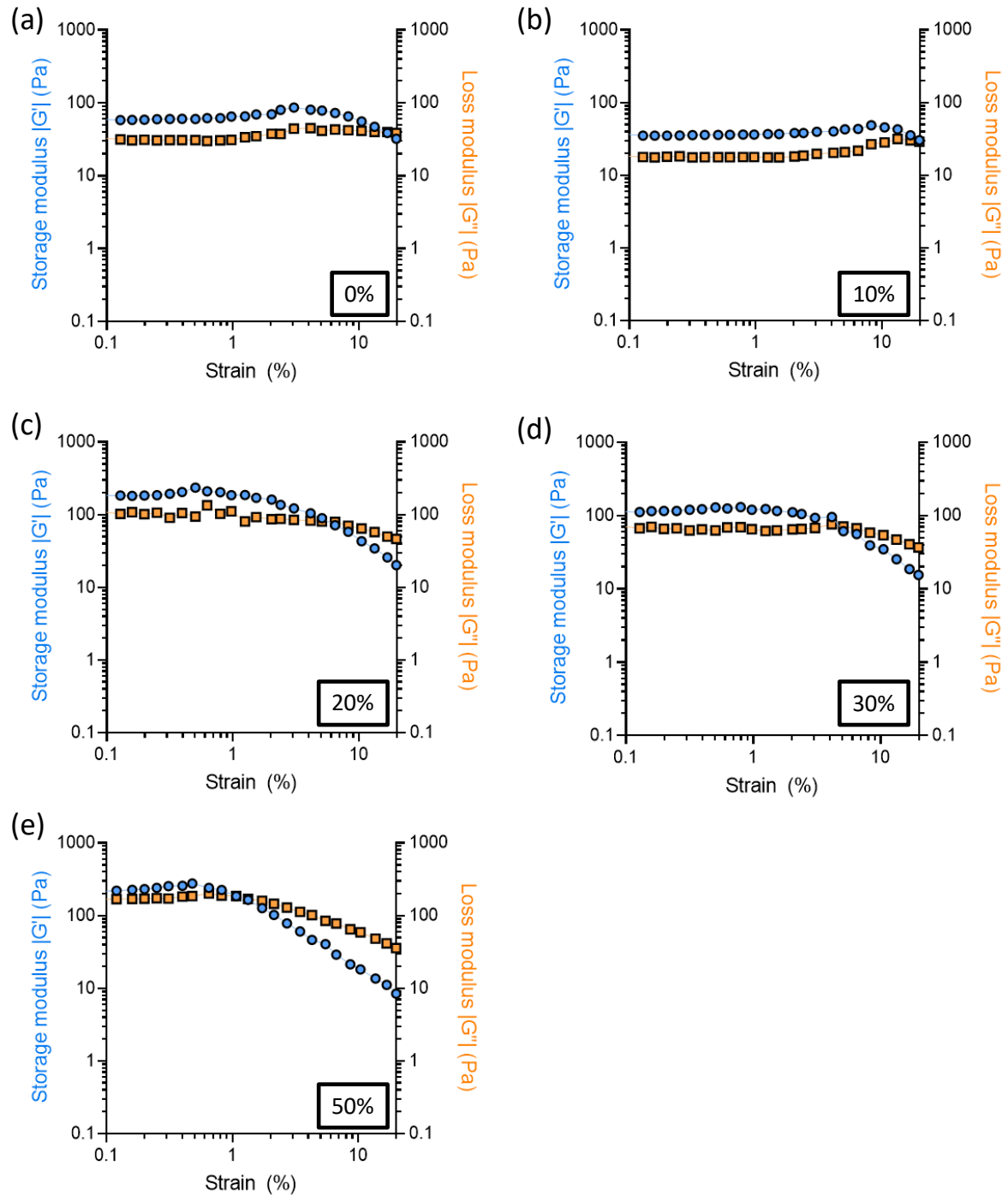
Appendix 6. Assigned ^1H NMR spectra (D_2O) recorded for (a) PAGEO5MA₃₇, (b) glycine-functionalised PGlyGEO5MA₃₇, (c) lysine-functionalised PLysGEO5MA₃₇ and (d) cysteine-functionalised PCysGEO5MA₃₇.



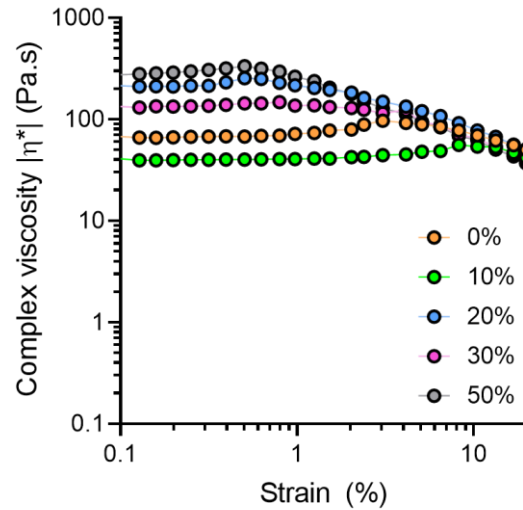
Appendix 7. Conversion vs. time and $\ln([M_0]/[M])$ vs. time plots obtained the RAFT aqueous dispersion polymerisation of HPMA in ethanol at $70\text{ }^\circ\text{C}$.



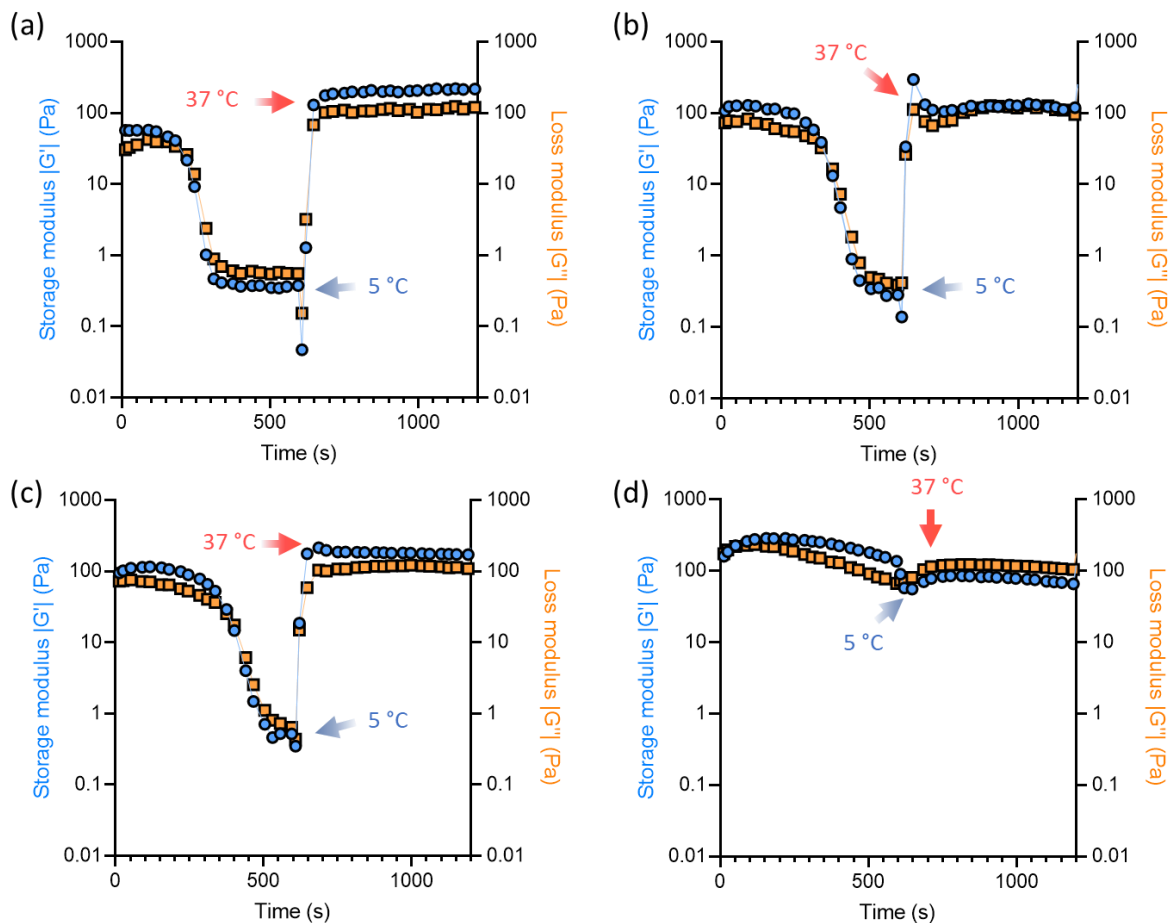
Appendix 8. Assigned ^1H NMR spectra (d_7 -DMF) recorded for (a) PGEO5MA₂₆-PHPMA₂₅₀, (b) PAGEO5MA₂₆-PHPMA₂₅₀ and (c) PHisGEO5MA₂₆-PHPMA₂₅₀.



Appendix 10. Storage and loss moduli (G' and G'' , respectively) vs. strain curves recorded at a constant angular frequency of 1.0 rad s^{-1} for PGE05MA₁₃-P(HPMA₁₅₅-*stat*-FMA_{0.15}) worms equilibrated at ambient temperature containing (a) 0%, (b) 10%, (c) 20%, (d) 30% and (e) 50% aldehyde functionality.



Appendix 11. Complex viscosity vs. strain curves recorded at a constant angular frequency of 1.0 rad s^{-1} for PGE05MA₁₃-P(HPMA₁₅₅-*stat*-FMA_{0.15}) worms equilibrated at ambient temperature containing varying degrees of aldehyde functionality.



Appendix 12. Variable temperature oscillatory rheology for storage and loss moduli (G' and G'' , respectively) recorded at either $5 \text{ }^\circ\text{C}$ or $37 \text{ }^\circ\text{C}$ for PGE05MA₁₃-P(HPMA₁₅₅-*stat*-FMA_{0.15}) worms containing (a) 10%, (b) 20%, (c) 30% and (d) 50% aldehyde functionality.



Appendix 13. Digital photographs recorded for $\text{PGE05MA}_{13}\text{-P}(\text{HPMA}_{155}\text{-stat-FMA}_{0.15})$ diblock copolymer nanoparticles at 25 °C and after cooling to 5 °C for (a) 0%, (b) 10%, (c) 20%, (d) 30% and (e) 50% aldehyde functionality.